

Sedimentary and volcanoclastic record of a mid-ocean spreading ridge: Macquarie Island, Southern Ocean

By: Ryan Adam Portner

January, 2010

to Jerry, Ethel, and Johanna Elise....

Presented to the Higher Degree of Research, Macquarie University in fulfillment
of the requirements for the degree of Doctor of Philosophy

**Sedimentary and volcanoclastic record of a mid-
ocean spreading ridge: Macquarie Island,
Southern Ocean**

Ryan Adam Portner

Bachelor of Science (Cum Laude honors)
University of Pittsburgh at Johnstown
Department of Geology
December 2000

Master of Science
University of Montana
Department of Geology
May 2005

Table of Contents:

Preface

Summary:.....	viii
---------------	------

Introduction:	1
Topic, scope, and significance:.....	3
Macquarie Island, a geological field laboratory:	6
“Island’s” age vs. “crustal” age	6
Thesis outline and time line:	8
Part 1 - Sedimentary rocks.....	9
Part 2 - Volcaniclastic rocks.....	12
References Cited:.....	15

Part 1

Chapter I: A detrital record of lower oceanic crust exhumation within a Miocene slow-spreading ridge: Macquarie Island, Southern Ocean	23
Abstract:	25
Introduction:	26
Geologic Setting:	28
Methods:.....	31
Lithofacies:	32
Basaltic breccias.....	33
Gabbroic sedimentary rocks.....	33
Stratigraphic Sections:	39
Major Lake Sections (central Macquarie Island)	39
Finch-Langdon Sections (northwest Macquarie Island)	40
Petrography:	46
Polymict basalt breccia	46
Gabbroic sedimentary rocks.....	51
Detrital clinopyroxene geochemistry:.....	53
Detrital ²⁰⁶ Pb/ ²³⁸ U zircon geochronology:	54
Discussion on provenance:	59
Polymict basalt breccias	59
Sandstones of the gabbro clast-bearing sedimentary intervals.....	60
Oceanic crustal exhumation and depositional environment:	74
Conclusions:.....	78
References Cited:.....	79

Chapter II: Gravity flow and bottom current interaction with a rugged mid-ocean ridge seafloor: an outcrop example from Macquarie Island	87
Abstract:	89
Introduction:	90
Geologic Setting:	92
Measured Sections:	96
Lithofacies:	106
Cobble breccia facies	106

Muddy diamictite facies	115
Pebble-granule breccia facies	116
Pebbly sandstone facies.....	117
Graded sandstone facies	118
Ripple-bedded sandstone facies	121
Sandy red mudstone facies.....	123
Arlstone facies	124
Discussion:	127
Detrital source and origin of gravity flows.....	127
Depositional Mechanisms.....	136
Paleobathymetry and depositional basin	142
Conclusions:.....	145
References Cited:.....	146
 Chapter III: Discussion on the depositional mechanism of massive sandstone and implications from detrital clay mineralogy	155
Introduction:	157
The deep-water massive sandstone conundrum	157
Clay mineralogy and low grade metamorphism	158
Results:.....	165
Mawson Point massive sandstone:.....	165
Sandstone clay petrography	173
Clay composition and mineralogy from electron microprobe data:	174
Clay mineralogy from X-ray diffraction.....	183
Discussion:	187
Diagenetic conditions	187
Implications for depositional flow mechanism	188
Conclusion:	189
References:	190
 Chapter IV: Oceanic zircon trace element and Hf-isotope geochemistry as a provenance tool and its implications for the proto-Macquarie Spreading ridge demise	193
Introduction:	195
Background:.....	196
Sample collection	196
Zircon host rock	197
Zircon characteristics.....	198
Methods:.....	203
$^{206}\text{Pb}/^{238}\text{U}$ geochronology and trace element geochemistry.....	203
$^{176}\text{Hf}/^{177}\text{Hf}$ isotopes	204
Results:.....	205
U-Pb concordia	205
Trace element data	206
Hf-isotopes	210
Discussion:	215
Depleted oceanic vs. enriched continental zircon provenance	215
Model ages, mantle reservoirs, and melt effects	219
Conclusions:.....	232

References Cited:.....	233
------------------------	-----

Part 2

Chapter V: Glassy fragmental rocks of Macquarie Island: Mechanism of formation and deposition.....241

Abstract	243
Introduction.....	243
Regional Geology.....	243
Methodology	244
Stratigraphy	244
Bauer Bay	246
Green Gorge.....	246
Pyramid Peak	247
Petrography of breccia matrix.....	249
Discussion	251
Fragmentation processes	251
Sediment Source.....	255
Transport mechanism.....	255
Lithification.....	256
Depositional model	257
Conclusions.....	259
References	259

Chapter VI: Geochemical fingerprint of hyaloclasts in glassy fragmental rocks of Macquarie Island (Southern Ocean): implications for volcanogenic sedimentary processes at a waning mid-ocean ridge261

Abstract:	263
Introduction.....	263
Regional Geology.....	264
Methods.....	264
Field methods	264
Geochemical methods and analytical techniques	264
Observations and results	267
Field relations	267
Petrography	267
Major element geochemistry of glasses	267
Glass classification and CIPW normative mineralogy	271
Trace element geochemistry of glasses.....	271
Discussion	273
Comparison of geochemical results with previous work	273
Implications for provenance	274
Depositional settings	275
Implications for the cessation of seafloor spreading at the Proto Macquarie Spreading Ridge (PMSR)	275
Conclusions.....	276
References	276

Chapter VII: Vitriclastic lithofacies from Macquarie Island (Southern Ocean): compositional influence on abyssal eruption explosivity in a dying Miocene spreading ridge.....	279
Abstract	281
Introduction	281
Geologic background and previous research	282
Lithofacies	283
Low vesicularity lithofacies characteristics.....	283
High vesicularity lithofacies characteristics.....	289
Major element geochemistry	289
Methodology.....	289
Glass shard geochemistry	289
Lithofacies Origin.....	293
Low vesicular glass facies	293
High vesicular glass facies.....	298
Eruptive explosivity and geochemistry	300
Conclusions.....	301
References	301
 Chapter VIII: Discussion about a fault-scarp source for hyaloclastite breccias	305
The problem:.....	307
The Davis Point example:	308
Description.....	308
Interpretation.....	313
The Green Gorge example:	314
Description.....	314
Interpretations	317
Conclusion:	317
References:	318
 Thesis synthesis.....	321

Appendices (DVD in back cover)

- A: Measured sections
- B: Field measurements from respective units in measured sections
- C: Representative CPX major and trace element geochemistry
- D: Zircon U-Pb data, Hf isotope, major and trace element geochemistry
- E: Amphibole, clay, zeolite and spinel major element geochemistry
- F: Clay mineral x-ray diffraction
- G: Volcanic glass major element geochemistry

List of tables:

- 0.1: Macquarie Island sedimentary and volcanoclastic rock types.....9
- 1.1: Representative point count data for basaltic and gabbroic sandstone49

2.1: Macquarie Island gabbroic sedimentary rock lithofacies	109
3.1: Averaged major element compositions for clay minerals	181
5.1: Hyaloclastite breccia and associated pillow basalt characteristics	246
6.1: Average sideromelane geochemical analyses	272
7.1: Macquarie Island volcanoclastic rock lithofacies	284
7.2: Averaged major element compositions for different vitriclastic facies	295

List of figures:

1.1: Location maps	29
1.2: Clast count data for gabbroic and basaltic breccia facies.....	35
1.3: Basaltic breccia and gabbroic sedimentary rock lithofacies photo mosaic..	35-37
1.4: Composite stratigraphic sections for central and northwest coast.....	41-43
1.5: Photomicrographs of basaltic and gabbroic sandstone.....	47
1.6: Clinopyroxene major element geochemistry plots	55
1.7: Chondrite normalized clinopyroxene rare earth element abundances	57
1.8: U-Pb zircon geochronology probability plots	61
1.9: Sandstone composition ternary diagrams.....	63
1.10: Rigid plate paleogeographic map reconstructions	69
1.11: Schematic representation of depositional basin.....	75
2.1: Location and paleogeographic reconstruction maps.....	93
2.2: Stratigraphic sections for gabbroic sedimentary rocks	97-103
2.3: Measured section bedding morphology photo mosaic.....	107
2.4: Gabbroic braccia clast count and sandstone point count data.....	111
2.5: Breccia facies photo mosaic	113
2.6: Sandstone facies photo mosaic	119
2.7: Sandy red mudstone and arlstone facies photo mosaic	125
2.8: Interpretive diagrams illustrating the distribution of sedimentary lithofacies	131
2.9: Schematic representation of mid-ocean ridge depositional basin.....	139
3.1: Composite stratigraphic section of Davis Point with clay compositions	161
3.2: Stratigraphic correlations for massive sandstone from northwest coast.....	163
3.3: Photograph and sketch montage of Mawson Point massive sandstone .	166-167
3.4: Bedform stability diagram.....	171
3.5: Relative abundance of clay types in Macquarie Island sandstones	175
3.6: Photomicrographs of Macquarie Island clay minerals.....	177
3.7: Electron microprobe data for clay minerals.....	179
3.8: X-ray diffractograms for clay minerals in Mawson Point mudstone.....	185
4.1: Sample location map	199
4.2: Photo montage of Macquarie Island zircon characteristics	201
4.3: Zircon U-Pb Terra Wasserburg diagrams	207
4.4: Trace element comparison for zircon host rocks.....	207
4.5: Zircon trace element geochemistry diagrams	211
4.6: Ti-in-zircon thermometry probability plot	211
4.7: Zircon Hf isotope compositions.....	213
4.8: Probability plot for zircon epsilon Hf	213
4.9: Calculated rare earth elements in melts for detrital clinopyroxene	217
4.10: Zircon model Hf ages	221

4.11: Paleogeographic map for eastern Gondwana at 130 Ma	223
4.12: Isotope abundances for Macquarie Island basalts	229
5.1: Tectonic map of South Pacific-Southern Ocean region	244
5.2: Sample location map for glassy fragmental rocks	244
5.3: Representative measured sections for glassy fragmental rocks.....	245
5.4: Photographs of glassy fragment-bearing breccias at Bauer Bay	247
5.5: Photographs of glassy fragment-bearing breccias at Green Gorge	249
5.6: Photographs of glassy fragment-bearing breccias at Pyramid Peak.....	251
5.7: Petrographic and scanning electron microscope images of glassy fragmental rocks	255
5.8: Total alkalis vs. silica diagram for glassy fragmental rocks	256
5.9: Depositional model for glassy fragmental rocks.....	257
6.1: Location and paleogeographic reconstruction maps.....	265
6.2: Sample locations and measured sections for glassy fragmental rocks	266
6.3: Photo mosaic of glassy fragmental rocks	269
6.4: Glassy fragmental rock major element compositions.....	271
6.5: Glassy fragmental rock mantle-normalized trace elements	273
6.6: Incompatible element variation diagrams for glassy fragmental rocks	274
7.1: Sample location map	282
7.2: Low vesicular (LV) glass facies photo montage	285
7.3: Measured sections of LV glass lithofacies along central west coast.....	287
7.4: Vitriclastic lithofacies in geologic map of Pyramid Peak area	288
7.5: High vesicular (HV) glass facies photo montage	291
7.6: Measured section and photo of HV facies from Pyramid peak.....	293
7.7: Major element discrimination diagram for different vitriclastic lithofacies and geochemical groups	97-103
7.8: Harker diagrams for vitriclastic lithofacies.....	296
7.9: Volatile compositions (Cl and H ₂ O) for vitriclastic facies	296
7.10: Hypothetical eruptive environments for vitriclastic lithofacies	297
8.1: Map and measured section illustrating the spatial relationship between hyaloclastite breccia and basalt breccia facies at Davis Bay	309
8.2: Photo mosaic of spatial relationship between hyaloclastite breccia and fault scarp at Davis Point	311
8.3: Structural data and photographs for Green Gorge hyaloclastite breccia	315

Summary:

Sedimentary and volcanoclastic rocks formed within mid-ocean ridge spreading centers have received relatively little documentation compared to their counterparts found in continental margin and volcanic arc systems. Results presented in this thesis characterize a diverse sedimentary and volcanoclastic lithofacies assemblage exposed on the Macquarie Island ophiolite, which formed within a waning slow-spreading mid-ocean ridge. Petrography, geochemistry, and geochronology of detritus indicate that the sedimentary rocks were derived from submarine exposures of faulted Oligocene to Miocene age oceanic crust. The interaction of fault-derived gravity flows with a rugged mid-ocean ridge sea floor and strong bottom current of the Southern Ocean produced a unique depositional environment. Low grade zeolite metamorphism and in-situ uplift of Macquarie Island sedimentary rocks aided the preservation of delicate sedimentary structures otherwise deformed during continental obduction or drilling of modern day mid-ocean ridge sediment.

Isotope and trace element geochemistry of sandstone, gabbroic colluvium, and basalt indicates that Miocene Macquarie Island crust was derived from a much more enriched mantle source compared to the Oligocene age detritus. The recorded covariance in enrichment with time may be attributed to changes in spreading direction and shortening of spreading segments. Alternatively, long-offset transforms associated with the shortened segments likely separated a heterogeneous mantle source. This is supported by paleogeographic reconstructions that show >300 km of offset between sources for the Oligocene detritus and Macquarie Island crust. Long-offset transforms along the waning spreading center also played a role in limiting magma mixing, which is preserved by geochemically variable sideromelane in volcanoclastic rocks. Distinct geochemistry within individual volcanoclastic rock units is attributed to discrete eruption episodes, which were primarily associated with non-explosive quench fragmentation processes along the steep slopes of growing pillow cones and active fault scarps. Rare explosive eruptions also occurred in relatively enriched magma compositions containing both fractionated and volatile components.

Author's declaration of originality:

I Ryan Portner declare that this is my own work and that it has not been submitted to any other institution for a higher degree.

Macquarie University
Earth and Planetary Sciences
North Ryde, Australia
rportner@els.mq.edu.au
+61 (0)2 9850 4400

Acknowledgements:

Support for this thesis primarily included an Australian Research Council (ARC) grant (Discovery Project ID DP0663373) to Nathan Daczko and Julie Dickinson. Logistical support for the field-based research was provided by the Australian Antarctic Division (AAD; project number 2515). Generous bursaries from the Petroleum Exploration Society of Australia (PESA; 2006, 2007) and Australia Institute of Geoscientists (AIG; 2008) were also vital resources for this thesis. The International Macquarie University Research Scholarship (iMURS), Post-Graduate Research Fund (PGRF) and Macquarie University International Travel Scholarship (MUIS) endowed the author with sufficient funding expenses (2006-2009) for laboratory analysis and presentation of the results from this thesis at several international conferences.

I am grateful for the tremendous efforts of four wonderful people intimately associated with the Macquarie Island project. My primary supervisor Nathan Daczko provided a tremendous amount of time, energy, enthusiasm, geofantasy, free rent, and money that made this project an amazing experience. My secondary supervisor Julie Dickinson was always there when I needed a sed head to bounce ideas off of and really helped when it counted. Keeping my spirits up during some of the most ridiculous weather conditions imaginable was Nicole Harb who always had a smile on her face. Another smiling face from the energetic Melissa Murphy cranked out some serious time in the lab and contributed a significant amount of analytical data to this thesis. These four people created the team this study is indebted to.

Field work was a main component of this dissertation and wouldn't have been possible without the help from everyone that spent time with me on Macquarie Island. Aleks, Rowan and Nick were personal escorts to some of the most "forbidden" and remote parts of Macquarie Island. Cheers to Wani, Paul (aka "the dude"), Hellsey, Doc, Eddie, Georgie, and Keith, for helping out with field work in some really crap weather. Not to mention, Damo who constructed the amazing Jacob staff that could withstand winds up to 60 knots. Upon return to the real world, the reality of doing lab work was imminent and was made bearable by the help of many working in the geochemical analysis unit of Macquarie University, namely including Norm, Kevin, Justin, Shelly, Luke, Manal, Steve, Russel, Stephan, and John. Pat

Quilty and Dick Flood must also be recognized for their seemingly unending reservoirs of geological knowledge I tapped into.

Lastly my dearest Siri was always there in my pain and continually educated me in the ways of my nemesis....the hyphen.

Introduction:

Sedimentary and volcanoclastic record of a mid-ocean spreading ridge: Macquarie Island, Southern Ocean

Topic, scope, and significance:

Mid-ocean spreading ridges comprise the most extensively connected mountain chain on planet Earth with over 50,000 km of global extent and an average relief of 1-2 km (Batiza 1996; Buck et al. 2005). Discovery of these deep-marine spreading centers in the 1950's lead to the plate tectonic paradigm shift of the 1960's and 70's, which prompted the connection between ophiolites and oceanic crust. Although ophiolites consist of subaerially exposed oceanic crust, their paleotectonic setting is often obscured during continental obduction. Geochemical data from ophiolites indicate that they are derived from a wide array of oceanic lithospheric domains including fast to slow mid-ocean spreading ridges, incipient rifts, arc-related rifts, and supra-subduction zones (Moores et al. 2000). The majority of ophiolitic rocks including the well-studied Oman and Troodos complexes are generally perceived to be akin to supra-subduction zone type oceanic crust, but controversy over their tectonic setting remains (Nicolas and Boudier 2003). Land based studies of mid-ocean ridge oceanic crust (*sensu-stricto*) within ophiolites is typically highly deformed such that the relationships between original tectonic and volcanic features (i.e. ridge-transform intersections) are obscured. However, these relationships are still preserved in modern ocean basins where oceanic crust is subaerially exposed as small islands, such as Iceland, but these examples are commonly influenced by mantle plumes/hot spots and thus do not adequately meet the definition of true mid-ocean ridge crust. Macquarie Island in the Southern Ocean is one such exception being a true non-plume related relatively in-situ exposure of oceanic crust (Varne et al. 2000).

In light of the remarkable nature of Macquarie Island, the primary aim of this thesis is to thoroughly describe and interpret the origin of sedimentary and volcanoclastic rocks within a mid-ocean ridge. This spreading ridge, the proto-Macquarie spreading ridge (PMSR), was active from the Eocene to Miocene and evolved into the present day amagmatic bathymetric ridge, the Macquarie Ridge Complex (MRC). Therefore, analysis of the detrital composition in volcanoclastic and sedimentary rocks on Macquarie Island will yield insight into the magmatic and tectonic evolution of a dying spreading ridge. Research on ancient and modern oceanic lithosphere has primarily focused on igneous, metamorphic, hydrothermal, geophysical, geochemical, and tectonic processes (e.g. Cann et al. 1999; Dilek et al. 2000; Dilek and Newcomb 2003) with relatively minor reference to synrift sedimentary or volcanoclastic rocks (e.g. Barret and Spooner 1977; Simonian and Gass 1978, Swift 1991; Clague et al. 2009). In continental basins, including embryonic rift basins, sedimentary and volcanoclastic rocks are primary targets for elucidating tectonic evolution (Dorsey et al. 2001; Gawthorpe and Leeder 2000; Sharp et al. 2000; Lappard and Gawthorpe 2006). Unfortunately, sedimentary and volcanic rocks in tectonically active basins of the mid-ocean ridge system have been neglected compared to their continental cousins. This is most likely due to the inherent difficulty in working in the deep-marine environment. Apart from sample collection and laboratory analysis, detailed documentation of sedimentary and volcanoclastic rocks within both ancient and active mid-ocean ridges have largely been overlooked due to their minor abundance compared to igneous rocks.

Apart from quiescent volcanic extrusion and pelagic sedimentation along active mid-ocean ridges, submersible studies and dredging have identified a plethora

of volcanoclastic and sedimentary rocks that range from syn-eruptive hyaloclastite deposits to hydrothermal chert and metaliferous sediments to ophiolitic breccia and sandstone (Fox and Heezen 1965; Bonatti et al. 1974; Lonsdale and Batiza 1980; Adachi et al. 1986; Barany and Karson 1989; German et al. 1999). Spreading-ridge volcano-sedimentary basins are important to the mining industry because they contain volcanic-hosted massive sulphide (VHMS) and sedimentary exhalative (SEDEX) deposits, which are economically viable ore bodies in land based localities (Robb 2005). For example, the Pb-Zn-Ag orebody in Broken Hill Australia is one of the largest of its kind to ever be discovered and believed to be a remnant of a hydrothermal-related volcanic- or sedimentary- exhalative deposit produced within a Proterozoic submarine spreading ridge (Parr et al. 2004). Furthermore, hydrothermal sediments and alteration of glassy volcanoclastic deposits within submarine rift-related environments are believed to be associated with the development of microbial life on Earth during the Archean and Proterozoic Eons (Fisk et al. 1998; Schopf et al. 2002; Fisk et al. 2003; Kato and Nakamura 2003; Furnes et al. 2005). A better understanding of the processes that generate mid-ocean ridge volcanoclastic and sedimentary deposits is needed and benefits from a hands-on field perspective based in appropriate subaerially exposed ophiolitic sections. Central to this goal is visual analysis via field research, which is a fundamental component to sedimentary geology and physical volcanology going “hand-in-hand” with laboratory work. Fieldwork and laboratory analytical results presented in this thesis provide a much needed building block into the “knowledge gap” of syntectonic mid-ocean ridge volcano/sedimentary basins.

Macquarie Island, a geological field laboratory:

Macquarie Island was discovered in 1810 by a sealing vessel. The island's geology was first summarized in 1880 by John H. Scott (University of Otago) and later examined in more detail by Leslie Blake between 1911 and 1913. The initial geological observations and notes were later published by Mawson and Blake (1943). An important conclusion from that first published work was that *Globigerina* ooze within pillow basalt selvages (interpillow ooze) was deposited between 2 and 4 km below sea level (b.s.l.). Over the next few decades several publications regarding Macquarie Island's unique geological character were realized and showed that it was a relatively well-preserved section of oceanic crust still within the context of the oceanic magnetic anomalies that it formed in (e.g. Varne et al. 1969). Due to its geologic uniqueness as an in-situ piece of well-preserved uplifted sea-floor, the best such example on earth, Macquarie Island was promoted to World Heritage status in 1997 (<http://whc.unesco.org/en/list/629>). It has therefore attracted numerous studies including several theses and thesis (e.g. Griffin 1982; Christodoulou 1990; Rivizzigno 2002; Meckel 2003; Wertz 2003; Lewis 2007).

“Island's” age vs. “crustal” age

The Macquarie Ridge Complex (MRC) is a south-southwest trending submarine ridge with 6 km of bathymetric relief and extends for 1500 km from the southern tip of New Zealand down to the Antarctic spreading corridor at ~62° south (Hayes and Talwani 1972; Ruff et al. 1989). Macquarie Island is situated along the apex of the MRC at 54°30'S and 158°54'E. Geomorphologic observations, including raised beach deposits 200 m above sea level, suggest that the island emerged ~700 to 600 kyr with an average uplift rate of 0.8-3.0 mm/year (Selkirk et al. 1990; Adamson

et al. 1996). Geodynamic reconstructions show that uplift of the presently forming MRC is inherited from transpressional tectonics along extensive transforms that connected short spreading segments of an older a Miocene spreading ridge (Meckel et al. 2005; Mosher and Massell-Symons 2008). This intermediate- to slow-rate spreading ridge, the proto-Macquarie spreading ridge (PMSR), was active from 47 to 6 Ma and formed the crust that makes up Macquarie Island (Lamarche et al. 1997; Varne et al. 2000).

Using foraminifera, nannoplankton and bolboforms from interpillow carbonate ooze from the Macquarie Island, Pat Quilty first suggested that the island was Miocene in age (Quilty et al. 1973), improving earlier interpretations of a Pliocene age (Mawson and Blake 1943). More recently Quilty et al. (2008) refined the stratigraphic age to be between 8.8 and 9.5 Ma. This stratigraphic age falls into the geodynamically modeled 12-6 Ma seafloor spreading age of the island (Varne et al. 2000). Although the validity of radiometric geochronologic data extracted from basalts is uncertain, Duncan and Varne (1988) report an 11.5 ± 0.3 Ma $^{40}\text{Ar}/^{39}\text{Ar}$ plateau age from a relatively pristine tabular basalt flow at Mawson Point. K/Ar data from other flows around the island have cooling ages indicating the end of greenschist metamorphism ($\sim 230^\circ\text{C}$ at 90 MPa) at 6.7 ± 0.6 to 7.2 ± 0.3 and the end of zeolite metamorphism ($\sim 120^\circ\text{C}$ at 50 MPa) at 5.8 ± 0.8 to 5.7 ± 0.8 (Duncan and Varne 1988). These ages are in general agreement with fission track cooling ages from zircon ($\sim 240^\circ\text{C}$) and apatite ($\sim 110^\circ\text{C}$) that yield ages between 5.5 to 6.5 Ma and 4.2 to 5.2 Ma respectively (Armstrong et al. 2004). These fission track ages are from late stage phlogopite pegmatoids in the island's north that also yield $^{206}\text{Pb}/^{238}\text{U}$ zircon

crystallization ages of 8.4 ± 0.3 to 8.8 ± 0.2 Ma (Armstrong et al. 2004) comparable to the other chronologic constraints for the crustal age of the island.

Thesis outline and time line:

This thesis is presented as a series of chapters written as journal articles that have been published or submitted (Chapters I, II, V, VI, and VII). These papers represent the main body of research. Also included are essay chapters (Chapters III, IV, VIII) written to highlight specific aspects of published chapters in more detail where data collected during the course of the study could not be included in journal articles due to length restrictions. The thesis is presented in two parts, the first addresses sedimentary rocks and the second volcaniclastic rocks. Chapters that are already published are presented in their final layout format according to the respective journal style, whereas other chapters are presented in standard thesis format. Therefore, bibliographic style and headings are not entirely consistent between published chapters.

This thesis is built upon a total of 9 months of field work during the 2006 and 2007 summer seasons on Macquarie Island. Using the 1:10,000 geologic maps for Macquarie Island (Goscombe and Everard 1998) sedimentary and volcaniclastic rocks were located and selected for analysis based on the best exposure, greatest thickness and most lateral extent. Table 1 lists generalized descriptions of the different sedimentary and volcaniclastic rocks found on Macquarie Island and the chapters that they are presented in. Nicole Harb assisted with data collection during the 2006 field season, part of which she used to complete her BSc honours thesis (Harb 2006). Melissa Murphy used samples collected from both field seasons for laboratory

analysis to complete her BSc honours thesis (Murphy 2008). Specific contributions from co-authors are noted under individual chapter explanations below. Otherwise all data was collected and analyzed by me.

Table 0.1: Macquarie Island sedimentary and volcanogenic rock types

Rock types, relative proportion, total abundance* on island	Associated lithologies	Clast/grain compositions, maximum detrital metamorphic grades	Bedding geometry, average thickness, lateral extent	Chapters
Basaltic sedimentary rocks, 45%, 6%	- autoclastic basalt breccia - fault-derived basalt breccia (\pm pillow fragments) - basaltic sandstone	polymict basalt, minor diabase, zeolite-greenschist grade	Irregular- to wedge-shaped, massive to crudely bedded, 30-150 m thick; <1000 m laterally extensive	I
Gabbroic sedimentary rocks, 10%, 1%	-gabbroic breccia -gabbroic sandstone -red sandy mudstone -chert/siliceous mudstone -micritic carbonate	Gabbro, diabase, polymict basalt, hydrothermal minerals, greenschist-amphibolite grade	Tabular-lenticular shaped, well bedded, 4-90 m thick; 80-3500 m laterally extensive	I, II, III, IV
volcaniclastic epiclastic, 30%, 1%	-pillow-fragment breccia -hyaloclastite tuff-breccia -vitriclastic sandstone -pyroclastic tuff and lapilli tuff	Monomict basalt, variably altered volcanic glass, zeolite-greenschist grade	Irregular-lenticular and massively to well bedded, <15 m thick; <700 m laterally extensive	V, VI, VII, VIII
Interpillow calcareous ooze, 15%, 2%	-carbonate ooze -sandstone	calcite, foraminifera, microplankton, minor ophiolitic grains	Irregular-well bedded, <2 m thick, <10 m laterally extensive	n/a

* Relative to the well-exposed extrusive section of Macquarie Island

Part 1 - Sedimentary rocks

Sedimentary rocks in this study refer to those which are intercalated within pillow and massive tabular basalt flow units and therefore must have been deposited during the volcanically active part of the rift-to-drift phase of mid-ocean ridge spreading. These rocks are not to be confused with the common ophiolitic sedimentary rock descriptions that abound in the literature, which primarily deal with post spreading pelagic accumulations or obduction-related ophiolitic breccias (e.g. Barrett 1982; Robertson 1990; Abbatte et al. 1994, Pessagno et al. 2000; Knipper et al. 2001; Chiari et al. 2003). Sedimentary rocks on Macquarie Island make up approximately 1% of the exposed ophiolitic sequence and are predominantly well-exposed along coastal wave-cut platforms and within cliff-line exposures of the islands upper plateau escarpment edge. The low total abundance of sedimentary rocks on the island is in part due to the prevalence of a plutonic to ultramafic sequence in the northern 1/5 of the island and poor to non-exposure in the island's

plateau, which makes up >75% of the islands aerial extent. Taking these factors into account sedimentary rocks makes up ~7% of the well-exposed volcanic section along the island's coast.

Chapter I - A detrital record of lower oceanic crust exhumation within a Miocene slow-spreading ridge: Macquarie Island, Southern Ocean

This chapter has been submitted to the Geological Society of America Bulletin and is currently in review (Portner, R.; Murphy, J.; Daczko, N.). Using sandstone petrography, breccia clast counts, clinopyroxene major and trace element geochemistry, and $^{206}\text{Pb}/^{238}\text{U}$ zircon geochronology, this contribution concludes that Macquarie Island's clastic rocks were derived from 1) locally uplifted young upper oceanic crust; and 2) distally uplifted old lower oceanic crust with more depleted compositions compared to presently exposed crust on the island. Petrographic analysis, field data collection, and evaluation of geochemical and geochronological data were conducted during 2007-2008. Geochemical and geochronological data collected by co-author Melissa Murphy during 2007 and 2008 as part of her BSc (honours) degree have been synthesized into this chapter. Nathan Daczko extensively reviewed the manuscript and provided numerous insights into tectonic plate reconstructions of the Macquarie Ridge region and as supervisor of the thesis has also been included as co-author.

Chapter II - Gravity flow and bottom current interaction with a rugged mid-ocean ridge seafloor: an outcrop example from Macquarie Island

This chapter has been submitted to Sedimentary Geology (Portner, R., Dickinson, J.; Daczko, N.). It presents a lithofacies scheme for sedimentary rocks deposited within active mid-ocean ridges with emphasis on coarser grained clastic sequences. Lithofacies interpretations are used to discuss the mechanics behind deep

marine gravity flows, bottom current controlled deposition, and the production of sand within the “erosionless” domain of the mid-ocean environment.

Paleoenvironmental interpretations and an idealized model for the depositional basin relative to mid-ocean ridge tectonic and volcanic features are explored. This paper is solely based on stratigraphic sections measured in 2007 with assistance from Nicole Harb in 2006. Julie Dickinson and Nathan Daczko provided extensive reviews of this manuscript and as thesis supervisors have been included as co-authors.

Chapter III - Discussion on the depositional mechanism of massive sandstone and implications from clay mineralogy

This chapter is supplementary to the data presented in Chapters I and II and explores the depositional mechanics that produce deep water massive sandstones, which form key hydrocarbon reservoirs in modern day petroleum fields. The rheologic properties of the depositing flow are partly dependant upon the amount of clay or mud matrix, which in turn controls the reservoir potential of the sandstone bodies. However, distinguishing between primary and secondary clay in sandstones can be problematic. In order to elucidate this dilemma, compositional variation in phyllosilicates from sandstone pore space and detrital minerals is compared with altered groundmass, minerals, and filled vesicles within interbedded basalt.

Chapter IV - Oceanic zircon trace element and Hf-isotope geochemistry as a provenance tool and implications for the proto-Macquarie Spreading ridge demise

This chapter is in preparation for submission to Earth and Planetary Science Letters (Portner, R.; Murphy, M.; Daczko, N.; Allchurch, S.). It presents trace element geochemistry and $^{176}\text{Hf}/^{177}\text{Hf}$ isotope data from zircon separated from detrital sandstones and modern day colluvium eroded from Macquarie Island's gabbroic

exposures. The $^{206}\text{Pb}/^{238}\text{U}$ age implications from the same zircon suite are discussed in Chapter I. The main finding of Chapter IV shows that detrital zircon trace element geochemistry varies with age indicating a more depleted oceanic source (old grains) toward a more enriched continental-like source (young grains). This is discussed with regard to mantle source heterogeneity, decreased partial melting affects along a dying spreading ridge, and zircon trace element geochemistry as a tool for discriminating between oceanic vs. continental sources. Melissa Murphy and Shelly Allchurch collected most of the geochemical and geochronological data on samples collected with some assistance from Paul Ferguson during the 2007 field season. Preliminary data analysis was conducted by Melissa Murphy with assistance from Elena Belosouva. Nathan Daczko provided reviews of the manuscript.

Part 2 - Volcaniclastic rocks

In this thesis, the term volcaniclastic refers to syneruptive particles produced as a direct consequence of a volcanic eruption (after White and Houghton 2006) and is not to be confused with older definitions that refer to any volcanic material without regard to an origin or environment (Bates et al. 1984 pg. 556 in the Dictionary of Geological Terms). Volcaniclastic rocks are generally better exposed than sedimentary rocks and are prevalent in both coastal and plateau exposures. They make up 1% of Macquarie Island's volcanic section and are referred to as hyaloclastite on the geologic map of Goscombe and Everard (1998). Hyaloclastite is defined as a non-explosively derived volcaniclastic deposit that forms by quenching and subsequent fragmentation of erupted lava during contact with water (after White and Houghton 2006). Along with explosively-derived pyroclastic rocks, hyaloclastites commonly contain fresh to partly altered volcanic glass, which can also

be termed vitriclastic (glassy) when the eruptive origin is uncertain (i.e. explosive vs. non-explosive).

Chapter V - Glassy fragmental rocks of Macquarie Island (Southern Ocean): Mechanism of formation and deposition

This chapter is published in *Sedimentary Geology* (Dickinson et al. 2009). This manuscript deals with depositional mechanics and paleoenvironment of the hyaloclastite formation in a mid-ocean ridge setting. It concludes that the majority of glassy (vitric) volcanoclastic rocks on Macquarie Island were formed by quench fragmentation of erupting lava and subsequent grain flows during gravitational collapse of a pillow cone flank during voluminous eruptions down steep slopes. Julie Dickinson assembled the manuscript based on Nicole Harb's BSc honours thesis. Nicole Harb and I collected most of the field data during the 2006 summer field season. During the 2007 field season, I revisited the locations described in Nicole's thesis and observed new field relationships that were implemented into the published manuscript. I drafted some of the figures, wrote some of the text, provided text reviews along with Nathan Daczko, and submitted the manuscript.

Chapter VI - Geochemical fingerprint of hyaloclasts in glassy fragmental rocks of Macquarie Island (Southern Ocean): implications for volcanogenic sedimentary processes at a waning mid-ocean ridge

This chapter is published in the *Australian Journal of Earth Sciences* (Daczko et al. 2009). Using major and trace element geochemistry this paper concludes that glass grains from the islands hyaloclastic rocks have a unique compositional "fingerprint" for specific eruption episode with little variation during the course of the eruption and laterally along a source vent. This conclusion is discussed relative to possible sources and the magmatically segregated environment of the proto-Macquarie spreading ridge (PMSR). Nathan Daczko assembled the manuscript based

on Nicole Harb's BSc honours thesis. Geochemical data was collected by Nicole Harb and Nathan Daczko. New field observations collected during my 2007 field season were a key element in the final conclusion of this published manuscript. Along with Julie Dickinson, I provided reviews of the manuscript and drafted some of the figures.

Chapter VII - Vitriclastic lithofacies from Macquarie Island (Southern Ocean): compositional influence on abyssal eruption explosivity in a dying Miocene spreading ridge

This chapter is published in the Bulletin of Volcanology (Portner et al. 2009).

The contribution outlines all the vitric (volcanic glass-bearing) volcanoclastic rocks on the island and concludes that hyaloclastic (non-explosive), pepperitic (sediment-magma mingling), epiclastic (re-sedimented), and pyroclastic (explosive) volcanogenic rocks occur on the island in relatively decreasing abundance. The major element geochemistry of the different facies is compared and used to explore magmatic control over eruption explosivity in a waning spreading ridge. Field observations and data analysis were collected during the 2007 field season. New geochemical data collected during 2008 was synthesized with data presented in Chapter VI. Nathan Daczko provided reviews along with Julie Dickinson.

Chapter VIII - Discussion about a fault-scarp source for hyaloclastite breccias

This chapter explores the conclusions made in Chapters V and VI, which refute a fault scarp-derived source for Macquarie Island hyaloclastites. New data collected during the 2007 field season is presented, which supports a fault-scarp source for some hyaloclastic breccias. Comparison between two specific examples is made for and against fault-scarp influenced hyaloclastic rocks. One of the examples,

Green Gorge, presents the new data collected during the 2007 field season that was instrumental in publication of Chapters V and VI.

References Cited:

- Abbate, E., Bortolotti, V., Passerini, P., Principi, G. and Treves, B., 1994. Oceanisation processes and sedimentary evolution of the Northern Apennine ophiolite suite; a discussion. In: V. Bortolotti and M. Chiari (Editors), *Memorie della Societa Geologica Italiana*, vol.48, Part 1, pp. 117-136.
- Adachi, M., Yamamoto, K. and Sugisaki, R., 1986. Hydrothermal chert and associated siliceous rocks from the northern Pacific their geological significance as indication of ocean ridge activity. *Sedimentary Geology*, 47(1-2): 125-148.
- Adamson, D.A., Selkirk, P.M., Price, D.M., Ward, N. and Selkirk, J.M., 1996. Pleistocene uplift and palaeoenvironments of Macquarie Island; evidences from palaeobeaches and sedimentary deposits. In: M.R. Banks and M.J. Brown (Editors), *Papers and Proceedings of the Royal Society of Tasmania*, vol.130, Part 2, pp. 25-32.
- Armstrong, R.A., Kohn, B., Goscombe, B.D. and Everard, J.L., 2004. U-Pb and fission track ages from oceanic crust at Macquarie Island. In: J. McPhie and P. McGoldrick (Editors), *Abstracts - Geological Society of Australia*, vol.73, pp. 197.
- Barany, I. and Karson, J.A., 1989. Basaltic breccias of the Clipperton fracture zone (East Pacific); sedimentation and tectonics in a fast-slipping oceanic transform. *Geological Society of America Bulletin*, 101(2): 204-220.
- Barrett, T.J., 1982. Stratigraphy and sedimentology of Jurassic bedded chert overlying ophiolites in the North Apennines, Italy. *Sedimentology*, 29(3): 353-373.
- Barrett, T.J. and Spooner, E.T.C., 1977. Ophiolitic breccias associated with allochthonous oceanic crustal rocks in the East Ligurian Apennines, Italy; a comparison with observations from rifted oceanic ridges. *Earth and Planetary Science Letters*, 35(1): 79-91.
- Bates, R.L. and Jackson, J.A., 1984. *Dictionary of geological terms*. American Geological Institute, Alexandria, 571 pp.
- Batiza, R., 1996. Magmatic segregation in mid-ocean ridges: A review. In: C.J. MacLeod and C.L. Walker (Editors), *Tectonic, magmatic, hydrothermal, and biological segmentation of mid-ocean ridges*, pp. 103-130.
- Bonatti, E., Emiliani, C., Ferrara, G., Honnorez, J. and Rydell, H., 1974. Ultramafic-carbonate breccias from the equatorial Mid Atlantic Ridge. *Marine Geology*, 16(2): 83-102.
- Buck, W.R., Lavier, L.L. and Poliakov, A.N.B., 2005. Modes of faulting at mid-ocean ridges. *Nature*, 434(7034): 719-723.
- Cann, J.R., Elderfield, H. and Loughton, A., 1999. *Mid-ocean ridges; dynamics of processes associated with creation of new ocean crust*. Cambridge University Press, Cambridge, 301 pp.

- Chiari, M., Bortolotti, V., Marcucci, M., Photiades, A. and Principi, G., 2003. The Middle Jurassic siliceous sedimentary cover at the top of the Vourinos Ophiolite. *Ophiolite*, 28(2): 95-103.
- Christodoulou, C., 1990. Petrology of the plutonic rocks of the Macquarie Island complex, University of Adelaide, Adelaide, 459 pp.
- Clague, D.A., Paduan, J.B. and Davis, A.S., 2009. Widespread strombolian eruptions of mid-ocean ridge basalt. *Journal of Volcanology and Geothermal Research*, 180(2-4): 171-188.
- Daczko, N., Harb, N., Portner, R.A. and Dickinson, J.A., 2009. Geochemical fingerprint of hyaloclasts in glassy fragmental rocks of Macquarie Island. *Australian Journal of Earth Sciences*, 56: 951-963.
- Dickinson, J.A., Harb, N., Portner, R.A. and Daczko, N., 2009. Glassy fragmental rocks of Macquarie Island: Mechanism of formation and deposition. *Sedimentary Geology*, 216: 91-103.
- Dilek, Y., Moores, E.M., Elthon, D. and Nicolas, A., 2000. Ophiolites and oceanic crust, new insights from field studies and the Ocean Drilling Program. Special Paper - Geological Society of America, vol.349, Boulder, 552 pp.
- Dilek, Y. and Newcomb, S., 2003. Ophiolite concept and the evolution of geological thought, 373. Special Paper - Geological Society of America, Boulder, 504 pp.
- Dorsey, R.J., Umhoefer, P.J., Ingle, J.C. and Mayer, L., 2001. Late Miocene to Pliocene stratigraphic evolution of Northeast Carmen Island, Gulf of California; implications for oblique-rifting tectonics. In: J. Halfar (Editor), *Sedimentary Geology*, pp. 97-123.
- Duncan, R.A. and Varne, R., 1988. The age and distribution of the igneous rocks of Macquarie Island. *Papers and Proceedings of the Royal Society of Tasmania*, 122: 45-50.
- Fisk, M.R., Giovannoni, S.J. and Thorseth, I.H., 1998. Alteration of Oceanic Volcanic Glass: Textural Evidence of Microbial Activity. *Science*, 281(5379): 978-980.
- Fisk, M.R., Storré-Lombardi, M. C., Douglas, S., Popa, R., McDonald, G., and Di Meo-Savoie, C., 2003. Evidence of biological activity in Hawaiian subsurface basalts. *Geochemistry, Geophysics, Geosystems - G (super 3)*, 4(12): 1103.
- Fox, P.J. and Heezen, B.C., 1965. Sands of the Mid-Atlantic Ridge. *Science*, 149(3690): 1367-1370.
- Furnes, H., Banerjee, N.R., Muehlenbachs, K. and Kontinen, A., 2005. Preservation of biosignatures in metaglassy volcanic rocks from the Jormua ophiolite complex, Finland. *Precambrian Research*, 136(2): 125-137.
- Gawthorpe, R.L. and Leeder, M.R., 2000. Tectono-sedimentary evolution of active extensional basins. *Basin Research*, 12(3/4): 195.
- German, C.R., Hergt, J., Palmer, M.R. and Edmond, J.M., 1999. Geochemistry of a hydrothermal sediment core from the OBS vent-field, 21°N East Pacific Rise. *Chemical Geology*, 155(1-2): 65-75.
- Goscombe, B.D. and Everard, J.L., 1998. 1:10,000 Geological Map of Macquarie Island, series of 7 maps, Mineral Resources Tasmania.
- Griffin, B.J., 1982. Igneous and metamorphic petrology of lavas and dykes of the Macquarie Island ophiolite complex. Ph.D. Thesis, University of Tasmania, Hobart, 220 pp.

- Harb, N., 2006. Fragmentation processes, depositional mechanisms and lithification of glassy fragmental rocks, Macquarie Island. BSc (hons) Thesis, Macquarie University, Sydney, 86 pp.
- Hayes, D.E. and Talwani, M., 1972. Geophysical investigation of the Macquarie Ridge Complex. Antarctic Research Series, 19: 211-234.
- Kato, Y. and Nakamura, K., 2003. Origin and global tectonic significance of early Archean cherts from the Marble Bar greenstone belt, Pilbara Craton, Western Australia. Precambrian Research, 125(3-4): 191-243.
- Knipper, A.L., Sharaskin, A.Y. and Voznesenskii, A.I., 2001. Ophiolite-clastic breccias of the Lesser Caucasus; structural features and origin. Geotectonics, 35(3): 199-206.
- Lamarche, G., Collot, J.-Y., Wood, R. A., Sosson, M., Sutherland, R., and Delteil, J., 1997. The Oligocene-Miocene Pacific-Australia plate boundary, south of New Zealand; evolution from oceanic spreading to strike-slip faulting. Earth and Planetary Science Letters, 148(1-2): 129-139.
- Leppard, C.W. and Gawthorpe, R.L., 2006. Sedimentology of rift climax deep water systems; Lower Rudeis Formation, Hammam Faraun Fault Block, Suez Rift, Egypt. Sedimentary Geology, 191(1-2): 67-87.
- Lewis, S.J., 2007. Focussed hydrothermal alteration in upper crustal oceanic faults on Macquarie Island. PhD Thesis, University of Tasmania, Hobart.
- Lonsdale, P. and Batiza, R., 1980. Hyaloclastite and lava flows on young seamounts examined with a submersible. Geological Society of America Bulletin, 91(9): I 545-I 554.
- Mawson, D. and Blake, L.R., 1943. Macquarie Island, its geography and geology. Australian Antarctic Expedition Science Report, 5(A): 194.
- Meckel, T.A., 2003. Tectonics of the Hjort region of the Macquarie Ridge Complex, southernmost Australian-Pacific plate boundary, Southwest Pacific Ocean. Doctoral Thesis, University of Texas, Austin, 192 pp.
- Meckel, T.A., Mann, P., Mosher, S. and Coffin, M.F., 2005. Influence of cumulative convergence on lithospheric thrust fault development and topography along the Australian-Pacific plate boundary south of New Zealand. Geochem. Geophys. Geosyst., 6(9): 20.
- Moores, E.M., Kellogg, L.H. and Dilek, Y., 2000. Tethyan ophiolites, mantle convection, and tectonic "historical contingency"; a resolution of the "ophiolite conundrum". In: Y. Dilek, E.M. Moores, D. Elthon and A. Nicolas (Editors), Ophiolites and oceanic crust, new insights from field studies and the Ocean Drilling Program. Special Paper - Geological Society of America, vol.349, Boulder, pp. 3-12.
- Mosher, S. and Massell-Symons, C., 2008. Ridge reorientation mechanisms: Macquarie Ridge Complex, Australia-Pacific plate boundary. Geology, 36(2): 119-122.
- Murphy, M., 2008. Petrography and geochemistry of oceanic crust: provenance of sedimentary detritus, Macquarie Island, Macquarie University, Sydney, 80 pp.
- Nicolas, A. and Boudier, F., 2003. Where ophiolites come from and what they tell us. In: Y. Dilek and S. Newcomb (Editors), Ophiolite concept and the evolution of geological thought. Special Paper - Geological Society of America, vol.373, pp. 137-152.

- Parr, J.M., Stevens, B.P.J., Carr, G.R. and Page, R.W., 2004. Subseafloor origin for Broken Hill Pb-Zn-Ag mineralization, New South Wales, Australia. *Geology*, 32(7): 589-592.
- Pessagno, E.A., Jr., Hull, D.M. and Hopson, C.A., 2000. Tectonostratigraphic significance of sedimentary strata occurring within and above the Coast Range Ophiolite (California Coast Ranges) and the Josephine Ophiolite (Klamath Mountains), northwestern California. In: Y. Dilek, E.M. Moores, D. Elthon and A. Nicolas (Editors), Special Paper - Geological Society of America, vol.349, pp. 383-394.
- Portner, R., Daczko, N. and Dickinson, J., 2009. Vitriclastic lithofacies from Macquarie Island (Southern Ocean): compositional influence on abyssal eruption explosivity in a dying Miocene spreading ridge. *Bulletin of Volcanology*, DOI 10.1007/s00445-009-0312-8: 19 p.
- Quilty, P.G., Crundwell, M. and Wise Jr., S.W., 2008. Microplankton provide 9 Ma age for sediment in the Macquarie Island ophiolite complex. *Australian Journal of Earth Sciences*, 55(8): 1119-1125.
- Quilty, P.G., Rubenach, M. and J.A., W., 1973. Miocene Ooze from Macquarie Island. *Search (Sydney)*, 4(5): 163-164.
- Rivizzigno, P.A., 2002. The major lake fault zone : an oblique spreading structure exposed in the Macquarie Island ophiolite, Southern Ocean. MS Thesis, Duke University, Durham, 72 pp.
- Robertson, A.H.F., 1990. Sedimentology and tectonic implications of ophiolite-derived clastics overlying the Jurassic Coast Range Ophiolite, Northern California. *American Journal of Science*, 290(2): 109-163.
- Ruff, L.J., Given, J.W., Sanders, C., O. and Sperber, C.M., 1989. Large earthquakes in the Macquarie Ridge Complex; transitional tectonics and subduction initiation. *Paleogeography*, 129(1/2): 71-129.
- Schopf, J.W., Kudryavtsev, A.B., Agresti, D.G., Wdowiak, T.J. and Czaja, A.D., 2002. Laser-Raman imagery of Earth's earliest fossils. *Nature*, 416(6876): 73-76.
- Selkirk, P.M., Adamson, D.A. and Wilson, M.E., 1990. Raised marine terrace on north-west coast of Macquarie Island. *Proceedings of the Linnean Society of New South Wales*, 112(1-4): 141-142.
- Sharp, I.R., Gawthorpe, R.L., Underhill, J.R. and Gupta, S., 2000. Fault-propagation folding in extensional settings; examples of structural style and synrift sedimentary response from the Suez Rift, Sinai, Egypt. *Geological Society of America Bulletin*, 112(12): 1877-1899.
- Simonian, K.O. and Gass, I.G., 1978. Arakapas fault belt, Cyprus: A fossil transform fault. *Geological Society of America Bulletin*, 89(8): 1220-1230.
- Swift, S.A., 1991. Gravels in the Atlantis II fracture zone. In: R.P. Von Herzen and P.T. Robinson (Editors), *Proceedings of the Ocean Drilling Program, Scientific Results*. Ocean Drilling Program, College Station, TX, pp. 431-438.
- Varne, R., Brown, A.V. and Falloon, T., 2000. Macquarie Island; its geology, structural history, and the timing and tectonic setting of its N-MORB to E-MORB magmatism. In: Y. Dilek, E.M. Moores, D. Elthon and A. Nicolas (Editors), Special Paper - Geological Society of America, vol.349, pp. 301-320.
- Varne, R., Gee, R.D. and Quilty, P., 1969. Macquarie island and the cause of oceanic linear magnetic anomalies. *Science*, 166(3902): 230-233.

- Wertz, K.L., 2003. From seafloor spreading to uplift; the structural and geochemical evolution of Macquarie Island on the Australian-Pacific Plate boundary. Doctoral Thesis, University of Texas, Austin, 169 pp.
- White, J.D.L. and Houghton, B.F., 2006. Primary volcanoclastic rocks. *Geology*, 34(8): 677-680.

Part 1:

Sedimentary rocks

I:

**A detrital record of lower oceanic crust
exhumation within a Miocene slow-spreading
ridge: Macquarie Island, Southern Ocean**

PORTNER, Ryan A.¹, MURPHY, Melissa J.¹, and DACZKO, Nathan
R.¹

¹GEMOC ARC National Key Centre, Department of Earth and Planetary Sciences,
Macquarie University, NSW 2109, Australia

Submitted to Geological Society of America Bulletin in April 2009
In review since, August 2009

Abstract:

Uplift, exhumation, and denudation of the lower oceanic crust is recorded by sedimentary rocks of Macquarie Island (54°30'S, 158°54'E), which were deposited within the slow-spreading proto-Macquarie Spreading Ridge (PMSR) between ~9 and 12 Ma. Measured stratigraphic sections typically contain basal basaltic breccia lithofacies that are overlain by a thick sequence of enriched mid-ocean ridge basalt (EMORB) with thin intercalations of gabbroic sedimentary lithofacies. Basaltic detritus has zeolite to lower greenschist metamorphic grades typical of the upper oceanic crust and gabbroic detritus has upper greenschist to amphibolite metamorphic grades typical of the lower oceanic crust. Breccia clast counts and sedimentary structures indicate that basaltic lithofacies were locally derived from the footwalls of adjacent spreading-related faults. Sedimentary structures, detrital clinopyroxene major and trace element geochemistry, and $^{206}\text{Pb}/^{238}\text{U}$ zircon geochronology indicate that the gabbroic lithofacies were more distally derived from a Paleogene aged tholeiitic MORB source. Detrital zircon populations of ~27 and ~33 Ma correspond to oceanic magnetic anomalies 8o and 13o respectively and exclude ~8.5 Ma gabbroic rocks of Macquarie Island as a potential source. Geodynamic reconstructions show that anomaly 8o crust from the Southeast Indian Ridge (SEIR) was juxtaposed against the active PMSR when sedimentary rocks of Macquarie Island were deposited and was a likely source for the gabbroic lithofacies. The PMSR and SEIR were connected by the Jurrut long-offset transform, which underwent significant transpression since 27 Ma. This transpression formed a bathymetric transverse ridge that was composed of heterogeneously aged Paleogene source crust and produced Macquarie Island's gabbroic sedimentary lithofacies.

Introduction:

Voluminous sedimentary sequences, up to 100 m thick, deposited within spreading ridge basins (Karson et al. 1984), have the potential to record the genesis and exhumation of the lower oceanic crust as is commonly described in continental basins flanking metamorphic core complexes (e.g. Wagner and Johnson 2006; Dunkl et al. 1998). Uplift of the lower oceanic crust, including sheeted diabase dykes, gabbro and serpentized peridotite, at spreading ridge/transform fault intersections has been thoroughly documented by submersible observations along currently active slow spreading ridges (Van Andel and Bowen 1968; Auzende et al. 1994; Blackman et al. 1998; Baines et al. 2003). These uplifted oceanic massifs, or megamullions, are juxtaposed against the upper crustal extrusive/sedimentary sequence by high to low angle detachment-style faults with up to 4000 m of bathymetric relief (MacLeod et al. 2002; Canales et al. 2004; Ildefonse et al. 2007). Breccias at the foot of these uplifted domains typically match the rock types in the footwall and are derived by mass wasting induced gravity flow processes (Bonatti et al. 1973; Tucholke et al. 1997; Gao 2006). Finer grained sediment identified within transform valley, median valley, ridge flanks, and nodal basins is classically assumed to be pelagic or its resedimented equivalent (Van Andel and Komar 1969; Karson and Dick 1983; Goud and Karson 1985). However, early studies identified small quantities of spreading-ridge-derived ultramafic- and mafic-rich sand (Fox and Heezen 1965; Siever and Kastner 1967). Apart from these early studies, detailed examination of this mafic detritus has largely been neglected primarily due to access difficulties in modern ocean basins and obduction dismemberment in ophiolite sequences.

The unique setting of nearly in-situ uplifted oceanic crust that forms Macquarie Island (Varne et al. 2000) offers an unparalleled natural laboratory to

characterize the relatively unstudied syntectonic spreading ridge sedimentary environment in the context of the ocean basin in which it was formed. The proximity of gabbroic sedimentary rocks to present day exposures of lower crustal rocks lead Daczko et al. (2005) to conclude that clastic sedimentary rocks were locally derived from fault scarps now exposed on Macquarie Island. However, that study noted the ambiguity of the complete absence of detrital serpentine in Macquarie Island breccias and the extensive exposures of serpentinitized harzburgite in the nearby spreading-related fault footwall (Fig. 1.1). Non-preservation of serpentine minerals in the submarine environment (Daczko et al. 2005) could not be the case, considering the presence of sedimentary serpentinites along the base of faulted serpentinitized peridotite horsts along the mid-Atlantic ridge (Bonatti et al. 1973). Phlogopite pegmatoids that cut gabbroic rocks currently exposed on the island yield $^{206}\text{Pb}/^{238}\text{U}$ zircon crystallization ages of ~ 8.6 Ma and zircon fission track ages of ~ 6 Ma (Armstrong et al. 2004) suggesting that they could not have been exposed during deposition of ~ 9 Ma Macquarie Island sedimentary rocks (Quilty et al. 2008). Furthermore, a paucity of detailed petrographic data from Macquarie Island sandstones and breccias precludes any interpretation of an oceanic crustal origin. Sandstone point counts and breccia clast counts have traditionally been used as necessary methods to statistically validate and clearly establish detrital mode (Dickinson and Suczek 1979; Ingersoll et al. 1984; Dorsey 1988; Garzanti et al. 2003). This study employs these petrographic methodologies along with detrital clinopyroxene major and trace element geochemistry, and detrital $^{206}\text{Pb}/^{238}\text{U}$ zircon geochronology to better establish the provenance for Macquarie Island sandstone and breccia. Clastic rocks and paleocurrent indicators within them are examined

from two volcano-sedimentary basins that are adjacent to the major-spreading-related faults on the island. These data are discussed relative to the database of surrounding ocean floor magnetic anomalies in order to reveal paleogeographic dispersal patterns and evolution of the Jurru long-offset transform that connected the Proto-Macquarie Spreading Ridge (PMSR) with the Southeast Indian Ridge (SEIR). This approach is the first of its kind to document the exhumation and unroofing of oceanic massifs along slow-spreading ridges.

Geologic Setting:

Rocks of Macquarie Island formed in the PMSR between 12 and 6 Ma (Duncan and Varne 1988; Armstrong et al. 2004; Quilty et al. 2008; Varne et al. 2000). This waning slow spreading ridge (half rates of 4.4-28 mm/yr) separated the Indo-Australian and Pacific plates from the mid-Eocene to late Miocene and was characterized by very short spreading corridors with long-offset transforms (>100 km) during formation of Macquarie Island crust (Massell et al. 2000; Varne et al. 2000; Mosher and Massell-Symons 2008). The majority of rocks exposed on the island consist of E-MORB pillow basalt (Kamenetsky and Mass; 2002) and to a lesser extent lower crustal rocks including sheeted diabase dykes, gabbro, and serpentinized harzburgite (Goscombe and Everard 1998). The upper crustal extrusive sequence is juxtaposed against the lower crustal intrusive sequence along major spreading-related faults (Fig. 1.1). One of these rift related faults in the north, the Finch-Langdon fault, is interpreted as a ridge-transform inside-corner structure with lower crustal rocks including peridotite in the footwall (Wertz et al. 2003). Another spreading-related structure in the central portion of the island, the Major Lake Fault,

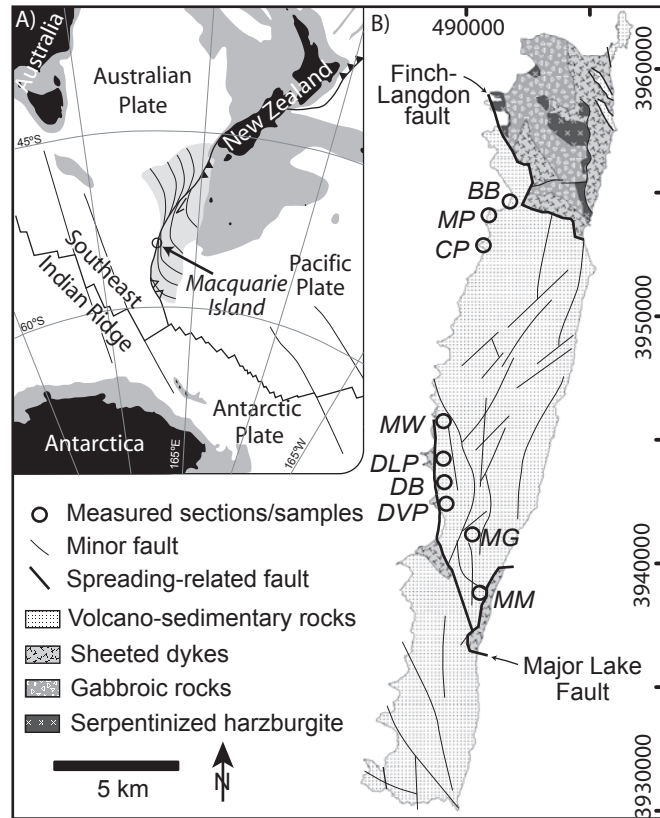


Figure 1.1:
 Location maps. A) Present day position of Macquarie Island in the Southern Ocean at 54.65°S, 158.83°E. Light grey represents oceanic crust formed at the Proto-Macquarie Spreading Ridge (PMSR). Dark grey represents bathymetric depths shallower than 2000 meters below sea level. Heavy black lines represent active plate boundaries, solid teeth on hanging walls of active subduction zones (hollow teeth on incipient subduction zones). Thin black lines represent spreading-related fracture zones. B) Simplified geologic map after Goscombe and Everard (1998) showing sample locations and/or measured sections, which are Bauer Bay (BB), Mawson Point (MP), Cormorant Point (CP), Mt. Waite (MW), Double Point (DLP), Davis Bay (DB), Davis Point (DVP), Mt. Gwynn (MG), and Mt. Martin (MM). Volcano-sedimentary rocks include pillow basalt, tabular basalt, clastic rocks, chert, and red pelagic mudstone. Most minor faults and modern alluvium omitted for clarity. Map projection is UTM 57S and grid is in meters.

has low-angle detachment-style geometry, pervasive hydrothermal mineralization including quartz-sulphide-chlorite-epidote-prehnite, and sheeted diabase dykes in the footwall (Davidson et al. 2004). These characteristics are comparable to modern day oceanic metamorphic core complexes (discussed above). Lower crustal exposures along these spreading-related faults have been interpreted to be the source for gabbro- and diabase-bearing synvolcanic clastic sedimentary rocks (Daczko et al. 2005) that are intercalated within the extrusive sequence adjacent to the faults (Fig. 1.1).

Methods:

Stratigraphic sections were measured along coastal outcrops where exposure is very good (Appendices A and B). 50 clasts from breccia units with average clast size were counted in the field using a square meter grid and a constant step interval of 10 cm. Representative medium- to coarse-grained sandstone units were point-counted using the Gazzi-Dickinson method (Ingersoll et al. 1984), in which individual sand-sized minerals within lithic grains are counted as mineral grains rather than lithic fragments. Provided sufficient area existed on the thin-section to avoid recounting the same grain multiple times, five hundred framework grains, not including cement and matrix, were counted from each sample using a constant step interval larger than the maximum grain size. Where framework grains showed complete alteration, they were tabulated as the secondary mineral rather than the primary mineral.

Random detrital clinopyroxene grains from medium grained sandstones and clinopyroxene groundmass in interbedded basalt were analyzed for major and trace

element compositions. Complete analytical procedure and representative samples are in Appendix C. Analyses were focused on the cores of all grains. All analyses were done using facilities within the Macquarie University geochemical analysis unit in Sydney, Australia. Major element compositions were measured using a Cameca SX100 electron microprobe operated with a 15 kV accelerating voltage, 20 nA beam current, and 1-2 μm beam size. Rare earth element (REE) concentrations were determined by laser ablation-inductively coupled plasma mass spectrometry (LA-ICPMS), which utilized a 7500cs Agilent ICP-MS along with a Merchantek 266 nm Nd laser operated with a 5 Hz frequency and 60-30 μm spot size.

Five of nineteen point counted sandstones were crushed for detrital zircon separation. For comparison we panned the sand sized fraction of 16 colluvium and lake shore sand locations in the northern portion of the island where gabbro exposures are predominant. Zircon was concentrated from these samples using magnetic and heavy liquid techniques. Representative zircon grains were hand picked for $^{206}\text{Pb}/^{238}\text{U}$ analysis. $^{206}\text{Pb}/^{238}\text{U}$ zircon geochronology was determined using LA-ICPMS instrumentation at Macquarie University as described in Belousova et al. (2001) and Jackson et al. (2004; operating conditions and isotope data are in Appendix D).

Lithofacies:

Sedimentary lithofacies of Macquarie Island primarily include clastic rocks, calcareous ooze, red pelagic mudstone, and chert. This paper describes the clastic (*sensu lato*) units, which are divided into two primary lithofacies described below not including vitriclastic rocks (i.e. glassy fragmental rocks).

Basaltic breccias

Basalt-bearing breccias are oligomict, ubiquitously comprised of basalt clasts (Fig. 1.2) and are the most voluminous type of sedimentary rock on Macquarie Island. Individual breccia sequences are up to 100 m thick and typically occur adjacent to faults. Clasts are typically between 2-13 cm, very angular to angular, and poorly to moderately sorted. Maximum clast sizes are <60 cm and have characteristics similar to pillow basalt fragments (Fig. 1.3A). These boulders have a rounded morphology on at least one side, which is oxidized similar to quenched margins of pillow basalts. Breccias are massively bedded and predominantly framework supported with local zones of matrix support typically along the basal and upper contacts. The matrix is composed of grayish red sandy mudstone and sand- to granule-sized basalt fragments. A planar clast fabric is well-developed in this facies and parallel to bedding (Fig. 1.3B). Bedding is indicated by localized thin beds of better sorted coarser clasts (Fig. 1.3C) and rare overlying very thin beds of basaltic sandstone. Basaltic breccia bedding is typically at an angle to bedding in overlying pillow basalt and gabbroic sedimentary intervals (Fig. 1.3D). Basaltic sandstones are rare on Macquarie Island, exhibit normal grading, and are coarse- to medium-grained.

Gabbroic sedimentary rocks

Polymict gabbroic sedimentary rock intervals are much more texturally and compositionally heterogeneous compared to basaltic breccias, and characteristically contain bluish-green amphibole-bearing diabase and epidote-bearing gabbro clasts (Fig. 1.2). These sedimentary intervals are 4-13 m thick, have a lenticular geometry with <85 m of lateral extent, and rapidly pinch into <10 cm thick red mudstone units

(Fig. 1.3E). The average clast size in gabbroic breccias is typically 8-16 mm. Clasts are very poorly sorted, very angular to subangular, and framework supported. Matrix varies from red clay in the base to sand in the upper portion of units. Bedding is lenticular, internally massive, and some sections exhibit reverse grading in the lower 20 cm. Units drape underlying pillow basalts (Fig. 1.3F) and basal contacts are erosional with underlying mudstone units (Fig. 1.3G). Cobble-sized red mudstone rip-up clasts are common. Overall breccias grade upward and laterally into planar laminated pebbly sandstone (Fig. 1.3F). Pebbly sandstones are very coarse- to coarse-grained, poorly sorted, planar laminated, and display planar-clast fabric.

In sections with basal granule-rich breccias, planar-laminated pebbly sandstones grade upward into massive and/or locally swaley-cross-stratified medium-grained sandstone and fine-grained ripple laminated sandstone (Fig. 1.3G). Sand grains are moderately sorted, subround to angular and have poor sphericity. Elongate grains are locally imbricated and match paleocurrent trends recorded from bedforms and scour marks. These sandstones grade up into a thickly to thinly laminated sequence of ripple-cross-stratified fine-grained sandstone and overlying sandy mudstone (Fig. 1.3H). The fine-grained laminated interval characteristically contains pervasive liquefaction features, including convolute laminations and asymmetric flame structures that indicate paleoflow direction (Fig. 1.3H). Together, this normal grading and sequence of sedimentary structures is comparable to type Bouma sequences (Fig. 1.3G; Bouma 1962). Thin sandstones show simple normal grading.

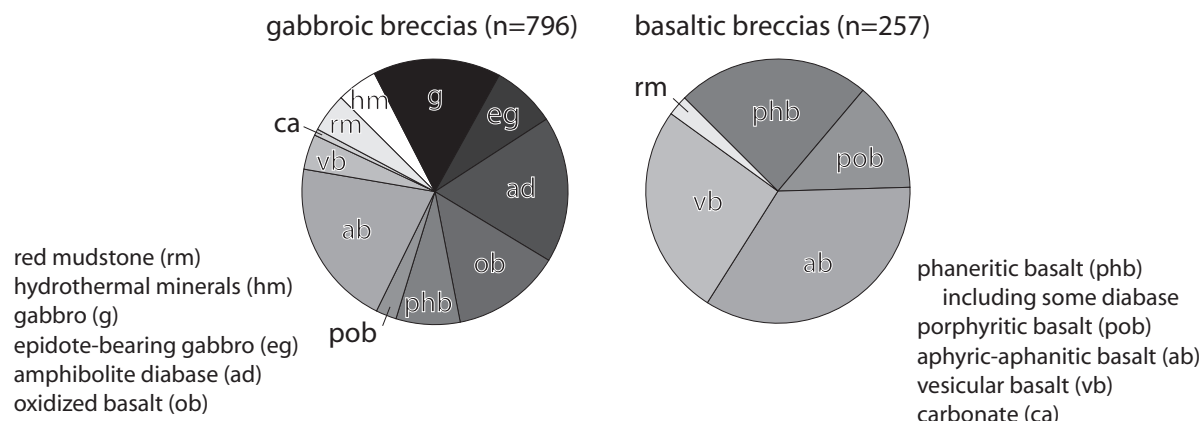


Figure 1.2:
Clast count data for gabbroic and basaltic breccia facies on Macquarie Island. Hydrothermal minerals (hm) include monocrystalline zeolite, quartz, epidote and prehnite.

Figure 1.3 (next page):

Basaltic breccia (A-D) and gabbroic sedimentary rock (E-H) lithofacies photo mosaic. Hammer is 28 cm long in A, C, and F. Pencil is 15 cm long in B and H. Measuring staff in D and E is 1.8 meters high and marked in 10 cm segments in G. A) Boulder-sized pillow fragment, Bauer Bay. B) Planar clast fabric, Bauer Bay. C) Thin cobble- to boulder-sized moderately sorted beds within pebble- to cobble-sized poorly sorted basaltic breccia from Bauer Bay. Dashed lines denote base of thin better sorted beds. D) Upper contact (black dashed line) of east (left) dipping basaltic breccia with west (right) dipping onlapping pillow basalt (dashed line) from base of Davis Point section. E) Lenticular geometry of a basal gabbroic breccia/sandstone sequence (base marked by dashed line) from Double Point section. Bottom of measuring staff is near the base of a tabular basalt unit (thin line) that pinches out into correlative red mudstone (dotted line), which overlies the basal breccia/sandstone sequence. F) Normal graded interval from Double Point with basal cobble-sized breccia (top of hammer) and overlying planar laminated sandstone. Note underlying pillow basalt morphology. Unit is capped by tabular basalt flow shown in E. G) Complete Bouma sequence with *a* though *e* horizons (shown to right) from Double Point. Red-mudstone rip-up clasts are prevalent at top of *a* horizon. Gabbroic breccias have erosive basal contacts (wavy line). H) Thickly to thinly laminated medium-grained and very fine-grained sandstone of Mawson Point. Paleocurrent direction (arrow) depicted by convolute laminations in middle of photo.

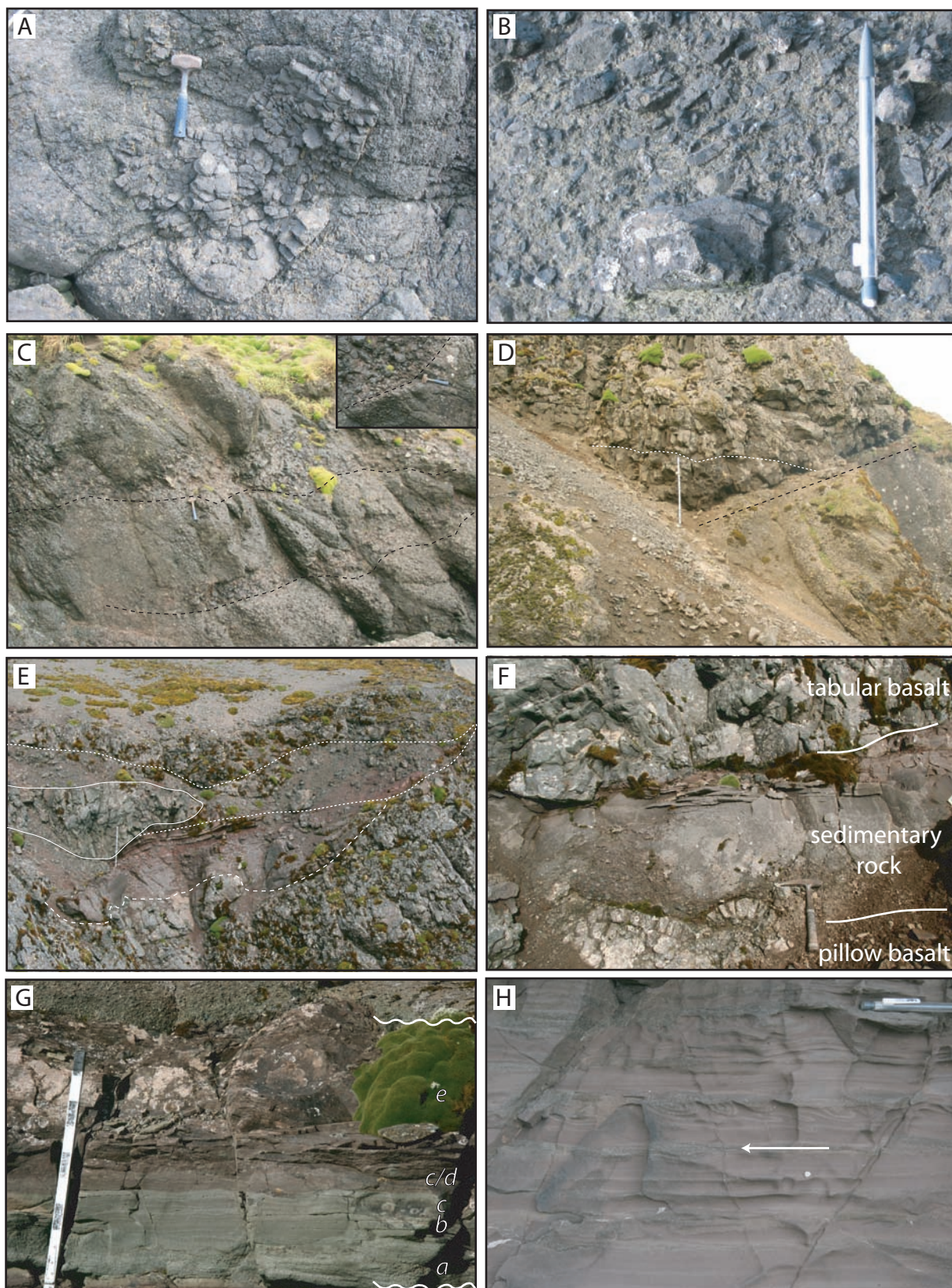


Figure 1.3 (caption on previous page)

Stratigraphic Sections:

Two representative sequences of sedimentary rocks that occur in the hanging wall of the Major Lake and Finch-Langdon spreading-related faults were measured from the central and northwestern parts of Macquarie Island (Fig. 1.4). Paleocurrent indicator orientations were measured in the field and rotated back to horizontal using “single-tilt” techniques (c.f. Potter and Pettijohn 1977; Appendix B).

Major Lake Sections (central Macquarie Island)

Davis Point, Double Point, and Mt. Waite (central west coast)

A 250 m thick section of relatively un-faulted upper oceanic crust was measured in well exposed cliffs along the central west coast escarpment of Macquarie Island between Mt. Waite and Davis Point (Figs. 1 and 4A). The base of the section starts directly above the Major Lake fault, which is locally buried by a 40-60 m thick unit of basaltic breccia that is laterally continuous for up to 2 km along Davis Bay. The basaltic breccia is overlapped by a very thick succession of compositionally variable pillow basalt with thin gabbroic sedimentary intercalations (Fig. 1.3D). These gabbroic sequences are longitudinally extensive for up to 3.5 km and only contain basal gabbroic breccia where they are thickest (Fig. 1.4B). Gabbroic breccia and sandstone units grade up into grayish red sandy mudstone units, which are laterally continuous where underlying breccia/sandstone units have pinched out. These mudstones locally contain <1 cm thick sandstone lenses that have bedding planar surfaces covered with scour marks, which are parallel to paleocurrent indicators in underlying coarser grained units. All paleocurrent indicators are typically orthogonal to the lenticular geometry of the sedimentary sequence and suggest paleoflow toward 340° -015° parallel to the nearby Major Lake fault (Fig.

1.4B). Microplankton-bearing interpillow calcareous ooze that is 1.3 km to the south and roughly equivalent with the basal west coast section; yield 9.01-8.78 Ma squat ovoid forms of the *Bolboforma metzmacheri* zonal marker species (Quilty et al. 2008).

Mt. Gwynn (central plateau) and Mt. Martin (central east coast)

The sedimentary rocks in the central west coast section laterally correlate with other gabbroic sedimentary intervals that occur within a 2.5 km wide zone across the central portion of the island. This zone parallels the Major Lake fault and was sampled at Mt. Gwynn in the middle plateau of the island and on the central east coast escarpment east of Mt. Martin (Fig. 1.1). The Mt Martin locality occurs in the hangingwall of a spreading-related fault that appears to be part of the Major Lake fault system. Basaltic breccia and heavily fractured pillow basalt occurs along the base of the section, similar to the central west coast sections, and rests against the fault with a near-vertical contact. These basaltic units are overlain by a gabbroic sedimentary interval that fines upward to red sandy mudstone.

Finch-Langdon Sections (northwest Macquarie Island)

Mawson Point-Bauer Bay

A well-exposed coastal section between Bauer Bay and Mawson Point contains several sedimentary sequences and occurs in the hangingwall of the Finch-Langdon fault (Fig. 1.1). Basaltic breccia is prominent in the hangingwall along the length of the Finch-Langdon fault and is exposed along the southern shore of Bauer Bay at the base of the northwest coast stratigraphic section. The breccia locally correlates with faulted pillow basalt and is capped by a thick sequence of tabular basalt with <5 m thick gabbroic sandstone intercalations. The tabular basalts are >10

Legend:







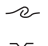




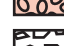












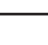
	gabbroic sedimentary interval		
	chert		pseudo-nodules
	mudstone		bioturbation
	siltstone		soft-sediment deformation
	gabbroic sandstone		scour features
	gabbroic breccia		water escape pipes
	basaltic breccia		grain imbrication
	autoclastic breccia		rip-up clasts
	hyaloclastic breccia		load casts
	pillow basalt		convolute lamination
	tabular basalt		ripple lamination
	hypabyssal sill/dyke		cross-stratification
			planar lamination
			reverse grading

Figure 1.4 (above and next page):

Legend above refers to stratigraphic sections on next page. A) Generalized central coast composite section compiled from several locations between Mt. Waite, Double Point, and Davis Point. B) Detailed representative measured section from Double Point gabbroic sedimentary interval shown in A (54°38'58"S and 158°49'39"E). Paleocurrent indicators were measured from 8 different stratigraphic sections along the central west coast. C) Northwest coast representative stratigraphic section from a gabbroic sedimentary interval (54°34'21"S and 158°51'17"E). Paleocurrent indicators measured from 7 different locations. Bidirectional paleocurrents measured from longitudinal ridges and furrows, channel thalweg axis, and gutter cast. Unidirectional paleocurrents measured from ripple lamination, cross-stratification aggradation direction, sand grain imbrication, flute casts, convolute laminations, and asymmetric flame structures.

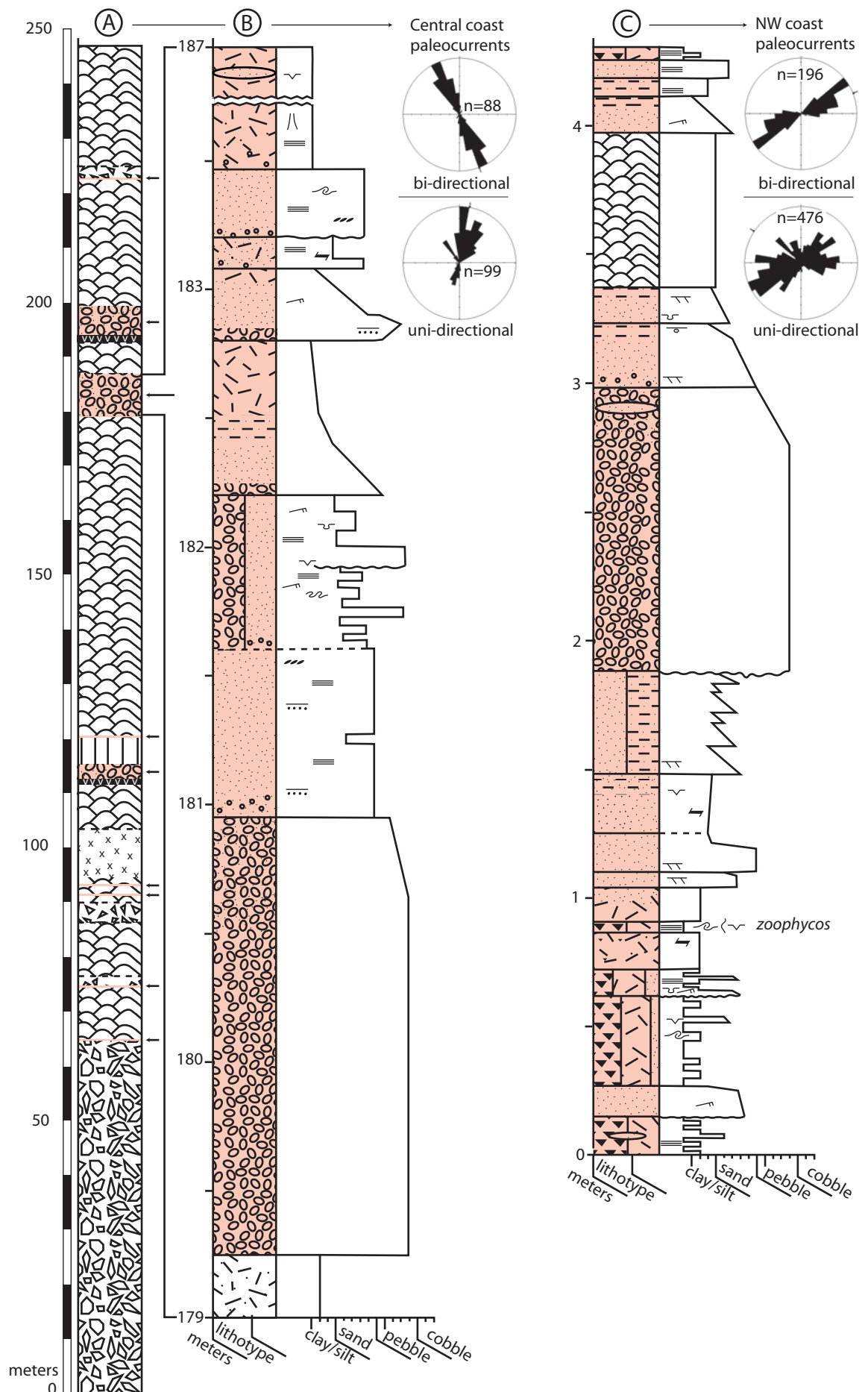


Figure 1.4 (caption on previous page)
Chapter I

thick and an $\text{Ar}^{40}/\text{Ar}^{39}$ plateau age from one of these tabular basalts gave an age of 11.5 Ma (Duncan and Varne 1988).

The gabbroic sedimentary intervals have an erosional basal contact with underlying thinly laminated mudstone and chert. Paleocurrent measurements taken from these gabbroic sedimentary units indicate a bi-directional NE-SW flow perpendicular to the Finch-Langdon fault (Fig. 1.4C). Complexly cross stratified swaley bedforms within the base of the section have southwesterly aggrading paleocurrent directions of 234° . These bedforms are overlain by well-preserved ripple cross laminae, convolute laminations and asymmetric flame structures that yield paleocurrents directed toward the northeast at 074° . A predominantly sandy mudstone interval stratigraphically above the breccia bearing sequence contains a thin sandstone bed with well-preserved basal scour marks with 232° - 052° orientations.

Cormorant Point

The gabbroic sedimentary sequence described for Mawson Point can be followed to Cormorant Point where it is overall much thicker, coarser grained and laterally more heterogeneous (Fig. 1.4C). *Zoophycos* trace fossils are preserved on the bedding planes of siliceous mudstones in a lower chert bearing interval, indicating anaerobic bathyl waters (Pemberton et al. 1992). A gradual upward reduction in the siliceous mudstone/chert sequence is paralleled by an upward increase in grain size and bedding thickness of interbedded sandstones. Extensive bedding planes covered by ridges and furrows mark the erosive basal contact of some normal graded coarse- to fine-grained sandstone units. These scour marks are oriented 250° - 070° perpendicular to the Finch-Langdon fault (Fig. 1.4C). The coarsening upward of

sandstone interbeds culminate into a very thick normal graded gabbroic breccia/sandstone interval. Paleoflow directions from ripple and cross-bed measurements change from 250° in stratigraphically lower finer grained units to 317° in stratigraphically higher coarser grained units.

Petrography:

Polymict basalt breccia

Basaltic breccias contain several varieties of basalt based on phenocryst content, color, grain size, mineralogy, and alteration characteristics (Fig. 1.2). Clinopyroxene groundmass and phenocrysts are colorless-brown/purple. These breccias also include minor sub-greenschist facies diabase clasts. Secondary alteration minerals predominantly occur in the intergranular groundmass space and replace olivine. These alteration minerals include analcime, clay, red hematitic oxides, calcite, and rare chlorite. Some clasts have a clear orange fibrous radiating zeolite (thomsonite and natrolite?) that grows around clay spherulites. Clasts commonly have albite-analcime cross-cutting veins. Therefore the metamorphic grade of all clasts is upper zeolite to lower greenschist facies similar to adjacent pillow basalts. Rare basaltic sandstones contain 50-80% basalt lithics, which are predominantly microlitic (Fig. 1.5A). Lathwork and devitrified vitric volcanic lithics are rare. Samples with the highest lithic proportion yield the lowest plagioclase (2%) and clinopyroxene (10%) fractions (Table 1.1) and do not contain any greenschist alteration minerals.

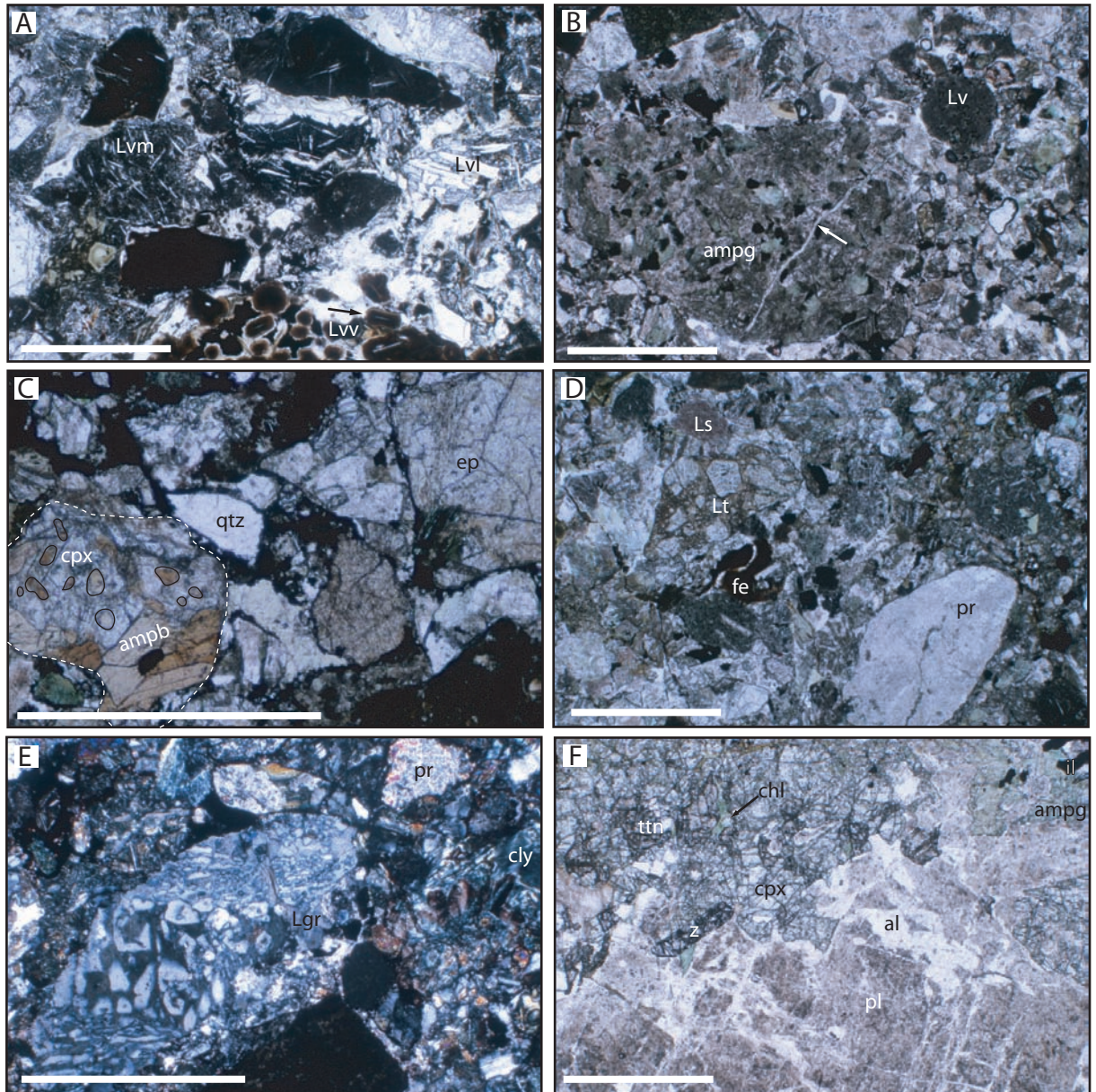


Figure 1.5:

Photomicrographs of medium- to coarse-grained basaltic sandstone (A) and gabbroic sandstone (B-F) with A-D and F in uncrossed-polars and E in crossed polars. All scale bars are 1 mm. A) Basaltic sandstone from Davis Bay showing predominance of microlitic volcanic lithic grains (Lvm) compared to lathwork lithics (Lvl) and vitric grains (Lvv). Lvv grains are devitrified to smectitic clay and have spherulitic plagioclase microlites (arrow). B) Plutonic lithic grain from Mt. Waite shows secondary green amphibole (ampg) replacement of clinopyroxene grains, which are cross cut by an intragranular prehnite vein (arrow). Very round volcanic lithics (Lv) are common in all gabbroic sandstones. C) Poikilitic (black outline) magmatic brown amphibole (ampb) within clinopyroxene (cpx) of a plutonic lithic grain (white dashed outline) from Double Point. Polycrystalline quartz (qtz) and epidote (ep) are common throughout sandstone. D) Tectonic lithic (Lt) composed of brecciated silt-sized epidote crystals, intrabasinal hematitic red-mudstone rip-up grains (fe), pink fine-grained sedimentary lithic (Ls), and monocrystalline prehnite grains from Cormorant Point. E) Quartz-feldspar granophyric lithic (Lgr) from Double Point with common monocrystalline prehnite (pr) and optically clear smectitic clay (cly). F) Plagiogranite clast from south coast of Macquarie Island exhibiting pervasive albitization (al) and sericite alteration of plagioclase (pl). Titanite (ttn), zircon (z), and ilmenite (il) commonly occur with clinopyroxene (cpx), which is locally replaced by green amphibole (ampg). Chlorite (chl) and prehnite (not shown) occur within intergranular space.

Location	NW	NW	NW	NW	NW	C	C	C	DLP1b- 5a	DLP3-3	DLP3-4	DLP3-20	DVP2-1b	DVP3-3	MG1-1	MM1-1	C	C
Sandstone lithofacies	GS	GS	GS	GS	BS	GS	GS	GS	GS	GS	GS	GS	GS	GS	GS	GS	GS	GS
Sample	MP1-3	MP1-4	CP1-3a	CP1-4a	CP1-5	CP3-11	BB3-3	MW4-1	MW4-2	MW6-2	DLP1b- 5a	DLP3-3	DLP3-4	DLP3-20	DVP2-1b	DVP3-3	MG1-1	DB1-6
quartz (qtz)	4	4	2	8	5	6		6	1	3		2	2	4	13	4		4
plagioclase (pl)	110	137	117	137	130	120	42	137	116	146	126	117	131	125	117	102	118	132
k-feldspar (k)					1									1				
clinopyroxene (cpx)	58	86	39	60	51	65	8	116	79	131	111	67	77	106	83	112	90	40
orthopyroxene (opx)							1	2	2		4	2	1	3	2		1	3
actinolite/hornblende (ampg)	23	21	50	45	39	35		54	53	52	51	33	34	48	42	68	38	1
paragassite/densite (ampb)	1	1	2			2		2	1	2					1		0	
olivine (ol)			1	1									1					
basalt lithic (Lv)	141	102	123	95	100	121	410	65	66	48	61	91	103	38	93	72	87	256
fault lithic (Lf)	5	21	19	28	15	17		4	6	16	2	5	7	9	14	2	13	
sedimentary lithic (Ls)	9		10	12	7	3					2	3		10	12	4	5	15
epidote, clinozoisite (ep)	11	13	18	7	10	6		6	14	22	26	15	8	34	9	11	32	27
prehnite (pr)	15	12	32	35	40	37		21	20	25	10	16	12	25	8	4	31	35
chlorite (chl)	13	21	31	19	14	26		20	28	17	31	33	29	50	30	39	22	44
smectitic clay (cly)	9	9	24	19	62	12	39	4	3	7	26	6	7	5	16	11	1	22
laumontite, albite (la)	83	30	14	7	4	9		31	7	2	12	56	62	16	27	18	9	39
analcite, wairakite (an)	1	20		1		4		4	5			2		2	11	1	22	1
zeolite (ze)*	2					1			1	9	1	3		4	4	6	5	4
opaques (op)†	15	19	13	23	22	36		24	8	20	35	33	18	20	18	44	26	9
carbonate (ca)		4	5	3				4	1			12	8			1		11
serpentine (s)																1	1	
total grains	500	500	500	500	500	500	500	500	411	500	500	500	500	500	500	500	500	470
%matrix/cement	5.8	6.0	10.2	21.0	8.3	6.2	-	7.8	1.9	9.3	6.9	5.7	3.1	8.1	5.8	7.4	3.3	5.3
dlopside/augite cpx ratio§	1/19	0/8	-	-	-	-	-	19/60	4/20	12/54	2/32	-	-	3/28	-	-	-	-
weighted average zircon age, errors are 2σ, n=##		33.1 ±2.5 n=16			33.6 ±1.7 n=20					27.27 ±0.48 n=49	27.25 ±0.60 n=52							28.0 ±1.1 n=20

† Opaques include intrabasinal hematitic rip-up clasts, ilmenite, pyrite, and magnetite.

Only Paleogene grains with less than 5 Ma internal error included in sample age.

Gabbroic sedimentary rocks

A higher proportion of monocrystalline minerals in gabbroic sandstones compared to basaltic sandstones reflects the coarser grained lithologies observed in associated gabbroic breccias relative to basaltic breccias (Fig. 1.2). Sandstone framework grain compositions are generally consistent across the island with minor variations between the stratigraphic sections described above (Table 1.1). Porosity and argillaceous matrix commonly make up between <5% to 10% of point-counted samples. Optically clear pale green smectite clay shows authigenic characteristics, which include an optically clear habit and growth textures that parallel grain boundaries. These clays commonly have titanite spherulitic intergrowths. Intergrown authigenic quartz-albite is the predominant cement in studied thin sections with subordinate laumontite and prehnite depending upon abundance in framework grains (Appendix E). These authigenic pore filling minerals indicate upper-zeolite to lower greenschist facies post-depositional conditions.

The most predominant sandstone framework components consist of Ca-plagioclase, colorless-green clinopyroxene, and volcanic lithic fragments (Table 1.1). Plagioclase grains typically have bytownite compositions of An₇₀₋₉₀ and are commonly altered to sericite, albite and laumontite. Clinopyroxene grains mostly have augite composition (see section on Detrital clinopyroxene geochemistry below) and many are entirely or partially replaced by chlorite and amphibole. Secondary amphiboles typically have brown-green, colorless-light green and deep green-bluish pleochroism, and yield magnesio-hornblende and actinolite compositions (Appendix E). Secondary amphibole is intergrown with and replaces chlorite in most lithic grains. These lithics are locally cross-cut by intragranular epidote/prehnite veins

(Fig. 1.5B). Rare edenite and pargasite compositions, that likely reflect high temperature primary magmatic amphiboles, have deep reddish-brown pleochroism (Fig. 1.5C).

Polymineralic mafic lithic fragments with >0.063 mm mineral grains typically have a subophitic/lathwork microstructure and commonly contain secondary amphibole particularly in coarser grain sizes (Fig. 1.5B). The grain size and texture of these lithic rock fragments are akin to a diabase or gabbro source. In comparison, polymineralic mafic lithic fragments with <0.063 mm mineral grains commonly have microlitic and less commonly granular textures and consist of chlorite-smectite clay alteration. Some microlitic grains have a monomineralic matrix that consists of clay, zeolite or opaque hematitic material with swallow tail plagioclase crystals. These lithics are regarded as altered vitric grains. Sedimentary lithics are rare and predominantly composed of light red polycrystalline grains and chert (Fig. 1.5D). Fault rock lithics are similar to silty sedimentary lithics but show slight attenuation around intralithic grains. These polymineralic tectonic lithic grains commonly contain the primary framework minerals mentioned above in addition to epidote and prehnite. Some tectonic lithics are completely composed of a brecciated array of silt sized epidote-prehnite, laumontite-quartz-chlorite, and analcime-quartz-albite grains set in a very fine-grained matrix (Fig. 1.5D). These minerals also occur as common monomineralic framework constituents in all thin sections and are the least altered grains in thin section (Table 1.1). Polycrystalline quartz makes up $<5\%$ of the major framework grain component and commonly contains thin veins of chlorite. A few samples contain granophyric feldspar-quartz grains and a very minor amount of biotite (Fig. 1.5E). Carbonate, orthopyroxene, olivine and serpentine are very minor

in abundance (<1%) in all samples. Common heavy minerals include pyrite, magnetite, titanite and zircon. A relatively high proportion of magmatic titanite and zircon were observed in a plagiogranite cobble, which contains <25% green clinopyroxene and pervasive prehnite-chlorite-epidote alteration (Fig. 1.5F)

Argillaceous grains commonly exhibit pseudomatrix textures and were counted as framework grains where they are at least fine-sand size. Reddish-brown opaque hematitic argillaceous grains have an association with larger red mudstone rip-up clasts seen throughout stratigraphically lower breccias. These intrabasinal clasts are a notable component of samples making up 5-10% of framework grains. Reflective opaque pyrite is noted in most hand samples but not more than 1% of total point counts.

Detrital clinopyroxene geochemistry:

Major element analysis of detrital clinopyroxene from gabbroic sandstone samples primarily yield tholeiitic compositions (Fig. 1.6). The compositional trend of these detrital grains in Fig. 1.6 has a slope that mimics the anorogenic (divergent) compositional spectrum of Loucks (1990). The extent of interbedded Macquarie Island basalt compositions is much more diverse than the detrital population with the most enriched compositions having subsilicic (<1.75 Si cations or <46% SiO₂) and titanian (>0.1 Ti cations) diopside compositions (on the basis of six oxygen; after Morimoto et al. 1988); a characteristic not observed in the detrital population (Fig. 1.6). Detrital compositions are more comparable to chromian (>0.01 Cr cations) diopside/augite grains typical of Macquarie Island sheeted dykes, gabbro and peridotite compositions. However, detrital grains are more fractionated than the

Island's plutonic clinopyroxene compositions as shown by their lower Mg#'s.

Representative detrital grains chosen from the <50% population densities are primarily augite in composition (Fig. 1.6) and <30% of detrital clinopyroxene from a given sample yield diopsidic compositions (Table 1.1).

Trace element analysis of detrital clinopyroxene grains is comparable to grains studied from NMORB rocks along the Mid-Atlantic Ridge and East Pacific Rise (Fig. 1.7). Calculated liquids from the detrital grain population have flat rare earth element patterns typical of NMORB. Depletion in incompatible light rare earth elements (LREE) from the detrital grain population differs from enrichment in these elements observed in interbedded basalts from the Davis Point section. Calculated liquid compositions from clinopyroxene grains in the Davis Point interbedded basalts have inclined rare earth element patterns akin to EMORB compositions. Very highly enriched patterns were calculated from subsilicic-titanian diopside grains.

Detrital $^{206}\text{Pb}/^{238}\text{U}$ zircon geochronology:

Detrital zircon grains separated from gabbroic sandstones have optically clear habits with rare zoning observed. Grain shapes are typically very angular to euhedral and are primarily colorless to pink and yellow. Due to the low yield in individual sandstone samples (Table 1.1) we combined sample populations into two datasets: 1) units that occur adjacent to the Major Lake fault (central west coast) and 2) those that occur adjacent to the Finch Langdon Fault (northwest coast). This was done to maximize grain populations for the two field locations described above and to reveal any distinctive age populations therein (c.f. Link et al. 2005). The central west coast dataset (n=123) is composed of a main peak population of 26.96 ± 0.12 Ma,

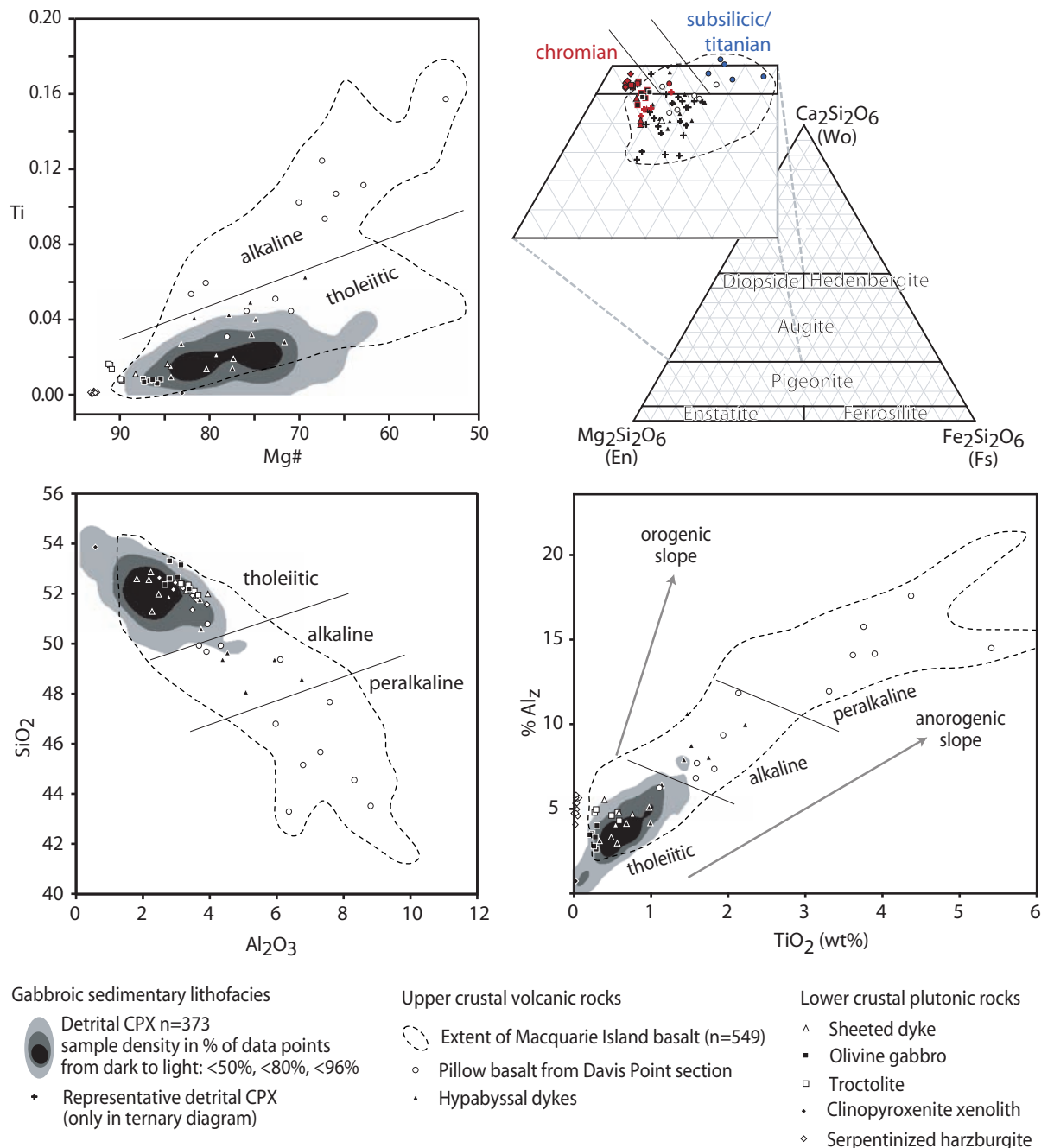


Figure 1.6: Clinopyroxene (cpx) major element geochemistry from Macquarie Island. Representative detrital cpx displayed in ternary diagram taken from the <50% sample density field shown in other plots. Data points on ternary diagram with red colors correspond to chromian cpx and points with blue colors correspond to subsilicic/titanian cpx. Extent of Macquarie Island basalt cpx compositions compiled from this study and Griffin (1982). Lower crustal cpx compositions compiled from Christodoulou (1990), Griffin (1982), Wertz (2003), and this study.

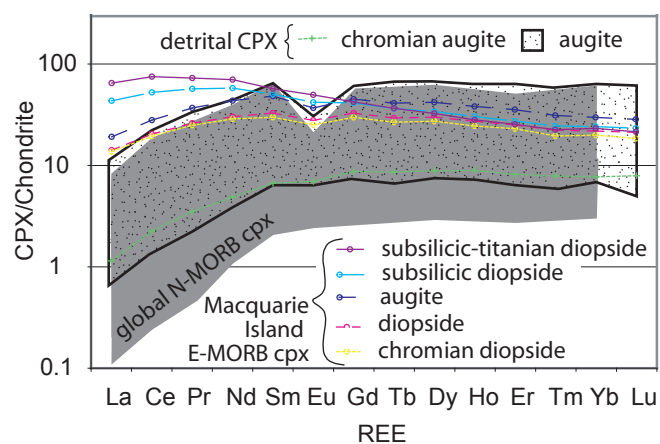


Figure 1.7:
Clinopyroxene (cpx) REE abundances normalized to chondrite values of Sun and McDonough (1989). Detrital cpx are from 19 representative grains in medium-grained sandstones of the west-central coast section. Macquarie Island E-MORB cpx are averaged from basalt ground mass in the west-central coast section. Global N-MORB cpx field is interpolated from Mid-Atlantic Ridge and East Pacific Rise gabbros and sheeted diabase dykes (Dick and Johnson, 1995; Ross and Elton, 1997; Coogan et al., 2000).

a smaller peak of 33.13 ± 0.84 Ma, and two anomalous grains with ~ 1200 Ma ages (Fig. 1.8). In comparison, the northwest coast dataset ($n=45$) yielded a main peak population of 32.45 ± 0.51 Ma, a smaller population of 27.84 ± 0.56 Ma, several older grains up to ~ 47 Ma and one very young 12.2 ± 0.3 Ma grain. The northwest coast dataset also includes several anomalously old grains including a weak ~ 1550 Ma population.

A robust zircon dataset ($n=88$) from modern colluvium derived from gabbroic outcrops in Macquarie Island's north, consist of very angular broken crystals with colorless to pink and yellow colors. All grains fall between 5 and 11 Ma with a main peak population between 8.14 ± 0.08 Ma and 8.76 ± 0.13 Ma (Fig. 1.8).

Discussion on provenance:

Polymict basalt breccias

The compositional similarities, including metamorphic grade, of polymict basalt breccias and the pillow basalt sequences they are interstratified with imply a proximal source. This is supported by their coarse-grained nature and the local preservation of relict pillow shapes. The low grade metamorphic character of rare diabase clasts implies that they were probably derived from hypabyssal sills and dykes that would have been associated with the pillow basalt sequence rather than the amphibole-bearing sheeted diabase dyke sequence described by Griffin (1982). Basaltic sandstones associated with these breccias have an undissected magmatic arc detrital mode and contain very low plagioclase and clinopyroxene detrital fractions, which reflect the relatively fine grained nature of the volcanic source terrain (Fig. 1.9).

The common spatial association of these very thick basalt breccias with unit bounding spreading-related faults indicates that the spreading-related faults presently exposed on Macquarie Island only exposed upper levels of the oceanic crust at the time of deposition. A syn-volcanic origin for these breccias is supported by onlap relationships by overlying pillow basalts and locally interstratified monomict hyaloclastite breccias. This negates the possibility that these breccias were produced after volcanism ceased during uplift of the modern day Macquarie Ridge Complex.

Sandstones of the gabbro clast-bearing sedimentary intervals

Source rock lithology and genesis

Sandstone framework grain compositions have a transitional dissected magmatic arc detrital mode in the classical quartz/feldspar/lithic (QFL) ternary plot (Fig. 1.9), yet lack primary magmatic amphibole, a common phase in hydrous magmatic arc settings (Davidson et al. 2007). Furthermore, the absence of monocrystalline quartz suggests little to no mixing with quartzose continental sources making utilization of the classical QFL diagram inadequate to effectively characterize the source terrain. This problem is resolved when interpreting the detrital mode in terms of an ophiolitic provenance similar to that employed by Garzanti et al. (2000, 2002). Ternary discrimination fields used in those studies incorporate an ultramafic source, which is largely ignored here due to the nearly complete lack of serpentinite and olivine grains in Macquarie Island sandstones. An ophiolitic provenance is substantiated by the high proportion of microlitic and lathwork volcanic lithics, which are more common in mafic volcanic lithics compared to felsic granular and seriate lithics (Ingersoll and Cavazza 1991). A tholeiitic source

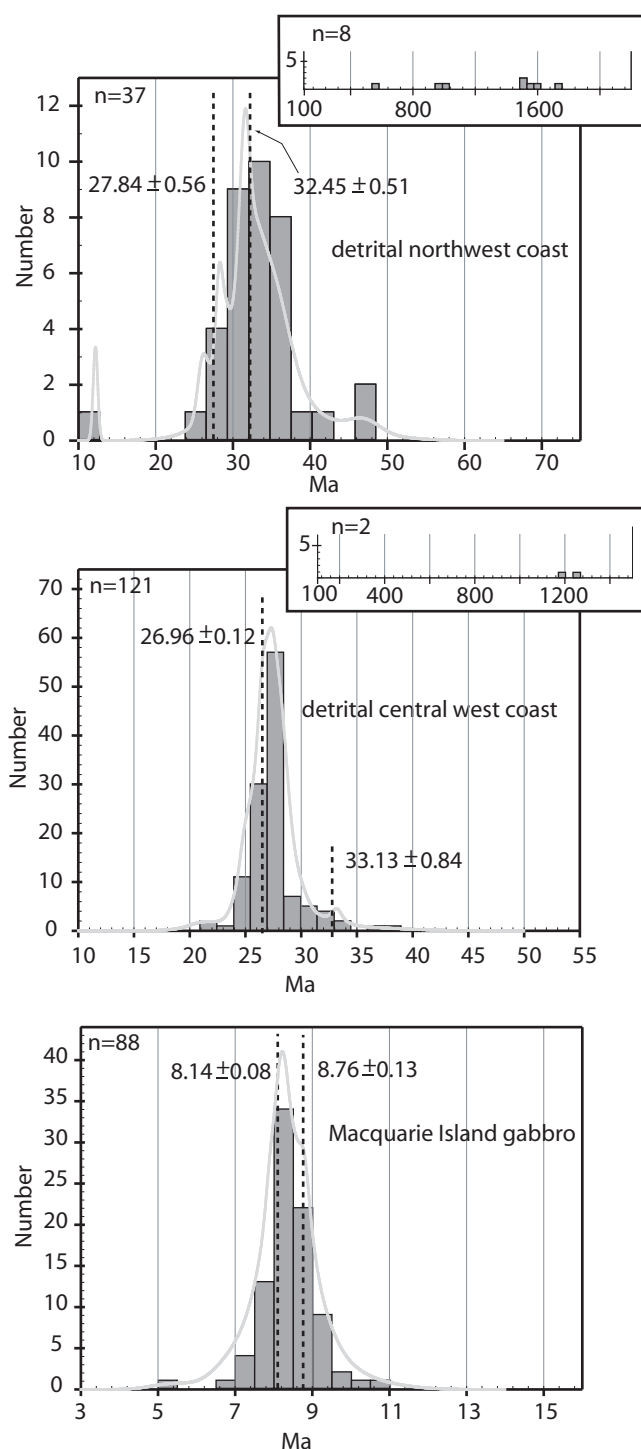


Figure 1.8:
 $^{206}\text{Pb}/^{238}\text{U}$ zircon geochronology. Bin widths are 2.7 Ma, 1.5 Ma, and 0.5 Ma for detrital northwest coast, detrital west-central coast, and Macquarie Island gabbro plots respectively. Peak ages shown by dashed lines are output by isoplot/Ex 3.0 software (K. Ludwig), which utilizes the Sambridge and Compton (1994) algorithm of a cumulative-Gaussian distribution (shown by light grey line).

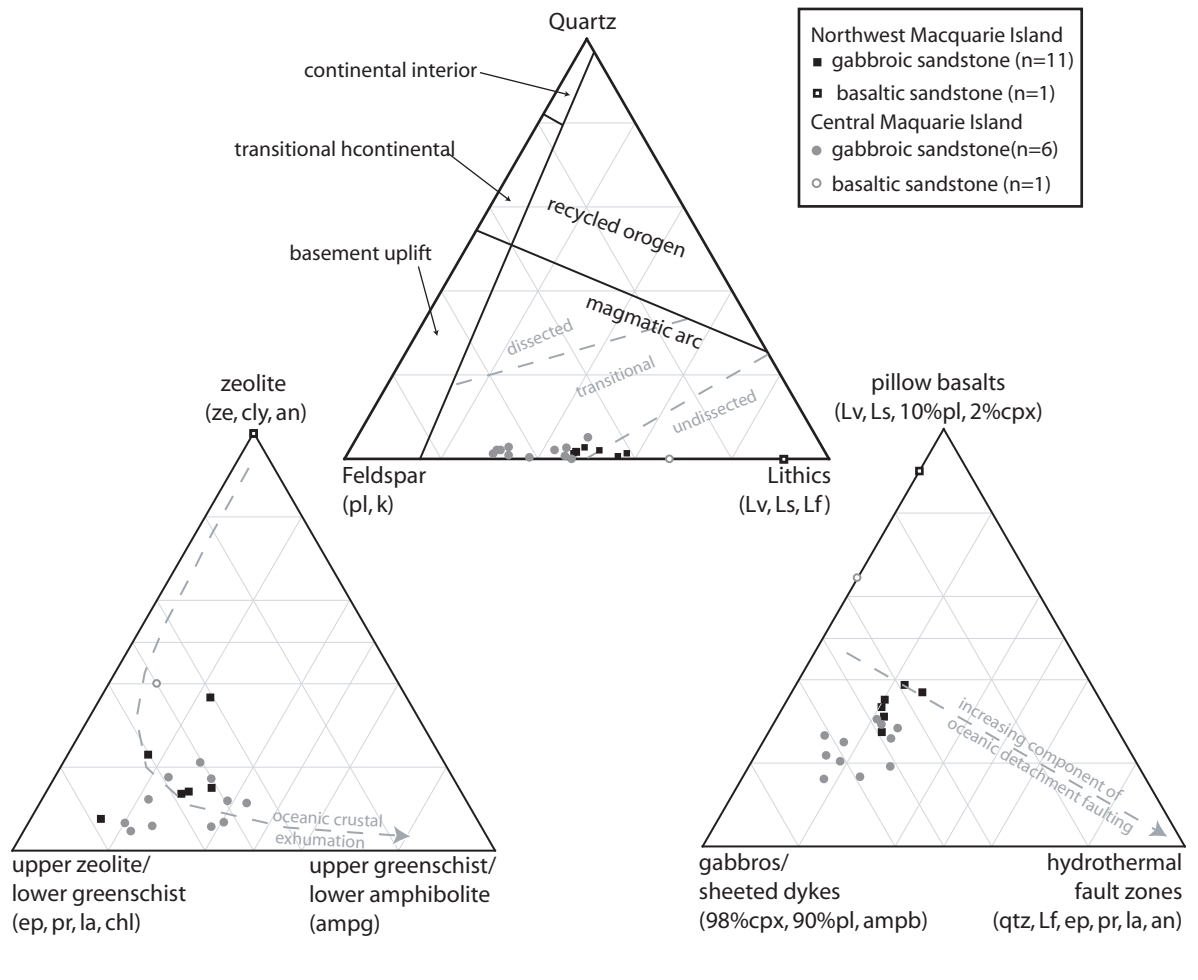


Figure 1.9: Sandstone ternary diagrams. Mineral acronyms are defined in Table 1.1. The Qtz/feldspar/lithic discrimination fields are taken from Dickinson (1985). Minerals used for metamorphic grade apices are taken from Griffin (1982). Plagioclase (pl) and clinopyroxene (cpx) percentages for the pillow basalt and gabbro/sheeted dyke apices match point counts from a basaltic sandstone with the highest volcanic lithic component (BB3-3 in Table 1.1).

is supported by detrital clinopyroxene geochemistry that typifies NMORB crust produced in a spreading-ridge setting. A low proportion of monocrystalline minerals in basaltic sandstone point counts, suggests that the greatest proportion of detrital plagioclase and clinopyroxene are from a plutonic source rather than basalt phenocrysts. This is supported by clast counts, which yield relatively high proportions of amphibolitic diabase and gabbroic clasts.

Prominent signs of chlorite alteration in volcanic lithics, actinolite/magnesio-hornblende in coarser grained subophitic lithics, and the presence of gabbro clasts suggest that deeper levels of the oceanic crust were exposed. This is demonstrated by sandstones plotting between the greenschist and amphibolite facies apices on the metamorphic grade ternary diagram (Fig. 1.9). These relatively high metamorphic grades are interpreted to be preserved from the source area since sandstone cements and interbedded basalts only exhibit zeolite to lower greenschist grade minerals. The common occurrence of secondary amphibole replacing secondary chlorite and primary clinopyroxene (uralitization) in plutonic lithic grains of Macquarie Island sandstones is a dehydrating prograde metamorphic reaction and is common in lower oceanic crustal levels (Griffin 1982; Gillis and Thompson 1993; Fagan and Day 1997). Intragranular veins of prehnite and epidote that cross cut these amphibolite lithics indicate a later hydrothermal event at lower greenschist conditions and marks the uplift of these lower crustal rocks.

The high proportion of greenschist grade hydrothermal minerals and tectonic lithics indicate that the source terrain likely incorporated the faulted remnants of the boundary between the upper and lower oceanic crust (Fig. 1.9). Faulting at this crustal level is observed at Double Point where significant hydrothermal

mineralization occurs along detachment faults between pillow basalt and sheeted diabase dykes (Davidson et al. 2004). In addition, rare granophyric lithic grains, magmatic amphibole, and zircon were likely derived from rare plagiogranite clasts, which are typically associated with late stage intrusions in stratigraphically higher gabbroic rocks in ophiolites and oceanic crust (Nicolas 1989; Dick et al. 2000; Grimes et al. 2008). The presence of these rare evolved plutonic clasts further supports a faulted upper/lower oceanic crustal boundary. Experiments have shown that oceanic plagiogranites can form by partial melting of the lower oceanic crust by hydrothermal infiltration along detachment faults that tap the dyke/gabbro boundary (Koepke et al. 2004; Koepke et al. 2007; Jöns et al. 2009). Being rare in mafic rocks, zircon can occur in these more siliceous differentiates that contain highly incompatible elements such as zirconium. This interpretation is substantiated by higher zirconium contents within shallower stratigraphic levels in the Macquarie Island gabbroic sequence (Christodoulou 1990).

The ~8.5 Ma zircon grains sampled from colluvium north of the Finch-Langdon fault are within error of 8.4 ± 0.3 and 8.8 ± 0.2 Ma SHRIMP $^{206}\text{Pb}/^{238}\text{U}$ data presented by Armstrong et al. (2004) for zircons collected from a late stage phlogopite pegmatoid also in the island's north. These gabbros are not the source for Macquarie Island gabbroic sandstones (Daczko et al. 2005) considering the disparity in zircon crystallization ages between them and the ~33 and ~27 Ma detrital populations in the sandstones. The absence of ~8.5 Ma zircon grains from the sandstones suggests that the gabbroic rocks, that are currently exposed along with peridotites and sheeted dikes across the Finch-Langdon fault, were not exposed during seafloor spreading. This interpretation is supported by the complete absence

of detrital serpentinite in the sandstones. Furthermore, a distal source is inferred from the complete absence of enriched subsilicic-titanian detrital diopside grains in the sandstones, which are common in the interbedded extrusive sequence. The older ages and unusual geochemistry of the detrital zircon and clinopyroxene populations, respectively, excludes actively forming igneous crust at the PMSR as a viable source for the gabbroic sedimentary intervals. Any likely provenance must have contained mixed aged crust that was not only older but also geochemically different to the interbedded volcanic rocks of Macquarie Island.

Paleogeography and dispersal patterns

Major changes in relative Australia-Pacific plate motion by ~27 Ma (Cande and Stock 2004) initiated reorientations in spreading direction of the PMSR (Lamarche et al. 1997; Massell et al. 2000). This reorganization manifested as ridge segment shortening, lengthening of transforms, and localized transpression along transforms (Mosher and Massell-Symons 2008). Rigid plate model geodynamic reconstructions (Meckel 2003) indicate overlap between the Australia and Pacific plates by ~20 Ma across the Jurru transform fault, which links the westernmost PMSR segment with the Australia-Pacific-Antarctic plate triple junction (Fig. 1.10, Massell et al. 2000). This overlap increases through time and by ~10 Ma, over 100 km of convergence is predicted across the Jurru transform fault (Fig. 1.10, Meckel 2003). Transpression along the Jurru long-offset transform fault between ~20-10 Ma began construction of a transverse ridge that over the past ~10 Myr has continued and built a 5 km high, 50 km wide bathymetric ridge at the latitude of Macquarie Island (Daczko et al. 2003, Meckel et al. 2005). Therefore uplift of oceanic crust and the formation of a prominent transverse ridge took place along the adjacent long-

offset transform at the time of seafloor spreading that formed Macquarie Island (Fig. 1.10). This transverse ridge was a likely source for the ~11-9 Ma Macquarie Island sedimentary rocks. Changes in spreading direction and transform migration along the Mid-Atlantic Ridge have also resulted in transpression across long-offset transforms, which formed transverse ridges with 1-4 km of bathymetric relief (Bonatti et al. 1994; Pockalny et al. 1996). These transverse ridges commonly parallel active and extinct modern day transform faults and occur adjacent to anomalously deep nodal basins on the active young crust (Pockalny et al. 1996). A geodynamic reconstruction for 10.9 Ma shows magnetic anomaly 8o (26.6 Ma) SEIR crust adjacent to the active PMSR (Fig. 1.10). Therefore, sedimentary rocks within the active Neogene volcano-sedimentary basin of the westernmost PMSR record the denudation of Paleogene aged crust that was transported >300 km northward over 19 Myr along the Jurrut transverse ridge. This implies that Macquarie Island gabbroic sandstones were mostly derived from crust that lay across the Jurrut transform fault and that gabbroic footwall rocks from the Finch-Langdon Fault were not a source (c.f. Daczko et al. 2005).

Detrital zircon grains from gabbroic sandstones have a wide spread in age with main peak populations of 27 Ma and 33 Ma for the central and northwestern volcano-sedimentary basins, respectively. This range in age likely reflects different source rocks and is also indicated by petrographic results, paleocurrents, and clinopyroxene geochemistry. Central coast samples were derived from younger oceanic crust that yielded a higher proportion of lower crustal rock detritus and more diopsidic pyroxenes (Table 1.1; Fig. 1.9). Garzanti et al. (2002) attributed diopside to gabbroic sources and augite to basaltic sources. A higher component of lower oceanic

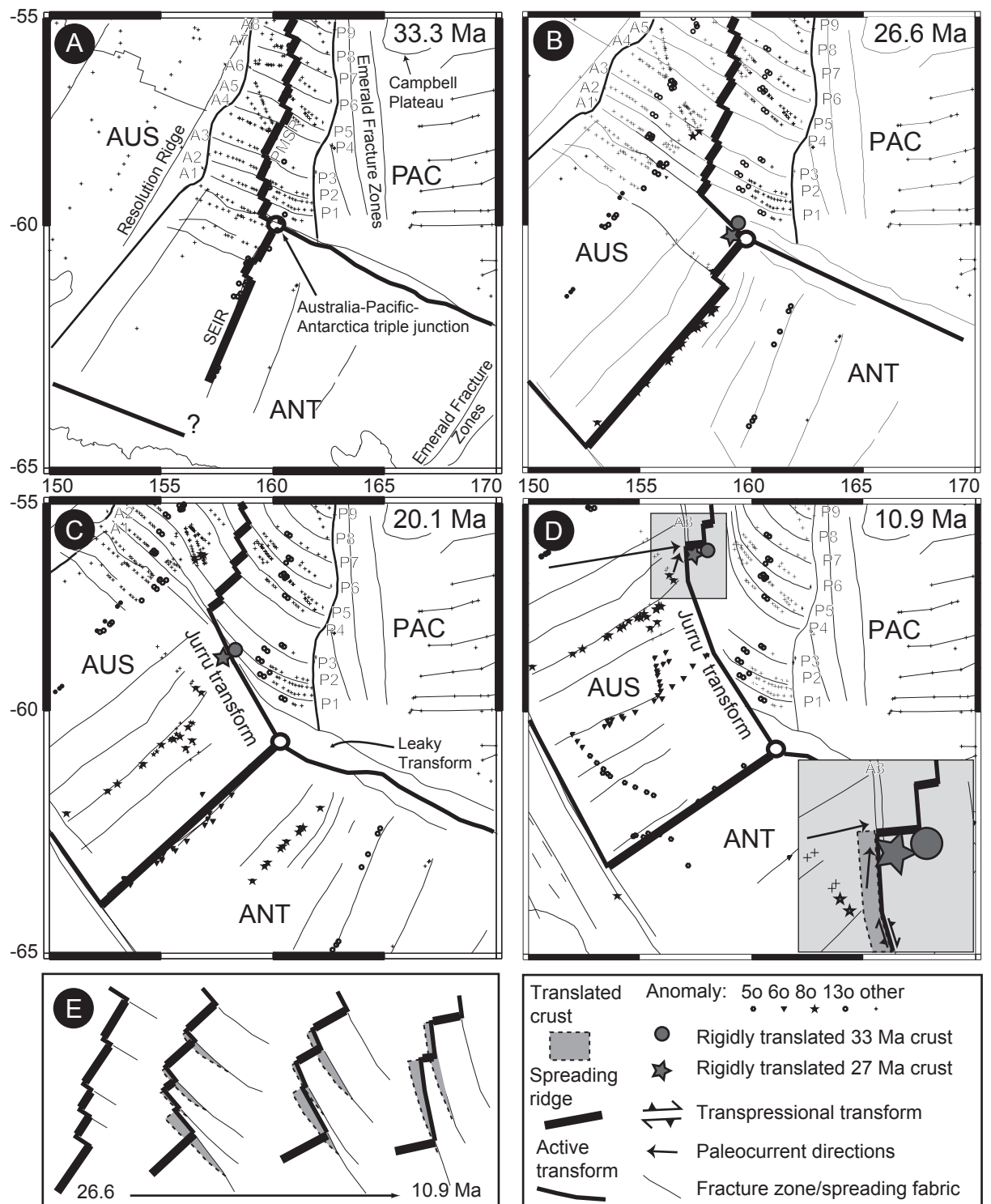


Figure 1.10: Rigid plate paleogeographic map reconstructions for the PMSR and SEIR modified from Meckel (2003), Keller (2004), and Mosher and Massell-Symons (2008). Pacific (PAC) plate fixed relative to Australia (AUS) and Antarctica (ANT) plates. Numbered fracture zones on AUS plate (A1-A9) correspond to conjugate fracture zones on PAC plate (P1-P9). A) Shows essentially continuous PMSR and SEIR at 33.3 Ma (anomaly 130). B) Initiation of plate motion reorganization at 26.6 Ma (anomaly 80). Translated 33 Ma PMSR crust is shown with circular marker. C) Development of long-offset Juru transform with failure of P0/A0-P1/A1-P2/A2 spreading corridors by 20.1 Ma (anomaly 60). D) Formation of Macquarie Island crust starting by 10.9 Ma (anomaly 50). Inset (light grey background) shows overlap in 33 Ma crust marker reflecting transpressional component across transform and paleocurrent directions recorded in gabbroic sedimentary intervals. E) Depicts crust translation across dead transforms during clockwise rotation of spreading direction, simultaneous shortening and propagation of spreading ridges, and transform migration.

crust for the central coast samples is also reflected in the higher recovery of detrital zircons in central west coast samples, which are more likely to have been derived from coarse-grained intrusive lithologies. Northwestern samples returned lower detrital zircon yields and were dominantly sourced from slightly older crust, partly consistent with an ~11.5 Ma depositional age for this basin compared with an ~9 Ma depositional age for the central west coast samples. However, the difference in detrital zircon age between the two basins corresponds to ~250 km of distance between magnetic anomalies 8o (26.6 Ma) and 13o (33.3 Ma) of the SEIR source crust (Fig. 1.10) and the possible few million years difference between the depositional age of the two basins is too short for ~250 km of offset across the Jurru transform.

This may be resolved by the difference in paleocurrent data between the two basins and probable reworking of sediment from older basins. The northerly paleocurrent data would predict younger ages in the central Macquarie Island basin relative to more easterly paleocurrent indicators in older source detritus of the northwestern basin (Fig. 1.10). This is constrained by a southerly younging direction of crust on the adjacent Australia plate. Single submarine gravity flows have the ability to deposit their sedimentary load across distances >500 km on slopes with <1° inclination (Talling et al. 2007) and would have the potential to tap the spatially separated source terrains envisioned for the PMSR volcano-sedimentary basins. However, sedimentary structures indicate that the paleocurrents of the depositing gravity currents may not represent the original direction of sediment transport. Forward modeling and field examples of turbidites with multilateral paleocurrents, indicate that submarine sediment gravity flows have the capacity to be reflected and deflected upon interaction with submerged obstacles (Pickering and Hiscott 1985;

Edwards et al. 1994; Kneller and McCaffery 1999), which would be expected in the fault bound basins of a mid-ocean ridge environment (Van Andel and Komar 1969). Considering this setback, the basal scour marks of the depositing gravity current are commonly believed to be the original passage of the flow and hence reflecting the true source area direction or basin morphology (Kneller et al. 1991; Kneller and McCaffery 1999). Scour marks in Macquarie Island gabbroic sandstones are generally bilateral and indicate nearly 90 degrees of separation between the source areas for the northwestern and central basins.

An alternate idea to explain how crust with both anomalies 8o and 13o lay within the vicinity of the nascent sedimentary basins of Macquarie Island is indicated by the geodynamic reconstruction at 26.6 Ma that shows the Australia-Pacific-Antarctic triple junction juxtaposing anomaly 8o crust actively forming at the SEIR near anomaly 13o PMSR crust (Fig. 1.10). Around this time propagation of the easternmost active SEIR segment into nearby anomaly 13o PMSR crust and/or transform migration could result in transfer of older Pacific plate crust to the Australian plate to produce heterogeneously aged crust (Fig. 1.10). This heterogeneous crust, now part of the Australia plate, would be transported northward toward the active PMSR along the Jurrul long-offset transform. However, shortening of the SEIR spreading corridor and southwestward migration of Australia-Pacific-Antarctic triple junction (Meckel 2003) does not support the ridge propagation model. Changing orientations of the spreading direction with simultaneous demise and propagation of spreading ridge tips have been shown to cause transform fault migration and translation of crust across dead transform boundaries with development of new transform orientations (Bonatti et al. 1994;

Mosher and Massell-Symons 2008). This is supported by the observed failure of the two westernmost PMSR corridors that were adjacent to the Jurru transform fault after ~27 Ma (ridge segments P0-P1-P2 on Fig. 1.10). Although, the lithospheric strength along the Jurru transverse ridge would impede transform migration and the translation of Pacific plate crust to the Australia plate. A most interesting point in the latter two models is that some of this source crust (anomaly 13o source) was created at the same spreading ridge ~22 Myr earlier, having been cannibalized into an adjacent transform fault during ridge reorientation and shortening only to be reintroduced as faulted detritus into basins of the active spreading corridor.

A final explanation for the heterogeneous source crust may reflect a very protracted magmatic accretion history for the SEIR spreading corridor. Modern day gabbroic rocks along slow-spreading mid-ocean ridges yield a span in zircon crystallization age of 0.1-2.5 Ma and have been interpreted to reflect uplift and assimilation of older crystallized rocks with younger shallow level intrusions (Grimes et al. 2008; Schwartz et al. 2005) and protracted zircon growth during gabbro crystallization (Lissenberg et al. 2009). The ~6 Myr time spread of our detrital zircon grains would then provide new insight into the accretion of oceanic crust on a much longer scale than previously recognized in sampling of in-situ igneous rocks. Off-axis intrusion would further complicate this model. Nevertheless, the wide “drainage area” recorded by detrital zircon sampling in modern ocean nodal basins could therefore provide further insight into the formation of oceanic crust. Future work on the detrital zircon trace element geochemistry may reveal differences in the heterogeneous source crust, which could argue for or against crust created at different or similar spreading centers.

Oceanic crustal exhumation and depositional environment:

A generalized stratigraphy recorded in Macquarie Island volcano-sedimentary basins of basaltic breccias overlain by gabbroic sediments document the exhumation and tectonic unroofing of the oceanic crust. The occurrence of locally-derived basaltic breccias within the base of stratigraphic sections and their common proximity to major spreading-related faults suggests that they mark the initial development of volcano-sedimentary basins. These basins were bounded by basaltic breccia talus piles and successively onlapped by newly extruded basalt and distally-derived gabbroic sandstones (Fig. 1.11). This detrital record reflects the tectonic removal of very thick sections of upper oceanic crust >2 km that has been documented along modern oceanic core complexes (Dick et al. 2000; John et al. 2004).

Due to the lack of erosional processes in the submarine environment the majority of sediment must have been created within fault zones. The latter is supported by fine grained sandy nature of fault gouge sampled from spreading-related faults on Macquarie Island (Daczko et al. 2005) that resembles faulted tectonic lithic grains within sandstones. We propose that tectonism along fault zones generated failure of unstable ophiolitic fault gouge. Extensive deformation within the Juru long-offset transform fault produced a higher proportion of finer grained gabbroic detritus relative to locally derived basaltic breccias. The gabbroic-sourced material moved en-masse down slope where it locally evolved into density-stratified gravity flows, which may have further disaggregated the sedimentary particles. The finer grained gabbroic gravity flows entrained intrabasinal pelagic mud before being ponded in fault-bound basins. The occurrence of very thick tabular basalts interbedded with gabbroic sandstones imply highly voluminous sheet flow extrusive episodes (Kennish and Lutz 1998) and therefore suggest that the sedimentary basins

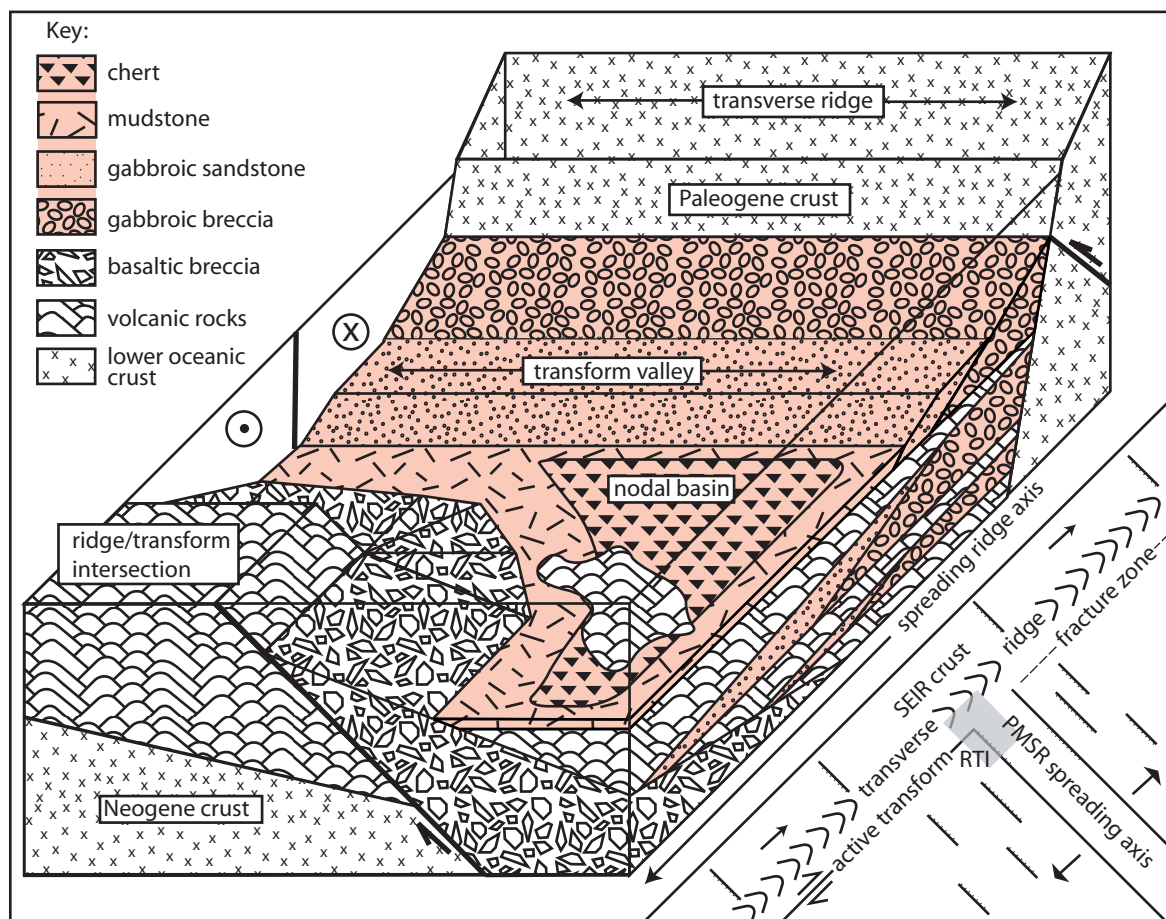


Figure 1.11:
Schematic representation of a depositional nodal basin flanking a transverse ridge at a ridge transform intersection. Neogene crust created at PMSR and Paleogene crust created at SEIR. Grey box in inset represents area depicted in 3-D block diagram.

were within the magmatically active spreading corridor of the westernmost PMSR (Fig. 1.11).

The absence of both ~8.5 Ma zircons and serpentinite lithics in gabbroic sandstones suggests that the lower oceanic crust and upper mantle presently observed on Macquarie Island was not exposed during deposition of these sandstones. Recent exposure due to subaerial erosion is unlikely considering the need for significant erosion during Macquarie Island's existence over the last 600-700 ka (Adamson et al. 1996) and the preservation of relatively young ocean floor seamount features (Varne et al. 2000). A likely explanation for this dilemma is that movement along Macquarie Island spreading-related faults continued long after filling of the volcano-sedimentary basins described here. Late uplift and denudation along spreading-related faults have been proposed to account for anomalously high temperature thermochronometers, 2-4 m.y. off axis along the slow-spreading SW Indian Ridge (John et al. 2004). Zircon and apatite fission track ages indicate that Macquarie Island gabbros cooled from ~240°C to 110°C between ~6.0 to 4.7 Ma (Armstrong et al. 2004) indicating that these rocks were still not exposed long after the depositional age of Macquarie Island sandstones. The depositional age for Macquarie Island gabbroic sandstones are constrained by the youngest detrital zircon grain of ~12 Ma in the northwest coastal dataset, interbedded tabular basalts that yield an ~11 Ma $\text{Ar}^{40}/\text{Ar}^{39}$ age in the northwest coast section (Duncan and Varne 1988), and ~9 Ma microplankton collected from interpillow calcareous ooze of the central west coast (Quilty et al. 2008).

Results from this study suggest that initial faulting of Macquarie Island spreading-related faults produced the basaltic breccias and created basins that

distally-derived older gabbroic sediment was also deposited into. During this time gabbroic rocks below the active PMSR crystallized. Upon cessation of magmatism and migration away from the active spreading corridor, continued faulting and uplift along Macquarie Island spreading-related faults exhumed the lower oceanic crust in bathymetric highs. Gabbroic detritus from these younger levels would have been incorporated into younger sedimentary basins that flanked the newly created transpressional Macquarie Ridge Complex.

Conclusions:

Clastic sedimentary rocks of Macquarie Island record the exhumation of lower oceanic crust at the intersection of a long-offset transform and a slow-spreading ridge. Initial development of Neogene volcano-sedimentary basins within the westernmost active PMSR corridor is preserved by locally derived very coarse grained basaltic breccias that typically occur adjacent to spreading-related faults. These spreading-related faults accommodated extension during volcanism in the active PMSR long after volcanism ceased. Fault-bound volcano-sedimentary basins were subsequently filled with thick sequences of pillowed and tabular basalt with thin intercalations of gabbroic sedimentary rocks. Petrographic analysis indicates that gabbroic breccias were primarily derived from the boundary between the lower and upper oceanic crust. Detrital clinopyroxene geochemistry from gabbroic sandstones, mostly yield tholeiitic augite compositions that have trends related to volcanic rocks produced in divergent rift settings. Trace element patterns of the detrital clinopyroxene have a depleted LREE signature indicative of an NMORB source in contrast to highly alkaline EMORB signatures of interbedded basalt

clinopyroxene grains. Detrital zircon $^{206}\text{Pb}/^{238}\text{U}$ geochronology yield ~27 and ~33 Ma grain populations suggesting that ~8.5 Ma Macquarie Island gabbroic rocks currently exposed in adjacent footwalls were not exposed during filling of the Neogene volcano-sedimentary basins. Geodynamic reconstructions show that heterogeneously aged Paleogene source crust in the SEIR spreading corridor was tectonically transported over 300 km in the Jurrut long-offset transform. This transform was subjected to significant transpression during this time, which produced a bathymetrically high transverse ridge. Denudation of this transverse ridge shed faulted Paleogene upper and lower oceanic crust into adjacent basins of the active PMSR. The heterogeneous source crust that supplied the ~27 (anomaly 80 crust) and ~33 Ma (anomaly 130 crust) detrital zircons appear to be separated by ~250 km in the SEIR spreading corridor. Several models are plausible for this mixture: 1) different paleocurrent directions from separate measured sections suggest that the very long transport of submarine gravity flows could potentially source these spatially separated source terrains; 2) rotation of spreading ridge segments, ridge segment shortening and propagation, and transform migration could assimilate 130 crust of the Pacific Plate with 80 crust of the Australia plate; and 3) a very protracted magmatic accretion history or off-axis magmatism within the SEIR spreading corridor.

References Cited:

- Adamson, D. A., Selkirk, P. M., Price, D. M., Ward, N., and Selkirk, J. M., 1996, Pleistocene uplift and palaeoenvironments of Macquarie Island; evidences from palaeobeaches and sedimentary deposits, in Banks, M. R., and Brown, M. J., eds., *Papers and Proceedings of the Royal Society of Tasmania*, vol.130, Part 2, p. 25-32.

- Armstrong, R. A., Kohn, B., Goscombe, B. D., and Everard, J. L., 2004, U-Pb and fission track ages from oceanic crust at Macquarie Island, in McPhie, J., and McGoldrick, P., eds., Abstracts - Geological Society of Australia, vol.73, p. 197.
- Auzende, J.-M., Cannat, M., Gente, P., Henriot, J.-P., Juteau, T., Karson, J., Lagabriele, Y., Mevel, C., and Tivey, M., 1994, Observation of sections of oceanic crust and mantle cropping out on the southern wall of Kane FZ (N. Atlantic): *Terra Nova*, v. 6, no. 2, p. 143-148.
- Baines, A. G., Cheadle, M. J., Dick, H. J. B., Scheirer, A. H., John, B. E., Kuszniir, N. J., and Matsumoto, T., 2003, Mechanism for generating the anomalous uplift of oceanic core complexes; Atlantis Bank, Southwest Indian Ridge: *Geology*, v. 31, no. 12, p. 1105-1108.
- Belousova, E. A., Griffin, W. L., Shee, S. R., Jackson, S. E., and O'Reilly, S. Y., 2001, Two age populations of zircons from the Timber Creek kimberlites, Northern Territory, as determined by laser-ablation ICP-MS analysis: *Australian Journal of Earth Sciences*, v. 48, p. 757-765.
- Blackman, D. K., Cann, J. R., Janssen, B., and Smith, D. K., 1998, Origin of extensional core complexes; evidence from the Mid-Atlantic Ridge at Atlantis fracture zone: *Journal of Geophysical Research*, v. 103, no. B9, p. 21,315-21,333.
- Bonatti, E., Honnorez, J., and Gartner, S., Jr., 1973, Sedimentary serpentinites from the Mid-Atlantic Ridge: *Journal of Sedimentary Petrology*, v. 43, no. 3, p. 728-735.
- Bonatti, E., Ligi, M., Gasperini, L., Peyve, A., Raznitsin, Y., and Chen, Y. J., 1994, Transform migration and vertical tectonics at the Romanche fracture zone, equatorial Atlantic: *Journal of Geophysical Research*, v. 99, no. B11, p. 21,779-21,802.
- Bouma, A. H., 1962, *Sedimentology of some flysch deposits: a graphic approach to facies interpretations*: Amsterdam, Elsevier, 168 p.
- Canales, J. P., Tucholke, B. E., and Collins, J. A., 2004, Seismic reflection imaging of an oceanic detachment fault: Atlantis megamullion (Mid-Atlantic Ridge, 30°10'N): *Earth and Planetary Science Letters*, v. 222, no. 2, p. 543-560.
- Cande, S. C., and Stock, J. M., 2004, Pacific-Antarctic-Australia motion and the formation of the Macquarie Plate: *Geophysical Journal International*, v. 157, no. 1, p. 399-414.
- Christodoulou, C., 1990, *Petrology of the plutonic rocks of the Macquarie Island complex*: University of Adelaide, 459 p.
- Coogan, L. A., Kempton, P. D., Saunders, A. D., and Norry, M. J., 2000, Melt aggregation within the crust beneath the Mid-Atlantic Ridge; evidence from plagioclase and clinopyroxene major and trace element compositions: *Earth and Planetary Science Letters*, v. 176, no. 2, p. 245-257.
- Daczko, N., Wertz, K. L., Mosher, S., Coffin, M. F., and Meckel, T. A., 2003, Extension along the Australian-Pacific transpressional transform plate boundary near Macquarie Island, *Geochemistry Geophysics Geosystems*, v. 4, no. 9, p. 22.
- Daczko, N. R., Mosher, S., Coffin, M. F., and Meckel, T.A., 2005, Tectonic implications of fault-scarp-derived volcanoclastic deposits on Macquarie Island; sedimentation at a fossil ridge-transform intersection?: *Geological Society of America Bulletin*, v. 117, no. 1-2, p. 18-31.

- Davidson, G. J., Varne, R., Brown, A. V., and Connell, R., 2004, Structural controls on sulphide deposition at the dyke-lava boundary, slow-spreading ocean crust, Macquarie Island: *Terra Nova*, v. 16, p. 9-15.
- Davidson, J., Turner, S., Handley, H., Macpherson, C., and Dosseto, A., 2007, Amphibole "sponge" in arc crust?: *Geology*, v. 35, no. 9, p. 787-790.
- Dick, H. J. B., and Johnson, K. T. M., 1995, REE and trace element composition of clinopyroxene megacrysts, xenocrysts, and phenocrysts in two diabase dikes from Leg 140, Hole 504B, Proceedings of the Ocean Drilling Program, Scientific Results, p. 121-130.
- Dick, H. J. B., Natland, J. H., Alt, J. C., Bach, W., Bideau, D., Gee, J. S., Haggas, S., Hertogen, J. G. H., Hirth, G., Holm, P. M., Ildefonse, B., Iturrino, G. J., John, B. E., Kelley, D. S., Kikawa, E., Kingdon, A., LeRoux, P. J., Maeda, J., Meyer, P. S., Miller, D. J., Naslund, H. R., Niu, Y.-L., Robinson, P. T., Snow, J., Stephen, R. A., Trimby, P. W., Worm, H.-U., and Yoshinobu, A., 2000, A long in situ section of the lower ocean crust: results of ODP Leg 176 drilling at the Southwest Indian Ridge: *Earth and Planetary Science Letters*, v. 179, no. 1, p. 31-51.
- Dickinson, W. R., 1985, Interpreting provenance relations from detrital modes of sandstones, in Zuffa, G. G., ed., *NATO Advanced Study Institutes Series. Series C: Mathematical and Physical Sciences*, vol. 148: Dordrecht-Boston, D. Reidel Publishing Company, p. 333-361.
- Dickinson, W. R., and Suczek, C. A., 1979, Plate tectonics and sandstone compositions: *American Association of Petroleum Geologists Bulletin*, v. 63, no. 12, p. 2164-2182.
- Dorsey, R. J., 1988, Provenance evolution and unroofing history of a modern arc-continent collision; evidence from petrography of Plio-Pleistocene sandstones, eastern Taiwan: *Journal of Sedimentary Petrology*, v. 58, no. 2, p. 208-218.
- Duncan, R. A., and Varne, R., 1988, The age and distribution of the igneous rocks of Macquarie Island: *Papers and Proceedings of the Royal Society of Tasmania*, v. 122, p. 45-50.
- Dunkl, I., Grasemann, B., and Frisch, W., 1998, Thermal effects of exhumation of a metamorphic core complex on hanging wall syn-rift sediments: an example from the Rechnitz Window, Eastern Alps: *Tectonophysics*, v. 297, no. 1-4, p. 31-50.
- Edwards, D. A., Leeder, M. R., Best, J. L., and Pantin, H. M., 1994, On experimental reflected density currents and the interpretation of certain turbidites: *Sedimentology*, v. 41, no. 3, p. 437.
- Fagan, T. J., and Day, H. W., 1997, Formation of amphibole after clinopyroxene by dehydration reactions: Implications for pseudomorphic replacement and mass fluxes: *Geology*, v. 25, no. 5, p. 395-398.
- Fox, P. J., and Heezen, B. C., 1965, Sands of the Mid-Atlantic Ridge: *Science*, v. 149, no. 3690, p. 1367-1370.
- Gao, D., 2006, Gravitational sliding on the Mid-Atlantic Ridge at the Kane Transform; implications for submarine basin-slope degradation and deformation: *American Association of Petroleum Geologists Bulletin*, v. 90, no. 2, p. 159-176.
- Garzanti, E., Ando, S., Vezzoli, G., and Dell'era, D., 2003, From Rifted Margins to Foreland Basins: Investigating Provenance and Sediment Dispersal Across

- Desert Arabia (Oman, U.A.E.): *Journal of Sedimentary Research*, v. 73, no. 4, p. 572-588.
- Garzanti, E., Andro, S., and Scutella, M., 2000, Actualistic ophiolite provenance; the Cyprus case: *Journal of Geology*, v. 108, no. 2, p. 199-218.
- Garzanti, E., Vezzoli, G., and Ando, S., 2002, Modern sand from obducted ophiolite belts (Sultanate of Oman and United Arab Emirates): *Journal of Geology*, v. 110, no. 4, p. 371-391.
- Gillis, K. M., and Thompson, G., 1993, Metabasalts from the Mid-Atlantic Ridge; new insights into hydrothermal systems in slow-spreading crust: *Contributions to Mineralogy and Petrology*, v. 113, no. 4, p. 502-523.
- Goscombe, B. D., and Everard, J. L., 1998, 1:10,000 Geological Map of Macquarie Island, series of 7 maps: Mineral Resources Tasmania.
- Goud, M. R., and Karson, J. A., 1985, Tectonics of short-offset, slow-slipping transform zones in the FAMOUS area, Mid-Atlantic Ridge: *Marine Geophysical Researches*, v. 7, no. 4, p. 489-514.
- Griffin, B. J., 1982, Igneous and metamorphic petrology of lavas and dykes of the Macquarie Island ophiolite complex [Ph.D. dissertation]: University of Tasmania, 220 p.
- Grimes, C. B., John, B. E., Cheadle, M. J., and Wooden, J. L., 2008, Protracted construction of gabbroic crust at a slow spreading ridge: Constraints from 206Pb/238U zircon ages from Atlantis Massif and IODP Hole U1309D (30°N, MAR): *Geochemistry Geophysics Geosystems*, v. 9.
- Ildefonse, B., Blackman, D. K., John, B. E., Ohara, Y., Miller, D. J., and MacLeod, C. J., 2007, Oceanic core complexes and crustal accretion at slow-spreading ridges: *Geology*, v. 35, no. 7, p. 623-626.
- Ingersoll, R. V., and Cavazza, W., 1991, Reconstruction of Oligo-Miocene volcanoclastic dispersal patterns in north-central New Mexico using sandstone petrofacies: Special Publication - Society of Economic Paleontologists and Mineralogists, v. 45, p. 227-236.
- Ingersoll, R. V., Fullard, T. F., Ford, R. L., Grimm, J. P., Pickle, J. D., and Sares, S. W., 1984, The effect of grain size on detrital modes; a test of the Gazzi-Dickinson point-counting method: *Journal of Sedimentary Petrology*, v. 54, no. 1, p. 103-116.
- Jackson, S. E., Pearson, N. J., Griffin, W. L., and Belousova, E. A., 2004, The application of laser ablation-inductively coupled plasma-mass spectrometry to in situ U-Pb zircon geochronology: *Chemical Geology*, v. 211, no. 1-2, p. 47-69.
- John, B. E., Foster, D. A., Murphy, J. M., Cheadle, M. J., Baines, A. G., Fanning, C. M., and Copeland, P., 2004, Determining the cooling history of in situ lower oceanic crust--Atlantis Bank, SW Indian Ridge: *Earth and Planetary Science Letters*, v. 222, no. 1, p. 145-160.
- Jöns, N., Bach, W., and Schroeder, T., 2009, Formation and alteration of plagiogranites in an ultramafic-hosted detachment fault at the Mid-Atlantic Ridge (ODP Leg 209): *Contributions to Mineralogy and Petrology*, v. 157, no. 5, p. 625-639.
- Kamenetsky, V. S., and Maas, R., 2002, Mantle-melt Evolution (Dynamic Source) in the Origin of a Single MORB Suite: a Perspective from Magnesian Glasses of Macquarie Island: *Journal of Petrology*, v. 43, no. 10, p. 1909-1922.

- Karson, J. A., and Dick, H. J. B., 1983, Tectonics of ridge-transform intersections at the Kane fracture zone: *Marine Geophysical Researches*, v. 6, no. 1, p. 51-98.
- Karson, J. A., Fox, P. J., Sloan, H., Crane, K. T., Kidd, W. S. F., Bonatti, E., Stroup, J. B., Fornari, D. J., Elthon, D., Hamlyn, P., Casey, J. F., Gallo, D. G., Needham, D., and Sartori, R., 1984, The geology of the Oceanographer Transform: The ridge-transform intersection: *Marine Geophysical Researches*, v. 6, no. 2, p. 109-141.
- Keller, W., 2004, Cenozoic plate tectonic reconstructions and plate boundary processes in the Southwest Pacific: California Institute of Technology.
- Kennish, M. J., and Lutz, R.A., 1998, Morphology and distribution of lava flows on mid-ocean ridges; a review: *Earth-Science Reviews*, v. 43, no. 3-4, p. 63-90.
- Kneller, B., Edwards, D., McCaffrey, W., and Moore, R., 1991, Oblique reflection of turbidity currents: *Geology*, v. 19, no. 3, p. 250-252.
- Kneller, B., and McCaffrey, W., 1999, Depositional effects of flow nonuniformity and stratification within turbidity currents approaching a bounding slope; deflection, reflection, and facies variation: *Journal of Sedimentary Research*, v. 69, no. 5, p. 980-991.
- Koepke, J., Berndt, J., Feig, S. T., and Holtz, F., 2007, The formation of SiO_2 -rich melts within the deep oceanic crust by hydrous partial melting of gabbros: *Contributions to Mineralogy & Petrology*, v. 153, no. 1, p. 67-84.
- Koepke, J., Feig, S., Snow, J., and Freise, M., 2004, Petrogenesis of oceanic plagiogranites by partial melting of gabbros: an experimental study: *Contributions to Mineralogy and Petrology*, v. 146, no. 4, p. 414-432.
- Lamarche, G., Collot, J.-Y., Wood, R. A., Sosson, M., Sutherland, R., and Delteil, J., 1997, The Oligocene-Miocene Pacific-Australia plate boundary, south of New Zealand; evolution from oceanic spreading to strike-slip faulting: *Earth and Planetary Science Letters*, v. 148, no. 1-2, p. 129-139.
- Link, P. K., Fanning, C. M., and Beranek, L. P., 2005, Reliability and longitudinal change of detrital-zircon age spectra in the Snake River system, Idaho and Wyoming; an example of reproducing the bumpy barcode: *Sedimentary Geology*, v. 182, no. 1-4, p. 101-142.
- Lissenberg, C. J., Rioux, M., Shimizu, N., Bowring, S. A., and Mevel, C., 2009, Zircon Dating of Oceanic Crustal Accretion: *Science*, v. 323, no. 5917, p. 1048-1050.
- Loucks, R. R., 1990, Discrimination of ophiolitic from nonophiolitic ultramafic-mafic allochthons in orogenic belts by the Al/Ti ratio in clinopyroxene: *Geology*, v. 18, no. 4, p. 346-349.
- MacLeod, C. J., Escartin, J., Banerji, D., Banks, G. J., Gleeson, M., Irving, D. H. B., Lilly, R. M., McCaig, A. M., Niu, Y., Allerton, S., and Smith, D. K., 2002, Direct geological evidence for oceanic detachment faulting; the Mid-Atlantic Ridge, 15 degrees 45'N: *Geology*, v. 30, no. 10, p. 879-882.
- Massell, C., Coffin, M. F., Mann, P., Mosher, S., Frohlich, C., Duncan, C. S., Karner, G., Ramsay, D., and Lebrun, J. F., 2000, Neotectonics of the Macquarie Ridge Complex, Australia-Pacific plate boundary: *Journal of Geophysical Research*, v. 105.
- Meckel, T. A., 2003, Tectonics of the Hjort region of the Macquarie Ridge Complex, southernmost Australian-Pacific plate boundary, Southwest Pacific Ocean [Ph.D. dissertation]: University of Texas, 192 p.

- Meckel, T. A., Mann, P., Mosher, S., and Coffin, M. F., 2005, Influence of cumulative convergence on lithospheric thrust fault development and topography along the Australian-Pacific plate boundary south of New Zealand: *Geochemistry Geophysics Geosystems*, v. 6.
- Morimoto, N., Fabries, J., Ferguson, A. K., Ginzburg, I. V., Ross, M., Seifert, F. A., Zussman, J., Aoki, K., and Gottardi, G., 1988, Nomenclature of pyroxenes: *American Mineralogist*, v. 73, no. 9-10, p. 1123-1133.
- Mosher, S., and Massell-Symons, C. M., 2008, Ridge reorientation mechanisms: Macquarie Ridge Complex, Australia-Pacific plate boundary: *Geology*, v. 36, no. 2, p. 119-122.
- Nicolas, A., 1989, Structures of ophiolites and dynamics of oceanic lithosphere: Dordrecht, Kluwer Academic, 367 p.
- Pemberton, S. G., MacEachern, J. A., and Frey, R. W., 1992, Trace fossil facies models; environmental and allostratigraphic significance, in Walker, R. G., and James, N. P., eds., *Facies models: responses to sea level change*: St. Johns, Geological Association of Canada, p. 47-72.
- Pickering, K. T., and Hiscott, R. N., 1985, Contained (reflected) turbidity from the Middle Ordovician Cloridorme Formation, Quebec, Canada: an alternative to the antidune hypothesis: *Sedimentology*, v. 32, no. 3, p. 373.
- Pockalny, R. A., Gente, P., and Buck, R., 1996, Oceanic transverse ridges: A flexural response to fracture-zone-normal extension: *Geology*, v. 24, no. 1, p. 71-74.
- Potter, P. E., and Pettijohn, F. J., 1977, *Paleocurrents and basin analysis*: Berlin Heidelberg New York, Springer-Verlag, 425 p.
- Quilty, P. G., Crundwell, M., and Wise Jr., S. W., 2008, Microplankton provide 9 Ma age for sediment in the Macquarie Island ophiolite complex: *Australian Journal of Earth Sciences*, v. 55, no. 8, p. 1119-1125.
- Ross, D. K., Elthon, D., Karson, J. A., Cannat, M., Miller, D. J., Agar, S. M., Barling, J., Casey, J. F., Ceuleneer, G., Dilek, Y., Fletcher, J. M., Fujibayashi, N., Gaggero, L., Gee, J. S., Hurst, S. D., Kelley, D. S., Kempton, P. D., Lawrence, R. M., Marchig, V., Mutter, C., Niida, K., Rodway, K., Ross, D. K., Stephens, C. J., Werner, C.-D., Whitechurch, H., and Miller, D. J., 1997, Cumulus and postcumulus crystallization in the oceanic crust; major and trace-element geochemistry of Leg 153 gabbroic rocks: *Proceedings of the Ocean Drilling Program, Scientific Results*, v. 153, p. 333-351.
- Sambridge, M. S., and Compston, W., 1994, Mixture modeling of multi-component data sets with application to ion-probe zircon ages: *Earth and Planetary Science Letters*, v. 128, no. 3-4, p. 373-390.
- Schwartz, J. J., John, B. E., Cheadle, M. J., Miranda, E. A., Grimes, C. B., Wooden, J. L., and Dick, H. J. B., 2005, Dating the Growth of Oceanic Crust at a Slow-Spreading Ridge: *Science*, v. 310, no. 5748, p. 654-657.
- Siever, R., and Kastner, M., 1967, Mineralogy and petrology of some Mid-Atlantic Ridge sediments: *Journal of Marine Research*, v. 25, no. 3, p. 263-278.
- Sun, S. s., and McDonough, W. F., 1989, Chemical and isotopic systematics of oceanic basalts: implications for mantle composition and processes: *Geological Society, London, Special Publications*, v. 42, no. 1, p. 313-345.
- Talling, P. J., Wynn, R. B., Masson, D. G., Frenz, M., Cronin, B. T., Schiebel, R., Akhmetzhanov, A. M., Dallmeier-Tiessen, S., Benetti, S., Weaver, P. P. E., Georgiopoulou, A., Zuhlsdorff, C., and Amy, L. A., 2007, Onset of submarine

- debris flow deposition far from original giant landslide: *Nature*, v. 450, no. 7169, p. 541(4).
- Tucholke, B. E., Kenneth Stewart, W., and Kleinrock, M. C., 1997, Long-term denudation of ocean crust in the central North Atlantic Ocean: *Geology*, v. 25, no. 2, p. 171-174.
- Van Andel, T. H., and Bowin, C. O., 1968, Mid-Atlantic ridge between 22 degrees and 23 degrees north latitude and the tectonics of mid-ocean rises: *Journal of Geophysical Research*, v. 73, no. 4, p. 1279-1298.
- Van Andel, T. H., and Komar, P. D., 1969, Ponded sediments of the Mid-Atlantic ridge between 22 degrees and 23 degrees north latitude: *Geological Society of America Bulletin*, v. 80, no. 7, p. 1163-1190.
- Varne, R., Brown, A. V., and Falloon, T., 2000, Macquarie Island; its geology, structural history, and the timing and tectonic setting of its N-MORB to E-MORB magmatism, in Dilek, Y., Moores, E. M., Elthon, D., and Nicolas, A., eds., *Special Paper - Geological Society of America*, vol.349, p. 301-320.
- Wagner, F. H., III, and Johnson, R. A., 2006, Coupled basin evolution and late-stage metamorphic core complex exhumation in the southern Basin and Range Province, southeastern Arizona, in Snyder, D. B., Eaton, D. W., and Hurich, C. A., eds., *Tectonophysics*: Amsterdam, Elsevier, p. 141-160.
- Wertz, K. L., 2003, From seafloor spreading to uplift; the structural and geochemical evolution of Macquarie Island on the Australian-Pacific Plate boundary [Ph.D. dissertation]: University of Texas, 169 p.
- Wertz, K. L., Mosher, S., Daczko, N. R., and Coffin, M. F., 2003, Macquarie Island's Finch-Langdon Fault; a ridge-transform inside-corner structure: *Geology*, v. 31, no. 8, p. 661-664.

II:

Gravity flow and bottom current interaction with a rugged mid-ocean ridge seafloor: an outcrop example from Macquarie Island

PORTNER, Ryan A.¹, DICKINSON, Julie A.¹, and DACZKO, Nathan R.¹

¹GEMOC ARC National Key Centre, Department of Earth and Planetary Sciences,
Macquarie University, NSW 2109, Australia

Submitted to Sedimentary Geology October 2009

Abstract:

Sedimentary lithofacies from the Miocene Macquarie Island ophiolite record the interplay between gravity flows, ocean bottom currents, volcanic constructional features, and faults within a mid-ocean ridge spreading center. Mafic gravel- to sand-sized detritus was primarily derived from mass wasting of hydrothermally altered volcanic and plutonic oceanic crust exposed by spreading-related faults. Lithofacies preserve the lateral transformation of fault proximal debris flows through density stratified gravity flows into distal turbidity flows in basin depocenters. Coarse-grained debrite-rich facies occur as channelized lenses within pillow basalts that formed close to magmatic spreading-segment tips. Finest grained facies occur as laterally extensive sheet-like intercalations within tabular basalt flows erupted in neovolcanic zones. Variation in individual turbidite beds indicate deflected gravity flow events during interaction with volcanic constructional features and intrabasinal faults. Abrupt thickness changes in breccia facies occur across small offsetting intrabasinal faults that were active during deposition. Gravity flow facies can be correlated into channel margin areas where they exhibit characteristics akin to bottom current reworking. Scoured bedding planes from contourite-rich facies that are intercalated within tabular basalts, indicate nearly perpendicular ocean bottom paleocurrents relative to paleoslope and gravity flows. In comparison, contourites from channelized sections within pillow basalt sequences have parallel paleocurrent indicators relative to gravity flow facies. These characteristics indicate confined pillow basalt basins close to spreading ridge tips/transform faults and unconfined tabular basalt basins in axial neovolcanic zones. Disseminated and laminated sulphides throughout pelagic chert units intercalated within tabular basalts suggest

that hydrothermal exhalation was most prevalent in neovolcanic zones.

Sedimentation primarily occurred during volcanically quiescent periods, during which *Helminthoides*, *Spirorhappe*, *Planolites*, *Zoophycos*, and *Paleodictyon* trace fossils formed.

Introduction:

Sedimentary lithofacies formed within submerged rift basins are typically associated with basin-marginal gravity flows and sediment-starved basin centers (Gawthorpe and Leeder 2000). Our knowledge of subaqueous gravity flows (i.e. debris flows, turbidity flows) is primarily based on ancient and modern submarine fan systems from continental margin settings (e.g. Kuenen and Migliorini 1950; Bouma 1962; Normark 1970; Mutti and Ricci Lucchi 1978; Jacobi 1976; Stow and Shanmugam 1980; Gee et al. 1999). This is in part due to the high petroleum reservoir potential in these sedimentary successions (Sullwold 1961; Walker 1978; Sanders and Friedman 1997). Despite a general bias toward research on these continentally-derived systems, clastic sedimentary lithofacies (i.e. sand- to gravel-rich) produced along the mid-ocean ridge system have received significantly less attention. Clastic sediment deposited along active mid-ocean spreading ridges is unique because it is not derived from continental landmass erosion, but rather from mass-wasting processes of uplifted oceanic ridges (Fox and Heezen 1965; Tucholke et al. 1997; Mitchell, et al. 2000). The production of sand-sized detritus by this erosionless process remains problematic (Swift 1991).

Coarse-grained talus ramparts bearing basalt, diabase, gabbro, and serpentinite clasts flank uplifted oceanic fault blocks within the mid-ocean ridge

system and are believed to represent mass wasting processes of denuded oceanic crust (Karson et al. 1984; Zonenshain et al. 1989; Tucholke et al. 1997; Tivey et al. 1998; Mitchell et al. 2000). Uplift of the lower oceanic crust within the inside corner of spreading-ridge/ transform intersections are commonly referred to as oceanic core complexes and typically occur along slow-spreading systems (van Andel and Bowin 1968; Auzende et al. 1994; Blackman et al. 2002; Canales et al. 2004). These core complexes are associated with tectonic removal of the upper oceanic crust along low angle detachment style faults (Dick et al. 2000; Macleod et al. 2002; Ildefonse et al. 2007). Uplifted lower crustal massifs are transported along active transforms where they typically form bathymetrically high transverse ridges with up to 4 km of relief (Dick et al. 1991; Bonatti et al. 1994; Pockalny et al. 1996). These bathymetric highs occur opposite the neovolcanic zone of the active spreading corridor at ridge-transform intersections, where they flank younger nodal basins that can contain sedimentary successions up to 100 m thick (Karson et al. 1984). In addition, seismic data along the Atlantis II transform valley indicate between 300 to 750 m thick deposits of ponded-turbidite sands and gravels derived from surrounding transverse ridges (Dick et al. 1991).

The spatial juxtaposition of sedimentary basins against faulted bathymetric “mountain ranges” implies that the coeval clastic detritus within the adjacent basins will provide a detrital record of their uplift and denudation as is commonly described in tectonically active subaqueous continental rift-basins (Dorsey et al. 2001; Leppard and Gawthorpe 2006). Aside from the typical coarse-grained breccias easily recognized by submersibles (e.g. Zonenshain et al. 1989; Tivey et al. 1998) finer grained mafic- and ultramafic-rich sandstone bodies have also been observed (Fox

and Heezen 1965; Siever and Kastner 1967; Flier-Keller 1991; Swift 1991), but lack any detailed sedimentological documentation aside from general surficial, geochemical, and petrographic characteristics. This is in part due to the inherent difficulty in locating and sampling sandy deposits along the mostly pelagic ooze covered mid-ocean ridge (Swift 1991; Tivey et al. 1998). Although ophiolites provide a window into the otherwise inaccessible oceanic floor, they are generally too deformed or do not contain clastic-rich sedimentary sections (Barrett and Spooner 1977; Karson and Dewey 1978). Simonian and Gass (1978) briefly describe 500 m thick sequences comprised of basalt flows intercalated with ophiolitic breccia-sandstone-mudstone units that were deposited by gravity flows believed to have filled a transform fault within the Troodos ophiolite. In the present study, we explore the generation, transport, and depositional environment of sandstones and associated lithofacies entirely produced within the slow-spreading proto-Macquarie spreading ridge (PMSR). The relationship between sedimentary lithofacies, volcanic basin morphology and faults is evaluated in terms of basin geometries along the dynamic spreading ridge environment. Measured stratigraphic sections, lithofacies analysis, and petrographic examination of sedimentary rocks from the well-exposed *in-situ* Macquarie Island ophiolite, provide a detailed land-based account of this relatively unstudied deep-marine depositional environment.

Geologic Setting:

Oceanic crust of the Macquarie Island ophiolite is located in the Southern Ocean approximately halfway between New Zealand and Antarctica (Fig. 2.1A). Rocks of the island formed in the westernmost active spreading segment of the slow-

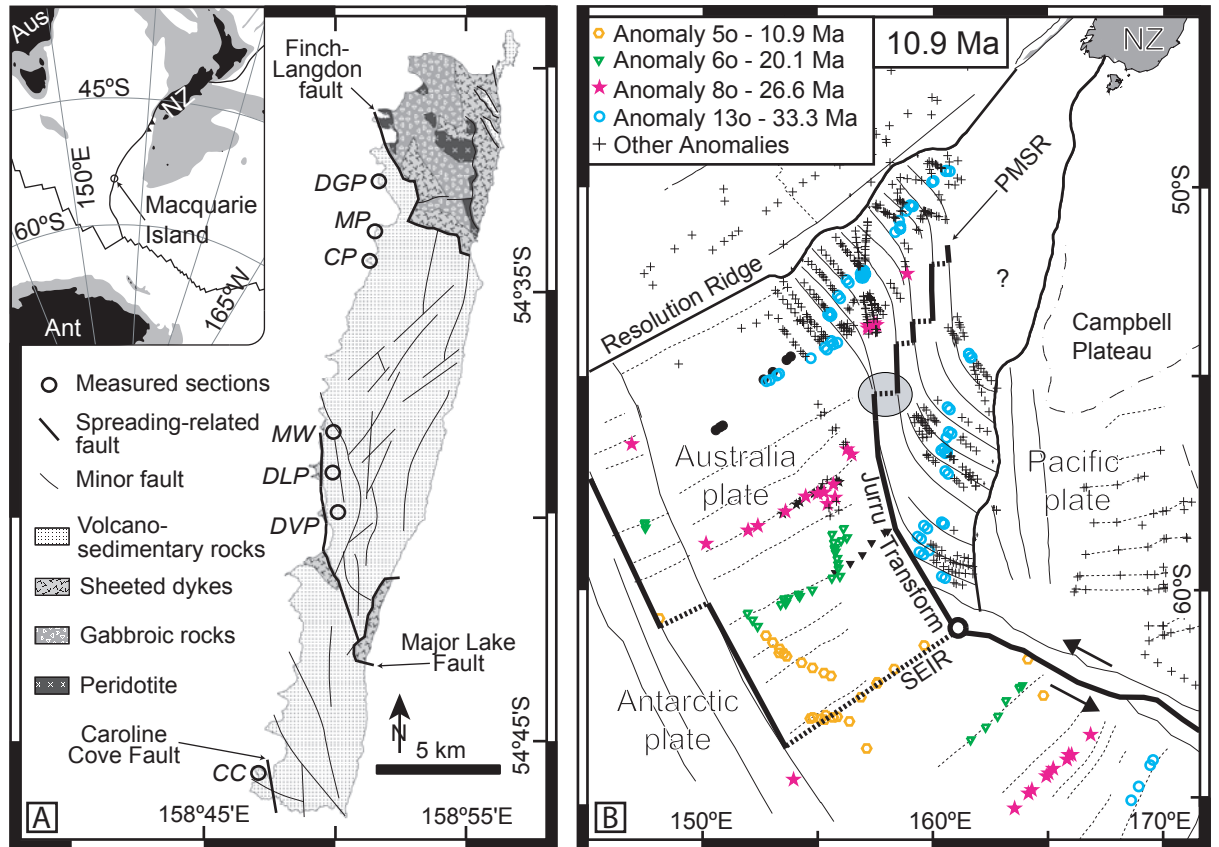


Figure 2.1:

A) Location and generalized geologic map of Macquarie Island. Dark bold lines in inset represent active plate boundaries. Measured section locations on geologic map include: Douglas Point (DGP), Mawson Point (MP), Cormorant Point (CP), Mt. Waite (MW), Double Point (DLP), Davis Point (DVP), and Caroline Cove (CC). B) Paleogeographic reconstruction for proto-Macquarie Spreading Ridge (PMSR) during late Miocene time (~10.9 Ma). Oceanic crust exposed on Macquarie Island formed in the westernmost PMSR spreading segment (circled). Transform/fracture zones (solid) and spreading-segment fabric (dashed) are represented by active bold lines and inactive thin lines. Medium weight lines correspond to conjugate rifted margins of the PMSR. Modified from Meckel (2003).

spreading PMSR (half rates of 4.4-28 mm/yr) between 12 and 8 Ma (Fig. 2.1B; Varne et al. 2000; Quilty et al. 2008; Mosher and Massell-Symons 2008). Intact pillow cones with radiating pillow basalt tubes can still be observed on the island and attest to the essentially *in-situ* nature of subaerially exposed oceanic crust that forms Macquarie Island (Varne et al. 2000). More than 75% of the exposed rocks on the island consist of enriched mid-ocean ridge basalt (EMORB) and minor amounts of normal mid-ocean ridge basalt (NMORB; Kamenetsky and Mass 2002). This extrusive sequence is locally in fault contact with lower crustal rocks that include sheeted diabase dykes, gabbro, and peridotite (Fig. 2.1A; Goscombe and Everard 1998). Metamorphic grades, cataclasis, mineralization, and cross-cutting relationships all suggest that these faults are spreading-related and were active during deposition of Macquarie Island's sedimentary rocks (Wertz et al. 2003; Davidson et al. 2004; Rivizzigno and Karson 2004; Daczko et al. 2005).

Sedimentary rocks make up 7% of the well-exposed extrusive sequence along coastal outcrops and typically occur as prominent horizons between individual basalt flow units. Apart from interpillow calcareous ooze, sedimentary rocks on the island primarily include basaltic and gabbroic lithofacies (Daczko et al. 2005). Basaltic lithofacies are invariably composed of basalt-clast-bearing breccias, whereas the more lithologically diverse gabbroic lithofacies contain mafic-clast-rich breccias with hydrothermally altered plutonic and extrusive clasts, sandstone, siltstone, mudstone, calcareous ooze, and chert. Chapter I concluded that basaltic breccia facies were locally derived from upper-crustal-cored faults now exposed on the island, and gabbroic clastic facies were derived from more distal (i.e. off island) lower crustal exposures in much older 27-33 Ma oceanic crust. Using geodynamic reconstructions

the cited study shows that a likely source for the gabbroic rocks would have been exposed along bathymetric highs of the adjacent Jurrut long-offset transform during Miocene time (Fig. 2.1B). Results presented here focus on the transport mechanisms and depositional environment of the gabbroic sedimentary rock lithofacies assemblage.

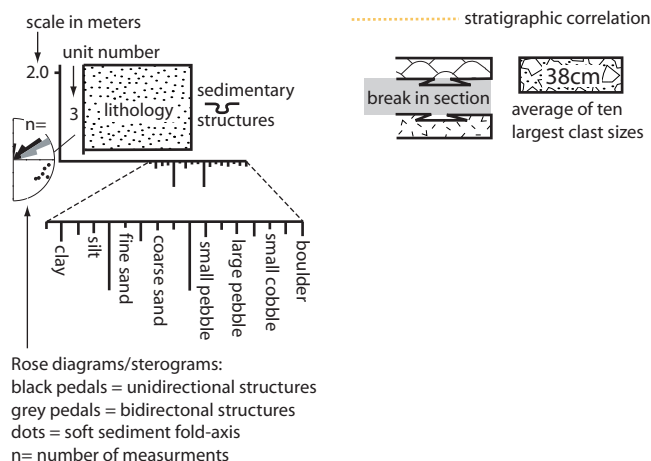
Measured Sections:

Detailed stratigraphic sections were measured from well-exposed coastal outcrops and within vertical cliff faces of the plateau escarpment on Macquarie Island (Fig. 2.1A). Sections containing lithofacies associated with gabbroic breccias are presented as they exhibit the most diverse lithology on the island relative to basaltic breccias and volcanoclastic rocks.

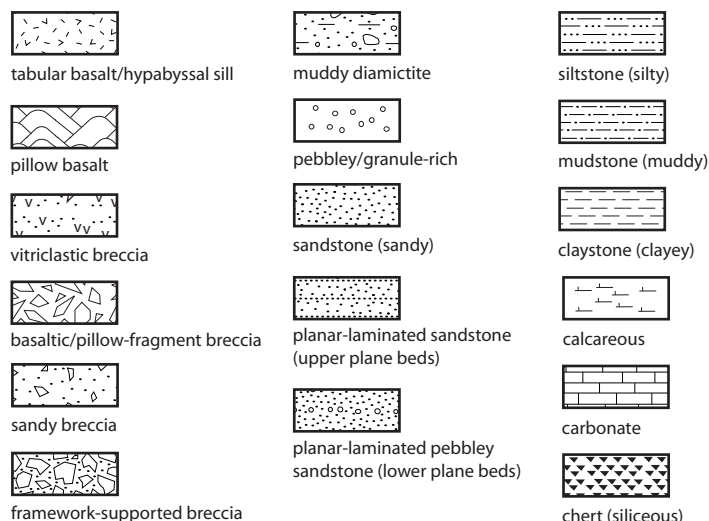
Douglas Point and Caroline Cove measured sections contain the coarsest and thickest sequence of gabbroic sedimentary rocks on Macquarie Island. They primarily include cobble breccias 5-50 m thick that are associated with pebble-granule breccia, muddy diamictite, and pebbly sandstones (Fig. 2.2A). Cobble breccias are locally interstratified with basaltic pillow-fragment breccias that laterally correlate with pillow basalt units. Both the Douglas Point and Caroline Cove sections have structural dips $>45^\circ$ and occur within 1 km of the Finch-Langdon and Caroline Cove spreading-related faults (respectively; Fig. 2.1A).

The most laterally extensive measured sections of gabbroic sedimentary rocks on the island can be correlated for 3.6 km between the Mt. Waite, Double Point, and Davis Point cliff escarpments (Fig. 2.2B). These sections have $<45^\circ$ structural dip and occur as thin intercalations within a continuously exposed >250 m thick pillow

Measured section key



Lithologies



Sedimentary structures

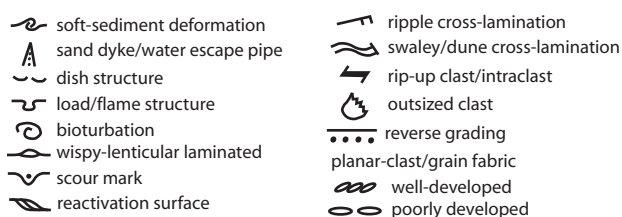


Figure 2.2 (above and following 3 pages):

Legend above explains representative stratigraphic sections from Macquarie Island depicted on following three pages. Paleocurrent indicators and soft-sediment deformation features are rotated to horizontal bedding (c.f. Potter and Pettijohn 1977).

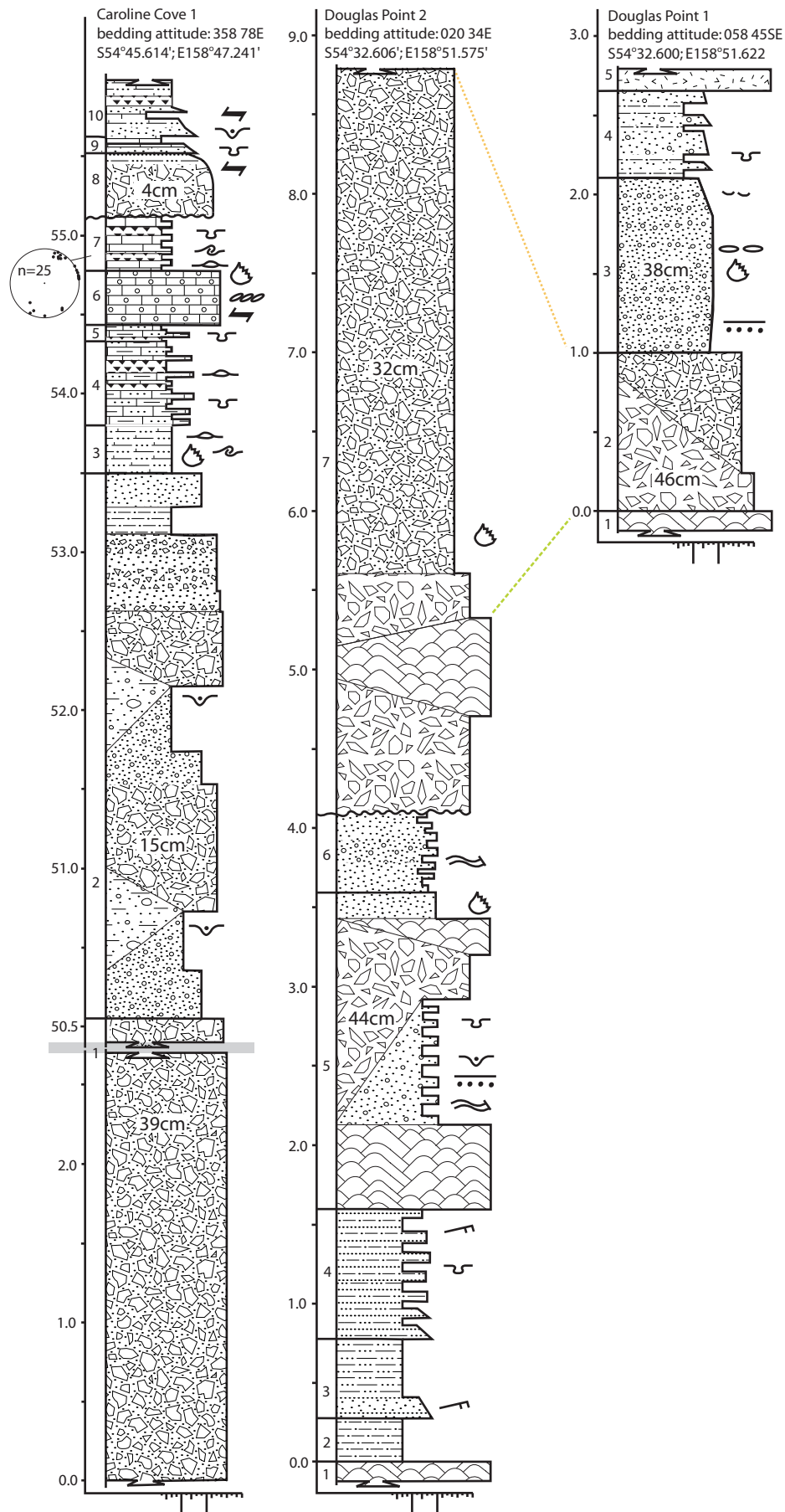


Figure 2.2A:
Very thick very coarse- to medium-grained sections from Caroline Cove and Douglas Point.

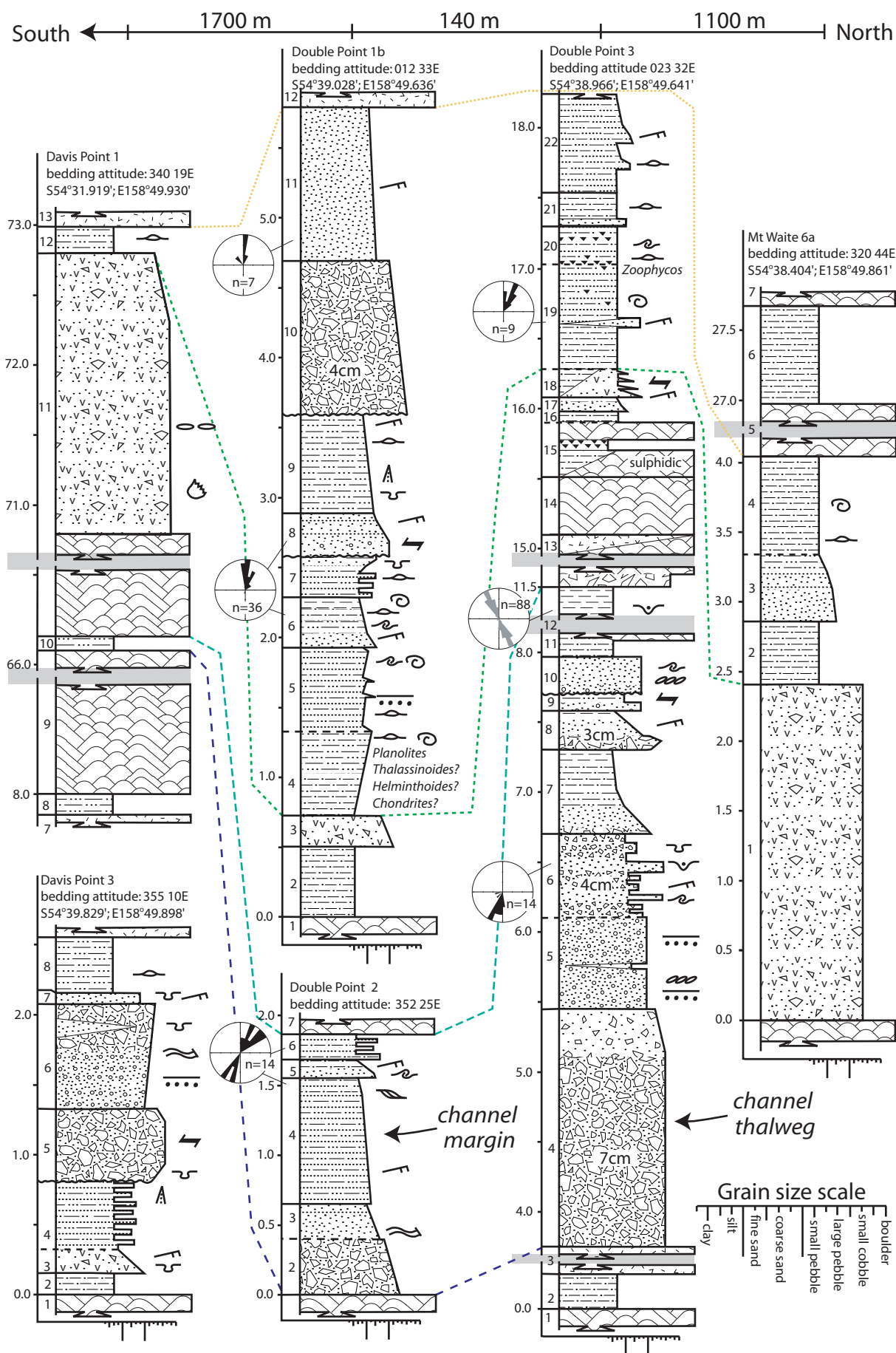


Figure 2.2B:
Laterally extensive coarse- to fine-grained sections with lenticular bedding geometries from Davis Point, Double Point, and Mt. Waite.

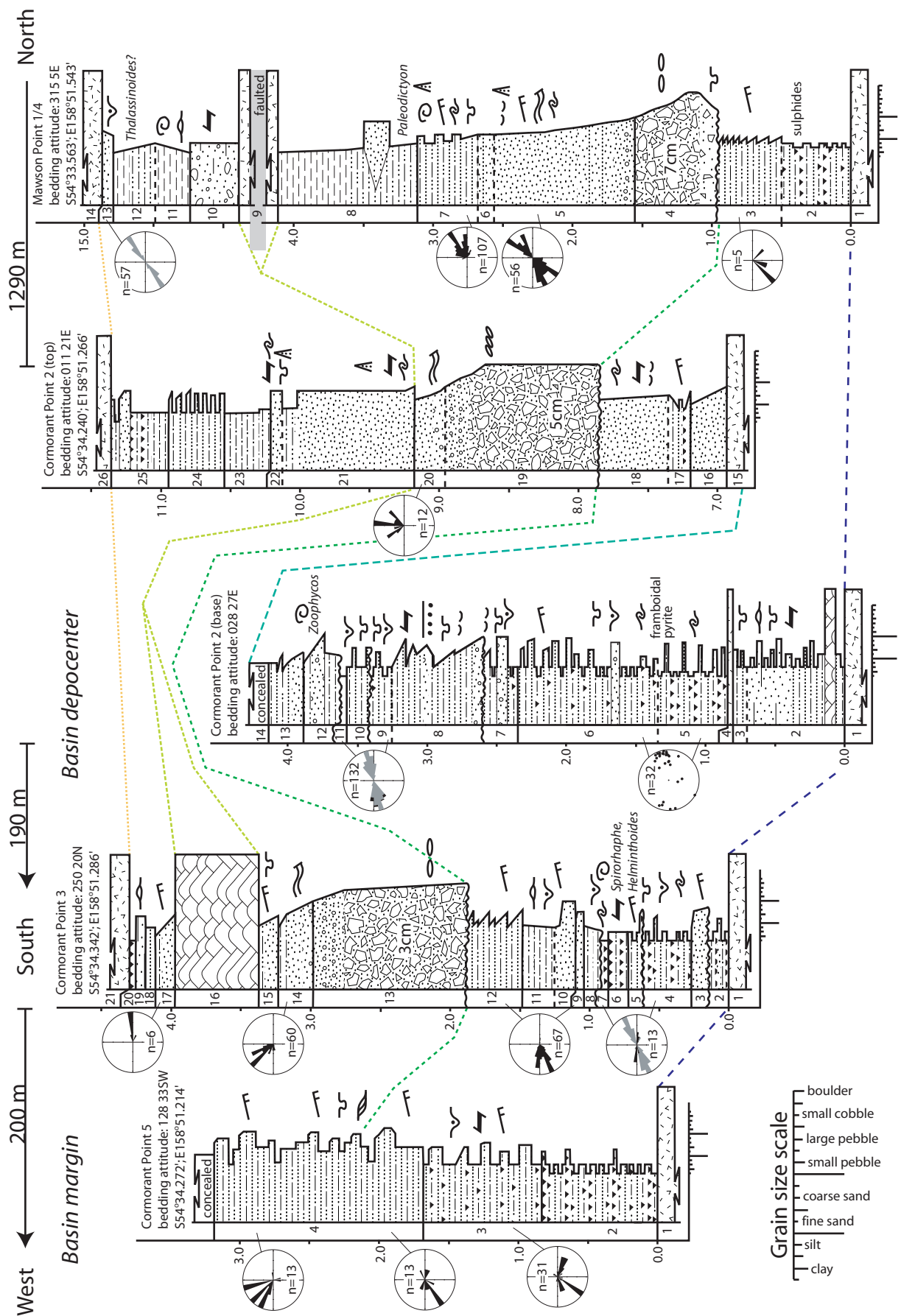


Figure 2.2C:
Tabular bedded medium- to very fine-grained sections from Cormorant Point and Mawson Point.

basalt/basaltic breccia sequence, which directly overlies low-angle listric faults and amphibolitized sheeted dykes associated with the Major Lake fault system. Section correlations are substantiated by interbedded basalt geochemistry (Murphy 2006). Outcrop sections exhibit <30 m wide channel-like morphologies that drape underlying pillow basalt (Fig. 2.3A). At Double Point an 8 m thick interval including pebble breccia, lenticular pebbly sandstone, and graded sandstone (Fig. 2.3B, C) abruptly pinches laterally into a 0.3 m thick interval of ripple-bedded sandstone and sandy mudstone (Fig. 2.2B, 3D). Paleocurrent indicators in all units indicate a northerly flow and are sub-parallel to the channel-axis trend.

The best preserved sections on Macquarie Island occur in tidal washed platform exposures for 1.6 km between Mawson and Cormorant points (Fig. 2.2C). Here, gabbroic sedimentary rocks occur as relatively thin tabular intercalations within tabular basalt flows that are >10 m thick (Fig. 2.3E). Sections can be correlated based upon basal key marker units enriched in sulphide minerals (Fig. 2.2C). Overall bedding in these sections coarsen and thicken upward from interbedded siltstone (siliceous mudstone; see Stow and Piper (1984) for terminology background) and ripple-bedded sandstones up into pebble-granule breccia, graded sandstone, and sandy red mudstones. Pebble-granule breccia and graded sandstones are prevalent in the thickest basin-center sections and laterally correlate with ripple-bedded sandstones in thinner condensed sections along basin margins. Paleocurrent indicators are variable, with some showing a nearly 180° difference within an individual graded sandstone facies (unit 5 in Mawson Point 1/4 of Fig. 2.2C).

Lithofacies:

Sedimentary facies analysis complimented with petrographic examination is used to characterize the depositional flow mechanisms that produced the relatively diverse gabbroic sedimentary rock assemblage. Eight lithofacies are recognized on the basis of grain size, texture, fabric, sedimentary structures, bedding geometry, and composition. Their diagnostic and most unique features are described below, with descriptions and associations presented in Table 2.1. All clast/grain compositions are ophiolitic unless otherwise noted. Gabbroic breccia clast counts identified basalt, gabbro, diabase, and their hydrothermally-altered equivalents (Fig. 2.4A). Primary hydrothermally-altered detrital minerals in petrographic thin sections of associated sandstones include laumontite, prehnite, epidote, iron oxides, phyllosilicates, wairakite, quartz, analcite, and sulphides (Fig. 2.4B).

Cobble breccia facies

Description

The cobble breccia lithofacies is characterized by very thick (>5 m) structureless beds of poorly sorted framework-supported breccia. Clasts average a maximum size of >7 cm. Large outsized boulders up to 3 m in diameter of both pillow basalt and diabase typically have smaller pebbles and cobbles of the same lithology surrounding them (Fig. 2.5A). This concentration of clast compositions is best observed between clasts that have easily recognizable lithologies (Fig. 2.5B). Matrix is composed of 20-40% red sandy mudstone. This facies has erosional basal contacts and sharp upper contacts with pebbly sandstone facies. It typically occurs proximal to major spreading-related faults.

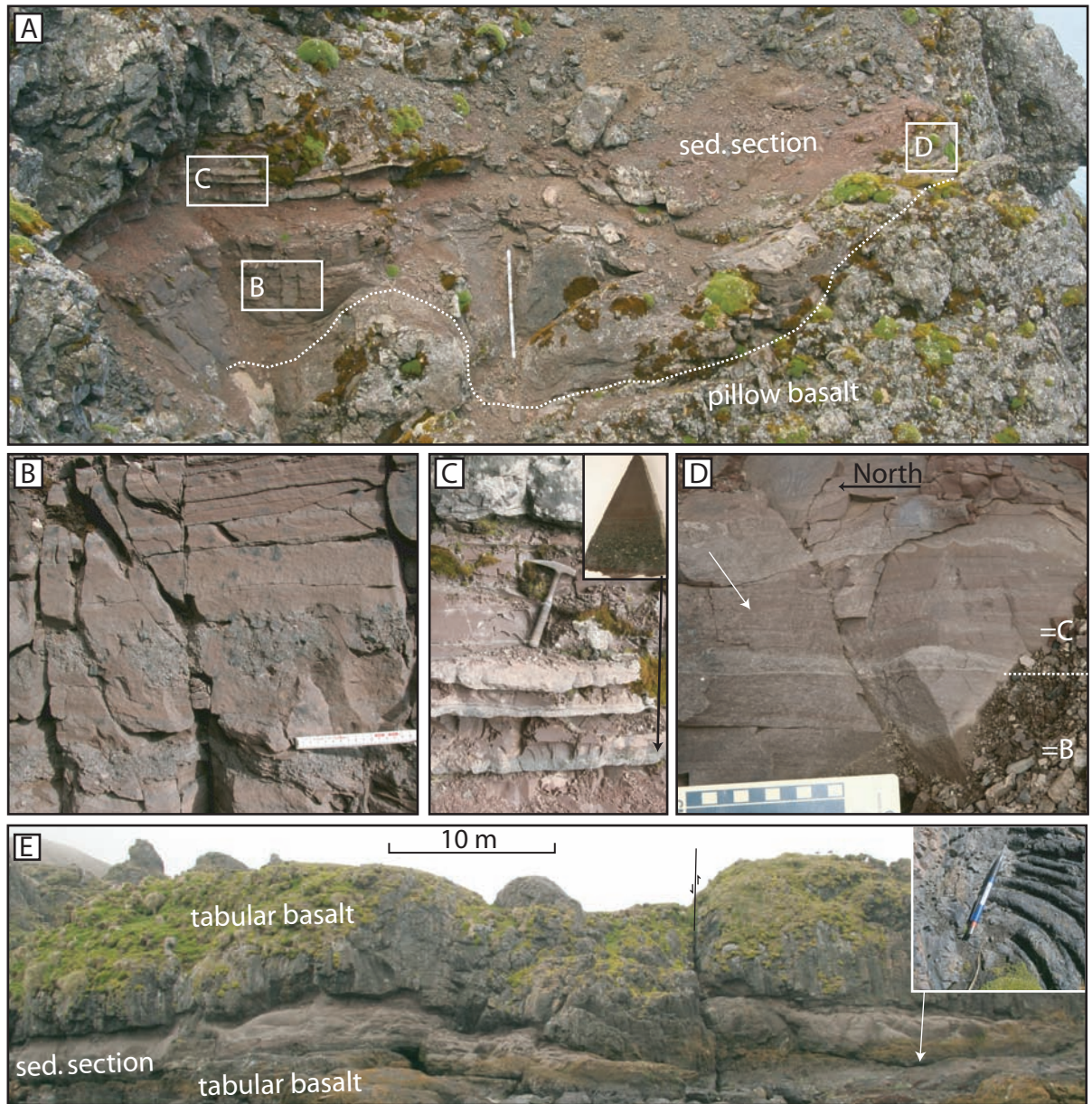


Figure 2.3:
Measured section bedding morphologies. A) Channelized sequence looking south from Double Point 3. Dashed line indicates boundary between pillow basalt and overlying sedimentary (sed.) section. Boxed letters refer to Figure 2.3B-D. Measuring staff is 1.8 m. B) Pebble breccia and pebbly sandstone with internal scour surfaces from basal units in channel center. Ruler shows 16 cm. C) Three sequential graded sandstone-mudstone units from upper units in channel center. Inset shows lowermost unit. Hammer is 30 cm. D) Channel margin units containing graded sandstone and overlying ripple bedded sandstone that are laterally equivalent to units shown in B and C, respectively. Ripple bedded unit contains reactivation surface (arrow). Scale in cm. E) Laterally extensive tabular bedded sedimentary section from Mawson Point intercalated within thick tabular basalt flows. Inset shows ropey corrugations on top of lower basalt, pencil is 14 cm.

Table 2.1.: Macquarie Island gabbroic sedimentary rock lithofacies

Facies; relative percentage	Diagnostic lithologies, average clast/grain size*	Lithology (if multiple): predominate sedimentary structures; clast/sand texture#	Average bed thickness and bedding geometry, <i>ichnogenera</i>	Lithofacies associations, nature of basal contacts	Primary depositional mechanisms
Cobble breccia 10%	Cobble breccia with scattered boulders. 20-40% sandy red mudstone matrix	Clast-supported, structureless; very angular, very poorly sorted	5 - 50 m thick beds, wedge shaped, lateral extent dependent upon localized faults.	Lateral gradation with pillow-fragment breccias, erosive contacts with lenticular pebbly sandstone and muddy diamictite facies	Gravelly cohesionless debris flows. Very proximal.
Muddy Diamictite 5%	Sandy brown marlstone with 10:1 biogenic ooze: ophiolitic clasts; sandy red mudstone with ophiolitic clasts. Pebble to cobble-sized clasts, >80% clayey matrix	Matrix-supported, structureless, well-developed planar clast fabric, rip-up clasts; very angular to plastically deformed ooze clasts, very poorly sorted	0.5-2.0 m thick beds, irregular to lenticular shaped,	Sharp lateral association with pebbly sandstone and sandy mudstone facies, sharp contacts with sandy mudstone and ripple bedded sandstone facies	Cohesive debris flow. Very proximal.
Pebble-granule Breccia 20%	Pebble to granule rich breccia ± scattered cobbles, 5-20% sandy red mudstone matrix (respectively)	Clast-supported, poorly developed planar-clast fabric, rip-up clasts, underlying detached flame structures, and coarse-tail graded with localized basal matrix support or reverse grading; angular, poorly sorted	0.3 - 1 m thick beds, pinch-and-swell shaped influenced by local faulting	Sharp lateral association with lenticular pebbly sandstone facies, erosive contacts with sandy mudstone and ripple bedded sandstone facies	Gravelly cohesionless debris flows and basal part of stratified density flows. Proximal to medial
Lenticular pebbly sandstone 20%	Very coarse- to medium-grained sandstone with scattered boulders, cobbles, and pebbles. 5-10% red mudstone matrix	Small-scale reverse graded intervals or large-scale normal grading, thick discontinuous wavy to planar 3-10 cm thick laminations, well-developed planar-clast fabric, internal scour surfaces; angular to subround, moderate sorting	0.5 - 1.0 m thick beds, lenticular shaped	Sharp contact with cobble breccia, sharp to gradational contact with pebble-granule breccia and lenticular pebbly sandstone facies, erosive contacts with sandy mudstone and ripple bedded sandstone facies	Sandy cohesionless debris flows and transitional interval in stratified density flows. Proximal.
Graded sandstone 20%	Very coarse-grained (± granules) to very fine-grained sandstone through siltstone, sandy to clayey mudstone. 1-7% red mudstone matrix	Sandstone: normal grading, continuous parallel lamination, swaley to sigmoidal cross-bedding /or/ structureless with water-escape structures, climbing ripple cross-stratification; angular - round, moderate to good sorting. Siltstone: planar to wavy laminated, convolute and contorted lamination, flame structures, rare bioturbation. Mudstone: graded sand to silt, structureless	0.1 - 3.0 m thick beds, tabular shaped, <i>Zoophycos</i> , <i>Paleodictyon</i>	Lateral gradation with sandy mudstone, Gradational contact with pebble-granule breccia and lenticular pebbly sandstone, erosive basal contacts with graded sandstone, sandy mudstone, arlstone, and ripple bedded sandstone facies	Turbidity currents and upper part of density stratified density flows, Proximal to medial
Ripple-bedded sandstone 5%	Fine to coarse-grained sandstone, granule lags	Sandstone: ripple cross-stratification, reactivation surfaces, mud-drapes, normal grading, wavy-laminated; angular - subround, very poorly to well sorted. Granules: structureless, scour surfaces, rip-up clasts: very angular, poorly sorted	1 - 10 cm thick beds, wedge to lenticular shaped	Lateral gradation with graded sandstone facies, sharp contacts with arlstone and sandy mudstone.	Channel margin turbidite levee deposits, sand-laden bottom currents
Sandy red mudstone-siltstone 15%	Siltstone, sandy red to umber colored mudstone ± siliceous or calcareous, coarse- to fine-grained sandstone, sand is 10:5:1 ophiolitic:biogenic:vitic	Sandy mudstone/siltstone: structureless to very thin wispy laminated, reverse and normal grading, moderate to pervasive bioturbation; sand is angular and poorly sorted. Sandstone: basal scour surfaces: angular - round, good sorting	Mudstone/siltstone: 0.5 - 3 m thick beds, tabular to pinch-and-swell shaped. Sandstone: 0.2 - 2 cm thick laminae, continuous, and planar to lenticular <i>Chondrites?</i> , <i>Planolites?</i> , <i>Thalassinoides?</i> , <i>Zoophycos</i>	Gradational lateral and basal contacts with graded sandstone and ripple bedded sandstone facies.	Mud-laden bottom current reworking of hemipelagic deposits
Arlstone 5%	Sandy marlstone (calcareous mudstone), sandy arlstone (siliceous mudstone), and chert ± disseminated sulphide laminae. Sand is 10:1 biogenic:ophiolitic	Pervasive to absent bioturbation, abundant soft sediment deformation, scoured surfaces, continuous planar/wavy/pinch-and-swell lamination; sand is angular and poorly sorted	1-3 cm thick laminae, tabular shaped <i>Spirorhaphe</i> , <i>Helminthoides</i>	Sharp contacts with interbedded ripple bedded sandstone, muddy diamictite, and graded sandstone facies	Hemipelagic to pelagic ± chemogenic deposits

* All clast/ grain compositions are ophiolitic unless noted.

Rounded grains only include volcanic lithic grains.

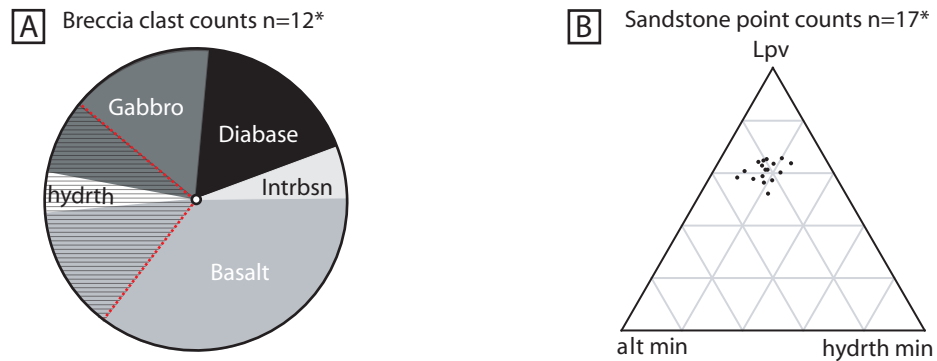


Figure 2.4:

A) Pie chart represents a total of 796 clasts counted from 12 gabbroic breccia exposures at >50 clasts per site. Hydrothermally altered plutonic (includes both gabbro and diabase) and volcanic clasts are shown by hatched overlay. Discrete hydrothermal mineral clasts (hydrth) include epidosite, prehnite, and zeolites minerals. Intrabasinal clasts (intrbsn) include sandy red mudstone and calcareous ooze.

B) Ternary diagram of 17 point counted medium-grained sandstones representing 500 grains counted per sample, not including cement, using the Gazzi-Dickinson method (Ingersoll et al. 1984). Plutonic/volcanic detritus (Lpv) includes igneous lithic grains, plagioclase, and clinopyroxene. Alteration minerals (alt min) include chlorite, amphibole, hematitic clays, and smectitic clays. Hydrothermal minerals (hydrth min) include epidote, prehnite, quartz, laumontite, analcite, wairakite, unidentified zeolites, and tectonic lithics.

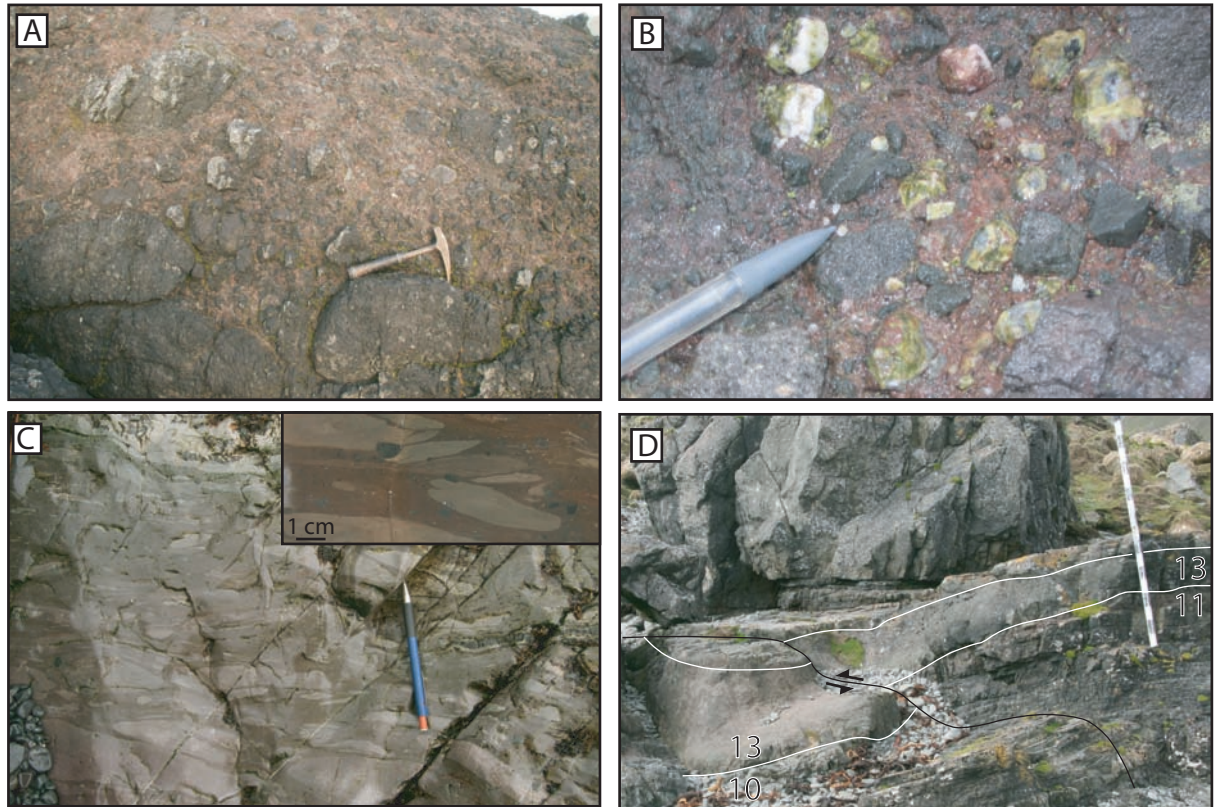


Figure 2.5:
Breccia facies from sections in Figure 2.2. A) Boulder-bearing cobble breccia facies with red mudstone matrix overlying pillow-fragment breccia and pillow basalt from Douglas Point 2 unit 7. Hammer is 30 cm long. B) Cobble breccia facies with epidote-prehnite clasts showing low clast disaggregation within red mudstone matrix. From Caroline Cove 1 unit 1. Pencil tip is 2 cm. C) Marlstone diamictite facies from Caroline Cove 1 unit 6. Pencil is 14 cm. Inset shows dark ophiolitic clasts and light plastically deformed cobbles of foraminifera ooze. D) Pebble-granule breccia facies from Cormorant Point 3 unit 13 truncating underlying units 12-10 (numbered). Unit 12 is completely truncated in photo. Breccia shows abrupt thickening change across syn-sedimentary fault. Staff is 1.8 m tall.

Interpretation

Very poor sorting, framework-support, relatively high matrix percentages, structureless nature, and coarse clast size in this facies indicate that the depositing flow had a high sediment concentration and high yield strength (Fisher 1971; Enos 1977; Lowe 1982). Clast support mechanisms would have been balanced between a cohesive muddy matrix and proficient dispersive pressures. These features are characteristic of cohesionless debris flows (c.f. Postma 1986; Gani 2004). The lack of prominent stratification or intra-unit pelagic beds indicates that this facies was emplaced without any significant hiatus during deposition.

Muddy diamictite facies

Description

Muddy diamictite facies is characterized by a matrix (>80%) of red sandy mudstone or brown to green marlstone with scattered small pebbles and large cobbles. Clasts within red mudstone diamictites are entirely ophiolitic in origin, but marlstone diamictites primarily contain 2-30 cm large clasts of foraminifera-rich carbonate ooze (Fig. 2.5C) and minor amounts (<10%) of ophiolitic clasts. Biogenic clasts show bedding-parallel attenuation and create a well-developed planar clast fabric. They have elongate ovoid geometries and locally exhibit plastic deformation. Basal contacts are sharp and generally non-erosive, but underlying units of marlstone facies locally occur as rip-up clasts within the diamictite. Bedding is structureless and generally <2 m thick.

Interpretation

A planar-clast fabric, high proportion of argillaceous matrix, and large outsized clasts diagnostic of this facies are typical of cohesive debrites (debris flow

deposits) that were deposited by a laminar flow with high matrix strength (Fisher 1971; Shanmugam 1996; Mulder and Alexander 2001). A plastic rheology and strong sense of shear in the flow is best expressed by a strong preferred orientation of clasts that show bedding-parallel plastic deformation.

Pebble-granule breccia facies

Description

The pebble-granule breccia facies is distinguished by framework-supported clasts with average sizes of 2-7 cm and 5-20% red mudstone matrix. This facies is typified by well-developed coarse-tail grading, but locally, the basal 10 cm exhibits matrix-support or reverse grading. Beds are 0.3 to 2.0 m thick with coarser clast sizes being more prevalent in thicker beds. Locally, abrupt changes in bedding thickness occur where this facies is cross-cut by faults and incorporated as matrix into the fault gouge (Fig. 2.5D). Erosional basal contacts are common with underlying mudstone units entrained into large flame structures and rip-up clasts (Fig. 2.3B). Breccias have sharp upper and lower contacts with pebbly sandstone facies and gradational upper contacts with graded sandstone facies.

Interpretation

Low matrix percentages indicate very high particle concentrations, which would have suppressed flow turbulence and maintained a non-Newtonian flow rheology (Gani 2004). Total argillaceous matrix compositions of <20% are not enough to provide the necessary matrix strength to support pebble-sized detritus (Hampton 1975). Therefore, dispersive pressure and buoyant lift were the likely clast-support mechanisms. These features, including coarse-tail grading, are characteristic of cohesionless debris flows (Fisher 1971; Middleton and Hampton 1976; Mulder and

Alexander 2001; Gani 2004; Amy et al. 2005). Rare basal reverse grading, matrix support, large flame structures in underlying units, and rip-up clasts indicate a basal cohesive shear surface that was maintained by erosion and entrainment of a muddy substrate.

Pebbly sandstone facies

Description

Lenticular beds 0.5-1.0 m thick that contain very coarse- to medium-grained sandstone with outsized clasts typify the pebbly sandstone facies. Clasts are boulder- to granule-sized depending upon clast sizes in associated breccia facies. Clasts are typically organized into elongate planar lags that have well-developed planar clast fabric (Fig. 2.6A). The facies comprises alternating cm-scale very coarse- and medium-grained sand laminae with planar to wavy geometries (Fig. 2.6B). Thicker laminations are locally reverse graded (Fig. 2.6C). Sandstones contain 5-10% red muddy matrix. This facies typically has sharp basal contacts with cobble and pebble-granule breccia facies. Locally pebbly sandstone facies occurs as a transitional normal graded unit that grades upward into overlying graded sandstone facies.

Interpretation

The presence of floating granules with well developed planar-clast fabric, planar to wavy lamination with localized reverse grading, and relatively low mud matrix percentages indicate that the depositing flow had a laminar state and frictional grain support. The localized association of reverse grading with planar stratified clast lags is comparable to the diffusely stratified traction carpets of Sohn (1997). Traction carpets indicate high-particle concentrations and dispersive pressures that suppress fluid turbulence creating a non-Newtonian flow rheology for

this facies. However, the local preservation of normal grading is more indicative of a Newtonian flow rheology. The common association of this facies with underlying pebble-granule breccia and/or overlying graded sandstone facies suggests that it provided a rheological transition between a contemporaneous cohesionless debris flow and/or turbidity flow (see graded sandstone facies). This transition between laminar and fluidal flow state is partly controlled by the original particle concentration during deposition and therefore indicates density stratification within the gravity flow. Therefore, we use the term *densite* (*sensu lato* Gani 2004) for the transitional lithofacies deposited by these density-stratified gravity flows (density flows).

Graded sandstone facies

Description

The graded sandstone facies is characterized by tabular beds that exhibit normal grading from granule-rich very coarse-grained sandstone up into sandy mudstone (e.g. Mawson Point 1/4 units 4-8 in Fig. 2.2C). Beds are laterally extensive for up to 1.6 km, < 3 m thick, and commonly have bioturbated tops. Thicker units contain a vertical succession of sedimentary structures including, from bottom to top, structureless, upper-plane bed, dune-scale sigmoidal to swaley cross-beds or critically-climbing ripples, planar to wavy laminated with ripple interbeds, planar silty laminae (Fig. 2.6D-E). Units that do not exhibit cross-bedded intervals are structureless with or without water escape pipes and dish structures (bottom of Fig. 2.6E). Convolute lamination and flame structures are common in upper finer grained sandstone and siltstone intervals. Capping mudstone units contain *Zoophycos* and *Paleodictyon* ichnogenera (Fig. 2.6F). Thin beds have erosive basal contacts and thick

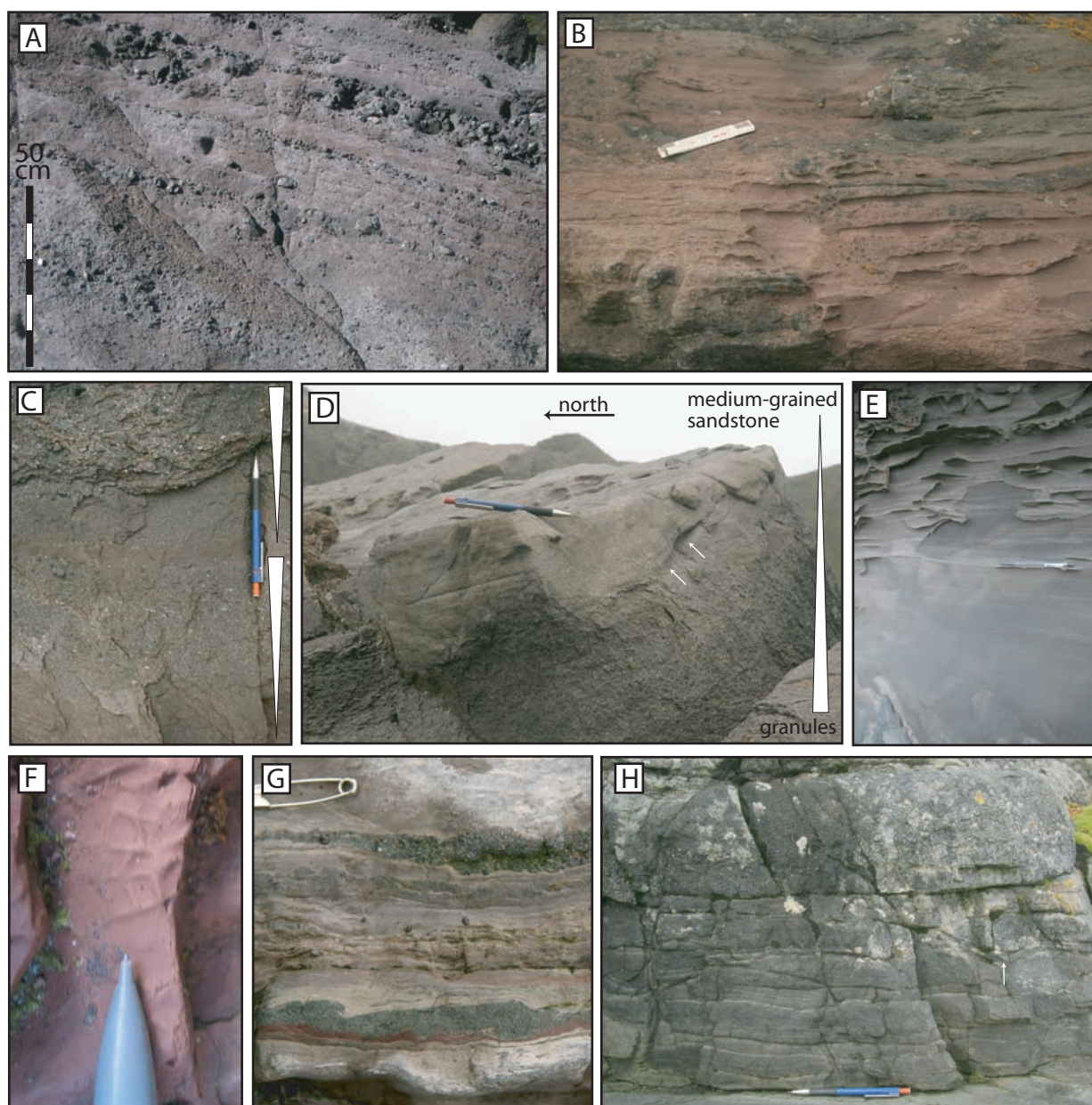


Figure 2.6:

Sandstone facies. Units and sections refer to Figure 2.2. A) Pebbly sandstone facies with planar laminations defined by cobbles and pebbles set within a very coarse-grained sandstone. From Douglas Point 1 unit 3. B) Thickly laminated fine and coarse-grained sandstone from pebbly sandstone facies in unit 5 of Douglas Point 2. Ruler is 14 cm long. C) Pebbly sandstone facies with a thin red mudstone parting between reverse graded fine/medium-grained sandstone to granule intervals. From unit 6 of Davis Point 3. Pencil is 14 cm long. D) Oblique 3D geometry of sigmoidal cross-beds (right of pencil) from graded sandstone facies. Granule lags along northwest dipping (i.e. out of page) bounding surfaces (arrow). From Cormorant Point 3 unit 14. E) Graded sandstone facies from units 5-7 in Mawson Point 1/4 with structureless base overlain by planar laminated and ripple laminated intervals. Structureless base is laterally equivalent to cross beds shown in D. F) *Paleodictyon* ichnogenes on bedding plane exposure of uppermost mudstone unit in graded sandstone facies from unit 8 Mawson Point 1/4. Pencil tip is 1 cm. G) Thin poorly sorted granule-rich lags of ripple bedded sandstone facies interbedded within marlstone facies. From Caroline Cove 1 unit 4. Paper clip is 3 cm. H) Thin bedded ripple- to wavy-laminated sandstone with mudstone partings in basin marginal ripple-bedded facies of Cormorant Point 5 unit 4. Note internal scour surface (arrow).

beds have gradational basal contacts with underlying pebbly sandstone and/or pebble-granule breccia facies.

Interpretation

The ubiquitous presence of normal graded sandstone in this facies is traditionally interpreted to be deposited from suspended fallout in a waning turbidity current (Kuenen and Migliorini 1950; Sanders 1965; Middleton 1967). The continuity of normal grading along with a vertical succession of bed forms in the thicker sections indicate waning flow regime along with bed load traction and typifies the classical Bouma sequence (Bouma 1962). Although the presence of bed load traction features in turbidites are controversial (see Shanmugam 1997 for review), the continuity of normal grading through the vertical succession of bedforms and the presence of climbing ripple lamination are diagnostic features of turbidity current deposition (Sanders 1965). Climbing ripple lamination indicates traction transport from a fluidal Newtonian current with a high sedimentation rate (Sanders 1965; Gani 2004). Lateral correlation of cross-stratified sandstone with structureless sandstone bearing water escape features suggests fluidization locally destroyed primary lamination.

Ripple-bedded sandstone facies

Description

Distinguishing characteristics of the ripple-bedded sandstone facies include very thin to thin lenticular beds of fine- to very coarse-grained sandstone with ripple to wavy lamination. Structureless granule lags are locally present (Fig. 2.6G). Sandstone beds are separated by very thin mudstone partings and drapes (Fig. 2.6H). Normal grading is rare. Reactivation surfaces locally occur within units that laterally

correlate with graded sandstone facies (Fig. 2.3D). Pebble-size rip-up clasts derived from underlying arlstone facies are common in coarser grained ripple bedded facies. Basal contacts are typically sharp to erosive. Bed form paleocurrent indicators within this facies are typically parallel to scoured and fluted surfaces within interbedded arlstone and sandy red mudstone facies. Locally, these indicators are near perpendicular to paleoslope directions measured from soft-sediment deformation folds and paleocurrent indicators in associated graded sandstone facies (Fig. 2.2C). This perpendicular relationship is only observed in facies intercalated within tabular basalt sequences, but not channelized facies associated with pillow basalt (Fig. 2.2B).

Interpretation

The near-perpendicular relationship between paleoflow directions in this facies vs. paleoslope and turbidity current directions measured from associated graded sandstone and arlstone facies, suggests that the depositing flow for ripple-bedded sandstone facies was subparallel to bathymetric contours. This relationship is by definition indicative of contour currents (Heezen et al. 1966). Although the paleoflow direction of bottom currents can be quite variable (Okada and Ohta 1993; Ito 1996), 90° of separation between gravity flow and bottom current directions is well documented in mixed turbidite-contourite sequences (e.g. Lovell and Stow 1981; Stanley 1993). A sandy contourite interpretation is also supported by the punctuation of this facies within muddy contourites of the sandy red mudstone facies (described next). In addition, fluctuating high to low velocity bottom currents and substrate winnowing is recorded by erosive gravel lags, truncation of underlying sandy red mudstone facies, reactivation surfaces, and mud partings. Where this facies laterally correlates with turbidites of the graded sandstone facies, it likely records the

reworking of channel levee and basin marginal “spill-over” turbidites (c.f. Stanley 1993).

Sandy red mudstone facies

Description

The sandy red mudstone facies is predominantly characterized by structureless and bioturbated red mudstone beds 0.5-3 m thick that contain 30-50% disseminated fine-grained sand to silt. The facies variably contains mm-scale laminations that are composed of silt to very fine-grained sand. Sand is primarily composed of ophiolitic grains with minor amounts of fragmented biogenic tests and devitrified glass shards. Silt laminae are commonly <1 mm thick, discontinuous, and wispy to mottled, and commonly exhibit pervasive to moderate bioturbation (Fig. 2.7A). Ichnogenera are commonly present and include *Planolites*, *Zoophycos*, *Chondrites?*, *Thalassinoides?*, and *Helminthoides?* (Fig. 2.7A, B). Sand laminae are 1-3 mm thick, continuous, planar, and locally occur above planar scour surfaces (Fig. 2.7C). Locally, sand laminae thicken upward within the lower half of reverse-to-normal graded sequences, which grades from mudstone into mottled sandy siltstone back into mudstone (Fig. 2.7A). These sequences typically have a gradational basal contact with thin underlying ripple-bedded or graded sandstone facies that truncates underlying sandy red mudstone facies (Fig. 2.7B). In addition, the sandy red mudstone facies commonly grades laterally into the upper mudstone interval of graded sandstone facies.

Interpretation

The local preservation of complete reverse-to-normal graded mudstone/siltstone sequences with pervasive bioturbation is similar to the classical contourite sequence described from the Faro Drift (Gonthier et al. 1984). Rare very

thin lenticular sand laminae above scour surfaces suggest that periodic pulses of bottom current erosion were associated with locally entrained starved ripples (c.f. Shanmugam et al. 1993; Stanley 1993). Bottom current velocity fluctuation is also supported by the superposition of coarsening/thickening-upward sandstone laminae within reverse graded mudstone-siltstone sequences. Sedimentary structures indicating fluctuating bottom current velocities typify contourites, though they could also be due to variation in sediment supply and/or biologic productivity (Stow et al. 1986; Faugères and Stow 1993). The sharp contacts of sand laminae are typical of sandy contourites (Shanmugam et al. 1993) and the mixture of biogenic tests with volcanoclastic sand and moderate to pervasive bioturbation within structureless mudstone is more common in muddy to silty contourites (Stow et al. 1998). A contourite drift interpretation is supported by the association of this facies with sandy contourites of the ripple-bedded sandstone facies.

Arlstone facies

Description

Structureless to well-laminated arlstone (siliceous mudstone), marlstone (calcareous mudstones), chert, and calcareous ooze characterize the arlstone lithofacies. Where bioturbation hasn't destroyed bedding this facies is well-bedded with sharp lithologic contacts (Fig. 2.7D). Bedding is typically on a cm-scale and typically exhibits pervasive soft-sediment slump-folds with local cross-cutting clastic dykes. Chert units contain recrystallized radiolarian tests, as well as, disseminated sulphide laminations and pyrite framboids. Bedding planes between chert and arlstone preserve horizontal grazing trace fossils akin to *Spirorhaphe* and *Helminthoides* (Fig. 2.7E). Upper siliceous bedding planes are extensively scoured

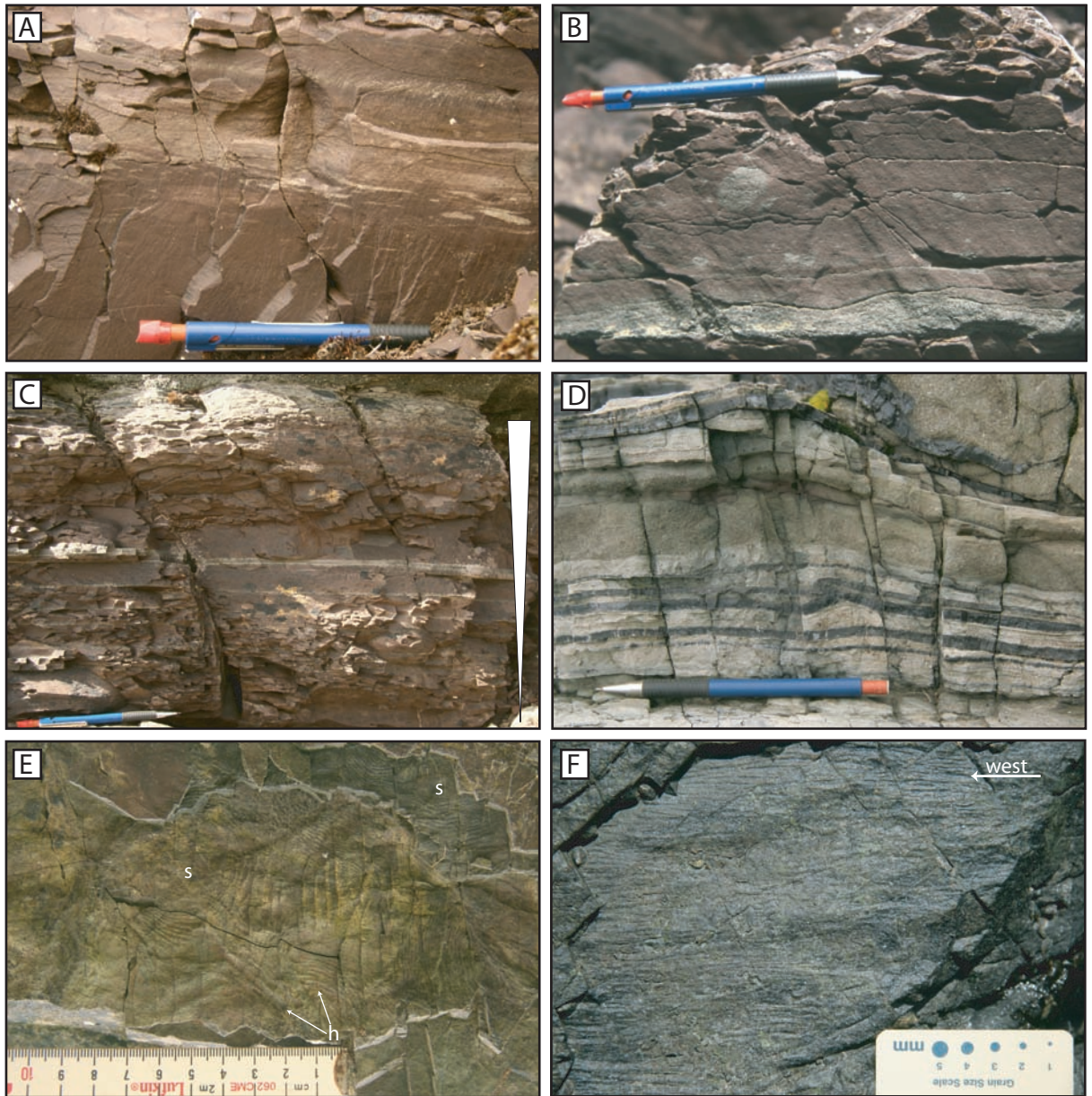


Figure 2.7:

Sandy red mudstone (A-D) and siltstone (E-F) facies. Units and sections refer to Figure 2.2. Pencil is 14 cm long. A) Lenticular laminated mudstone grading upward into wispy laminated siltstone that fines up into massive mudstone with planar silt laminae. Pervasive bioturbation has forms akin to *Chondrites?* and/or *Helminthoides?* ichnogenera. From Double Point 1 unit 5. B) Ripple bed fining upward into massive sandy red mudstone with subspherical *Planolites* and burrow fills. From Double Point 1 unit 6. C) Very thin planar sandstone laminae thicken upward within a coarsening upward sequence from massive mudstone into wispy laminated siltstone. From Double Point 1 unit 7. D) Thickly laminated chert (black) and siltstone (white) interbedded with ripple bedded sandstone facies from Cormorant Point unit 6. E) *Spirorhappe* (s) and *Helminthoides* (h) grazing traces on underside of siltstone bed from Cormorant Point unit 6. Scale in cm. F) Flute mold from scoured chert bedding plane from unit 11 in Cormorant Point 2.

(Fig. 2.7F) where interbedding with invariably associated ripple bedded sandstone facies is most prevalent.

Interpretation

High proportions of well-preserved biogenic tests and very little sand-sized detritus in chert and ooze beds typify pelagic deposition, whereas sandy siltstone and marlstone lithologies at the high paleolatitude of the PMSR (~56°S) is more indicative of hemipelagic sedimentation (Stow et al. 1996; Stow and Tabrez 1998). A hemipelagic interpretation is used in its widest sense, since the sand composition in the siltstones is invariably oceanic crust derived rather than terrigenous as initially intended for hemipelagites (see Stow and Tabrez 1998). A concentration of sand in the argillaceous units may also be due to bottom current winnowing of other sandy facies, but the well-preserved nature of biogenic grains attests to a low degree of traction transport. Disseminated sulphide in the siliceous units also indicates some chemogenic input from hydrothermal exhalation (James et al. 1998).

Discussion:

Detrital source and origin of gravity flows

Despite an acceptable source of sediment being derived from hydrothermally-altered fault zones along the PMSR (Daczko et al. 2005; Chapter I); its generation within the marine environment remains unexplained. Unlike sedimentary and volcanoclastic rocks derived from continents and volcanic arcs, sediment production through erosion in the abyssal mid-ocean environment is subdued. Possible mechanisms to generate the sand- to gravel-sized detritus prevalent in Macquarie Island's gabbroic sedimentary lithofacies are discussed below.

Fault zone source

Hydrothermally altered clasts and associated minerals make up 20-40% of gabbroic breccias and associated sandstones (Fig. 2.4) and are comparable in composition to authigenic mineral assemblages within spreading-related fault zones of the island (Wertz et al. 2003; Daczko et al. 2005; Davidson et al. 2004).

Hydrothermally altered cataclastic zones along Macquarie Island's major spreading-related faults are 1-2 km wide and are composed of highly fractured igneous bedrock with networks of 0.1-20 cm wide hydrothermal mineral veins (Wertz et al. 2003, Davidson et al. 2004; Rivizzigno and Karson 2004). This lead Daczko et al. (2005) to the conclusion that the "physical disintegration and tectonic abrasion" of oceanic crust in hydrothermally altered fault zones could produce the gravel- to sand-sized detritus observed in Macquarie Island sedimentary rocks. Such an interpretation is supported by the presence of thick talus ramparts that flank uplifted fault blocks along active mid-ocean ridge transforms (Karson and Dick 1983; Karson et al. 1984; Tivey et al. 1998). Furthermore, denudation of weakened bedrock along modern mid-ocean ridge fault zones typically exploits joints, fissures and fractures where hydrothermal alteration and seafloor weathering are most prevalent (Alt et al. 1986; Zonenshain et al. 1989; Swift 1991; Mitchell et al. 2000).

Compared to Macquarie Island fault zones, a much more voluminous source of fault zone generated sediment would have been available along the proposed ~550 km long Jurru transform source region (Chapter I; Fig. 2.1B). At least 10 Myr of "tectonic grinding" during the lag time between the detrital zircon crystallization ages (27-33 Ma) and the depositional age (~9 Ma) for Macquarie Island's sedimentary rocks (Quilty et al. 2008; Chapter I) could theoretically have generated a large quantity of potential detrital material to be tectonically denuded. This lag time is

poorly constrained and relies upon maximum estimates of 10 Myr for cooling and uplift of plutonic oceanic crust (c.f. John et al. 2004). Transpression along the Juru transform between 20 and 10 Ma (Meckel 2005; Mosher and Massell-Symons 2008) formed a robust transverse ridge that created the necessary bathymetric relief to generate large submarine gravity flows (Fig. 2.8A). Up to 4000 m of bathymetric relief has been observed along the Romanche transverse ridge of the mid-Atlantic ocean (Bonatti et al. 1994; Pockalny et al. 1996) and between 600-1200 m of relief along individual transform-parallel fault scarps along the Atlantis Bank transverse ridge in the Indian Ocean (Baines et al. 2003). Tectonism and associated seismicity focused along the Juru transverse ridge initiated fault rupture and mass wasting of hydrothermally altered fault zone sediment, which was released in copious amounts to the PMSR sea floor via gravity flows (Fig. 2.8A). Syn-depositional seismicity is preserved in Macquarie Island lithofacies by: i) fault gouge that contains breccia matrix from adjacent units; and ii) gravity flow deposits that abruptly thicken into cross-cutting faults. The latter characteristic is comparable to growth strata in tectonically active continental rift basins (c.f. Sharp et al. 2000).

Transport-related sediment generation

Sediment production would have occurred during transport of gravity flows through substrate erosion and frictional clast support mechanisms (Fig. 2.8B). A weakened bedrock substrate along fault scarps is thought to be particularly susceptible to erosion by clastic-rich flows with the necessary component of basal frictional stress. Tucholke et al. (1997) suggest that mass flow events have caused up to 500 m of incision into mid-Atlantic Ridge fault scarps by opening up already weakened fracture zones. In addition, the fractured and brittle nature of fault zone-

derived detritus would be particularly susceptible to desegregation by frictional stress brought on by clast-to-clast interaction during transport of cohesionless debris flows.

Lithofacies interpreted as cohesionless debrites include cobble breccia and pebble-granule breccia. Framework-support, relatively low percentages of muddy matrix (<40%), and large outsized clasts in these gravel-rich debrite facies suggest that grain-to-grain interactions (dispersive pressure) provided the primary grain/clast support mechanism during transport. Hence, a frictional strength, rather than a cohesive or plastic strength, transported the boulder- to pebble-size clasts. Frictional clast-support mechanisms are preserved in coarser grained breccias by local concentrations of clasts with similar lithologies (i.e. poor mixing) that would have been broken up from larger parent clasts during transport (Fig. 2.5B). Distribution of these syn-transport-produced clasts was inhibited by the suppression of turbulence and frictional-freezing intrinsic to these non-Newtonian cohesionless debris flows.

Hampered grain segregation and frictional locking is also produced in traction carpets (Sohn 1997), which occur in the locally reverse graded pebbly sandstone densite facies. Traction carpets form by the progressive upward aggradation and freezing of high-density gravity flows from the bottom up (Sohn 1997; Gani 2004; Sumner et al. 2008). Traction carpet depositional mechanisms are debated, and thought to occur from particle-size variation during sediment supply by near-bed flow velocity fluctuations of an unsteady flow ("spaced stratification" of Hiscott 1994) or by laminar shear of an overriding less dense turbidity flow (Lowe 1982; Sohn et al. 2002). The latter mechanism is supported by lithofacies associations on

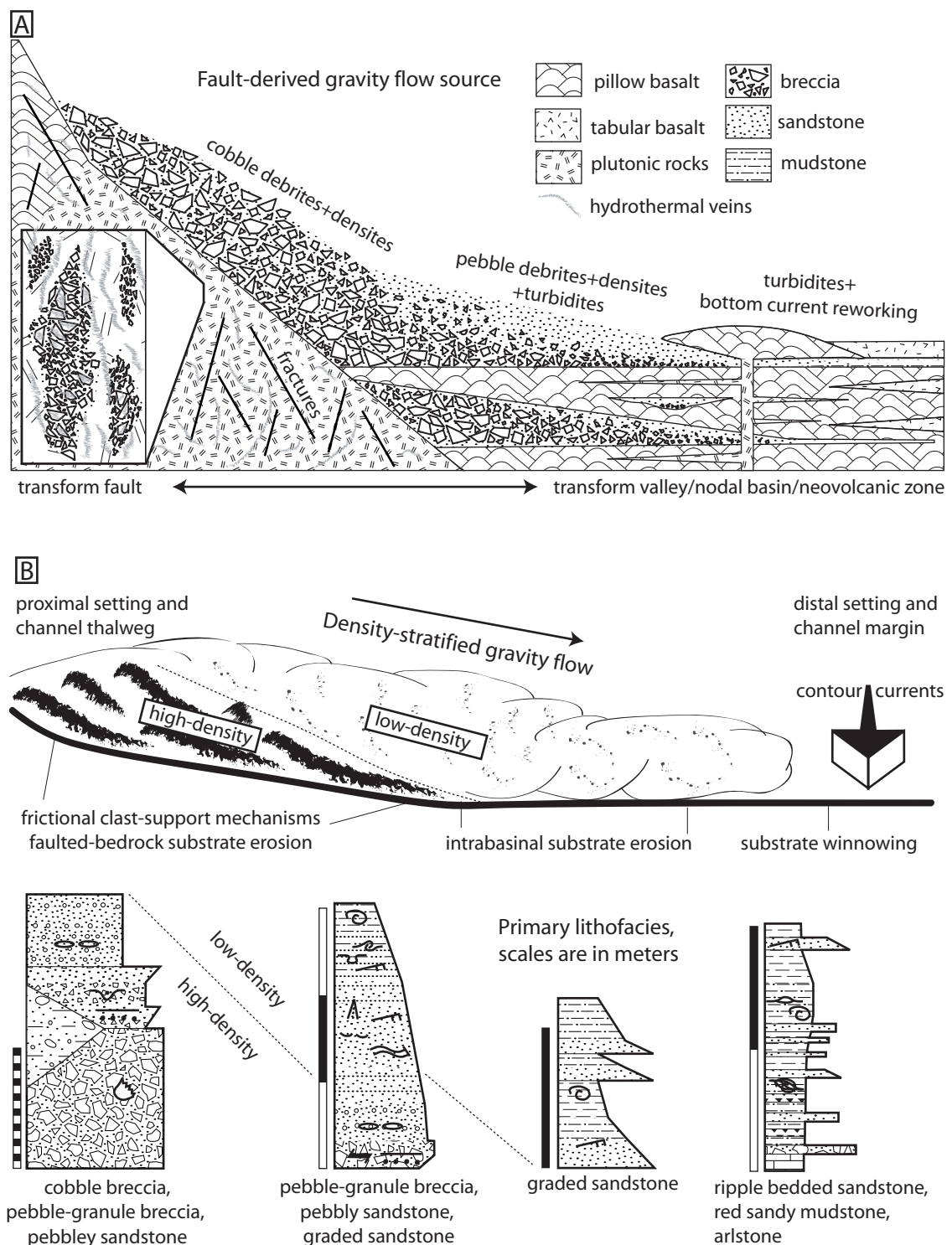


Figure 2.8:

A) Cross-section of depositional basin showing lateral variation in fault-derived gravity flow lithofacies flanking a transform fault. Note gradual shift from pillow to tabular basalt going away from transform fault. B) Architecture of density-stratified gravity flow showing various syn-transport sediment generation mechanisms in proximal and distal depositional settings. Idealized stratigraphic sections use symbology key from Fig. 2.2.

Macquarie Island between planar stratified pebbly sandstone densite facies and overlying graded sandstone turbidite facies (Fig. 2.8B). However, in sections that contain cobble breccia and pebbly sandstone (e.g. Douglas Point), overlying turbidite facies are absent. This is most likely due to the passage of the overlying co-genetic turbidity current in very proximal settings (Fig. 2.8B). Nevertheless, traction carpets are made up of lower frictional region in contact with the substrate and an upper collisional region that is characterized by grain collisions. Both these regions likely played a major role in producing finer grained sand along the PMSR. However, sediment production by this mechanism would be suppressed by turbulence in more distal settings where turbidity flows predominate (Fig. 2.8B).

Upon encountering the basin floor in a distal depositional setting, additional erosion of underlying sedimentary rocks would also be incorporated into the gravity flows (Fig. 2.8B). This is supported by erosional basal contacts, detached flame structures, mudstone rip-up clasts, and argillaceous matrix-support along the basal contact of pebble-granule breccia debrites and graded sandstone turbidites, which are attributed to incorporation of a muddy substrate during erosion, entrainment, and desegregation. Substrate entrainment into submarine gravity flows is common and depends upon the degree of lithification, composition, slope angle and gravity flow mechanics (Butler and Tavarnelli 2006). A poorly consolidated muddy substrate would have likely contributed a significant proportion of finer grained clayey material to PMSR gravity flows.

Although frictional stress would have been overwhelmed by significant matrix strength in the muddy diamictite cohesive debrites, foraminifera-rich marly rip-up clasts suggest that an underlying pelagic ooze succession was eroded and

entrained into the flow. Gee et al. (1999) also document seafloor erosion by a pelagic ooze-rich debris flow that removed 8 stratigraphic meters of its underlying volcanoclastic substrate. This is unusual as subaqueous cohesive debris flows are traditionally not associated with erosive bases due to a hydroplaning mechanism below the head of the flow (Fisher 1971; Mohrig et al. 1998; Mulder and Alexander 2001). However, recent experimental data has shown that frictional stress is concentrated below the body of the flow where erosion facilitates a basal lubricated interface (Ilstad, et al. 2004). Substrate erosion may explain the otherwise peculiar occurrence of ophiolitic pebbles and cobbles in the Caroline Cove marly diamictite, which could have been entrained from underlying gravel-rich debrite deposits or weakened bedrock.

Glacial and bottom current origin

An alternative source for some of the sand in contourite and hemipelagic deposits might be ice-rafted debris from the Antarctic continental margin. Abundant poorly sorted sand- to gravel-sized sediment on the modern abyssal seafloor in high latitude ocean basins is partly associated with ice-rafted debris (Lucchi et al. 2002). Ice-rafted debris mixes with pelagic biogenic material to form hemipelagic deposits (Stow and Tabrez 1998) and locally is winnowed and reworked by bottom currents into gravel lags of glaciogenic contourite drifts (Gilbert et al. 1998; Stoker et al. 1998; Lucchi et al. 2002). Macquarie Island crust formed close to the northern extent of ice rafted debris at ~9 Ma (Kennett 1977), but sand compositions in hemipelagites and contourites described here generally do not have continentally-derived signatures. However, a small proportion (<18%) of detrital zircon grains with ages between 500-1600 Ma (Chapter I) do support some component of glacially ice-rafted debris

and/or reworked continental sediment, most likely from Antarctica. Any continentally-derived debris was likely reworked and winnowed by bottom currents and locally entrained by gravity flows in the PMSR basins (Fig. 2.8B). However, the predominance of oceanic crustal source detritus in Macquarie Island sedimentary rocks masks any significant contribution of continental sediment input, glacial or not.

Bottom current erosion, winnowing, and reworking of ophiolitic detritus along the surrounding seafloor is another potential source for sediment within PMSR basins. Wide areas of volcanic seafloor in the north Atlantic and vast manganese pavements west of the Macquarie Ridge Complex in the Southern Ocean have been subject to erosion and sediment bypass by very strong bottom currents (Connolly and Payne 1972; Glasby 2000; Howe et al. 2001). Modern observations indicate that large turbulent eddies occur where the strong Antarctic circumpolar current intersects the bathymetrically robust SEIR and Macquarie Ridge Complex systems (Schuur et al. 1998; Ansorge and Lutjeharms 2005). A thick contourite drift has developed in association with one of these eddies on the leeward side of the Macquarie Ridge Complex and is primarily composed of reworked biogenic ooze and terrigenous sediment from the southern New Zealand continental margin (Connolly and Payne 1972; Schuur et al. 1998). However, New Zealand as a sediment source would not have been available until late Miocene time (i.e. after deposition of Macquarie Island sedimentary rocks) when the onset of rapid convergence, uplift, glaciation, and erosion occurred (Carter 1996). In any case, sand and gravel composition in coarse-grained contourite systems primarily corresponds to the regional sedimentation regime (Stoker et al. 1998) and any terrigenous input from New Zealand would have been diluted by ophiolitic sand reworked along the PMSR.

The Antarctic circumpolar current and Antarctic bottom water would have been developed by Miocene time in the Southern Ocean (Kennett 1977) and today have combined mean flow velocities of 10-29 cm s⁻¹ east of Macquarie Island along the base of the Campbell Plateau (Gordon 1975). Therefore the late Miocene Antarctic bottom current would have had peak flow velocities sufficient to resuspend and transport sand-sized material (>30 cm s⁻¹; McCave and Hall 2006) along the PMSR. Such elevated bottom current velocities would typify flow constriction within the narrow passageways created by the PMSR transforms. Consequently, it is feasible that some of the detritus in Macquarie Island's sedimentary lithofacies were introduced by bottom currents.

Depositional Mechanisms

The cohesionless debrite-densite-turbidite continuum

Recent work in deep-marine gravity flow deposits has diligently focused on the depositional mechanisms that operate within density-stratified flows with bipartite rheological behavior (Gani 2004). Of particular interest has been the high particle-concentration transitional zone between basal gravelly cohesionless debris flows and upper sandy turbidity flows (Fig. 2.8B). A variety of nomenclature has been used to describe these density-stratified flows partly including: high-density turbidity currents, density-modified grain flows, concentrated density flows, sandy debris flows, and densites (used in this study after Gani 2004). Average fault scarp gradients between 32 and 43° (Mitchell et al. 2000) and large variations in sediment clast/grain sizes along the immature mid-ocean ridge environment, such as the PMSR, create a type deep-marine environment to study these unusual deposits.

The association between debrite, densite, and turbidite is best preserved on Macquarie Island at Mawson Point where a basal pebble-granule breccia debrite facies is overlain by a planar laminated pebbly sandstone densite facies that grade upward into a graded sandstone turbidite facies (MP1-4 in Fig. 2.2C). In addition, a near perpendicular change in paleocurrent direction is recorded between bedforms in the higher density transitional interval and the upper low density turbidite interval. A genetic relationship amongst these three lithofacies to the same gravity flow event is inferred from the relative continuity of grading and lack of internal bedding/erosion surfaces through the sequence. We interpret the paleocurrent reversal as a deflection of the upper less dense turbid portion of a density-stratified gravity flow (Fig. 2.9A). Turbidity current reflection and deflection have been documented from ancient turbidite sequences and experimentally produced (Pickering and Hiscott 1985; Kneller 1991; Haughton 1994). Kneller and McCaffrey (1999) demonstrated that reflected turbidity currents commonly occur within the upper dilute portion of density-stratified flows where they do not have sufficient inertia to carry on past any obstacles encountered. Interbedded ripple laminated sandstone and siltstone within the upper deflected turbidite portion of the Mawson Point density-stratified flow deposit suggests repeated pulses of current energy and sedimentation. The interbeds don't show evidence of being small fine-grained turbidites, which commonly display vertical repetition in sedimentary structures and internal grading (Stow and Shanmugam 1980). Rather, these pulses may be associated with velocity fluctuations or eddies during the surging passage of the deflected turbidity current tail (c.f. Kneller 1995).

A “surging” gravity flow mechanism may also explain the presence of thin gravel lags along bounding surfaces within sigmoidal cross-bed sets of a turbidite unit at Cormorant Point (Fig. 2.2C). Dune-scale bedforms are unusual in turbidites and their absence has been attributed to the lack of appropriate grain-size when turbidity current velocities reach the dune stability field (Arnott and Hand 1989). However, a relatively coarse load in Macquarie Island gravity currents would provide a consistent amount of suitable detritus to form dune-scale bed forms. By corollary, granule lags along the bounding surfaces result from differential settling rates of a coarse suspended load during unsteady flow conditions. Considering the fact that the Cormorant Point turbidite is continuously graded without internal amalgamated subunits, sequential gravity flow events would likely not have produced the granule lags.

Bottom current reworked turbidites and hemipelagites

Bottom current reworking is a common counterpart to post-depositional turbidite modification along deep-marine continental margins (Stanley 1993) and results from this study extends this turbidite-contourite association into the mid-ocean ridge depositional environment. Reactivation surfaces, internal scours, and mud drapes within ripple-bedded sandstone facies of Macquarie Island channel/basin margins (e.g. Double Point and Cormorant Point) laterally correlate with thin successive graded sandstone facies within channel/basin centers (Fig. 2.3C-D). Reactivation surfaces and internal erosion surfaces in deep-marine sandstones characterize bottom current reworking (Shanmugam 1993; Martín-Chivelet et al. 2003). Lateral correlations in this case indicate reworking of “spilled over” turbidity current deposits in channel/basin margin “levee” areas (Fig. 2.9A). Therefore, the

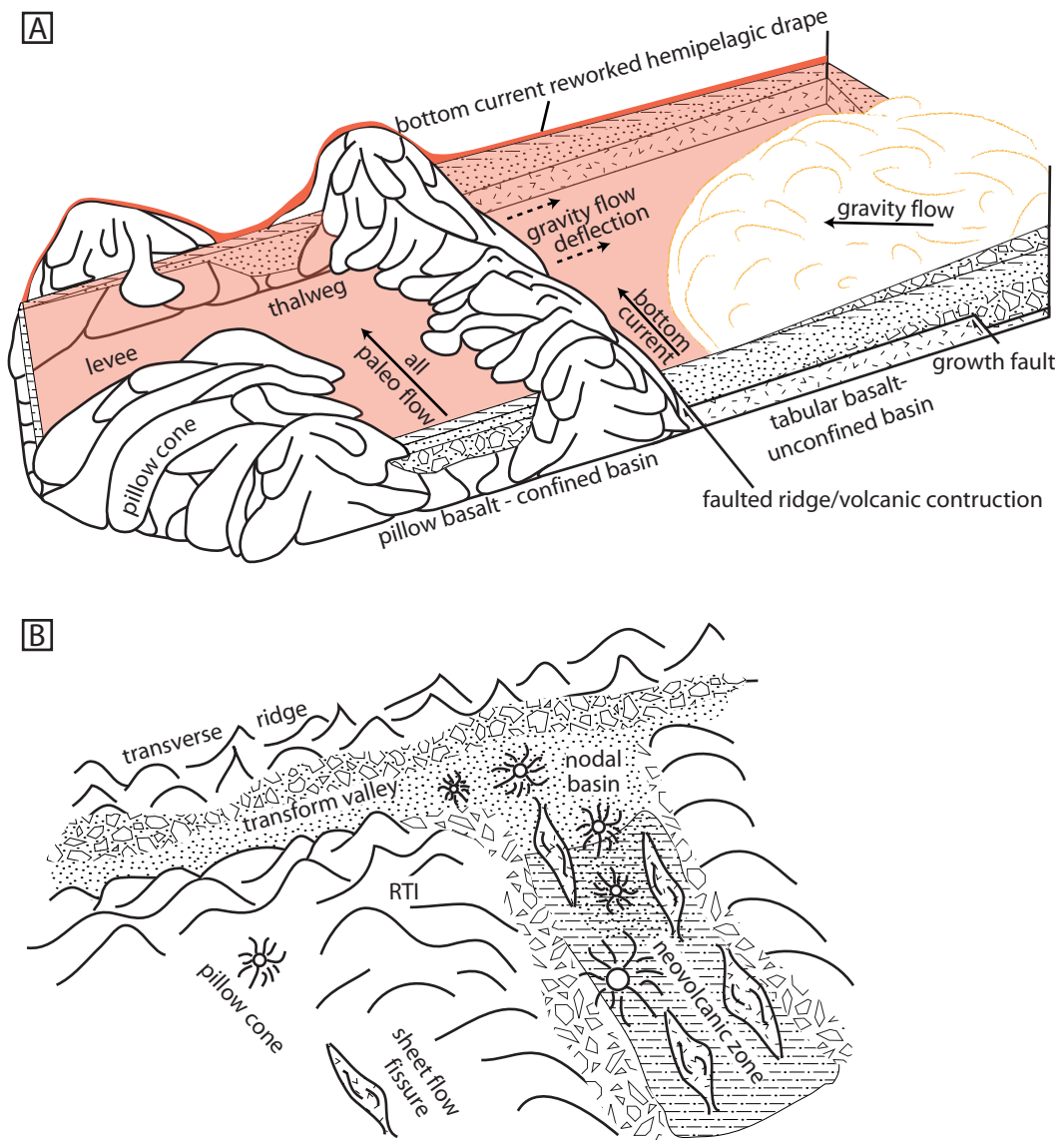


Figure 2.9:

A) Schematic representation of channelized gravity flows within confined basin of pillow basalt terrain vs. non-channelized flows within unconfined basin of sheet flow basalt terrain. Local fault blocks cause deflection of gravity flows and growth strata. Coarse-grained facies fill in bathymetric lows with bottom current reworked hemipelagic drape. B) Sedimentary-volcanic depositional environment around ridge-transform intersection (RTI) of PMSR. Gabbroic detritus derived from mass-wasting of uplifted transverse ridge and deposited between active pillow cones and sheet flow fields of active spreading corridor and within transform valley. Highly voluminous tabular sheet flows more common in axial neo-volcanic zone.

upper muddy dilute portions of the very thin channel/basin marginal turbidites would have been reduced to very thin mud drapes by bottom current winnowing between gravity flow events.

Evidence for erosive bottom currents along the PMSR are preserved by extensive scour surfaces and starved ripples within interbedded sandy red mudstone, arlstone, and ripple-bedded sandstone facies. These features are comparable to lineated scour surfaces commonly observed on the modern seafloor (Tucholke et al. 1985; Okada and Ohta 1993) and bottom-current generated bed forms documented from active mid-ocean ridge slopes (Karson et al. 1984). The general absence of gravity flow facies (i.e. graded sandstone turbidite facies) above the scoured surfaces indicate that they were either produced during sediment bypass of erosive gravity flows or by discrete contour currents. A bottom current origin is preferred due to the locally perpendicular relationship between paleocurrents recorded by scour surfaces vs. gravity flow bed forms and paleoslope indicators (Fig. 2.2C).

Bioturbation has been used as diagnostic criteria for contourites, as described in the sandy red mudstone facies, but it can be quite variable (Ito 1996; Viana et al. 1998) and this use has been questioned (Shanmugam et al. 1993; Martín-Chivelet et al. 2008). Arguments against its use typically include coarser grained sandy contourites that contain sedimentary structures and lack bioturbation. The lack of bioturbation in Macquarie Island ripple-bedded contourite facies may be due to the fact that organic matter is typically adsorbed to finer-grained argillaceous particles rather than mineral sand (Mayer 1994). Therefore, the muddy to silty contourites will have provided more nutrients for benthic communities and hence show more intense

degrees of bioturbation. Other reasons for bioturbation variability between contourite systems also include availability of nutrients, oxygenation, and erosion in sufficiently strong currents (Chough and Hess 1985; Tucholke et al. 1985; Thistle et al. 1985). Macquarie Island's pelagites and hemipelagites (i.e. arlstone facies) also contain bioturbation, but do not contain sandy to silty traction structures, lack inverse grading, and commonly have a higher proportion of well-preserved biogenic tests. The preservation potential of biogenic tests is decreased during winnowing by the erosive bottom currents.

Paleobathymetry and depositional basin

Trace fossils observed in Macquarie Island sedimentary facies are comparable to modern and ancient deep marine to continental slope *Nereites* and *Zoophycos* ichnofacies. In particular *Spirorhaphe* has only been observed in modern day environments below depths of 2.2 km and *Paleodictyon* above depths of 3.9 km (Buatois et al. 2001). The ubiquitous presence of carbonate in Macquarie Island sedimentary rocks also constrain paleobathymetric depths to <4 km, which was the approximate level of the Southern Ocean carbonate compensation depth during the late Miocene (Van Andel 1975). Dissolution resistant benthic foraminifera (e.g. *Pullenia*, *Melonis*, *Globocassidulina*) from inter- and intra-pillow calcareous oozes compare with south Pacific fauna associations that indicate upper abyssal depths between 2.0-3.5 km below sea level (Hayward et al. 2004, Quilty et al. 2008). Together these data suggest that sedimentary lithofacies described in this study were deposited between 2.2 and 3.5 km below sea level, which is common for basins along young mid-ocean ridge axes (Orton 1996). However, the depths of uplifted fault blocks that bounded the basin floors still remain unclear.

The greatest bathymetric relief along the modern mid-ocean ridge system is 2.0-5.5 km and typically occurs along slow-spreading ridges (Bonatti et al. 1994; Tivey et al. 1998; Baines et al. 2003). Such exaggerated bathymetry is most common along the ends of spreading ridge segments between transverse ridges and adjacent transform valleys or nodal basins (i.e. ridge/transform intersections). Deep basins associated with the high bathymetric relief of transform faults are prime targets for thick sedimentary successions along mid-ocean ridges (Karson et al. 1983; Tivey et al. 1998) including sedimentary rocks of Macquarie Island (Fig. 2.8A). Due to the rugged nature of the faulted seafloor (Mitchell et al. 2000), gravity flow reflection and/or deflection would seem like a common phenomenon along slow-spreading centers (Fig. 2.9A). This is supported by experimental and observational evidence for the reflection and ponding of bioclastic turbidites within constricted basins of the mid-Atlantic Ridge (Van Andel and Komar 1969) and results presented here.

Sedimentary lithofacies variation on Macquarie Island also corresponds to differences in basin geometry, which is primarily controlled by the nature of volcanic constructional features and the presence of faults. For example, the perpendicular nature of bottom current vs. gravity current/paleoslope directions is only observed in laterally extensive facies associated with tabular basalt sequences where currents were relatively unconfined (Fig. 2.9A). In comparison, facies within channelized sections of pillow basalt sequences preserve nearly parallel bottom and gravity current directions indicating confined basins. In general, tabular basalt flows are commonly associated with highly voluminous and rapid basalt flows that pond in bathymetric lows of the neo-volcanic zone, whereas pillow basalt flows indicate slower less voluminous flows associated with a lower magma budget along the

spreading-segment tips (Fig. 2.9A; Kennish and Lutz 1998). Alternatively, magmatically active transtensional pull-apart basins can form along transform valleys that are undergoing reorientation associated with ridge propagation like the PMSR (Dick et al. 1991; Bonatti et al. 1994). More voluminous volcanism (i.e. tabular basalt flows) in these settings may be expected. Despite a transpressional regime along some PMSR transforms by 10 Ma (Meckel et al. 2005), transtensional relay zones are also known to occur along the currently active transpressional Australia-Pacific plate boundary (Daczko et al. 2003). Nevertheless, on Macquarie Island tabular basalt flows are interbedded with distally derived fine-grained turbidite, contourite and pelagic facies, which have shallow structural dips and occur far from any major spreading-related fault. More proximally derived coarse-grained debrite facies are interbedded with pillow basalt, have steep to vertical structural dips, and occur very close to spreading-related faults. These characteristics create an idealized lithofacies continuum that changes from debrite-rich confined pillow basalt floored basins along faulted transform flanks to turbidite-rich unconfined tabular basalt floored basins along spreading ridge axes, nodal basins, and/or magmatically active transform valleys (Fig. 2.8).

Lithofacies architecture preserved in Macquarie Island likely records the evolutionary transition from fault-proximal cohesionless debris flows basin-ward through density-stratified flows into turbidity flows of the neovolcanic zone (Fig. 2.8). This lateral transition between co-genetic lithofacies is commonly described from continental margin settings (Walker 1978; Mulder and Alexander 2001; Leppard and Gawthorpe 2006) and subaqueous continental rift basins (e.g. Leppard and Gawthorpe 2006). Furthermore, the coarsening and thickening upward of turbidite

facies at Cormorant Point is comparable to the vertical sequence of facies produced by prograding submarine fans along continental margins (Walker 1978). Along the PMSR, increasing tectonic activity would have supplied submarine fans with increasing amounts of coarser-grained detritus during volcanically quiescent periods. In addition, vertical facies architecture was subject to changing source directions that depended upon the loci of tectonic activity along the transform ridge. When sediment supply was low, bottom current reworking and hemipelagic draping was most pronounced and therefore best preserved in the more distal sediment-starved neovolcanic basin centers.

Conclusions:

Diverse sedimentary lithofacies preserved on Macquarie Island record the mass wasting of oceanic crust in a slow-spreading center between 2.2 and 3.5 km below sea level. Seismic activity along spreading center transforms initiated mass gravity flows of hydrothermally-altered oceanic crust disaggregated from cataclastic gouge and fractured bedrock. Gravity flows produced a lithofacies continuum from transform fault-proximal debrites to densites and turbidites in more distal neovolcanic basins. Lateral spreading of gravity flows occurred in magmatically-charged neovolcanic centers where tabular basalts produced unconfined basins. In comparison pillow basalt terrains along the more amagmatic spreading-ridge tips produced more confined basins that channelized incoming gravity flows. The rugged nature of the slow-spreading proto-Macquarie spreading ridge (PMSR) seafloor caused reflection and ponding of gravity flows in bathymetric lows of the neovolcanic centers. Gravity flows developed into submarine fans that prograded

into basin depocenters where they interfingered with hemipelagic, pelagic, and chemogenic deposits. During basin infilling, facies were continually reworked by Antarctic-related bottom currents that introduced small amounts of extrabasinal detritus during volcanic- and tectonic-quiescent periods. Small contourite drifts formed in bottom current eddies, which would have been focused around the bathymetrically robust PMSR transverse ridge. Primary depocenters existed within transform valleys and nodal basins where bathymetric relief was greatest.

References Cited:

- Alt, J.C., Honnorez, J., Laverne, C. and Emmermann, R., 1986. Hydrothermal Alteration of a 1 km section through the upper oceanic crust, Deep Sea Drilling Project Hole 504B: Mineralogy, Chemistry and Evolution of Seawater-Basalt Interactions. *J. Geophys. Res.*, 91.
- Amy, L.A., Talling, P.J., Peakall, J., Wynn, R.B. and Arzola Thynne, R.G., 2005. Bed geometry used to test recognition criteria of turbidites and (sandy) debrites. *Sedimentary Geology*, 179(1-2): 163-174.
- Ansorge, I.J. and Lutjeharms, J.R.E., 2005. Direct observations of eddy turbulence at a ridge in the Southern Ocean. *Geophysical Research Letters*, 32: no.14, 4.
- Arnott, R.W.C. and Hand, B.M., 1989. Bedforms, primary structures and grain fabric in the presence of suspended sediment rain. *Journal of Sedimentary Petrology*, 59(6): 1062-1069.
- Auzende, J.-M., Cannat, M., Gente, P., Henriot, J.-P., Juteau, T., Karson, J., Lagabriele, Y., Mevel, C. and Tivey, M., 1994. Observation of sections of oceanic crust and mantle cropping out on the southern wall of Kane FZ (N. Atlantic). *Terra Nova*, 6(2): 143-148.
- Baines, A.G., Cheadle, M. J., Dick, H. J. B., Scheirer, A. H., John, B. E., Kuszniir, N. J. and Matsumoto, T., 2003. Mechanism for generating the anomalous uplift of oceanic core complexes; Atlantis Bank, Southwest Indian Ridge. *Geology*, 31(12): 1105-1108.
- Barrett, T.J. and Spooner, E.T.C., 1977. Ophiolitic breccias associated with allochthonous oceanic crustal rocks in the East Ligurian Apennines, Italy; a comparison with observations from rifted oceanic ridges. *Earth and Planetary Science Letters*, 35(1): 79-91.
- Blackman, D.K., Karson, J. A., Kelley, D. S., Cann, J. R., Frueh-Green, G. L., Gee, J. S., Hurst, S. D., John, B. E., Morgan, J., Nooner, S. L., Ross, D. K., Schroeder, T. J. and Williams, E. A., 2002. Geology of the Atlantis Massif (Mid-Atlantic Ridge, 30 degrees N); implications for the evolution of an ultramafic oceanic core complex. *Marine Geophysical Researches*, 23(5-6): 443-469.

- Bonatti, E., Ligi, M., Gasperini, L., Peyve, A., Raznitsin, Y. and Chen, Y. J., 1994. Transform migration and vertical tectonics at the Romanche fracture zone, equatorial Atlantic. *J. Geophys. Res.*, 99(B11): 21,779-21,802.
- Bouma, A.H., 1962. *Sedimentology of some flysch deposits: a graphic approach to facies interpretations*. Elsevier, Amsterdam, 168 pp.
- Buatois, L.A., Mángano, M.G. and Sylvester, Z., 2001. A diverse deep-marine Ichnofauna from the Eocene Tarcau sandstone of the Eastern Carpathians, Romania. *Ichnos: An International Journal for Plant and Animal Traces*, 8(1): 23 - 62.
- Carter, L., Carter, R.M., McCave, I.N. and Gamble, J., 1996. Regional sediment recycling in the abyssal Southwest Pacific Ocean. *Geology*, 24(8): 735-738.
- Chough, S.K. and Hesse, R., 1984. Contourites from Eirik Ridge, south of Greenland. *Sedimentary Geology*, 41(2-4): 185-199.
- Conolly, J.R. and Payne, R.R., 1972. Sedimentary patterns within a continent-mid-oceanic ridge-continent profile; Indian Ocean south of Australia. *Antarctic Research Series*, 19: 295-315.
- Daczko, N., Wertz, K.L., Mosher, S., Coffin, M.F. and Meckel, T.A., 2003. Extension along the Australian-Pacific transpressional transform plate boundary near Macquarie Island, *Geochemistry Geophysics Geosystems* 4(9): 22.
- Daczko, N.R., Mosher, S., Coffin, M.F. and T.A., M., 2005. Tectonic implications of fault-scarp-derived volcanoclastic deposits on Macquarie Island; sedimentation at a fossil ridge-transform intersection? *Geological Society of America Bulletin*, 117(1-2): 18-31.
- Davidson, G.J., Varne, R., Brown, A.V. and Connell, R., 2004. Structural controls on sulphide deposition at the dyke-lava boundary, slow-spreading ocean crust, Macquarie Island. *Terra Nova*, 16: 9-15.
- Dick, H.J.B., Natland, J. H., Alt, J. C., Bach, W., Bideau, D., Gee, J. S., Haggas, S., Hertogen, J. G. H., Hirth, G., Holm, P. M., Ildefonse, B., Iturrino, G. J., John, B. E., Kelley, D. S., Kikawa, E., Kingdon, A., LeRoux, P. J., Maeda, J., Meyer, P. S., Miller, D. J., Naslund, H. R., Niu, Y.-L., Robinson, P. T., Snow, J., Stephen, R. A., Trimby, P. W., Worm, H.-U. and Yoshinobu, A., 2000. A long in situ section of the lower ocean crust: results of ODP Leg 176 drilling at the Southwest Indian Ridge. *Earth and Planetary Science Letters*, 179(1): 31-51.
- Dick, H.J.B., Schouten, H., Meyer, P. S., Gallo, D. G., Bergh, H., Tyce, R., Patriat, P., Johnson, K. T. M., Snow, J. and Fisher, A., 1991. Tectonic evolution of the Atlantis II fracture zone. In: R.P. von Herzen and P.T. Robinson (Editors). *Ocean Drilling Program, Scientific Results*, College Station, pp. 359-398.
- Dorsey, R.J., Umhoefer, P.J., Ingle, J.C. and Mayer, L., 2001. Late Miocene to Pliocene stratigraphic evolution of Northeast Carmen Island, Gulf of California; implications for oblique-rifting tectonics. In: J. Halfar (Editor), *Sedimentary Geology*, pp. 97-123.
- Enos, P., 1977. Flow regimes in debris flow. *Sedimentology*, 24(1): 133-142.
- Faugères, J.-C. and Stow, D.A.V., 1993. Bottom-current-controlled sedimentation: a synthesis of the contourite problem. *Sedimentary Geology*, 82(1-4): 287-297.
- Fisher, R.V., 1971. Features of coarse-grained, high-concentration fluids and their deposits. *Journal of Sedimentary Petrology*, 41(4): 916-927.
- Flier-Keller, E.V.d., 1991. Geochemistry and mineralogy of sediments, Atlantis II fracture zone, Southwest Indian Ocean. In: R.P. Von Herzen and P.T.

- Robinson (Editors), Proceedings of the Ocean Drilling Program, Scientific Results. Ocean Drilling Program, College Station, TX, pp. 145-151.
- Fox, P.J. and Heezen, B.C., 1965. Sands of the Mid-Atlantic Ridge. *Science*, 149(3690): 1367-1370.
- Gani, M.R., 2004. From turbid to lucid; a straightforward approach to sediment gravity flows and their deposits. *The Sedimentary Record*, 2(3): 4-8.
- Gawthorpe, R.L. and Leeder, M.R., 2000. Tectono-sedimentary evolution of active extensional basins. *Basin Research*, 12(3/4): 195.
- Gee, M. J. R., Masson, D. G., Watts, A. B. and Allen, P. A., 1999. The Saharan debris flow: an insight into the mechanics of long runout submarine debris flows. *Sedimentology*, 46(2): 317-335.
- Gilbert, I.M., Pudsey, C.J. and Murray, J.W., 1998. A sediment record of cyclic bottom-current variability from the northwest Weddell Sea. *Sedimentary Geology*, 115(1-4): 185-214.
- Glasby, G.P., 2000. Manganese: predominant role of nodules and crusts. In: H.D. Schulz and M. Zabel (Editors), *Marine Geochemistry*. Springer-Verlag, Berlin-Heidelberg, pp. 335-372.
- Gonthier, E.G., Faugeres, J.C. and Stow, D.A.V., 1984. Contourite facies of the Faro Drift, Gulf of Cadiz. In: D.A.V. Stow and D.J.W. Piper (Editors), *Geological Society Special Publications*, vol.15. Geological Society of London, London, pp. 275-292.
- Gordon, A.L., 1975. An Antarctic oceanographic section along 170 degrees E. *Deep-Sea Research and Oceanographic Abstracts*, 22(6): 357-377.
- Goscombe, B.D. and Everard, J.L., 1998. 1:10,000 Geological Map of Macquarie Island, series of 7 maps, Mineral Resources Tasmania.
- Hampton, M., 1975. Competence of fine-grained debris flows. *Journal of Sedimentary Petrology*, 45(4): 834-844.
- Haughton, P.D.W., 1994. Deposits of deflected and ponded turbidity currents, Sorbas basin, Southeast Spain. *Journal of Sedimentary Research*, 64: 233-246.
- Hayward, B.W., Grenfell, H.R., Carter, R. and Hayward, J.J., 2004. Benthic foraminiferal proxy evidence for the Neogene palaeoceanographic history of the Southwest Pacific, east of New Zealand. *Marine Geology*, 205(1-4): 147-184.
- Heezen, B.C., Hollister, C.D. and Ruddiman, W.F., 1966. Shaping of the Continental Rise by Deep Geostrophic Contour Currents. *Science*, 152(3721): 502-508.
- Hiscott, R.N., 1994. Traction-carpet stratification in turbidites; fact or fiction? *Journal of Sedimentary Research*, 64(2a): 204-208.
- Howe, J.A., Stoker, M.S. and Woolfe, K.J., 2001. Deep-marine seabed erosion and gravel lags in the northwestern Rockall Trough, North Atlantic Ocean. *Journal of the Geological Society of London*, 158(3): 427-438.
- Ildefonse, B., Blackman, D. K., John, B. E., Ohara, Y., Miller, D. J. and MacLeod, C. J., 2007. Oceanic core complexes and crustal accretion at slow-spreading ridges. *Geology*, 35(7): 623-626.
- Ilstad, T., Elverhøi, A., Issler, D. and Marr, J.G., 2004. Subaqueous debris flow behaviour and its dependence on the sand/clay ratio: a laboratory study using particle tracking. *Marine Geology*, 213(1-4): 415-438.
- Ito, M., 1996. Sandy contourites of the lower Kazusa Group in the Boso Peninsula, Japan; Kuroshio-current-influenced deep-sea sedimentation in a Plio-

- Pleistocene forearc basin. *JOURNAL OF SEDIMENTARY RESEARCH*, 66(3): 587-598.
- Jacobi, R.D., 1976. Sediment slides on the northwestern continental margin of Africa. *Marine Geology*, 22(3): 157-173.
- James, R.H., Duckworth, R.C. and Palmer, M.R., 1998. Drilling of sediment-hosted massive sulphide deposits at the Middle Valley and Escanabe Trough spreading centres: ODP Leg 169. In: R.A. Mills and K. Harrison (Editors), *Modern Ocean Floor Processes and the Geological Record*. Special Publications. Geological Society, London, pp. 177-199.
- John, B.E., Foster, D. A., Murphy, J. M., Cheadle, M. J., Baines, A. G., Fanning, C. M. and Copeland, P., 2004. Determining the cooling history of in situ lower oceanic crust--Atlantis Bank, SW Indian Ridge. *Earth and Planetary Science Letters*, 222(1): 145-160.
- Kamenetsky, V.S. and Maas, R., 2002. Mantle-melt Evolution (Dynamic Source) in the Origin of a Single MORB Suite: a Perspective from Magnesian Glasses of Macquarie Island. *J. Petrology*, 43(10): 1909-1922.
- Karson, J. and Dewey, J.F., 1978. Coastal Complex, western Newfoundland: An Early Ordovician oceanic fracture zone. *Geological Society of America Bulletin*, 89(7): 1037-1049.
- Karson, J.A. and Dick, H.J.B., 1983. Tectonics of ridge-transform intersections at the Kane fracture zone. *Marine Geophysical Researches*, 6(1): 51-98.
- Karson, J.A., Fox, P. J., Sloan, H., Crane, K. T., Kidd, W. S. F., Bonatti, E., Stroup, J. B., Fornari, D. J., Elthon, D., Hamlyn, P., Casey, J. F., Gallo, D. G., Needham, D. and Sartori, R., 1984. The geology of the Oceanographer Transform: The ridge-transform intersection. *Marine Geophysical Researches*, 6(2): 109-141.
- Kennett, J.P., 1977. Cenozoic Evolution of Antarctic Glaciation, the Circum-Antarctic Ocean, and Their Impact on Global Paleooceanography. *J. Geophys. Res.*, 82.
- Kennish, M.J. and Lutz, R.A., 1998. Morphology and distribution of lava flows on mid-ocean ridges; a review. *Earth-Science Reviews*, 43(3-4): 63-90.
- Kneller, B., 1995. Beyond the turbidite paradigm; physical models for deposition of turbidites and their implications for reservoir prediction. In: A.J. Hartley, and Prosser, D.J. (Editor), *Characterization of Deep Marine Clastic Systems*. Geological Society Special Publications, London, pp. 31-49.
- Kneller, B., Edwards, D., McCaffrey, W. and Moore, R., 1991. Oblique reflection of turbidity currents. *Geology*, 19(3): 250-252.
- Kneller, B. and McCaffrey, W., 1999. Depositional effects of flow nonuniformity and stratification within turbidity currents approaching a bounding slope; deflection, reflection, and facies variation. *Journal of Sedimentary Research*, 69(5): 980-991.
- Kuenen, P.H. and Migliorini, C.I., 1950. Turbidity currents as a cause of graded bedding. *The Journal of Geology*, 58(2): 91-127.
- Leppard, C.W. and Gawthorpe, R.L., 2006. Sedimentology of rift climax deep water systems; Lower Rudeis Formation, Hammam Faraun Fault Block, Suez Rift, Egypt. *Sedimentary Geology*, 191(1-2): 67-87.
- Lovell, J.P.B. and Stow, D.A.V., 1981. Identification of ancient sandy contourites. *Geology*, 9(8): 347-349.
- Lowe, D.R., 1976. Grain flow and grain flow deposits. *Journal of Sedimentary Petrology*, 46(1): 188-199.

- Lowe, D.R., 1982. Sediment gravity flows; II, Depositional models with special reference to the deposits of high-density turbidity currents. *Journal of Sedimentary Petrology*, 52(1): 279-297.
- Lucchi, R.G., Rebesco, M., Camerlenghi, A., Busetti, M., Tomadin, L., Villa, G., Persico, D., Morigi, C., Bonci, M. C. and Giorgetti, G., 2002. Mid-late Pleistocene glacimarine sedimentary processes of a high-latitude, deep-sea sediment drift (Antarctic Peninsula Pacific margin). *Marine Geology*, 189(3-4): 343-370.
- MacLeod, C.J., Escartin, J., Banerji, D., Banks, G. J., Gleeson, M., Irving, D. H. B., Lilly, R. M., McCaig, A. M., Niu, Y., Allerton, S. and Smith, D. K., 2002. Direct geological evidence for oceanic detachment faulting; the Mid-Atlantic Ridge, 15 degrees 45'N. *Geology*, 30(10): 879-882.
- Martín -Chivelet, J., Fregenal-Martínez, M.A. and Chacón, B., 2003. Mid-depth calcareous contourites in the latest Cretaceous of Caravaca (Subbetic Zone, SE Spain). Origin and palaeohydrological significance. *Sedimentary Geology*, 163(1-2): 131-146.
- Martín -Chivelet, J., Fregenal-Martínez, M.A. and Chacón, B., 2008. Traction structures in contourites. In: M. Rebesco and A. Camerlenghi (Editors), *Contourites. Developments in Sedimentology*. Elsevier, pp. 159-182.
- Mayer, L.M., 1994. Surface area control of organic carbon accumulation in continental shelf sediments. *Geochimica et Cosmochimica Acta*, 58(4): 1271-1284.
- McCave, I.N. and Hall, I.R., 2006. Size sorting in marine muds: Processes, pitfalls, and prospects for paleoflow-speed proxies. *Geochem. Geophys. Geosyst.*, 7.
- Meckel, T.A., 2003. Tectonics of the Hjort region of the Macquarie Ridge Complex, southernmost Australian-Pacific plate boundary, Southwest Pacific Ocean. Doctoral Thesis, University of Texas, Austin, 192 pp.
- Meckel, T.A., Mann, P., Mosher, S. and Coffin, M.F., 2005. Influence of cumulative convergence on lithospheric thrust fault development and topography along the Australian-Pacific plate boundary south of New Zealand. *Geochem. Geophys. Geosyst.*, 6(9): 20.
- Middleton, G.V., 1967. Experiments on density and turbidity currents; [Part] 3, Deposition of sediment. *Canadian Jour. Earth Sci.*; with French abs., 4(3): 475-505.
- Middleton, G.V. and Hampton, M.A., 1976. Subaqueous sediment transport and deposition by sediment gravity flows. In: D.J. Stanley and D.J.P. Swift (Editors), *Marine Sediment Transport and Environmental Management*. John Wiley & Sons, New York, pp. 197-218.
- Mitchell, N.C., Tivey, M.A. and Gente, P., 2000. Seafloor slopes at mid-ocean ridges from submersible observations and implications for interpreting geology from seafloor topography. *Earth and Planetary Science Letters*, 183(3-4): 543-555.
- Mohrig, D., Whipple, K.X., Hondzo, M., Ellis, C. and Parker, G., 1998. Hydroplaning of subaqueous debris flows. *Geological Society of America Bulletin*, 110(3): 387-394.
- Mosher, S. and Massell-Symons, C., 2008. Ridge reorientation mechanisms: Macquarie Ridge Complex, Australia-Pacific plate boundary. *Geology*, 36(2): 119-122.
- Mulder, T. and Alexander, J., 2001. The physical character of subaqueous sedimentary density flows and their deposits. *Sedimentology*, 48(2): 269-299.

- Mutti, E. and Ricci Lucchi, F., 1978. Turbidites of the northern Apennines; introduction to facies analysis. *International Geology Review*, 20(2): 125-166.
- Normark, W.R., 1970. Growth patterns of deep-sea fans. *The American Association of Petroleum Geologists Bulletin*, 54(11): 2170-2195.
- Okada, H. and Ohta, S., 1993. Photographic evidence of variable bottom-current activity in the Suruga and Sagami Bays, central Japan. *Sedimentary Geology*, 82(1-4): 221-237.
- Orton, G.J., 1996. Volcanic environments. In: H.G. Reading (Editor), *Sedimentary Environments: Processes, facies and Stratigraphy*. Blackwell Science, Oxford, pp. 485-567.
- Pickering, K.T. and Hiscott, R.N., 1985. Contained (reflected) turbidity from the Middle Ordovician Cloridorme Formation, Quebec, Canada: an alternative to the antidune hypothesis. *Sedimentology*, 32(3): 373.
- Pockalny, R.A., Gente, P. and Buck, R., 1996. Oceanic transverse ridges: A flexural response to fracture-zone-normal extension. *Geology*, 24(1): 71-74.
- Postma, G., 1986. Classification for sediment gravity-flow deposits based on flow conditions during sedimentation. *Geology*, 14(4): 291-294.
- Potter, P.E. and Pettijohn, F.J., 1977. *Paleocurrents and basin analysis*. Springer-Verlag, Berlin Heidelberg New York, 425 pp.
- Quilty, P.G., Crundwell, M. and Wise Jr., S.W., 2008. Microplankton provide 9 Ma age for sediment in the Macquarie Island ophiolite complex. *Australian Journal of Earth Sciences*, 55(8): 1119-1125.
- Rivizzigno, P.A. and Karson, J.A., 2004. Structural expression of oblique seafloor spreading in the Macquarie Island ophiolite, Southern Ocean. *Geology*, 32(2): 125-128.
- Sanders, J.E., 1965. Primary sedimentary structures formed by turbidity currents and related resedimentation mechanisms. In: G.V. Middleton (Editor), *Primary Sedimentary Structures and their Hydrodynamic Interpretation*. Soc. Econ. Paleontol. Mineral., Spec. Publ., pp. 192-219.
- Sanders, J.E. and Friedman, G.M., 1997. History of petroleum exploration in turbidites and related deep-water deposits. *Northeastern Geology and Environmental Sciences*, 19(1-2): 67-102.
- Schuur, C.L., Coffin, M.F., Frohlich, C., Massell, C.G., Karner, G.D., Ramsay, D., and Caress, D.W., 1998. Sedimentary regimes at the Macquarie Ridge complex; interaction of Southern Ocean circulation and plate boundary bathymetry. *Paleoceanography*, 13(6): 646-670.
- Shanmugam, G., 1996. High-density turbidity currents; are they sandy debris flows? *Journal of Sedimentary Research*, 66(1): 2-10.
- Shanmugam, G., 1997. The Bouma Sequence and the turbidite mind set. *Earth-Science Reviews*, 42(4): 201-229.
- Shanmugam, G., 2002. Ten turbidite myths. *Earth-Science Reviews*, 58(3-4): 311-341.
- Shanmugam, G., Spalding, T.D. and Rofheart, D.H., 1993. Traction structures in deep-marine, bottom-current-reworked sands in the Pliocene and Pleistocene, Gulf of Mexico. *Geology*, 21(10): 929-932.
- Sharp, I.R., Gawthorpe, R.L., Underhill, J.R. and Gupta, S., 2000. Fault-propagation folding in extensional settings; examples of structural style and synrift sedimentary response from the Suez Rift, Sinai, Egypt. *Geological Society of America Bulletin*, 112(12): 1877-1899.

- Siever, R. and Kastner, M., 1967. Mineralogy and petrology of some Mid-Atlantic Ridge sediments. *Journal of Marine Research*, 25(3): 263-278.
- Simonian, K.O. and Gass, I.G., 1978. Arakapas fault belt, Cyprus: A fossil transform fault. *Geological Society of America Bulletin*, 89(8): 1220-1230.
- Sohn, Y.K., 1997. On traction-carpet sedimentation. *Journal of Sedimentary Research*, 67(3): 502-509.
- Sohn, Y.K., Choe, M.Y. and Jo, H.R., 2002. Transition from debris flow to hyperconcentrated flow in a submarine channel (the Cretaceous Cerro Toro Formation, southern Chile). *Terra Nova*, 14(5): 405-415.
- Stanley, D.J., 1993. Model for turbidite-to-contourite continuum and multiple process transport in deep marine settings: examples in the rock record. *Sedimentary Geology*, 82(1-4): 241-255.
- Stoker, M.S., Akhurst, M.C., Howe, J.A. and Stow, D.A.V., 1998. Sediment drifts and contourites on the continental margin off northwest Britain. *Sedimentary Geology*, 115(1-4): 33-51.
- Stow, D.A.V., Faugères, J.-C. and Gonthier, E., 1986. Facies distribution and textural variation in Faro Drift contourites: Velocity fluctuation and drift growth. *Marine Geology*, 72(1-2): 71-100.
- Stow, D.A.V., Faugeres, J.-C., Viana, A.R. and Gonthier, E., 1998. Fossil contourites; a critical review. In: D.A.V. Stow and J.-C. Faugeres (Editors), *Sedimentary Geology*, pp. 3-31.
- Stow, D. A. V., and Piper, D. J. W., 1984, Deep-water fine-grained sediments; history, methodology and terminology: *Geological Society Special Publications*, v. 15, p. 3-14.
- Stow, D.A.V., Reading, H.G. and Collinson, J.D., 1996. Deep seas. In: H.G. Reading (Editor), *Sedimentary Environments: Processes, facies and Stratigraphy*. Blackwell Science, Oxford, pp. 395-453.
- Stow, D.A.V. and Shanmugam, G., 1980. Sequence of structures in fine-grained turbidites: Comparison of recent deep-sea and ancient flysch sediments. *Sedimentary Geology*, 25(1-2): 23-42.
- Stow, D.A.V. and Tabrez, A.R., 1998. Hemipelagites: processes, facies and model. In: M.S. Stoker, D. Evans and A. Cramp (Editors), *Geological Processes on Continental Margins: Sedimentation, Mass Wasting and Stability*. Geological Society, Special Publications, London, pp. 317-337.
- Sullwold, H.H., Jr., 1961. Turbidites in oil exploration. In: J.A. Peterson and J.C. Osmond (Editors), *Geometry of sandstone bodies*. American Association of Petroleum Geologists, Tulsa, pp. 63-81.
- Sumner, E.J., Amy, L.A. and Talling, P.J., 2008. Deposit Structure and Processes of Sand Deposition from Decelerating Sediment Suspensions. *JOURNAL OF SEDIMENTARY RESEARCH*, 78(8): 529-547.
- Swift, S.A., 1991. Gravels in the Atlantis II fracture zone. In: R.P. Von Herzen and P.T. Robinson (Editors), *Proceedings of the Ocean Drilling Program, Scientific Results*. Ocean Drilling Program, College Station, TX, pp. 431-438.
- Thistle, D., Yingst, J.Y. and Fauchald, K., 1985. A deep-sea benthic community exposed to strong near-bottom currents on the Scotian Rise (western Atlantic). *Marine Geology*, 66(1-4): 91-112.

- Tivey, M., Takeuchi, A. and Scientific Party, W., 1998. A submersible study of the western intersection of the Mid-Atlantic ridge and Kane fracture zone (WMARK). *Marine Geophysical Researches*, 20(3): 195-218.
- Tucholke, B. E., Houtz, R. E., and Ludwig, W. J., 1982, Sediment thickness and depth to basement in western North Atlantic Ocean basin: *AAPG Bulletin*, v. 66, no. 9, p. 1384-1395.
- Tucholke, B.E., Hollister, C.D., Biscaye, P.E. and Gardner, W.D., 1985. Abyssal current character determined from sediment bedforms on the Nova Scotian continental rise. *Marine Geology*, 66(1-4): 43-57.
- Tucholke, B.E., Kenneth Stewart, W. and Kleinrock, M.C., 1997. Long-term denudation of ocean crust in the central North Atlantic Ocean. *Geology*, 25(2): 171-174.
- Van Andel, T.H., 1975. Mesozoic/cenozoic calcite compensation depth and the global distribution of calcareous sediments. *Earth and Planetary Science Letters*, 26(2): 187-194.
- van Andel, T.H. and Bowin, C.O., 1968. Mid-Atlantic ridge between 22 degrees and 23 degrees north latitude and the tectonics of mid-ocean rises. *Journal of Geophysical Research*, 73(4): 1279-1298.
- van Andel, T.H. and Komar, P.D., 1969. Ponded sediments of the Mid-Atlantic ridge between 22 degrees and 23 degrees north latitude. *Geological Society of America Bulletin*, 80(7): 1163-1190.
- Varne, R., Brown, A.V. and Falloon, T., 2000. Macquarie Island; its geology, structural history, and the timing and tectonic setting of its N-MORB to E-MORB magmatism. In: Y. Dilek, E.M. Moores, D. Elthon and A. Nicolas (Editors), *Special Paper - Geological Society of America*, vol.349, pp. 301-320.
- Viana, A.R., Faugères, J.C. and Stow, D.A.V., 1998. Bottom-current-controlled sand deposits -- a review of modern shallow- to deep-water environments. *Sedimentary Geology*, 115(1-4): 53-80.
- Walker, R.G., 1978. Deep-water sandstone facies and ancient submarine fans; models for exploration for stratigraphic traps. *AAPG Bulletin*, 62(6): 932-966.
- Wertz, K.L., Mosher, S., Daczko, N.R. and Coffin, M.F., 2003. Macquarie Island's Finch-Langdon Fault; a ridge-transform inside-corner structure. *Geology*, 31(8): 661-664.
- Zonenshain, L.P., Kuzmin, M.I., Lisitsin, A.P., Bogdanov, Y.A. and Baranov, B.V., 1989. Tectonics of the Mid-Atlantic rift valley between the TAG and MARK areas (26-24°N): Evidence for vertical tectonism. *Tectonophysics*, 159(1-2): 1-23.

III:

Discussion on the depositional mechanism of massive sandstone and implications from detrital clay mineralogy

Introduction:

The deep-water massive sandstone conundrum

Offshore petroleum exploration over the past two decades has increasingly sought out deep water massive sands, which commonly form key hydrocarbon reservoirs (Stow and Johansson 2000). However, the depositional flow dynamics that produce these massive sands are still enveloped in controversy (e.g. Arnott and Hand 1989; Kneller and Branney 1995; Shanmugam 1996; Amy et al. 2005; Talling et al. 2007). Experimental work has shown that high sedimentation rates and/or rapid flow deceleration within turbidity currents can impede traction transport and bed load reworking, thus producing massive sand of the Bouma A division (Lowe 1988; Arnott and Hand 1989; Allen 1991; Kneller 1995; Sumner et al. 2008). This is in stark contrast to other modes of formation for deep-marine massive sandstone which include: 1) a sandy debris flow origin with laminar non-Newtonian flow rheology (Shanmugam 1996; Stow and Johansson 2000); 2) fluidized flow with upward water-escape grain support mechanisms (Lowe 1976); and 3) post-depositional fluidization (Lowe 1975; this study). Distinguishing between these different mechanisms and transitions between them (Stow and Johansson 2000) is important because proximal remobilization processes (e.g. fluidized flow) vs. long distance transport processes (e.g. high-density turbidity flow) will create different hydrocarbon reservoir characteristics.

In this chapter the mechanism that produced the very well-exposed massive sandstone exposed at Mawson Point (Fig. 2.2C Mawson Point 1/4 unit 5) is explored in more detail. For the purpose of this study, massive sandstone is synonymous with structureless sandstone without regard to thickness. Typically, the thickness (~1 m)

of the Mawson Point massive sandstone and its occurrence within a normal graded turbidite sequence precludes it from being classified as a true very thick deep-water massive sandstone (*sensu stricto* Stow and Johansson 2000), but meter-scale massive sandstone debrites (sandy debris flow origin) do occur within co-genetic turbidite sequences (Talling et al. 2004; Talling et al. 2007). A total mud matrix percentage between 15 and 50% in these “turbidite-sandwiched-debrites” is used as a proxy for interpreting massive sandstone of debris flow origin from turbidite origin (Talling et al. 2007). However, due to problems encountered from the inherent difficulty of recognizing authigenic (diagenetic) clay from detrital clay, the importance of relative differences in clay contents rather than absolute amounts has been noted (Amy et al. 2005). Furthermore, Amy et al. (2005) proposed the usage of bed geometry to infer gravity flow mechanism for deposition of massive sandstones. Bed geometry in Macquarie Island sedimentary lithofacies is partly constrained by the lateral confinement by intrabasinal faults and/or volcanic constructions (see Chapter II) and therefore is not a reliable criterion to use. This chapter reconciles this dilemma by complementing detailed sedimentology, stratigraphy, and petrography with clay mineralogy from sandstone and interbedded basalt alteration. Clay mineralogy is inferred from geochemical data collected with the electron microprobe (method in Appendix E) and validated with X-ray diffraction data collected (method in Appendix F) from interbedded mudstones.

Clay mineralogy and low grade metamorphism

Clay alteration minerals from metabasite terrains and deep-sea drilling project boreholes show an array of compositions between ideal end-members of celadonite (dioctahedral mica) through saponite (trioctahedral smectite) to chlorite (Schiffman

and Fridleifsson 1991; Neuhoff et al. 1999; Demant et al. 1998; Neuhoff et al. 2006). This compositional array is associated with burial depth and/or hydrothermal system influence (Chang et al. 1986; Schiffman and Staudigel 1995). Low temperature seawater alteration (15-65°C) of pillow basalts on the young seafloor typically produce mixtures of iddingsite (Fe-oxyhydroxide and clay mixture), celadonite, and saponite compositions, the latter becoming more pervasive with increasing degrees of alteration (Marescotti et al. 2000). In addition, smectitic clays may change from di- to trioctahedral varieties with increasing temperatures (Schiffman and Fridleifsson 1991; Neuhoff et al. 2006). Discrete smectite is stable up to 60-100 °C in burial metamorphosed settings (Helmold and van de Kamp 1984; Chang et al. 1986) and 150-210°C in geothermal settings when corrensite (interlayered trioctahedral smectite and chlorite) and/or discrete chlorite become the dominant clay mineral (Robinson et al. 2002). The reaction pathway during the smectite to chlorite transition is dependant upon fluid-rock ratios and can be continuously or discontinuously interlayered with a corrensite compositional midpoint, as well as, direct with no progressive interlayering phase (Robinson et al. 1993; Robinson et al. 2002). Discrete chlorite generally occurs at the zeolite-greenschist metamorphic facies boundary.

On Macquarie Island the smectite to chlorite transition occurs along with the upper stability limit for laumontite and marks the boundary between zeolite and greenschist metamorphic grades in the islands extrusive sequence (Griffin 1982). The zeolite-greenschist metamorphic boundary exists in the middle of the island between Davis Bay on the west-coast and Pyramid Peak on the plateau, which make up the base and top, respectively, of a relatively intact block of oceanic crust with the Major

Lake spreading-related fault at its base (Fig. 3.1). A composite stratigraphic section through this crustal block (Fig. 3.1) contains a relatively continuous variation in clay mineral non-interlayer cations, $\text{Si}+\text{Al}+\text{Fe}+\text{Mg}+\text{Mn}$, measured in altered basalt groundmass. This geochemical technique has proven to be a good tool in discriminating the transition from smectite to corrensite to chlorite, where higher percentages of the non-interlayer cations correspond to more chloritic compositions (Schiffman and Staudigel 1995; Neuhoﬀ et al. 2006). Figure 3.1 shows chloritic clays within the base of the section (Davis Bay) through a chlorite-rich corrensite phase in its middle (Davis Point escarpment) to smectitic-rich corrensite clays (Pyramid Peak) in the top. This stratigraphic change in clay mineralogy is not matched by a similar covariation in basalt geochemistry, thus ruling out host rock control of the clay composition progression (Fig. 3.1). Therefore, the gradual change in basalt clay species provides good constraint on the burial temperatures of interbedded sandstone and associated authigenic clay minerals. A thin graded sandstone facies in the middle of the Davis Point section was selected for comparison against the Mawson Point sandstone. The Davis Point sandstone is at a near equivalent stratigraphic position to where clay alteration from a Mawson Point tabular basalt unit (MP1-10 of Fig. 3.2) would hypothetically occur according to its non-interlayer cation composition (Fig. 3.1). By comparing clay mineralogy and composition from sandstones and interbedded basalt clays at both Davis Point and Mawson Point it is possible to identify primary (detrital or syn-metamorphic) vs. secondary (authigenic or post-metamorphic) clay minerals in the context of the sandstones' diagenetic history. This distinction can then be used to interpret the primary depositional

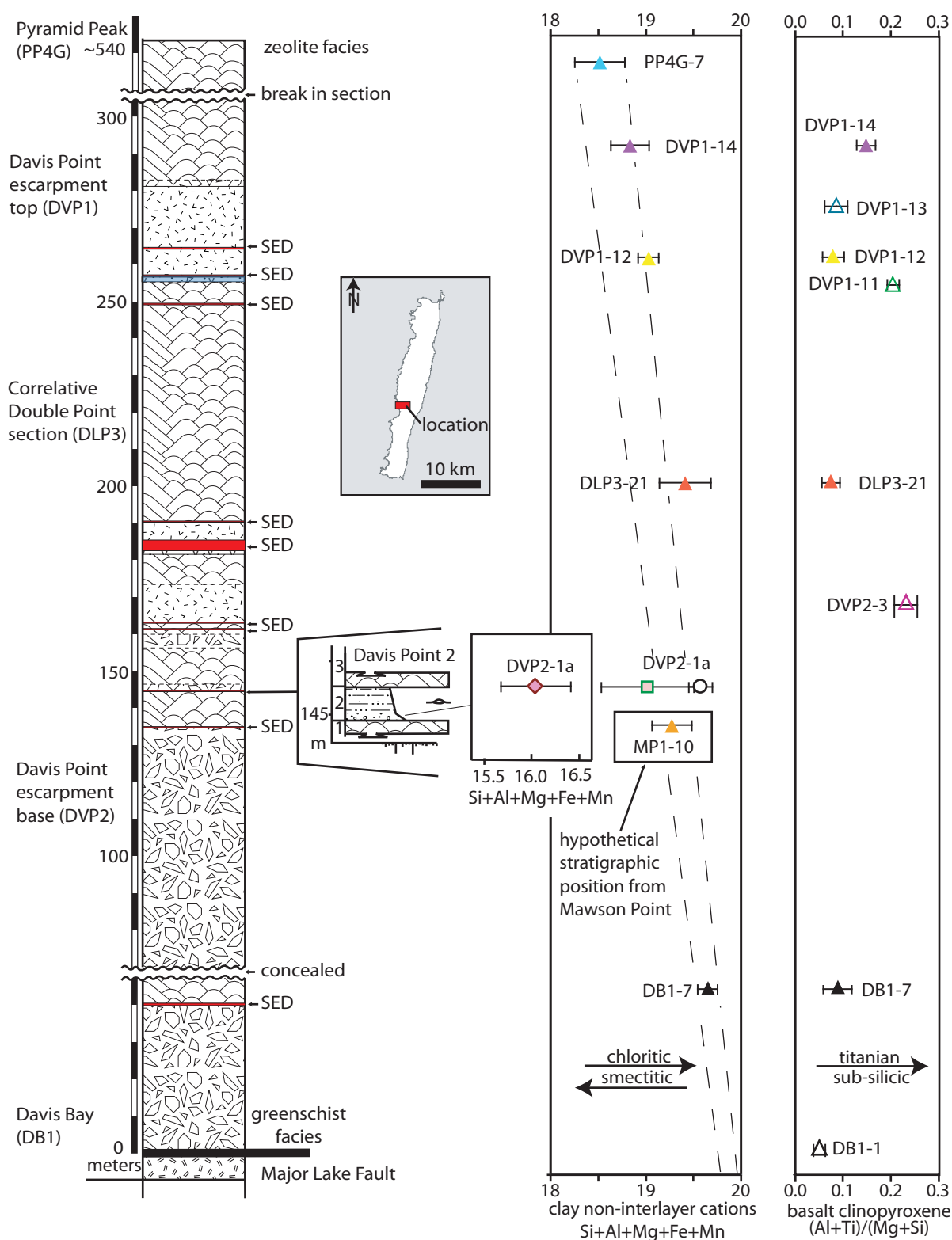
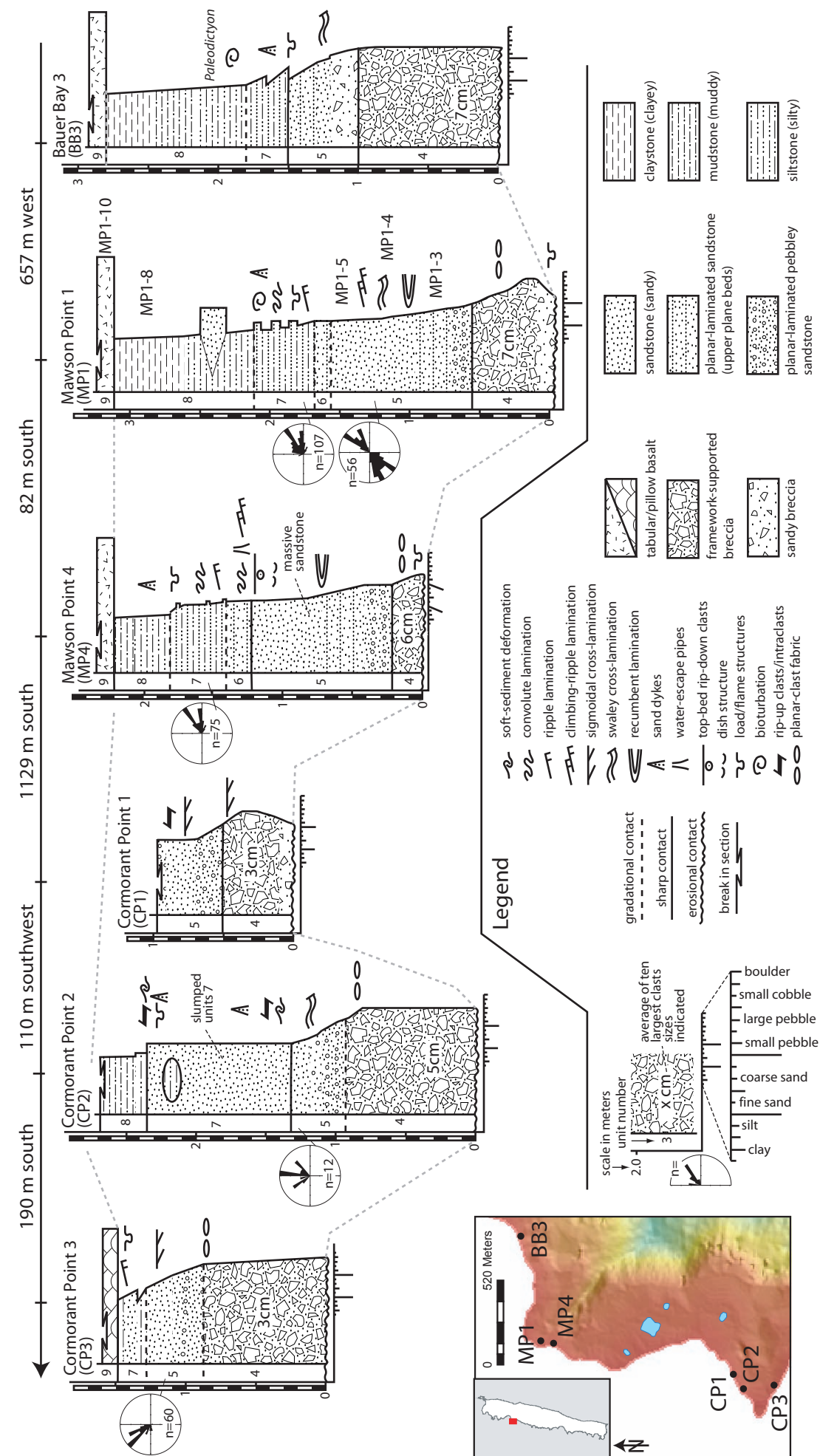


Figure 3.1: Composite stratigraphic section from Davis Bay up through the Davis Point/Double Point escarpment to Pyramid Peak. Section thickness across break in section between Davis Point and Pyramid Peak is approximated based on stratigraphic dips. Several sedimentary sections (SED) shown as red markers are generally thin (<1 m) gabbroic sedimentary rock intervals. Averaged non-interlayer cation, $\text{Si}+\text{Al}+\text{Mg}+\text{Fe}+\text{Mn}$, abundances from clay alteration in basalt units (triangles) and clay within one SED sample DVP2-1a (circles, diamonds, squares) show relative decrease upward through the section from chloritic to smectitic clay. A basalt unit from the Mawson Point sedimentary section is shown for comparison (see sample MP1-10 on Fig. 3.2). Averaged clinopyroxene major element ratios $(\text{Al}+\text{Ti})/(\text{Mg}+\text{Si})$ from Davis Point basalt units show variable titanian-subsilicic compositions. See Chapter I for basalt clinopyroxene data and methodology. All error bars are 1 sigma.



mechanism for the Mawson Point massive sandstone in terms of its original clay matrix component.

Results:

Mawson Point massive sandstone:

Description

Well-preserved graded sandstone facies from the Mawson Point 4 measured section (MP4) contains a 0.5 m thick massive sandstone unit that correlates with units to the east at Bauer Bay and to the south at Cormorant Point over a 1.5 km distance (Fig. 3.2). These stratigraphically equivalent sections contain a vertical succession of bed forms (units 5-7 in MP1 Fig. 3.2). Planar lamination within the lowermost coarse-grained sandstone (unit 5i) becomes inclined at progressively higher angles up-section from 5° to 22° where it exhibits overturned recumbent fold geometries (unit 5ii; Fig. 3.3A-B). In MP1 these recumbent folds are overlain by dune-scale swaley bedforms that show vertical to low-angles of climb similar to associated critically-climbing ripples (unit 5iii; Fig. 3.3B-C). Laterally this bedform sequence correlates with sigmoidal-shape cross-beds at Cormorant Point (Fig. 3.3D). Sigmoidal cross-beds contain bounding surfaces with small gravel lags and become progressively lower-angle down depositional-dip where they have planar geometries. This cross-stratified interval laterally correlates with massive sandstone in the MP4 section (Fig. 3.3E), which exhibits water-escape pipes and rare dish structures. The massive sandstone and correlative cross-bedded intervals are overlain by fine-grained planar laminated sandstone, which locally contains convolute laminations that verge toward the inclination direction of cross-cutting water escape pipes (Fig. 3.3F). At

Figure 3.3 (opposite):

Photograph and sketch montage of units associated with the Mawson Point massive sandstone. A) Recumbent lamination toward the base of unit 5 at MP1. Scale is in cm. B) Sketch of complexly cross laminated sandstone of unit 5 at MP1. Shows planar laminated granule-rich unit 5i, recumbent folded low-angle laminations of unit 5ii, and critically-climbing ripples and swaley dune-scale cross bedding of unit 5iii. C) Portion of outcrop shown in B. Scale is 20 cm long. D) Equivalents units at Cormorant Point (CP3) containing structureless granule-rich breccia of unit 4 grading up into medium-grained sandstone with sigmoidal cross-bedding of unit 5. Sketch depicts cross-bed bounding surfaces with granules and small pebbles. E) Turbidite sequence at MP4 with massive sandstone (units 5ii-iii). Red mudstone cap of unit 8 is not shown. F) Convolute planar lamination of unit 6 at MP4 with cross-cutting water-escape pipes. Paleocurrent to left (northeast). Red clay fractures are late dilational features. G) Sharp contact between massive sandstone of unit 5iii with overlying planar laminated sandstone of unit 6 at MP4. Note wispy-shaped top-bed rip-down clasts locally suspended in underlying massive sandstone (arrows). H) Coarse-grained clastic dykes from unit 5 cross cutting unit 7 at Bauer Bay 3.

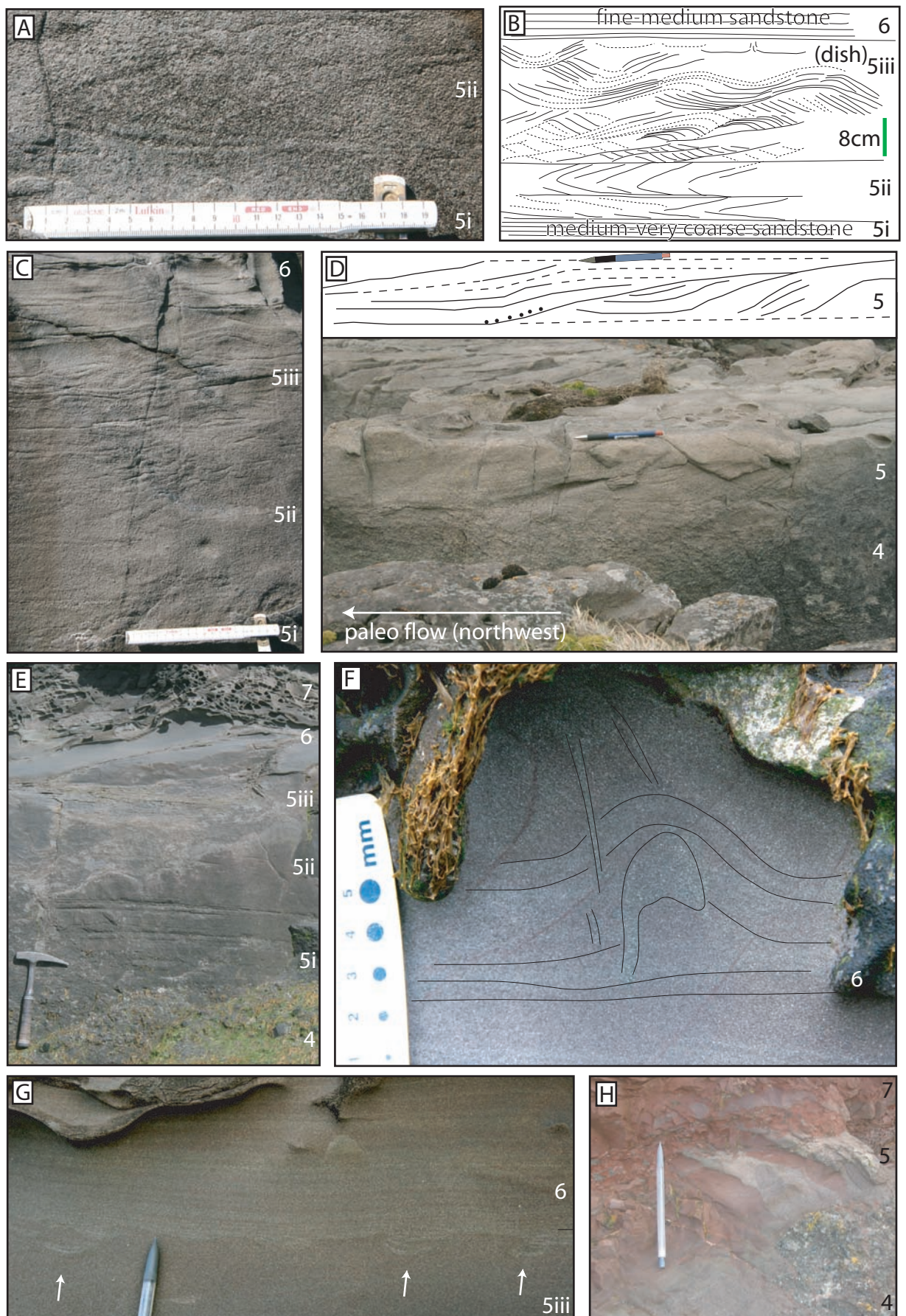


Figure 3.3

MP4 the boundary between the massive and overlying planar-laminated sandstone intervals exhibits concave up top-bed rip-down clasts (Fig. 3.3G). There is no distinct grain size break across this sharp contact, but a change in paleocurrent direction is notable in the Mawson Point section (MP1). Clastic dykes emanating from the massive sandstone interval penetrate upward into uppermost finest-grained mudstone units (Fig. 3.3 H).

Interpretation

Results from Chapter II suggest that massive sandstone from the Mawson Point unit was deposited by a turbidity current that underwent post-depositional fluidization. This interpretation is based upon the occurrence of massive sandstone within a continuously normal graded succession, presence of water-escape features along its upper contact, and its correlation with dune-scale cross-bedded sandstone. Overturned cross-lamination that directly underlies the massive/cross-bedded interval is generally attributed to: 1) liquefied- or fluidized-shear induced by an overriding current; 2) gravitational slip; or 3) seismic shock (Allen and Banks 1972; Allen 1982). Røe and Hermansen (2006) also document the lateral transition of large-scale sigmoidal cross-bedding to overturned recumbent folds and massive zones in medium- to fine-grained fluvial sandstone. They concluded that the deformation was caused by fluidal shear-induced drag from an overlying high-density flow, which underwent fluid turbulence instabilities along the dune/upper-stage plane-bed flow regime transition. The sequence of bed forms in the Mawson Point example goes from upper plane bed up through recumbent folds into swaley dunes (Fig. 3.3B). This progression also suggests that turbidity current conditions were close to the lower/upper flow regime boundary (Fig. 3.4) and therefore the Mawson Point

recumbent folds likely formed by turbulent current-induced drag. Climbing-ripple and swaley bed forms in overlying units indicate that the current had a high sediment concentration or fall-out rate (Mulder et al. 2009; Postma et al. 2009) and would have provided the essential inertia to cause drag in underlying traction structures.

The upward and/or lateral transition of overturned cross-beds to massive sandstone lead Røe and Hermansen (2006) to conclude that a liquefied bed rheology permitted erosion and destruction of primary laminations by the overriding current. At Mawson Point we do not see sharp surfaces suggestive of erosion, but rather gradual diffuse boundaries suggesting that passive disaggregation/ homogenization of the sand occurred. This process would have destroyed primary sedimentary structures by: 1) upward and/or lateral density current-induced fluid drag; and/or 2) load-induced compaction that caused water-escape and reorganization of the primary structures. The inclined down-paleocurrent vergence of asymmetric convolute laminations and cross-cutting water-escape pipes suggests that both upward and lateral grain movement would have been under the influence of current-induced drag during water-escape. This mechanism of grain support by an upward force exerted by water-escape during lateral down slope movement is by definition a fluidized flow (Lowe 1975). However, the preservation of these features suggests that a post-depositional fluidization process occurred without any significant lateral transport. This conclusion complies with a previous detailed investigation by Lowe (1975) on the timing of pervasive water-escape during the load-induced consolidation of a rapidly deposited “quick” bed.

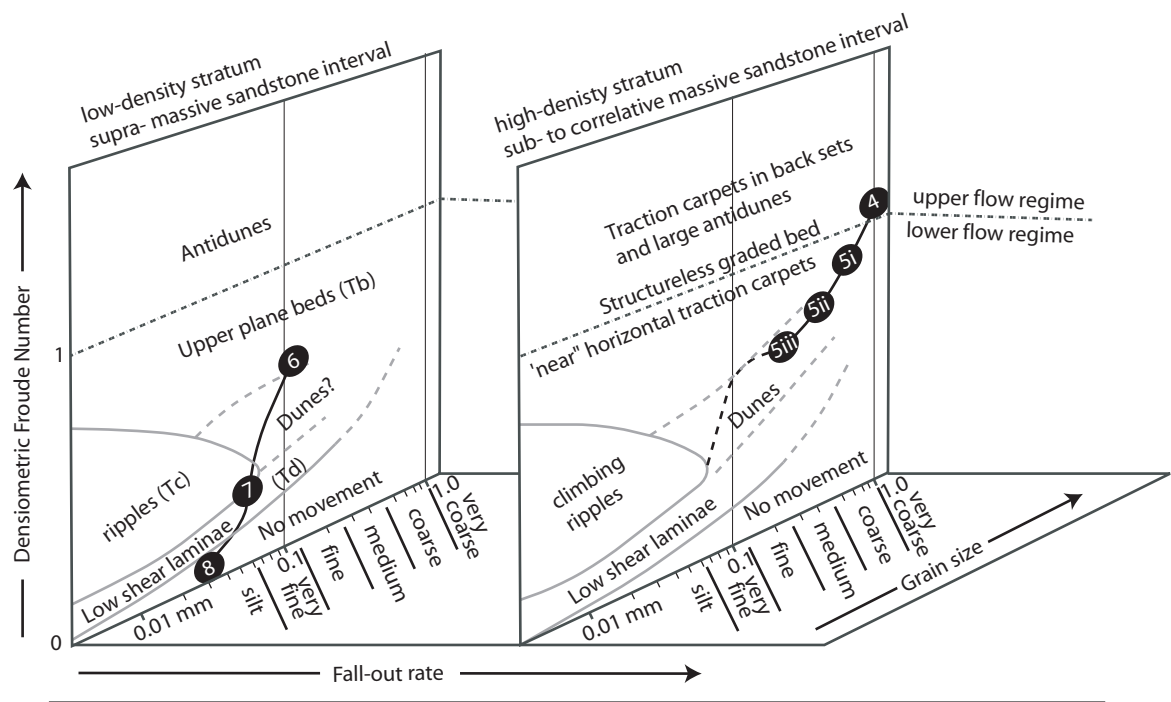


Figure 3.4:
 Bed form stability diagram with Mawson Point section 1 units overlain for comparison. Sedimentation fall-out rate is a qualitative distinction between relatively low- and high-density (sediment-laden) turbidity current end-members produced in saline water. Modified from Postma et al. (2009).

Therefore, both current-induced drag and a load-induced compaction stress caused fluidization of the turbidite bed and creation of the Mawson Point massive sandstone. In addition, a post-depositional fluidization origin rather than a syndepositional origin from debris flow or high sedimentation rates for the Mawson Point massive sandstone is supported by top-bed rip-down clasts. These clasts appear to form by a stoping process as a fluidization front sweeps up through the bed (Allen 1982; Stow and Johansson 2000). The fluidization front boundary exists along the transition from cross-stratified lamination to planar lamination and most likely occurs here due to the relative impermeability of bedding-parallel clay-rich laminae (after Lowe 1975).

Sandstone clay petrography

Medium- to coarse-grained massive sandstone from the Mawson Point and Davis Point sequence is moderately to well-sorted and well-cemented with ~6% intergrown quartz-albite-laumontite and minor amounts of calcite. Argillaceous minerals make up between 7-19% of point counted framework grains (see Chapter I for methodology) and matrix (Fig. 3.5). Petrographically four clay mineral types can be recognized and include light green, brownish-green, brownish-red, and dark red opaque clay. Non-discrete argillaceous grains are ubiquitously composed of dark red and brownish-red clay and were not tallied with phyllosilicate minerals on point counts shown in Fig. 3.5. These grains primarily include volcanic lithic grains that exhibit clay alteration of vitric groundmass domains with included microphenocrysts, spherulites, and/or vesicles (Fig. 3.6A).

All discrete argillaceous grains, including light green, brownish green and dark red clay, exhibit pseudolithic matrix cement characteristics. Both light green and

brownish-green clay are coarsely crystalline and optically clear (Fig. 3.6B). Most light green clay is easily recognizable as chlorite in thin section by anomalous blue-brown interference colors and the common presence of amphibole needle intergrowths (Fig. 3.6C). Light green clay that does not display blue-brown interference colors and most brownish-green clay commonly exhibit authigenic growth rings parallel to grain boundaries (Fig. 3.6D). Both of these varieties locally contain titanite crystals and have authigenic crystal habits similar to clay alteration of interbedded basalt ground mass (Fig. 3.6E). Dark red clay is similar in appearance to intrabasinal rip-up clasts in underlying breccias, thin argillic laminations in overlying siltstone, and red mudstones (Fig. 3.6F).

Clay composition and mineralogy from electron microprobe data:

Three varieties of corrensite from Robinson et al. (1993) are plotted on Fig. 3.7A and include randomly interlayered (RO) and regularly interlayered (R1) chlorite:trioctahedral smectite (C/S) compositions with the latter having 65% and 85% chlorite interlayers relative to smectite. Basalt compositions from the Davis Point section range from discrete chlorite along its greenschist-grade base through decreasing amounts of chlorite interlayers within R1 ordered corrensite to RO ordered corrensite in its zeolite-grade top (Fig. 3.1; 3.7A). Sandstone chlorite grains plot with alteration clays from greenschist facies basalt sample DB1-7 (Fig. 3.7B). Light green clay exhibiting authigenic growth rings yield a chloritic corrensite composition. Dark red clay in the sandstones has variable compositions that yield two distinctly different phase end-members based on $\text{FeO}^{\text{total}}$, which averages 50-60 wt% or 20-30 wt% (Table 3.1). The average composition of the low-Fe red clay end-member plots near the 50% R1 ordered corrensite midway point along with

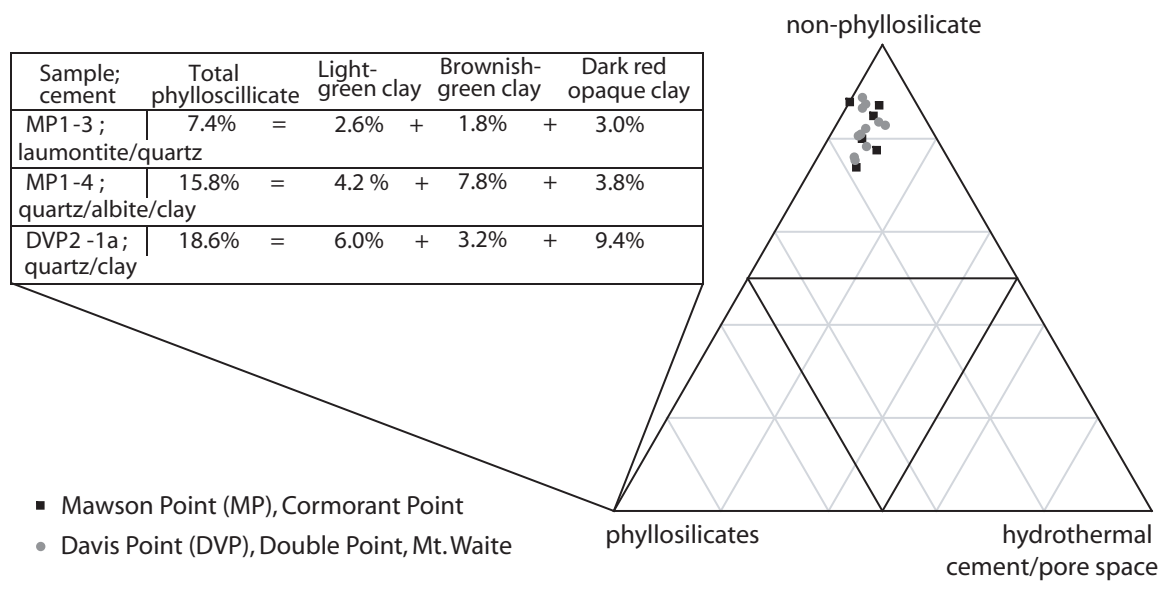


Figure 3.5:
Ternary diagram showing point counts from several sandstone units collected from sections associated with the Mawson Point location and Davis Point location. The relative proportions and total amount of discrete clay minerals identified in thin-sections of Mawson Point and Davis Point samples are shown for comparison.

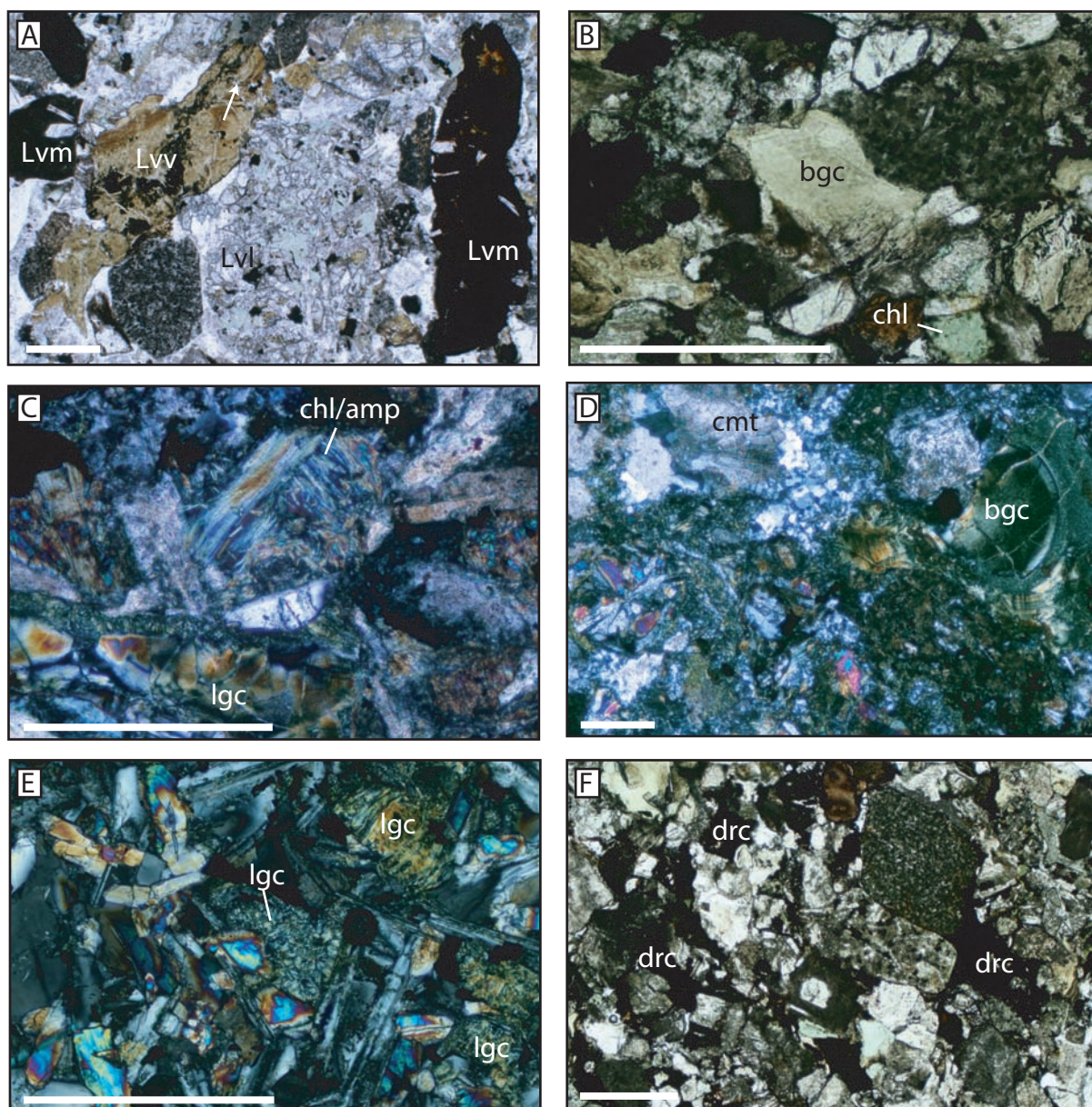


Figure 3.6:

Photomicrographs of Macquarie Island clay minerals. All scales are 0.5 mm long. A) Argillaceous volcanic and subvolcanic lithics including red-clay altered microlitic grains (Lvm), brownish-red devitrified grain (Lvv) with internal authigenic growth ring (arrow), and a chlorite-altered lathwork grains (Lvl). From Cormoarnt Point sandstone. B) Comparison of brownish-green clay (bgc) and light-green chlorite (chl) in uncrossed polars from DVP2-1a sandstone. C) Comparison of light green clay (lgc) lacking blue interference colors, which are very prevalent in adjacent chl grain. Chlorite grain also contains amphibole (amp) needle intergrowths. Crossed polars from Unity Point sandstone. D) Growth rings in bgc adjacent to pore cement (cmt) containing calcite, quartz, and albite from Cormorant Point sandstone. E) Lgc groundmass alteration within MP1-10 basalt. F) Dark red clay (drc) exhibiting pseudo-matrix morphology (right) from DVP2-1a sandstone.

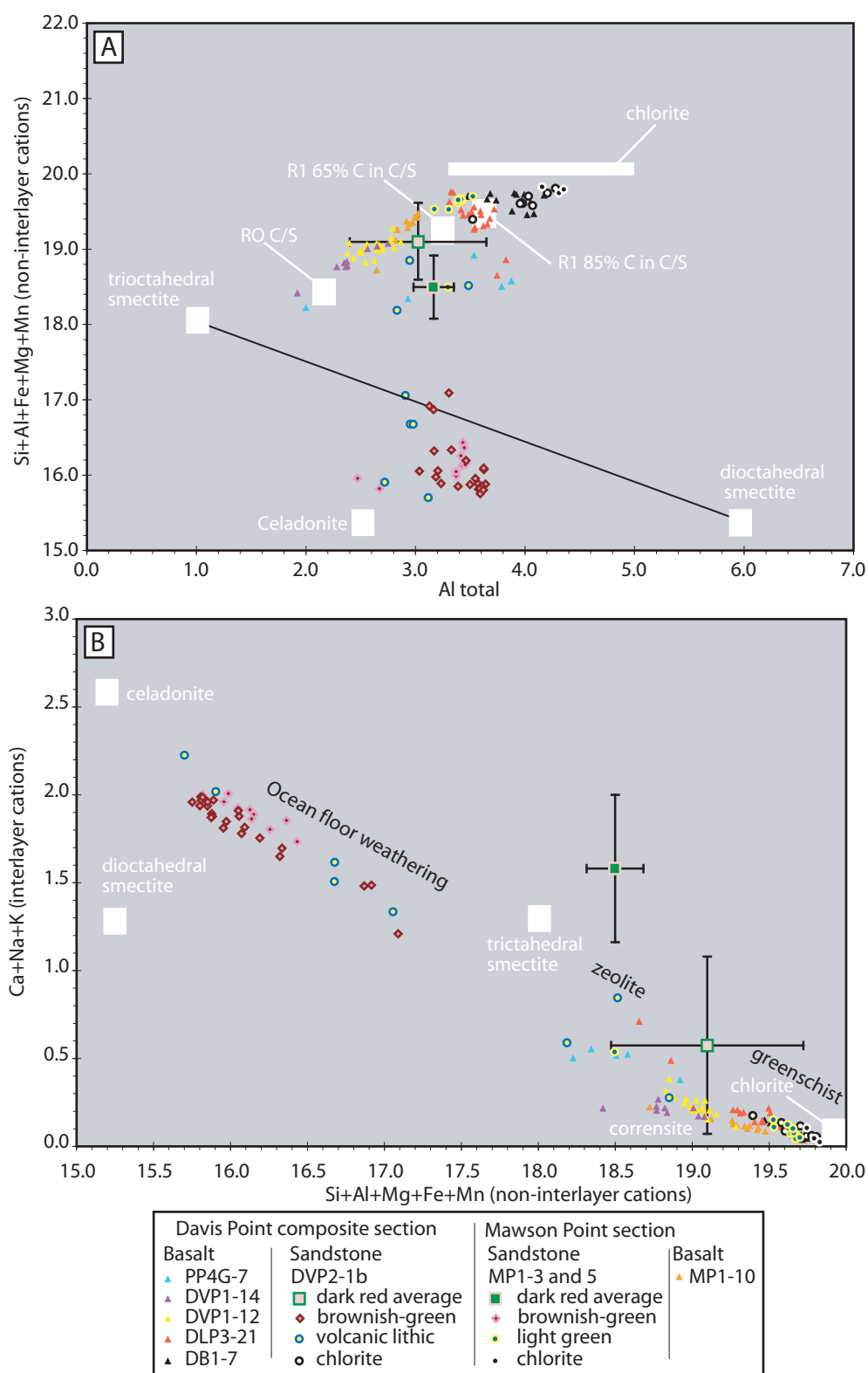


Figure 3.7: Clay composition and inferred mineralogy in sandstone and basalt from the Davis Point and Mawson Point section location. Cation abundances are based on 28 Oxygens. Error bars on dark red detrital clay averaged samples are 1 standard deviation. Numbers of analyses for all samples are listed in Table 3.1. Trioctahedral smectite includes: saponite and stevensite. Dioctahedral smectite includes: beidellite (tetrahedral substitution), nontronite (Fe-rich), and montmorillonite (Al-rich). A) Non-interlayer cations (Si+Al+Fe+Mg+Mn) against total Aluminum. Ideal mineral end-members are taken from Robinson (1993). Randomly-ordered (RO) and regularly-ordered chlorite/smectite (C/S) interlayered clay list relevant proportion of chlorite interlayers in percent. B) Exchangeable interlayer cations (Ca+Na+K) against non-interlayer cations (Si+Al+Fe+Mg+Mn). Ideal mineral end-members are taken from Neuhoﬀ et al. (1996). Relevant metamorphic grades from Macquarie Island clay species are inferred from Griﬃn (1982).

Table 3.1: Averaged sandstone (DVP2-1a and MP1-3/5) and basalt (MP1-10) clay compositions in wt%. Cation formulas based on 28 oxygens. Analyses with totals less than 80% were not included in the averages.

Sample Clay color, mineral	DVP2-1a Brown- green, smectite	DVP2-1a Dark red, corrensite	DVP2-1a Light green, chlorite	MP1-3/5 Brown- green, smectite	MP1-3/5 Light green, corrensite	MP1-3/5 Dark red, corrensite	MP1-3/5 Dark red, Fe-oxy hydroxide	MP1-3/5 Light green, chlorite	MP1-10 Light green, corrensite
n=	23	19	8	10	9	4	3	3	11
SiO ₂	51.44	32.66	30.92	45.65	31.86	28.78	15.17	28.98	35.78
TiO ₂	0.28	0.37	0.01	0.18	0.29	0.15	0.66	0.03	0.03
Al ₂ O ₃	16.32	12.21	16.75	13.69	13.82	12.26	5.99	17.50	12.37
Cr ₂ O ₃	0.03	0.02	0.01	0.02	0.01	0.01	0.01	0.02	0.01
FeO ^{total}	10.04	21.08	16.96	11.22	22.15	27.82	57.74	22.96	15.63
MnO	0.22	0.43	0.43	0.10	0.29	0.31	0.14	0.32	0.09
MgO	7.47	17.34	21.21	5.83	18.33	11.82	5.26	17.74	22.43
CaO	0.54	1.00	0.34	0.19	0.56	6.47	1.59	0.21	0.42
Na ₂ O	0.08	0.22	0.05	0.08	0.03	0.08	0.10	0.01	0.05
K ₂ O	7.40	0.97	0.05	7.08	0.03	0.08	0.59	0.03	0.07
NiO	0.02	0.03	0.05	0.02	0.02	0.02	0.01	0.02	0.08
Total	93.84	86.33	86.78	84.06	87.39	87.80	87.25	87.82	86.98
Si	9.16	6.86	6.27	9.21	6.59	6.31	4.23	6.00	7.12
Ti	0.04	0.06	0.00	0.03	0.05	0.03	0.14	0.00	0.00
Al	3.42	3.02	4.00	3.25	3.37	3.17	1.97	4.27	2.90
Cr	0.00	0.00	0.00	0.00	0.00	0.00	0.00	0.00	0.00
Fe	1.49	3.70	2.87	1.89	3.83	5.10	13.47	3.98	2.60
Mn	0.03	0.08	0.07	0.02	0.05	0.06	0.03	0.06	0.02
Mg	1.98	5.43	6.41	1.75	5.65	3.86	2.19	5.48	6.65
Ca	0.10	0.22	0.07	0.04	0.12	1.52	0.48	0.05	0.09
Na	0.03	0.09	0.02	0.03	0.01	0.03	0.06	0.00	0.02
K	1.68	0.26	0.01	1.82	0.01	0.02	0.21	0.01	0.02
Ni	0.00	0.01	0.01	0.00	0.00	0.00	0.00	0.00	0.01
Si+Al+Mg +Fe+Mn	16.09	19.10	19.63	16.13	19.49	18.50	21.89	19.79	19.28
Ca+Na+K	1.81	0.57	0.11	1.90	0.14	1.58	0.74	0.06	0.13
Fe/Fe+Mg	0.43	0.41	0.31	0.52	0.40	0.57	0.86	0.42	0.28
Si/Si+Al	0.73	0.69	0.61	0.74	0.66	0.67	0.68	0.58	0.71

associated interbedded basalts (MP1-10 and DVP1-12 in Fig. 3.7A). The high Fe end-member is most likely a Fe-oxyhydroxide phase mixed in with the red clay phase (i.e. iddingsite) and therefore only analysis with low-Fe values are included in the phyllosilicate plots. Sandstone volcanic lithic grains (Lv) with extensive red clay alteration in thin section exhibit a compositional array stretching between the 50% R1-ordered corrensite to a celadonite-like smectite composition. This celadonite-like composition also dominates the brownish-green clay in sandstones, which have intermediate compositions between di- and trioctahedral smectite end-members.

Clay mineralogy from X-ray diffraction

Due to the variable geochemical results obtained from the dark red clay in sandstones, X-ray diffraction was used to determine the clay mineralogy of the red capping mudstone unit in the Mawson Point turbidite (MP1-8 in Fig. 3.2). This approach assumes that clay within the mudstone cap is of a similar composition and mineralogy to red clay in the sandstone. This inference is based upon a genetic relationship between the basal sandstone and upper mudstone from the same turbidite, which exhibits upward-increasing red clay contents from bottom to top.

A diffractogram output from an oriented sample of the glycolated clay size-fraction (<2 μ) separated from the Mawson Point turbidite mudstone cap was modeled using NEWMOD software (Reynolds 1985). The results shown in Fig. 3.8 indicate that the mudstone is primarily composed of 47% chlorite, 38% corrensite (interlayered chlorite/smectite), and 15% trioctahedral smectite (saponite). Discrete Fe-rich chlorite is best observed by the relative stability of the 14.5Å (d001) peak and disappearance of the higher intensity 7.2Å (d002) and 4.8Å (d003) peaks after heat treatment of 550°C (Fig. 3.8). The d001 chlorite peak is masked by strong 15.6Å and

16.5Å reflections of corrensite (d002) and discrete smectite (d001), respectively, in the unheated glycolated sample. The presence of the 31.5Å peak (d001) in the glycolated sample and its disappearance upon heat treatment is indicative of R1 ordered (regularly interlayered) corrensite. In addition, the crude reappearance of the corrensite d001 peak at 23.9Å after 550°C heat treatment further indicates an R1 ordered type. Modeling shows that corrensite is composed of Fe-rich trioctahedral smectite (ferrosaponite) and chlorite with a 1:1 ratio. This variety of corrensite would hypothetically fall into the same position as that measured using the microprobe for sandstone red clay and associated basalt interbeds (i.e. between RO and 65% R1 corrensite on Fig. 3.7A).

In addition to clay minerals, quartz, ca-rich plagioclase, calcite, and sulphides are also a notable constituent, with some being ground down into the clay fraction during sample preparation (Fig. 3.8). A 2.71Å peak prevalent throughout all treatments corresponds to the most intense basal reflection for marcasite (FeS₂) and second most intense peak for pyrite. The presence of these minerals and other unidentified minerals is supported by bulk random powder diffraction analysis (Appendix F), and likely causes the high percentages of Si, Al, Ca, and Fe observed in the microprobe data results for dark red clay grains (Table 3.1). This multi-phase mineralogy, including different discrete clay minerals, of the dark red clay causes it to have the widely variable chemical compositions demonstrated by large error bars in Fig. 3.7. Nevertheless, comparing clay mineralogy identified by microprobe analysis (sandstone, basalt) vs. x-ray diffraction methods (mudstone) is validated by a nearly equivalent composition of corrensite determined by both methods.

Compared to the electron microprobe technique x-ray diffraction is less sensitive to

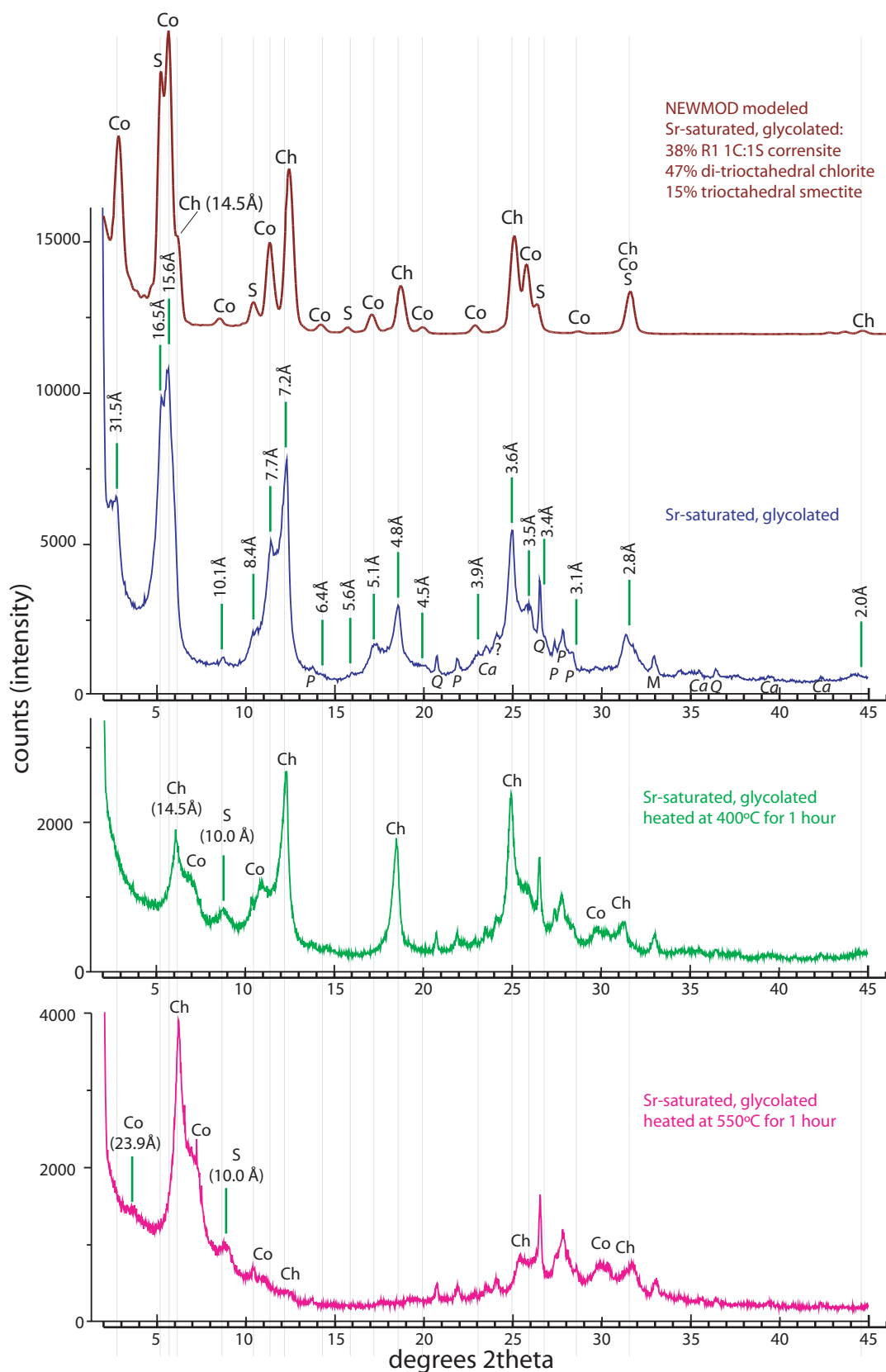


Figure 3.8: X-ray diffraction patterns for MP1-8 red mudstone unit at top of Mawson Point turbidite sequence. All diffractograms are for the clay fraction ($<2\mu$) of a centrifuged sample, which was saturated with SrCl. The top-most pattern is a modeled diffractogram output from NEWMOD (Reynolds 1985) software with peaks identified as Corrensite (Co), Smectite (S), and Chlorite (Ch). Full parameters used in the modeling software are in Appendix F. The model diffractogram matches very closely with the glycolated sample (second down), which has peaks identified in d-spacing (Å). Sharp peaks not observed in the model are due to contamination by quartz (Q), ca-rich plagioclase (P), calcite (Ca), and Marcasite (M), which ground down into the $<2\mu$ fraction during sample preparation. The stability of these contaminant minerals is observed in successive heat treatments at 400°C and 550°C.

the presence of small amounts of chlorite interlayers within corrensite (Schiffman and Fridleifsson 1991), but is irrelevant in Mawson Point samples that contain ~50% chlorite interlayers.

Discussion:

Diagenetic conditions

Corrensite clay alteration in interbedded basalt units supports an upper zeolite metamorphic grade for both the Mawson Point and Davis Point sandstone samples. This is substantiated by laumontite cement in both sandstones, which indicates temperatures between 110 and 190° C (Demant et al. 1998; Helmold and van de Kamp 1984). An upper zeolite metamorphic grade in the studied sandstones is also supported by the absence of prehnite pore-filling cement, which is indicative of greenschist conditions on Macquarie Island (Griffin 1982).

Based on these results, it appears that the brownish-green di/trioctahedral smectitic clay component in sandstone samples is not in equilibrium with the higher metamorphic grade of corrensite clay in associated mudstone units and interbedded basalt (see diamond DVP2-1a in Fig. 3.1). The mineralogic discontinuity between the correlative mudstone and sandstone clays could be due to the impermeable nature of the mudstone unit, which would impede hydrothermal circulation and cause lower temperature replacement of discrete smectite between 60 and 100°C (c.f. Chang et al. 1986; Robinson et al. 2002). In comparison, the more porous sandstones would readily permit hydrothermal circulation that could have sustained smectitic clay compositions at significantly higher temperatures. For example, Di/trioctahedral smectite clay from Icelandic geothermal fields is stable up to ~150°C (Schiffman and

Fridleifsson 1991). However, the occurrence of light green corrensite clay with well-developed authigenic growth rings suggests that the burial condition for the Mawson Point sandstone was similar to conditions that produced corrensite clay in interbedded basalts. A celadonite-like composition for the brownish-green clay and the presence of authigenic growth rings may indicate a later growth of this mineral during lower temperature alteration that could have accompanied uplift of the island.

Implications for depositional flow mechanism

An authigenic origin for the brownish-green clay suggests that 2-8% (see Fig. 3.5) of the total tabulated mud in the Macquarie Island sandstones is diagenetic or hydrothermal in origin. After accounting for these secondary clays in the Mawson Point example, primary detrital clays primarily composed of deep-red corrensite clay and discrete chlorite would have been between 6 and 8% during deposition. This is supported by the predominance of deep-red corrensite clay throughout Macquarie Island normal graded sequences as breccia/sandstone matrix, sandstone laminations, and mudstone caps. The latter of which would have been deposited by the dilute tail of a turbidity current.

Recalculated mud-matrix percentages for massive sandstones on Macquarie Island are just below the suggested threshold for sandy debrites examined by Talling et al. (2004, 2007). Experimental work by Hampton (1975) showed that a sandstone would need >19% mud in very coarse grain sizes and >2.3% mud in finest grain sizes in order to have a debris flow origin. Therefore, it is unlikely that 6-8% detrital clay within the coarse- to medium-grained massive sandstone of Mawson Point was able to sustain transport by a sandy debris flow origin. This supports detailed

sedimentologic and stratigraphic analysis, which highlighted characteristics indicative of post-depositional fluidization and destruction of primary sedimentary structures.

In addition to the amount of mud matrix, clay mineralogy also plays a role in determining the mode of gravity flow transport. Marr et al. (2001) showed that sandy debris flows were possible in very fine grained sand immersed in fresh water with 7-25% low charge kaolinite and only 0.7-5.0% high charge bentonite (smectite), with the higher values being required at greater initial fluid:sediment ratios. This difference in clay type dependency for sandy debris flow initiation is likely due to the high swelling capability of the higher charge clays (Marr et al. 2001). Chlorite has a moderate expandability, which is further suppressed when immersed in salt water. Hence, high chloritic clay content in gravity flows produced along the deep-marine PMSR would only be able to generate debris flows when an efficiently high clay content (>20%) was available.

Conclusion:

Using total clay content as a proxy for inferring a debris flow origin vs. a turbidite flow origin is problematic when care is not taken to identify primary from secondary clays. This conundrum can be resolved by identifying clay mineralogies and pore-filling cements in gravity flow sandstones and comparing them with low-grade metamorphic clays in correlative rocks. It is also important to determine a burial or hydrothermal origin for the secondary minerals, due to differences in clay mineral stability under both diagenetic regimes. In addition, the method must be used in accord with prospective host rock properties and apparent fluid:rock ratios,

which can control the clay transition process. In oceanic crustal rocks the smectite to chlorite transition proved to be a good tool for this technique. Future work applied to the smectite-illite transition in continental sedimentary basins may also prove to be helpful.

References Cited:

- Allen, J.R.L., 1982. Sedimentary structures, their character and physical basis; Volume II. Developments in Sedimentology, 2. Elsevier, Amsterdam.
- Allen, J.R.L., 1991. The Bouma division A and the possible duration of turbidity currents. *Journal of Sedimentary Petrology*, 61: 291-295.
- Allen, J.R.L. and Banks, N.L., 1972. An interpretation and analysis of recumbent-folded deformed cross-bedding. *Sedimentology*, 19(3/4): 257-283.
- Amy, L.A., Talling, P.J., Peakall, J., Wynn, R.B. and Arzola Thynne, R.G., 2005. Bed geometry used to test recognition criteria of turbidites and (sandy) debrites. *Sedimentary Geology*, 179(1-2): 163-174.
- Arnott, R.W.C. and Hand, B.M., 1989. Bedforms, primary structures and grain fabric in the presence of suspended sediment rain. *Journal of Sedimentary Petrology*, 59(6): 1062-1069.
- Chang, H.K., MacKenzie, F.T. and Schoonmaker, J., 1986. Comparisons between the diagenesis of dioctahedral and trioctahedral smectite, Brazilian offshore basins. *Clays and Clay Minerals*, 34(4): 407-423.
- Demant, A., Munch, P., Romeuf, N. and Morata, D., 1998. Distribution and chemistry of secondary minerals (zeolites and clay minerals) from hole 917A, southeast Greenland margin. In: A.D. Saunders, H.C. Larsen and S.W. Wise Jr. (Editors), *Proceedings of the Ocean Drilling Program, Scientific Results*.
- Griffin, B.J., 1982. Igneous and metamorphic petrology of lavas and dykes of the Macquarie Island ophiolite complex. Ph.D. Thesis, University of Tasmania, Hobart, 220 pp.
- Hampton, M., 1975. Competence of fine-grained debris flows. *Journal of Sedimentary Petrology*, 45(4): 834-844.
- Helmold, K.P. and van de Kamp, P.C., 1984. Diagenetic mineralogy and controls on albitization and laumontite formation in Paleogene arkoses, Santa Ynez Mountains, California. *AAPG Memoir*, 37: 239-276.
- Kneller, B., 1995. Beyond the turbidite paradigm; physical models for deposition of turbidites and their implications for reservoir prediction. In: A.J. Hartley, and Prosser, D.J. (Editor), *Characterization of Deep Marine Clastic Systems*. Geological Society Special Publications, London, pp. 31-49.
- Kneller, B.C. and Branney, M.J., 1995. Sustained high-density turbidity currents and the deposition of thick massive sands. *Sedimentology*, 42(4): 607-616.
- Lowe, D.R., 1975. Water-escape structures in coarse-grained sediments. *Sedimentology*, 22(2): 157.

- Lowe, D.R., 1976. Grain flow and grain flow deposits. *Journal of Sedimentary Petrology*, 46(1): 188-199.
- Lowe, D.R., 1988. Suspended-load fallout rate as an independent variable in the analysis of current structures. *Sedimentology*, 35(5): 765.
- Marescotti, P., Vanko, D.A. and Cabella, R., 2000. From oxidizing to reducing alteration: mineralogical variations in pillow basalts from the east flank, Juan De Fuca Ridge. In: A. Fisher, E.E. Davis and C. Escutia (Editors), *Proceedings of the Ocean Drilling Program, Scientific Results*, pp. 119-163.
- Marr, J.G., Harff, P.A., Shanmugam, G. and Parker, G., 2001. Experiments on subaqueous sandy gravity flows: The role of clay and water content in flow dynamics and depositional structures. *Geological Society of America Bulletin*, 113(11): 1377-1386.
- Mulder, T., Razin, P. and Faugeres, J.-C., 2009. Hummocky cross-stratification-like structures in deep-sea turbidites: Upper Cretaceous Basque basins (Western Pyrenees, France). *Sedimentology*, 56(4): 997-1015.
- Neuhoff, P.S., Fridriksson, T., Amórsson, S. and Bird, D.K., 1999. Porosity changes and mineral paragenesis during low-grade metamorphism at Teigarhorn, eastern Iceland. *American Journal of Science*, 299: 467-501.
- Neuhoff, P.S., Rogers, K.L., Stannius, L.S., Bird, D.K. and Pedersen, A.K., 2006. Regional very low-grade metamorphism of basaltic lavas, Disko-Nuussuaq region, West Greenland. *Lithos*, 92(1-2): 33-54.
- Postma, G., Cartigny, M. and Kleverlaan, K., 2009. Structureless, coarse-tail graded Bouma Ta formed by internal hydraulic jump of the turbidity current? *Sedimentary Geology*, 219(1-4): 1-6.
- Reynolds, R.C., Jr., 1985. NEWMOD a computer program for the calculation of one-dimensional diffraction patterns of mixed-layer clays. Reynolds, R. C., 8 Brook rd, Hanover, NH 03775, USA.
- Robinson, D., Bevins, R.E. and Rowbotham, G., 1993. The characterization of mafic phyllosilicates in low-grade metabasalts from eastern North Greenland. *American Mineralogist*, 78(3-4): 377-390.
- Robinson, D., Schmidt, S.T. and Santana de Zamora, A., 2002. Reaction pathways and reaction progress from the smectite-to-chlorite transformation; evidence from hydrothermally altered metabasites. In: G.L. Clarke and M. Brown (Editors), *Journal of Metamorphic Geology*, pp. 167-174.
- Røe, S.-L. and Hermansen, M., 2006. New aspects of deformed cross-strata in fluvial sandstones: Examples from Neoproterozoic formations in northern Norway. *Sedimentary Geology*, 186(3-4): 283-293.
- Shanmugam, G., 1996. High-density turbidity currents; are they sandy debris flows? *Journal of Sedimentary Research*, 66(1): 2-10.
- Schiffman, P. and Fridleifsson, G.O., 1991. The smectite-chlorite transition in drillhole NJ-15, Nesjavellir geothermal field, Iceland; XRD, BSE and electron microprobe investigations. *Journal of Metamorphic Geology*, 9: 679-696.
- Schiffman, P. and Staudigel, H., 1995. The smectite to chlorite transition in a fossil seamount hydrothermal system; the basement complex of La Palma, Canary Islands. *Journal of Metamorphic Geology*, 13(4): 487-498.
- Staudigel, H. and Schmincke, H.-U., 1984. The Pliocene seamount series of La Palma/Canary Islands, *Journal of Geophysical Research*, pp. 11,195-11,215.

- Stow, D.A.V. and Johansson, M., 2000. Deep-water massive sands; nature, origin and hydrocarbon implications. In: D.A.V. Stov and M. Mayall (Editors), *Marine and Petroleum Geology*, pp. 145-174.
- Sumner, E.J., Amy, L.A. and Talling, P.J., 2008. Deposit Structure and Processes of Sand Deposition from Decelerating Sediment Suspensions. *Journal of Sedimentary Research*, 78(8): 529-547.
- Talling, P.J., Amy, L.A., Wynn, R.B., Peakall, J. and Robinson, M., 2004. Beds comprising debrite sandwiched within co-genetic turbidite: origin and widespread occurrence in distal depositional environments. *Sedimentology*, 51(1): 163-194.
- Talling, P.J. Wynn, R. B., Masson, D. G., Frenz, M., Cronin, B. T., Schiebel, R., Akhmetzhanov, A. M., Dallmeier-Tiessen, S., Benetti, S., Weaver, P. P. E., Georgiopoulou, A., Zuhlsdorff, C. and Amy, L. A., 2007. Onset of submarine debris flow deposition far from original giant landslide. *Nature*, 450(7169): 541(4).

IV:

Oceanic zircon trace element and Hf-isotope geochemistry as a provenance tool and its implications for the proto-Macquarie Spreading ridge demise

Introduction:

In recent years zircon trace element geochemistry has been sought out as a provenance tool for elucidating parent rock type (Heaman et al. 1990; Belousova et al. 2002). In particular, U, Yb, Y, and Hf concentrations have proven very useful for provenance studies and show good covariation for discriminating continental vs. oceanic crustal sources (Grimes et al. 2007). In comparison, rare earth elements (REE) exhibit considerable overlap between mafic and felsic parent sources, thus precluding their usage as a reliable provenance tool (Hoskin and Ireland 2000). Ti-in-zircon thermometry does provide a reliable estimate of zircon crystallization temperature (Watson and Harrison 2005; Ferry and Watson 2007) and correlates with other trace element gauges of magma evolution (Fu et al. 2008).

Hafnium (Hf) isotope compositions in zircon have proven to be an invaluable tool in assessing the genesis of magmatic rocks, timing of continental crust differentiation on early Earth, and provenance of sedimentary rocks (Amelin et al. 1999; Vervoort and Blichert-Toft 1999; Griffin et al. 2004; Belousova et al. 2006; Nebel et al. 2007). This is due to (i) relatively high (up to weight percent) Hf concentrations and very low Lu/Hf ratios in zircon, (ii) resilience of the zircon crystal lattice to trace element mobility and contamination, (iii) well-established methods of evaluating zircon U-Pb crystallization ages, and (iv) detecting metamorphic overprints in discordant grains (Dickin 2005). Despite the great utility of the zircon Lu-Hf system in elucidating continental crustal generation, its application to oceanic crustal evolution has, as of yet, been neglected.

In this chapter, detrital zircon $^{176}\text{Hf}/^{177}\text{Hf}$ isotope compositions are used in conjunction with trace element data and Ti-in-zircon thermometry to elucidate the provenance and mantle source reservoir for detrital sandstone and colluvial sand

from Macquarie Island. Results from Chapter I show that the source for Macquarie Island's gabbroic sedimentary rocks was ~20 Myr older (Oligocene) and more depleted in nature than the igneous section currently exposed on the island (Miocene). Furthermore, paleotectonic reconstructions indicate that the detrital source was produced along the eastern-most spreading segment of the Southeast Indian Ridge (SEIR), which was offset by >300 km from the proto-Macquarie spreading ridge (PMSR) where igneous crust exposed on Macquarie Island was formed (see Fig 1.10). This relationship suggests that the mantle source for melts along the SEIR-PMSR system varied from a depleted to enriched composition with distance and/or time. This chapter examines this variation amongst old and young zircon age groups through trace element and isotope geochemistry. Furthermore, results are used to test the validity of oceanic vs. continental zircon discrimination schemes for provenance studies (e.g. Grimes et al. 2007), which has implications for the development of continental crust on early Earth (Coogan and Hinton 2006).

Background:

Sample collection

Five medium-grained sandstone samples were collected from gabbroic sedimentary sections (see Chapter I for facies description) in the central part of the island at Double Point (DLP1B-5A), Mt. Waite (MW6-2) and Mt. Martin (MM1-1), and the northwestern part of the island at Cormorant Point (CP1-5) and Mawson Point (MP1-4; Fig. 4.1). Correlations indicate that the Double Point and Mt. Waite "detrital" samples are stratigraphically equivalent (see unit 11 DLP1b and unit 3 MW6 in Fig 2.2B), as well as, the Cormorant Point and Mawson Point "detrital"

samples (unit 5 of both CP1 and MP1 in Fig. 3.2). Several colluvium sites in the northern 1/5 of the island, where gabbro exposures predominate, were chosen for heavy mineral panning. The sand-size fraction of 13 stream sites running through gabbroic colluvium and 3 sandy lake shore sites (Fig. 4.1) were combined as one “colluvial” sample (sample MI). This colluvial sample and crushed detrital sandstone samples were separated for zircon using magnetic and heavy liquid techniques at GEOTRACK facilities in Victoria Australia. Concentrated zircon separates from these six samples were hand picked to maximize variation in zircon morphology, color, and shape.

Zircon host rock

Results from Chapters I and II showed the source for the sandstone samples was hydrothermally altered lower to upper oceanic crust. Although it is difficult to directly infer the source of detrital zircon separated from sandstone samples, zircon-bearing cobbles do occur in associated breccia lithofacies. These cobbles are composed of coarse-grained leucocratic diorite that contains >60% plagioclase (An_{35}) + 20% green diopside ($En_{36}Wo_{47}Fs_{17}$) + 10% titanite + <5% ilmenite, zircon and apatite (Fig. 4.2A-B). Alteration minerals make up >5% of the whole rock mineralogy and generally occur within intergranular space and are composed of epidote, prehnite, chlorite, and albite. A large boulder-sized clast of amphibolitic dolerite from Southwest Point (Fig. 4.1) contains a 3 cm thick dyke of zircon-bearing leucocratic diorite. The margins of the leucocratic dyke have 2mm thick brown-green amphibole alteration halos with abundant Fe-Ti oxides where it is in contact with the dolerite host rock. These alteration halos also occur around >1cm fine-grained porphyritic basalt xenoliths (Fig. 4.2C). Other potential zircon host rocks include

detrital lithic grains that contain brown amphibole (pargasite) and k-feldspar, and granophyric texture (see Chapter I results). These mineralogies, including the leucocratic diorite clasts, typically occur in evolved plutonic suites along mid-ocean ridges and in ophiolites (e.g. Aumento 1969; Tribuzio et al. 2000). They are commonly referred to as oceanic plagiogranites (*sensu stricto* Koepke et al. 2007), which are SiO₂ enriched (>52 wt%) oceanic rocks primarily including leucocratic tonalite, trondhjemite, diorite, quartz diorite, and anorthosite.

The colluvial nature of zircon from sample MI is by nature out-of-context from its original host rock. Panning locations only in the northern plateau portion of the island in and around non-layered gabbro to dolerite outcrops minimize potential colluvial zircon host rocks to upper level plutonic bodies. Zircon collected from evolved late-stage phlogopite-bearing pegmatoids in Macquarie Island's north yield an ~8.5 Ma age (Armstrong et al. 2004), which is within error of colluvial zircon reported in Chapter I and in this chapter. Hence, suggesting a similar host rock affinity.

Zircon characteristics

All zircon grains have characteristics of igneous zircon. For example, those observed in-situ within leucocratic diorite clasts are euhedral to subhedral. Grains typically occur as 50-100µm inclusions within plagioclase and diopside or amongst titanite-ilmenite grain aggregates (Fig. 4.2A-B). Rare grains are 600-500 µm in size (Fig. 1.5F). They all display a flat back-scattered image with only few showing oscillatory zoning in cathodoluminescence imaging (Fig. 4.2D). Most grains have euhedral crystal faces with many exhibiting angular shapes likely due to the grain separation process. Grains are primarily colorless to pink and yellow. Most grains

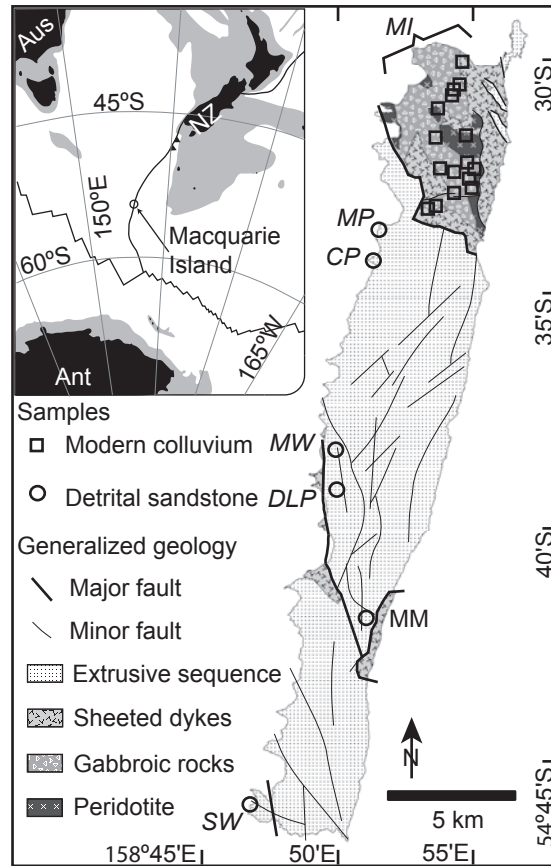


Figure 4.1:

Map showing colluvial stream and lake sand sites panned for zircon in northern part of the island (sample MI), and detrital sandstone sample localities along the northwestern coast (Mawson Point-MP, Cormorant Point-CP) and central coast (Double Point-DLP, Mt. Martin-MM, and Mt. Waite-MW). Detrital zircon identified in thin section, but not analyzed in this chapter, was also recovered from breccia clasts at Southwest Point (SW).

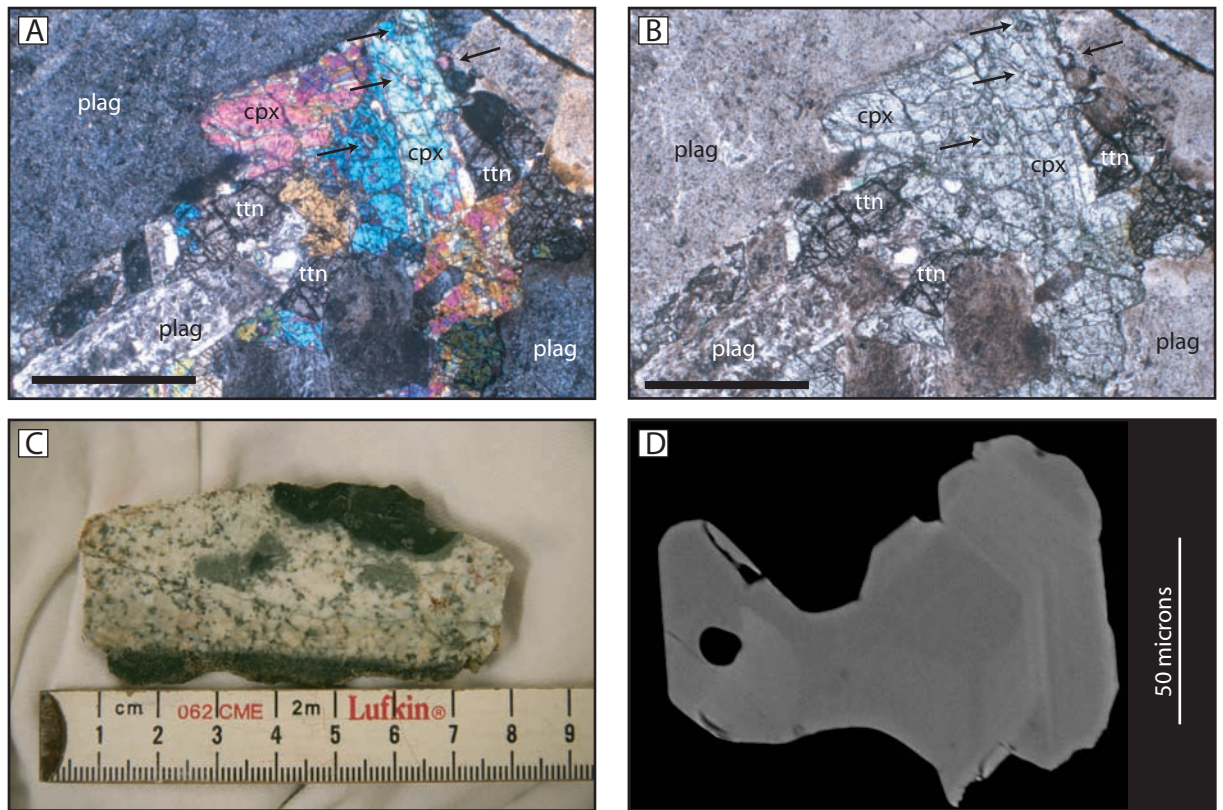


Figure 4.2:
Photographic montage of zircon from Macquarie Island. A) Photomicrograph in crossed polarized light of leucocratic diorite clast bearing titanite (tn) from Southwest Point. Diopsidic clinopyroxene (cpx) contains inclusions of euhedral zircon (arrows), which also occur along grain boundaries with plagioclase (plag). Scale is 1mm. B) Same as in A under plane-polarized light. C) Leucocratic diorite dyke cross-cutting amphibolitized dolerite (bottom of sample) with fine-grained basalt xenoliths. From Southwest Point. D) Back-scattered reflection image of zircon from colluvial sample MI. Note faint oscillatory zoning in right side of grain. Crystal shape is partly controlled by the grain mounting process.

have a textural affinity to the euhedral type 1 and rarely subhedral type 2 oceanic zircons described by Grimes et al. (2009).

Methods:

²⁰⁶Pb/²³⁸U geochronology and trace element geochemistry

Simultaneous U-Pb dating and trace element analysis of zircon grains was determined using a New Wave 213 nm Nd: YAG laser system linked to an Agilent 7500s ICP-MS at GEMOC Macquarie University, Australia. The technique (LA-ICPMS) along with analytical uncertainty is described by Jackson et al. (2004). Analyses used a beam diameter of 30-40 μm , a 5 Hz (pulses per second) repetition rate, and an output energy of ~ 0.9 mJ per pulse. Each analysis took 180 s, with a “gas blank” measurement of the carrier gas (He) taken over the first ~ 50 s, before ablation of the sample for ~ 130 s. Samples were analyzed in runs of 20 analyses consisting of two analyses of a gem quality GJ zircon standard for calibration of U-Pb isotopes, two analyses of synthetic glass NIST-610 standard for calibration of trace-elements, one each of Mud Tank and 91500 zircon reference materials to monitor the accuracy and precision of the method, 10 analyses of unknowns, and a further two GJ zircon standards and two NIST-610 standards. The zircon 91500 and Mud-Tank zircons have accepted $^{206}\text{Pb}/^{238}\text{U}$ age of 1065.4 ± 0.6 Ma (Wiedenbeck et al. 1995) and 732 ± 5 Ma (Black and Gulson 1978), respectively. The 91500 zircon reference material was also used as a control for the accuracy and precision of trace-element measurements (values in Wiedenbeck et al. 2004). Hafnium-176 was used as an internal standard for trace-element quantification and measured using electron microprobe measurements of HfO_2 (see Appendix E for electron microprobe method).

U-Pb ages were calculated from the raw signal data using the online software package GLITTER, Version 4.4 (van Achterbergh et al. 1999). The time-resolved analysis software, in which the signal intensity data for each mass and each ratio is displayed as a function of time (ablation depth) during the analysis, allows for the most stable portion of the signal to be selected for integration, thereby enabling isotopic heterogeneities such as inherited cores or inclusions to be identified and avoided. The ^{204}Pb isotope cannot be precisely measured with this technique, due to a combination of low signal and isobaric interference from ^{204}Hg contaminants in the Ar gas supply. Consequently, the common-Pb contents were evaluated using the algorithm described by Anderson (2002) where applicable. Because of low concentrations of ^{207}Pb present in young (i.e. <1.6 Ga) zircons and low count rates and large analytical uncertainties, the determination of the ages for 'young' zircons is based on their $^{206}\text{Pb}/^{238}\text{U}$ ratios. Concordia ages were determined using Isoplot version 2.35 (Ludwig 2006).

$^{176}\text{Hf}/^{177}\text{Hf}$ isotopes

Hf-isotope analyses of zircon used a New Wave Research 213 nm Nd:YAG laser, attached to a Nu Plasma multi-collector ICP-MS, at GEMOC Macquarie University, Australia. The complete analytical method with full analytical accuracy and precision is thoroughly described in Griffin et al. (2000, 2004). Analyses used a beam diameter of $\sim 55\text{ }\mu\text{m}$, a 5 Hz repetition rate, and output energies of 0.6–1.3 mJ per pulse. Laser ablation times ran for 30–120 s after background was collected for 45 s. Resulting ablation pits were 20–60 μm deep.

Stable portions of the laser-ablation analyses were selected using Nu Plasma time-resolved analysis software before the data was processed to give final results.

The selected interval is divided into 40 replicates for the calculation of the standard error. The measurement of accurate $^{176}\text{Hf}/^{177}\text{Hf}$ ratios in zircon was corrected for the isobaric interferences of ^{176}Lu and ^{176}Yb on ^{176}Hf (after Griffin et al. 2004). Corrections were applied relative to zircon standard 61.308, which yields a wide range in $^{176}\text{Yb}/^{177}\text{Hf}$ (0.005–0.065) and $^{176}\text{Lu}/^{177}\text{Hf}$ (0.00016–0.002) and shows no correlation with $^{176}\text{Hf}/^{177}\text{Hf}$.

Measured $^{176}\text{Lu}/^{177}\text{Hf}$ ratios were used to calculate initial $^{176}\text{Hf}/^{177}\text{Hf}$ ratios by implementing the Lu decay constant of Scherer et al. (2001). Typical 2σ uncertainty on a single analysis of $^{176}\text{Lu}/^{177}\text{Hf}$ was $\pm 1\text{--}2\%$, which reflects both the analytical uncertainties and spatial variation of Lu/Hf across many zircons. Data were normalized to $^{179}\text{Hf}/^{177}\text{Hf} = 0.7325$, using an exponential correction for mass bias.

Results:

U-Pb concordia

Chapter I presented both the detrital and colluvial zircon U-Pb ages, which had primary Gaussian age distribution peaks and 2σ deviations of 32.45 ± 0.51 Ma ($n=45$), 26.96 ± 0.12 Ma ($n=123$), and 8.14 ± 0.08 Ma ($n=88$) for the two northwest coast detrital sandstone samples, three central coast detrital sandstone samples, and northern plateau colluvial sample, respectively (Fig. 1.8). Several older grains in both the middle and northwest coastal sandstones yield ages between 500 and 1800 Ma. One very young grain in the MP detrital sandstone yields a 12.2 ± 0.6 Ma age (2σ).

Uranium-lead results for some grains from the dataset used in Chapter I are not presented in this chapter due to the absence of Hf or trace element analysis.

Furthermore, grains that show a mismatch between concordance of their Pb/Pb and

Th/U isotopic systems are not included in the Hf-isotope analysis (M. Murphy pers. comm. 2009) and shown as blue error ellipses on the Terra-Wasserburg concordia diagrams in Fig. 4.3. After removal of these discordant grains average ages with 2σ deviation are 30.79 ± 5.4 Ma ($n=12$), 27.48 ± 3.30 ($n=60$), and 8.50 ± 1.1 ($n=22$) for the northwest coast detrital, central coast detrital, and colluvial samples, respectively. The northwest coast detrital average does not include one anomalously young grain shown in the Fig. 4.3 inset.

Trace element data

Apart from four grains with anomalously high trace element contents, likely due to ablation of inclusions, all grains analyzed for trace elements are used in this chapter. This ensures that a large population of zircon grain chemistry is used for trace element discrimination schemes, which are subject to the typically wide variation in zircon trace element composition (Grimes et al. 2009).

Detrital and colluvial zircon from Macquarie Island show nearly complete overlap with oceanic zircon collected from MORB terrains along the Mid-Atlantic and Southwest Indian ridges (Fig. 4.4). The detrital zircon from the island define a new field on the Y vs. U rock type discrimination diagram of Belousova et al. (2002), distinct from felsic and mafic continental crust. In general, only colluvial grains and the anomalously old (>500 Ma) detrital grains fall into the overlap area between oceanic and continental discrimination fields outlined in Fig. 4.4. This disparity is also portrayed in Fig. 4.5, which shows the majority of 23-47 Ma aged detrital grains ($\sim 88\%$) plotting on the oceanic crustal side of the discrimination line determined by Grimes et al. (2007) and <12 Ma aged grains plotting on the continental side along with anomalously old (>500 Ma) detrital grains. Plotting Macquarie Island zircon by

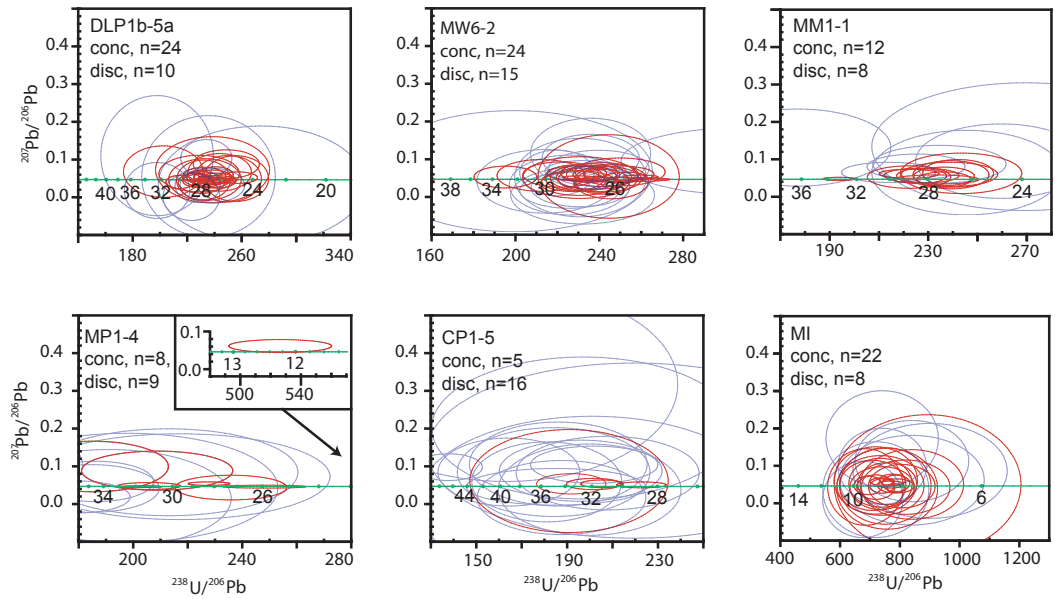


Figure 4.3:
U-Pb Terra Wasserburg diagrams for 23-47 Ma detrital and 7-10 Ma colluvial zircon grains from Macquarie Island. Error ellipses are 2 sigma. Concordant grains (conc) used for Hf-isotope analysis are shown by red error ellipses and discordant (disc) grains are shown by blue ellipses.

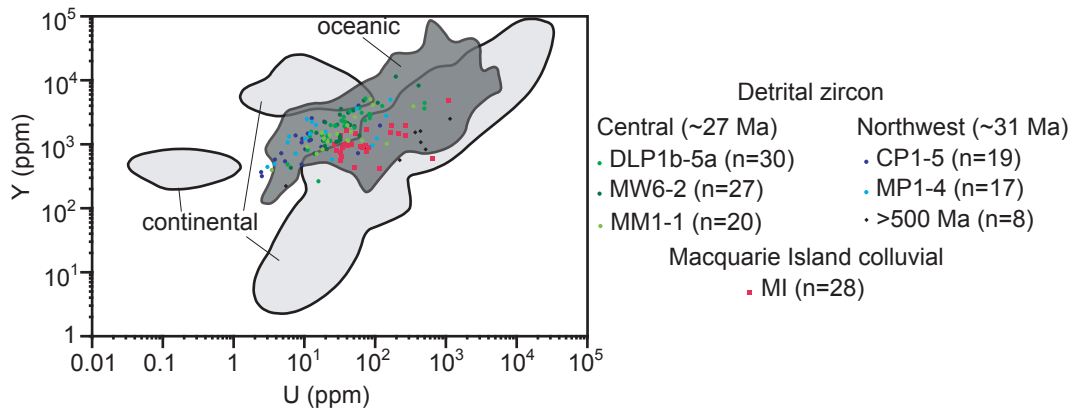


Figure 4.4:
Zircon host rock type comparison between continental rock types outlined in light gray (Belousova et al. 2002) and oceanic crust dark gray (Grimes et al. 2007, 2009; Jöns et al. 2008). The continental field includes both felsic and mafic rock types. Greater than 500 Ma grains are all from the northwest coast samples except one analysis from MM1-1.

age groupings shows that the older (29-47 Ma) grains plot closely with the NMORB variety of oceanic zircon at low U and relatively high Yb and Y values. A comparatively younger detrital zircon age-grouping of 23-29 Ma plots with the EMORB variant of oceanic zircon. Nearly all of the colluvial zircon grains collected from the island (86%) have more enriched compositions compared to global zircon collected from EMORB crust.

Ti-in-zircon thermometry (after Ferry and Watson 2007) shows a peak Gaussian distribution at $\sim 795^{\circ}\text{C}$ for the crystallization temperature of both detrital and colluvial zircon populations on Macquarie Island (Fig. 4.6). Grains in both the colluvial sample and central detrital samples have average crystallization temperatures of $805 \pm 56^{\circ}\text{C}$ (2σ) compared to a slightly lower average temperature of $770 \pm 54^{\circ}\text{C}$ (2σ) for the northwest coast detrital sample. These Ti-in-zircon thermometry calculations are calibrated for 1.33 ± 0.67 kbar pressure, 0.8 ± 0.15 for a_{TiO_2} , and 1.0 for a_{SiO_2} (after Ferry and Watson 2007). Values for a_{TiO_2} and a_{SiO_2} take into account average compositions of 61.71% SiO_2 and 0.87% TiO_2 for zircon-bearing oceanic plagiogranite along the Atlantis Bank of the Southwest Indian ridge (Koepke et al. 2007; Jöns et al. 2009). The pressure calibration assumes a 4 ± 2 km crystallization depth, which is average for shallowly emplaced plagiogranites and Fe-Ti oxide gabbros intrusions in slow-spreading-ridges (Dick et al. 2000; John et al. 2004; Baines et al. 2008; Grimes et al. 2008). These calibrations are substantiated by the presence of ilmenite, titanite, diopside, and $>60\%$ plagioclase in zircon-bearing leucocratic diorite clasts in Southwest Point cobble breccias (Fig. 1.5F).

Hf-isotopes

Average $^{176}\text{Hf}/^{177}\text{Hf}$ isotope composition for the Macquarie Island colluvial sample is 0.283143 ± 0.000042 (2σ), which is slightly less radiogenic than the averaged detrital sandstone composition of 0.283170 ± 0.000061 (2σ). These averages exclude the discordant zircons described in the U-Pb results section, which are shown by blue error ellipses in Fig. 4.3 and open symbols on Fig. 4.7A. Initial Hf isotope compositions were calculated using the $^{176}\text{Lu}/^{177}\text{Hf}$ decay constant of Scherer et al. (2001). The average 1σ error on individual grains measurements are <0.00003 , which is equivalent to an analytical uncertainty of one epsilon unit. $^{176}\text{Hf}/^{177}\text{Hf}$ compositions in Fig. 4.7A generally fall in between Hf isotope evolution lines for an average depleted MORB mantle (DMM) and an enriched DMM (E-DMM). The E-DMM mantle reservoir is enriched 2σ over the average isotope composition of non-plume-related DMM source away from subduction zones (Workman and Hart 2005). The evolution line for the DMM uses a Lu/Hf of 0.0384 (Vervoort and Patchett 1996) and is used as a base to calculate a 2σ enriched E-DMM Lu/Hf of 0.0366. Starting $^{176}\text{Hf}/^{177}\text{Hf}$ and Lu/Hf for the CHUR evolution line are from Blichert-Toft and Albarede (1997), which is used to calculate epsilon ϵ_{Hf} for the Macquarie Island samples. Averaged ϵ_{Hf} values are well above the CHUR line ($\epsilon_{\text{Hf}} = 0$) and range from 13.32 ± 0.74 (1σ) for colluvial samples and 14.70 ± 2.14 (1σ) for detrital samples (Fig. 4.8). Within their respective age distributions, colluvial samples generally plot closer to the E-DMM evolution line compared to detrital samples, which fall approximately midway between the E-DMM and DMM lines.

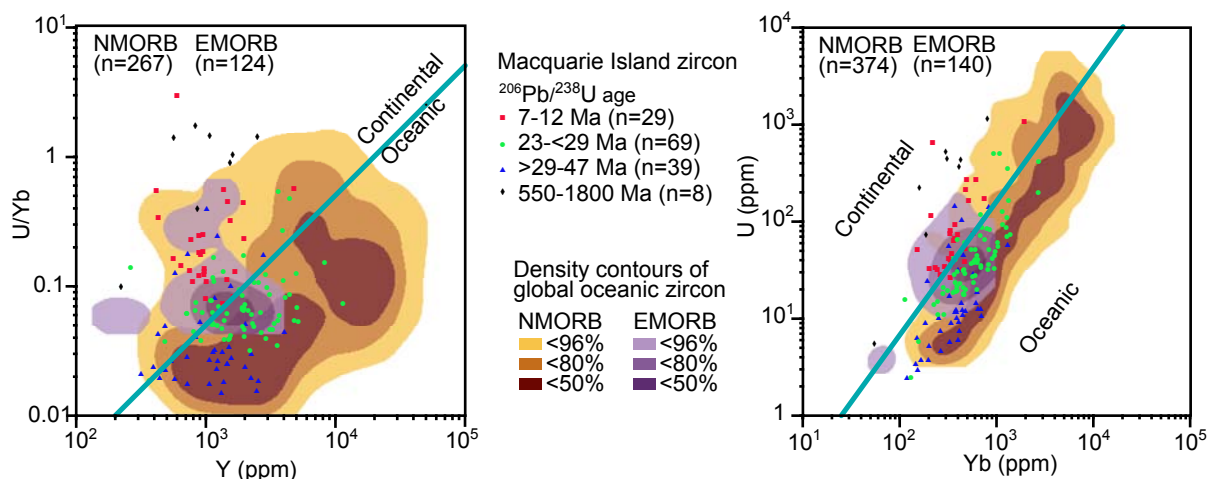


Figure 4.5:

Trace element discrimination diagrams of Macquarie Island zircons (points) by relative age groupings. The continental vs. oceanic zircon discrimination line is from Grimes et al. (2007). Density contour plot shaded colors depict <50%, <80%, and <96% of oceanic zircon grains that fall within their outer boundaries. Outlier points outside of the density plots include <4% of the total MORB database and thereby excluded from the spatial analysis. Zircon from EMORB crust is from 15°45' N and 14° 44' N along the Mid-Atlantic ridge. Zircon from NMORB crust is from 30°N Atlantis massif and 23°N Kane fracture zone of the Mid-Atlantic Ridge. Included with the NMORB data are grains from more depleted NMORB crust along the Atlantis Bank of the Southwest Indian Ridge at 57° E. MORB data is compiled from Grimes et al. (2007, 2009), and Jöns et al. (2009).

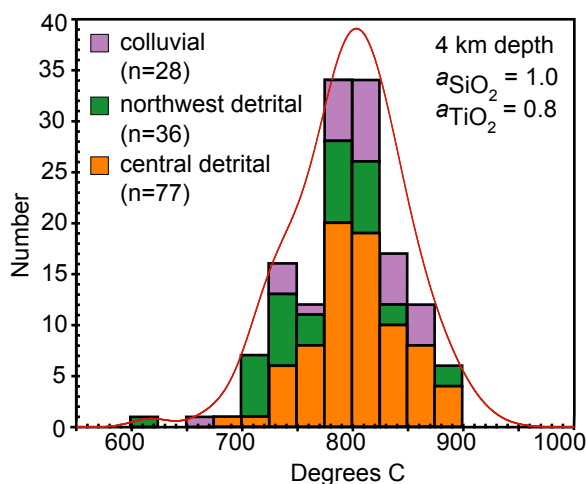


Figure 4.6:

Ti-in zircon thermometry showing peak Gaussian distribution of combined colluvial and detrital Macquarie Island samples at ~795°C. Calibrations for pressure (depth of emplacement), a_{TiO_2} , and a_{SiO_2} are described in text.

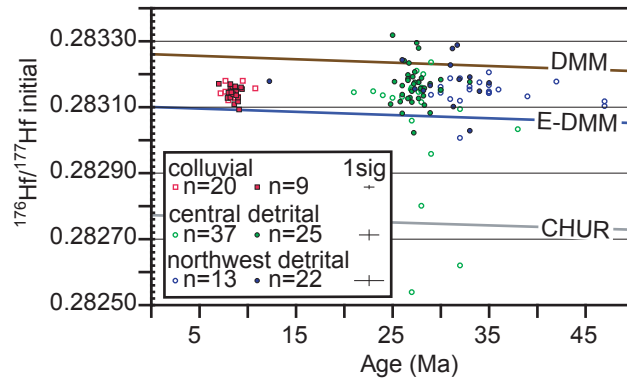


Figure 4.7:
Initial $^{176}\text{Hf}/^{177}\text{Hf}$ isotope compositions with respect to $^{206}\text{Pb}/^{238}\text{U}$ ages for modern colluvium sample, central detrital, and northwestern detrital samples. Maximum 1 sigma error bars are shown for individual grains. Filled symbols represent concordant grains and open symbols represent grains that show discordance between Pb-Pb and U-Th concordia analysis. Isotope compositions for DMM, E-DMM and CHUR are described in text.

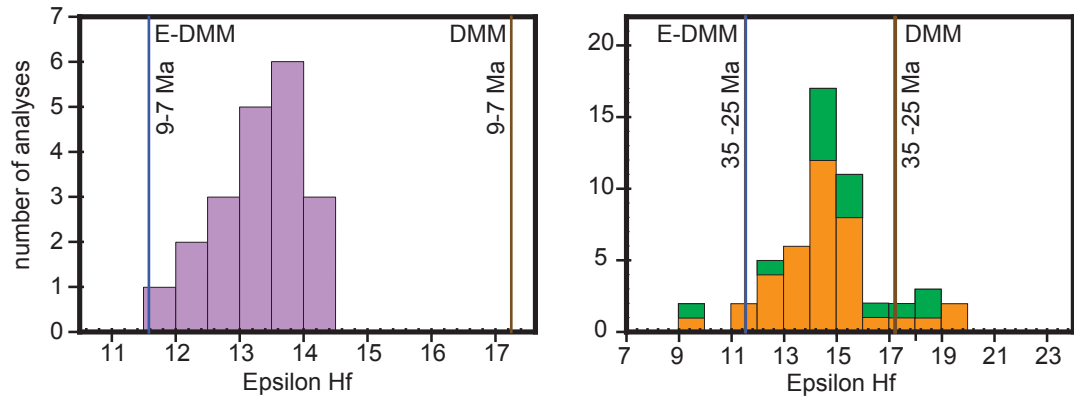


Figure 4.8:
Probability plot of epsilon Hf for concordant colluvial and detrital zircon grains from Macquarie Island. Mantle reservoir source values are for 7-9 Ma and 25-35 Ma on the colluvial and detrital plots, respectively. Isotope systematics described in text.

Discussion:

Depleted oceanic vs. enriched continental zircon provenance

Although the majority of zircon collected from the Mid-Atlantic and Southwest Indian Ridges, plots within the oceanic crustal source provenance field of Grimes et al. (2007), zircon crystallized within more enriched varieties of MORB crust plot closer to the continental field. This is best demonstrated by plotting density contours of zircon grains collected from EMORB crust between 15°45' N and 14° 44' N along the Mid-Atlantic Ridge (Dosso et al. 1993), against grains collected from NMORB crust along the Atlantis Bank, Kane fracture zone and Atlantis Massif (Coogan et al. 2004; Debaille et al. 2006). This relationship is also observed between depleted detrital zircon and enriched colluvial zircon on Macquarie Island. A more depleted oceanic crustal source for all of the detrital sandstone samples, relative to enriched Macquarie Island basalt, is in good agreement with calculated melt compositions for detrital clinopyroxene presented in Chapter I (Fig. 4.9). In addition, the detrital population shows increasingly more enriched compositions in younger grains. This is demonstrated in Fig. 4.5 by the similarities in trace element concentrations between the 29-47 Ma detrital population and NMORB zircon (N-zircon), relative to the 23-29 Ma detrital population and EMORB zircon (E-zircon). Disparity amongst the ~8 Ma colluvial zircons and the oceanic zircon field likely reflects the unusual very highly enriched composition of some Macquarie Island basalts (Kamenetsky et al. 2000). Therefore, discrimination between a continental vs. oceanic crustal provenance for detrital zircons must take into account trace element compositions imposed by partial melting of a more enriched mantle source (i.e. E-zircons) or relatively low degrees of partial melting. This is especially important for

elucidating the development of continental crust on early Earth by comparison of modern oceanic and continental crustal zircon chemistry with detrital zircon from Hadean rocks (e.g. Grimes et al. 2007).

Ti-in-zircon thermometry has also been used as a proxy to suggest the existence of continental crust in Hadean rocks (Watson and Harrison 2005). Using this thermometer, average zircon crystallization temperatures are generally higher in mafic rocks at $758 \pm 111^{\circ}\text{C}$ (2σ) compared to $653 \pm 124^{\circ}\text{C}$ (2σ) in felsic rocks (Fu et al. 2008). However, a large overlap between different rock types and grains formed in oceanic vs. continental crust requires the application of the Ti-zircon-thermometer to large datasets (Coogan and Hinton 2006; Fu et al. 2008). In addition, this method typically yields a wide spread in individual sample suite crystallization temperatures of $65\text{--}34^{\circ}\text{C}$ (2σ). Average temperatures of $774 \pm 169^{\circ}\text{C}$ and $818 \pm 161^{\circ}\text{C}$ are common for oceanic plagiogranites and gabbros \pm Fe-Ti oxides (Grimes et al. 2009; Jöns et al. 2009). These temperatures are comparable to a spread of $700\text{--}900^{\circ}\text{C}$ (Fig. 4.6) in the majority of grains (138/141 analyses) for Macquarie Island detrital and colluvial samples reflecting the mafic nature of their host rock. These results stress the importance of large datasets to accurately assess the host rock provenance for detrital Ti-in-zircon thermometry. An average $805 \pm 56^{\circ}\text{C}$ (2σ) Ti-in-zircon thermometry for Macquarie Island colluvial zircon is also consistent with their oceanic crustal source, despite a continental trace element signature as deduced from the discrimination line of Grimes et al. (2007). Hence, there is no covariation between Ti-in-zircon thermometry and trace element enrichment in samples studied here.

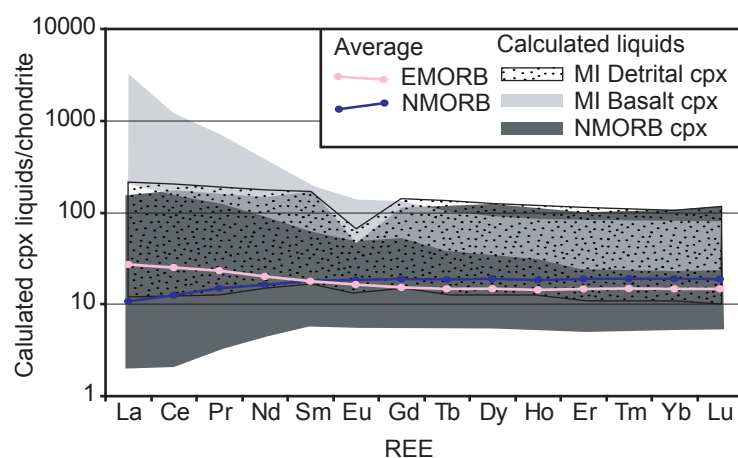


Figure 4.9:
Chondrite-normalized calculated melts from detrital clinopyroxene in Macquarie Island sandstone and groundmass clinopyroxene in Macquarie Island basalts of the Davis Point section. Partition coefficients are from Green (2000) and chondrite normalization values are from Sun and McDonough (1989).

Model ages, mantle reservoirs, and melt effects

Magmatic zircon with mantle-derived signatures typically lay within error of or above the CHUR line having $\epsilon_{\text{Hf}} \gg 0$ (Belosouva et al. 2006) as portrayed by both colluvial and detrital Macquarie Island zircon grains. A mantle-derived signature for Macquarie Island zircons is also reflected by the general lack of internal structure (i.e. zoning) on backscatter and cathodoluminescence images (Griffin et al. 2004 and references therein). Using the Lu/Hf values of individual zircon grains, a 130-160 Ma minimum model age is calculated for the time when the zircon source melt would have separated from a depleted mantle reservoir (T_{DM} ; Fig. 4.10). Rather, it is common practice to assume a value for average mafic or felsic crust to obtain a maximum “model” age for the separation of a zircon-source melt from a chosen mantle reservoir (Nebel et al. 2007). Due to the ophiolitic nature of Macquarie Island (colluvial sample) and the detrital sample source (Chapter I), a Lu/Hf ratio of 0.022, which is appropriate for mafic crust (Vervoort and Patchett 1996; Nebel et al. 2007), was used to model average “crustal” model ages ($T_{\text{DM}^{\text{C}}}$). By using the commonly chosen DMM source (e.g. Griffin et al. 2004), Macquarie Island Hf crustal model ages fall within a range of 280 to 380 Ma for detrital and colluvial samples, respectively (Fig. 4.10). Several models for these anomalously “old” Hf model ages are discussed below.

Gondwana legacy

One scenario that may explain the old model age could be the fingerprint of the long-lived Paleozoic-Mesozoic subduction zone along the eastern margin of the Gondwana supercontinent, which was largely active between 500 and 100 Myr (Li and Powell 2001). Paleogeographic reconstructions show that the eastern Gondwana

subduction zone was adjacent to the future mantle source for the spreading segments of the SEIR and PMSR (Fig. 4.11). Therefore, the underlying mantle-source for Macquarie Island's igneous rocks and colluvial zircon may have been enriched during Paleozoic-Mesozoic subduction (also see Wertz, 2003).

High degrees of hydrous partial melting, commonly associated with subduction, is preserved in exposed peridotite on Macquarie Island by spoon-shaped trace element patterns in clinopyroxene, positive Sr anomalies, and relatively high spinel Cr-numbers between 39 and 48 (Wertz 2003). Although there is evidence for syn-transpressional rifting along discrete portions of the PMSR by 10.5 Ma (Meckel et al. 2005), under-thrusting would likely not have been enough (i.e. incipient subduction) to cause hydrous partial melting. Instead, the hydrous partial melting geochemical signature in Macquarie Island peridotites may represent the lingering presence of a stubborn mantle source contaminant long after cessation of the Gondwana subduction zone. Therefore, a Gondwana subduction fingerprint could explain the anomalously the old 130-380 Ma ϵHf model ages for gabbroic zircons on Macquarie Island (Fig. 4.10). The persistence of the old subduction contaminant is supported by the presence of an ancient mantle wedge identified by geophysics at the Australian-Antarctic Discordance below the present day SEIR (Gurnis and Müller 2003).

A Gondwana mantle contaminant model does not explain the absence of a residue-melt association between Macquarie Island peridotite and basalt (Wertz 2003), which instead represents the base-up growth of the PMSR oceanic crust (Dijkstra and Cawood 2004). Base-up growth on the island is preserved by cross-cutting relationships between basalt/hypabyssal dykes, sheeted dolerite dykes,

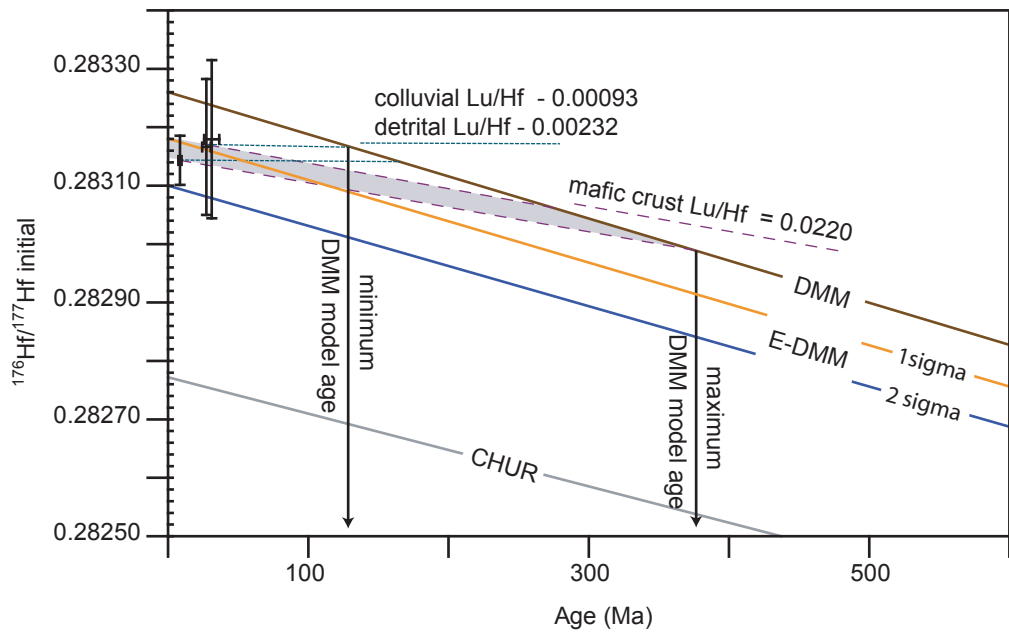


Figure 4.10:
Modeled Hf crustal ages for averaged detrital and colluvial samples with respect to DMM source. Error bars are 2 sigma for three sample averages. Averaged Lu/Hf values for detrital samples are combined. Isotope systematics described in text.

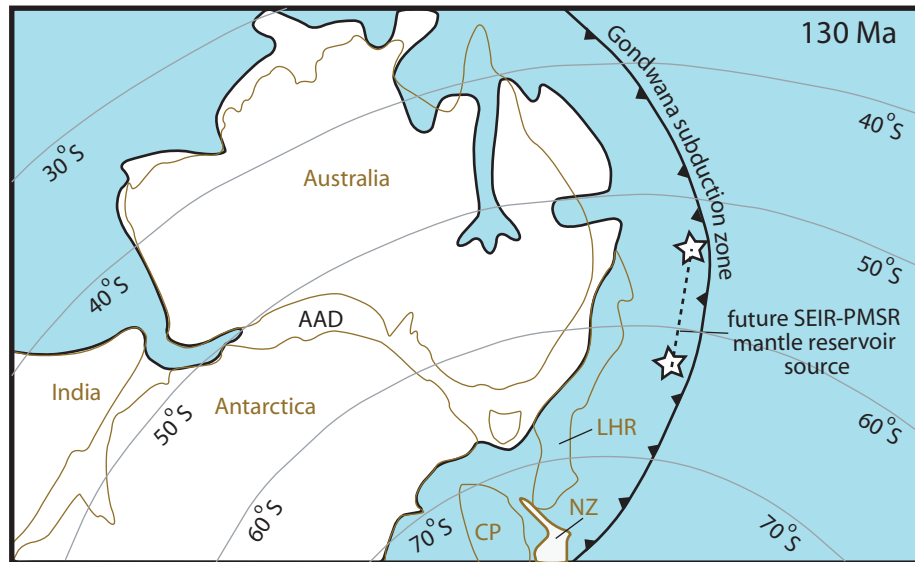


Figure 4.11:

Paleogeographic reconstruction of Australia-Pacific region for 130 Ma (Li and Powell 2001). This time corresponds to the minimum Hf-isotope model age for Macquarie Island zircons. Reconstruction shows the relative proximity of the Gondwana subduction zone (teeth on down-going plate) to the future position of the eastern Southeast Indian ridge (SEIR) and proto-Macquarie spreading ridge (PMSR) mantle source (stars). The mantle source stars are approximately positioned with respect to the latitude where the spreading segments that produced Macquarie Island crust and detrital source crust formed. Longitude is poorly constrained using palinspastic restorations from the present day position of continental margins (Lawver et al. 1999). Present day position of the Australian-Antarctic-Discordance (AAD) relative to Australia and Antarctica is shown for comparison. Lord Howe Rise (LHR), New Zealand (NZ), and Campbell Plateau (CP) would have moved north and east of the inferred positions of the SEIR-PMSR mantle source by the time of formation for Macquarie Island crust.

gabbro, and peridotite (in corresponding order). These relationships are comparable to models for oceanic crustal growth along slow-spreading ridges where older mantle components are exhumed along low-angle detachment faults where they are intruded by late-stage zircon-bearing differentiates (Schwartz et al. 2005; Grimes et al. 2008; Lissenberg et al. 2009). Hence, it is a moot point to argue for a genetic mantle reservoir source between detrital zircon and peridotite exposed on Macquarie Island. In addition, if the Gondwana fingerprint persisted up until formation of Macquarie Island crust, a more enriched character might also be expected in zircon of the older detrital sandstone samples, which is not the case.

A dynamic mantle source

Another explanation for the enriched composition of colluvial zircon relative to detrital zircon could be due to decreasing amounts of partial melting along the PMSR-SEIR system between 30 and 10 Ma. As incompatible elements are sequestered by melts, enriched and depleted MORB compositions can be produced by low and high degrees of partial melting, respectively. Therefore, EMORB oceanic crust is generally produced along slow-spreading ridges where mantle upwelling is suppressed (Niu and Hekinian 1997) and short spreading segments separated by long transforms where magma mixing is limited (see Chapter VI). This relationship may also apply to the PMSR-SEIR system, which generally had long transforms and slow spreading rates that decreased up until the complete cessation of rifting at 6 Ma shortly after production of Macquarie Island crust (Mosher and Massell-Symons 2008; Varne et al. 2000). Hence, a faster spreading rate along the SEIR and adjacent PMSR during the Oligocene could have produced more depleted NMORB-associated detrital zircon, and slower spreading rates during the Miocene produced more

EMORB-associated colluvial zircon. However, a wide array of basalt compositions on Macquarie Island lead Kamenetsky et al. (2000) to conclude that regional mantle source heterogeneity was the primary control on depleted vs. enriched compositions, rather than melting effects.

Alternatively, Kamenetsky and Mass (2002) suggest that the continuous production and extraction of melts along with changing degrees of partial melting caused a complementary evolution, heterogeneity, of the PMSR mantle-source. This model combines the aspects of both a heterogeneous mantle and partial melting effects. This dynamically changing mantle-source produced Macquarie Island's wide array of basalt compositions, specifically including unusual very highly enriched primitive basalts (Kamenetsky et al. 2000; Wertz 2003). The lack of a fractionated component to these most enriched primitive melts lead Kamenetsky and Mass (2002) to conclude that they were the primary melts, which were then followed in time by less enriched more fractionated compositions. However, this time-transgressive depletion of the mantle-source only explains the wide variance in MORB geochemistry relatively to the short time-frame of Macquarie Island crust formation. It does not explain the longer term enrichment suggested by zircon trace element and Hf-isotope geochemistry in this chapter. Therefore, it is ambiguous to employ the model of Kamenetsky and Mass (2002) in explaining the relative enrichment of Miocene Macquarie Island crust compared to the Oligocene detrital source.

The long term enrichment from Oligocene detrital to Miocene colluvial zircons may instead represent a dynamically changing mantle source reservoir that accompanied increased melt enrichment and lower degrees of partial melting during the waning stages of magmatism along the PMSR. However, Macquarie Island

peridotite and basalt have higher average spinel Cr#’s (>35 ; Griffin 1982; Wertz 2003) compared to rare detrital spinel (Cr# <30 ; Appendix E), suggesting higher degrees of partial melting of the Miocene mantle source relative to the Oligocene mantle source. Thus, different mantle melting regimes (i.e. high vs. low) between Oligocene and Miocene spreading episodes is uncertain.

An enriched mantle source

A more straightforward model to explain the relatively old Hf-model ages is by utilizing an E-DMM reservoir for the more enriched colluvial zircons. Geochemical data collected from Macquarie Island volcanic rocks generally have an enriched mid-ocean ridge basalt (EMORB) affinity and were produced along a true mid-ocean spreading center (Kamanetsky et al. 2000; Varne et al. 2000; Wertz 2003). This is supported by clinopyroxene REE abundances presented in Chapter I (Fig. 4.9). Although many Macquarie Island basalt samples show unusual degrees of enrichment for MORB, they do not exhibit any characteristics akin to an ocean island basalt mantle-source origin (Kamanetsky et al. 2000; HIMU, EMI and EMII in Fig. 4.12). Rather, the mantle-source for Macquarie island basalts is comparable to the 2σ enriched variety of the average MORB end-member of Workman and Hart (2005; E-DMM in Fig. 4.12).

The DMM and 2σ E-DMM end-members for the Nd-Sr and Pb-Pb isotopic systems shown for basalts in Fig. 4.12 correspond to starting mantle-source Hf isotope compositions shown for zircons in Fig. 10. The similarity, relative to DMM and E-DMM mantle reservoirs, between Macquarie Island basalt Nd-Sr isotope and gabbroic zircon Hf-isotopes compositions compliments the good harmony commonly observed between the two isotopic systems in mantle-derived melts

(Patchett and Tatsumoto 1980; Salters and Hart 1991; Vervoort and Blichert-Toft 1999). Therefore, it seems reasonable to utilize a more enriched starting mantle source reservoir (E-DMM), relative to the commonly used DMM, for the highly enriched Macquarie Island igneous rock suite.

Calculating a 1σ enriched E-DMM from isotopic end-members presented by Workman and Hart (2005), yields a Lu/Hf of 0.03768 and initial $^{176}\text{Hf}/^{177}\text{Hf}$ of 0.283180 (Fig. 4.10). This 1σ E-DMM is roughly midway between the DMM and 2σ E-DMM on Fig. 4.12, roughly where Macquarie Island basalt compositions fall on the Nd-Sr isotopic array. The average Hf isotope composition for Macquarie Island detrital zircon plots along the 1σ enriched version of the DMM reservoir suggesting a nearly equivalent Hf model age and zircon crystallization age. Furthermore, slightly less radiogenic Hf isotopes in the colluvial sample suggests that the source for the Macquarie Island gabbro was isotopically different to the detrital samples. If they had shared a co-genetic mantle source reservoir, the younger colluvial samples should be slightly more radiogenic (higher $^{176}\text{Hf}/^{177}\text{Hf}$) and lie along a common Hf evolution line to the older detrital samples. Both Nd and Hf (daughter products) are more incompatible compared to Sm and Lu (parent products; Salters and Hart 1991) and therefore should produce lower $^{143}\text{Nd}/^{144}\text{Nd}$ and $^{176}\text{Hf}/^{177}\text{Hf}$ ratios in the more enriched ~ 8 Ma PMSR melts. This is also indicated by zircon trace element compositions, which show more depleted detrital samples (N-zircon) relative to the highly enriched colluvial sample (E-zircon). Disparate mantle source reservoirs for the old detrital sample and young colluvial samples is supported by an apparent >300 km offset along the Jurru Transform fault, which separated their host spreading-segments (described Chapter I).

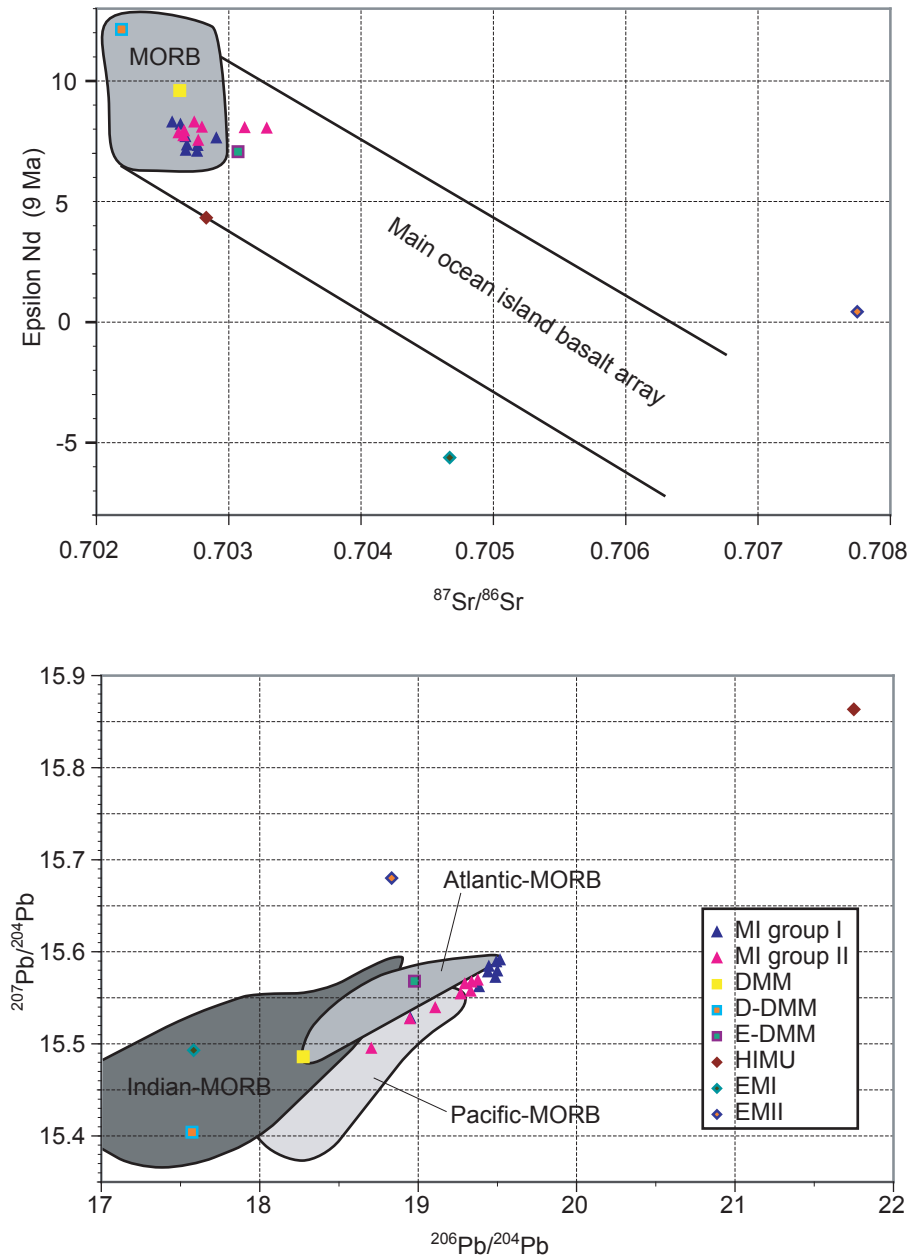


Figure 4.12:
 Indian and Pacific MORB and Macquarie Island (MI) data are from Kamenetsky et al. (2000) and Atlantic MORB from Ito et al. (1987). Group I and Group II MI data correspond to primitive and fractionated basalts, respectively. Depleted mantle (DMM) composition end member and its 2sigma enriched and 2sigma depleted variants (E-DMM and D-DMM) are from Workman and Hart (2005). Mantle-source end members for ocean island basalts HIMU, EMI, and EMII are from Zindler and Hart (1986).

Proposed model for detrital zircon provenance

The enriched ϵ_{Hf} composition of the detrital samples, relative to the global DMM reservoir source average, is still not explained by relatively flat detrital clinopyroxene patterns, more suggestive of a depleted NMORB source. Therefore, it may be expected that the detrital samples should have Hf-isotope values closer to the average DMM value of Workman and Hart (2005). This relative discrepancy may be due to the formation of the zircon host rock. Oceanic plagiogranite can form by hydrous partial melting of gabbros, liquid immiscibility affects, and MORB differentiation (see Koepke et al. 2007 for discussion). Partial melting of a gabbro source would preferentially enrich the segregated plagiogranite melt in Hf relative to more compatible Lu. This partial melt enrichment, with respect to the average DMM source, is preserved by lower $^{176}\text{Hf}/^{177}\text{Hf}$ ratios in zircons, which are artifacts of the radiogenic decay of Lu to ^{176}Hf . This process could then explain the production of depleted clinopyroxene and slightly enriched zircon relative to a common DMM source observed in Macquarie Island detrital sandstone samples. Evolved oceanic plagiogranites formed by anatexis typically have TiO_2 concentrations <1 wt%, which is generally much less than that found in plagiogranites formed by liquid immiscibility affects and MORB differentiation (Koepke et al. 2007). Although detrital zircon trace element compositions are out of context with their host rock bulk geochemistry, they have roughly equivalent Ti-in-zircon crystallization temperatures to oceanic plagiogranites interpreted to have formed by hydrous partial melting. In addition, $<15\%$ modal titanite and ilmenite, and non-titanian diopside in zircon bearing leucocratic diorite clasts from Southwest Point support relatively low total

TiO₂ concentrations and a partial melt-derived source for the detrital zircon host rocks.

Conclusions:

Trace element and Hf-isotope geochemistry from Oligocene and Miocene age zircon on Macquarie Island record the transition from a depleted to an enriched mantle source reservoir during transition of the PMSR toward the present day transform setting. Results caution the comparison between oceanic and continental crust zircon trace element geochemistry when interpreting detrital zircon provenance. Enriched oceanic crust (i.e. EMORB) contains zircons that are comparatively enriched in incompatible elements. This is portrayed by complimentary enrichment in Macquarie Island basalt and colluvial zircon collected from the islands plutonic section. Therefore, models for the generation of continental crust on early Earth may instead represent partial melting of an enriched mantle source. This enrichment is also observed in Hf-isotope compositions, which plot close to the 1 σ enriched variety of the modern global depleted mantle source average. Such enrichment changes ϵ_{Hf} crustal model ages by 350 Ma using a Lu/Hf ratio for mafic crust and has dire implications for crustal evolution models that assume a depleted mantle reservoir source.

A time-transgressive enrichment for the Macquarie Island detrital and colluvial zircon source can be explained by several models. The contamination of the source reservoir by Paleozoic-Mesozoic subduction along the eastern margin of Gondwana may explain the younger enriched zircons, but do not necessarily agree with more depleted zircon and detrital clinopyroxene with NMORB crustal affinity.

A geochemical disparity between the older detrital samples compared to the younger colluvial samples may instead represent changing melting regimes during demise of the PMSR. In this model, reduced partial melting in the waning stages of rifting could produce more enriched melts that Macquarie Island basalt and zircon would have formed from. However, relatively low Cr#’s in rare detrital spinel grains suggest lower degrees of partial melting than that inferred for the Macquarie Island melt source. More data from detrital chromian spinel may elucidate this explanation.

The best supported model for the time-transgressive enrichment of the SEIR-PMSR mantle source envisages a heterogeneous mantle source in both time and spatial scales. Greater than three hundred kilometers of offset along the Jurru transform between the SEIR detrital source and PMSR colluvial source was most likely associated with major mantle heterogeneities that were inherited by melts crystallizing zircon. The evolved host melts that formed the zircon, notably the detrital zircon, also played a role in their overall enriched ϵ_{Hf} character relative to the average DMM. Zircon-host plagiogranites formed by hydrous partial melting of gabbros would have been enriched in highly incompatible elements including Hf relative to radiogenic Lu; causing slightly lower $^{176}\text{Hf}/^{177}\text{Hf}$ compositions than would be expected. This is supported by Ti-in-zircon thermometry, which yields roughly equivalent crystallization temperatures to low-Ti plagiogranites formed by partial melting.

References Cited:

Amelin, Y., Lee, D.-C., Halliday, A.N. and Pidgeon, R.T., 1999. Nature of the Earth's earliest crust from hafnium isotopes in single detrital zircons. *Nature*, 399(6733): 252-255.

- Anderson, T., 2002. Correction of common-lead in U-Pb analyses that do not report ^{204}Pb . *Chemical Geology*, 192: 59-79.
- Armstrong, R.A., Kohn, B., Goscombe, B.D. and Everard, J.L., 2004. U-Pb and fission track ages from oceanic crust at Macquarie Island. In: J. McPhie and P. McGoldrick (Editors), *Abstracts - Geological Society of Australia*, vol.73, pp. 197.
- Aumento, F., 1969. Diorites from the Mid-Atlantic Ridge at 45° N. *Science*, 165(3898): 1112-1113.
- Baines, A.G., Cheadle, M.J., John, B.E. and Schwartz, J.J., 2008. The rate of oceanic detachment faulting at Atlantis Bank, SW Indian Ridge. *Earth and Planetary Science Letters*, 273(1-2): 105-114.
- Belousova, E., Griffin, W., O'Reilly, S. and Fisher, N., 2002. Igneous zircon: trace element composition as an indicator of source rock type. *Contributions to Mineralogy and Petrology*, 143(5): 602-622.
- Belousova, E.A., Griffin, W.L. and O'Reilly, S.Y., 2006. Zircon Crystal Morphology, Trace Element Signatures and Hf Isotope Composition as a Tool for Petrogenetic Modelling: Examples From Eastern Australian Granitoids. *J. Petrology*, 47(2): 329-353.
- Black, L.P. and Gulson, B.L., 1978. The age of the Mud Tank carbonatite, Strangways Range, Northern Territory. *BMR Journal of Australian Geology and Geophysics*, 3: 227-232.
- Blichert-Toft, J. and Albarède, F., 1997. The Lu-Hf isotope geochemistry of chondrites and the evolution of the mantle-crust system. *Earth and Planetary Science Letters*, 148(1-2): 243-258.
- Coogan, L.A. and Hinton, R.W., 2006. Do the trace element compositions of detrital zircons require Hadean continental crust? *Geology*, 34(8): 633-636.
- Coogan, L.A., Thompson, G. M., MacLeod, C. J., Dick, H. J. B., Edwards, S. J., Hosford-Scheirer, A., and Barry, T. L., 2004. A combined basalt and peridotite perspective on 14 million years of melt generation at the Atlantis Bank segment of the Southwest Indian Ridge: evidence for temporal changes in mantle dynamics? *Chemical Geology*, 207(1-2): 13-30.
- Debaille, V., Blichert-Toft, J., Agranier, A., Doucelance, R., Schiano, P. and Albarede, F., 2006. Geochemical component relationships in MORB from the Mid-Atlantic Ridge, 22-35°N. *Earth and Planetary Science Letters*, 241(3-4): 844-862.
- Dick, H.J.B., Natland, J. H., Alt, J. C., Bach, W., Bideau, D., Gee, J. S., Haggas, S., Hertogen, J. G. H., Hirth, G., Holm, P. M., Ildefonse, B., Iturrino, G. J., John, B. E., Kelley, D. S., Kikawa, E., Kingdon, A., LeRoux, P. J., Maeda, J., Meyer, P. S., Miller, D. J., Naslund, H. R., Niu, Y.-L., Robinson, P. T., Snow, J., Stephen, R. A., Trimby, P. W., Worm, H.-U. and Yoshinobu, A., 2000. A long in situ section of the lower ocean crust: results of ODP Leg 176 drilling at the Southwest Indian Ridge. *Earth and Planetary Science Letters*, 179(1): 31-51.
- Dickin, A.P., 2005. *Radiogenic isotope geology*. Cambridge University Press, Cambridge, United Kingdom (GBR), 492 pp.
- Dijkstra, A.H., and Cawood, P.A., 2004. Base-up growth of ocean crust by multiple phases of magmatism; field evidence from Macquarie Island. *Journal of the Geological Society of London*, 161(5): 739-742.

- Dosso, L., Bougault, H. and Joron, J.-L., 1993. Geochemical morphology of the North Mid-Atlantic Ridge, 10°-24°N: Trace element-isotope complementarity. *Earth and Planetary Science Letters*, 120(3-4): 443-462.
- Ferry, J.M. and Watson, E.B., 2007. New thermodynamic models and revised calibrations for the Ti-in-zircon and Zr-in-rutile thermometers. *Contributions to Mineralogy & Petrology*, 154(4): 429-437.
- Fu, B., Page, F., Cavosie, A., Fournelle, J., Kita, N., Lackey, J., Wilde, S. and Valley, J., 2008. Ti-in-zircon thermometry: applications and limitations. *Contributions to Mineralogy and Petrology*, 156(2): 197-215.
- Green, T.H., Blundy, J.D., Adam, J. and Yaxley, G.M., 2000. SIMS determination of trace element partition coefficients between garnet, clinopyroxene and hydrous basaltic liquids at 2-7.5 GPa and 1080-1200 degrees C. *Lithos*, 53(3-4): 165-187.
- Griffin, W.L., Belousova, E.A., Shee, S.R., Pearson, N.J. and O'Reilly, S.Y., 2004. Archean crustal evolution in the northern Yilgarn Craton: U-Pb and Hf-isotope evidence from detrital zircons. *Precambrian Research*, 131(3-4): 231-282.
- Griffin, W.L., Pearson, N. J., Belousova, E., Jackson, S. E., van Achterbergh, E., O'Reilly, S. Y. and Shee, S. R., 2000. The Hf isotope composition of cratonic mantle; LAM-MC-ICPMS analysis of zircon megacrysts in kimberlites. *Geochimica et Cosmochimica Acta*, 64(1): 133-147.
- Grimes, C.B., John, B. E., Cheadle, M. J., Mazdab, F. K., Wooden, J. L., Swapp, S. and Schwartz, J. J., 2009. On the occurrence, trace element geochemistry, and crystallization history of zircon from in situ ocean lithosphere. *Contributions to Mineralogy & Petrology*, 10.1007/s00410-009-0409-2.
- Grimes, C.B., John, B.E., Cheadle, M.J. and Wooden, J.L., 2008. Protracted construction of gabbroic crust at a slow spreading ridge: Constraints from $^{206}\text{Pb}/^{238}\text{U}$ zircon ages from Atlantis Massif and IODP Hole U1309D (30°N, MAR). *Geochem. Geophys. Geosyst.*, 9.
- Grimes, C.B., John, B. E., Kelemen, P. B., Mazdab, F. K., Wooden, J. L., Cheadle, M. J., Hanghoj, K. and Schwartz, J. J., 2007. Trace element chemistry of zircons from oceanic crust: A method for distinguishing detrital zircon provenance. *Geology*, 35(7): 643-646.
- Gurnis, M. and Mueller, R.D., 2003. Origin of the Australian-Antarctic discordance from an ancient slab and mantle wedge. In: R.R. Hills and R.D. Mueller (Editors), *Special Paper - Geological Society of America*, vol.372. Geological Society of America (GSA), Boulder, pp. 417-429.
- Heaman, L.M., Bowins, R. and Crocket, J., 1990. The chemical composition of igneous zircon suites: implications for geochemical tracer studies. *Geochimica et Cosmochimica Acta*, 54(6): 1597-1607.
- Hoskin, P.W.O. and Ireland, T.R., 2000. Rare earth element chemistry of zircon and its use as a provenance indicator. *Geology*, 28(7): 627-630.
- Ito, E., White, W.M. and Gopel, C., 1987. The O, Sr, Nd and Pb isotope geochemistry of MORB. *Chemical Geology*, 62: 157-176.
- Jackson, S.E., Pearson, N.J., Griffin, W.L. and Belousova, E.A., 2004. The application of laser ablation-inductively coupled plasma-mass spectrometry to in situ U-Pb zircon geochronology. *Chemical Geology*, 211(1-2): 47-69.

- John, B.E., Foster, D. A., Murphy, J. M., Cheadle, M. J., Baines, A. G., Fanning, C. M. and Copeland, P., 2004. Determining the cooling history of in situ lower oceanic crust--Atlantis Bank, SW Indian Ridge. *Earth and Planetary Science Letters*, 222(1): 145-160.
- Jons, N., Bach, W. and Schroeder, T., 2009. Formation and alteration of plagiogranites in an ultramafic-hosted detachment fault at the Mid-Atlantic Ridge (ODP Leg 209). *Contributions to Mineralogy and Petrology*, 157(5): 625-639.
- Kamenetsky, V.S., Everard, J. L., Crawford, A. J., Varne, R., Eggins, S. M. and Lanyon, R., 2000. Enriched end-member of primitive MORB melts; petrology and geochemistry of glasses from Macquarie Island (SW Pacific). *Journal of Petrology*, 41(3): 411-430.
- Kamenetsky, V.S. and Maas, R., 2002. Mantle-melt Evolution (Dynamic Source) in the Origin of a Single MORB Suite: a Perspective from Magnesian Glasses of Macquarie Island. *J. Petrology*, 43(10): 1909-1922.
- Koepke, J., Berndt, J., Feig, S.T. and Holtz, F., 2007. The formation of SiO_2 -rich melts within the deep oceanic crust by hydrous partial melting of gabbros. *Contributions to Mineralogy & Petrology*, 153(1): 67-84.
- Lawver, L.A., Dalziel, I.W.D. and Gahagan, L.M., 1999. PLATES - Antarctica keystone of Gondwana. University of Texas Institute for Geophysics, Austin.
- Li, Z.X. and Powell, C.M., 2001. An outline of the palaeogeographic evolution of the Australasian region since the beginning of the Neoproterozoic. *Earth-Science Reviews*, 53(3-4): 237-277.
- Lissenberg, C.J., Rioux, M., Shimizu, N., Bowring, S.A. and Mevel, C., 2009. Zircon Dating of Oceanic Crustal Accretion. *Science*, 323(5917): 1048-1050.
- Ludwig, K.R., 2006. Isoplot v. 3.5: a computer program for plotting geochronological data. Berkeley Geochronology Center, Berkeley.
- Meckel, T.A., Mann, P., Mosher, S. and Coffin, M.F., 2005. Influence of cumulative convergence on lithospheric thrust fault development and topography along the Australian-Pacific plate boundary south of New Zealand. *Geochem. Geophys. Geosyst.*, 6.
- Murphy, M., 2009. Petrography and geochemistry of oceanic crust: Provenance of sedimentary detritus, Macquarie Island. BSc honours thesis, Macquarie University, Sydney, 80 pp.
- Mosher, S. and Massell-Symons, C., 2008. Ridge reorientation mechanisms: Macquarie Ridge Complex, Australia-Pacific plate boundary. *Geology*, 36(2): 119-122.
- Nebel, O., Nebel-Jacobsen, Y., Mezger, K. and Berndt, J., 2007. Initial Hf isotope compositions in magmatic zircon from early Proterozoic rocks from the Gawler Craton, Australia: A test for zircon model ages. *Chemical Geology*, 241(1-2): 23-37.
- Niu, Y. and Hekinian, R., 1997. Spreading-rate dependence of the extent of mantle melting beneath ocean ridges. *Nature*, 385: 326-329.
- Patchett, P.J. and Tatsumoto, M., 1980. Hafnium Isotope Variations in Oceanic Basalts. *Geophys. Res. Lett.*, 7: 1077-1080.
- Salters, V.J.M. and Hart, S.R., 1991. The mantle sources of ocean ridges, islands and arcs: the Hf-isotope connection. *Earth and Planetary Science Letters*, 104(2-4): 364-380.

- Scherer, E., Munker, C. and Mezger, K., 2001. Calibration of the Lutetium-Hafnium Clock. *Science*, 293(5530): 683-687.
- Schwartz, J.J., John, B. E., Cheadle, M. J., Miranda, E. A., Grimes, C. B., Wooden, J. L. and Dick, H. J. B., 2005. Dating the Growth of Oceanic Crust at a Slow-Spreading Ridge. *Science*, 310(5748): 654-657.
- Sun, S.s. and McDonough, W.F., 1989. Chemical and isotopic systematics of oceanic basalts: implications for mantle composition and processes. Geological Society, London, Special Publications, 42(1): 313-345.
- Tribuzio, R., Tiepolo, M. and Vannucci, R., 2000. Evolution of gabbroic rocks of the Northern Apennine ophiolites (Italy); comparison with the lower oceanic crust from modern slow-spreading ridges. In: Y. Dilek, E.M. Moores, D. Elthon and A. Nicolas (Editors), Special Paper - Geological Society of America, vol.349. Geological Society of America (GSA), Boulder, pp. 129-138.
- van Achterbergh, E., Ryan, C.G. and Griffin, W.L., 1999. GLITTER: On-line interactive data reduction for the laser ablation ICPMS microprobe, The 9th V. M. Goldschmidt Conference. Cambridge, Massachusetts, pp. 305.
- Varne, R., Brown, A.V. and Falloon, T., 2000. Macquarie Island; its geology, structural history, and the timing and tectonic setting of its N-MORB to E-MORB magmatism. In: Y. Dilek, E.M. Moores, D. Elthon and A. Nicolas (Editors), Special Paper - Geological Society of America, vol.349, pp. 301-320.
- Vervoort, J.D. and Blichert-Toft, J., 1999. Evolution of the depleted mantle: Hf isotope evidence from juvenile rocks through time. *Geochimica et Cosmochimica Acta*, 63(3-4): 533-556.
- Vervoort, J.D. and Jonathan Patchett, P., 1996. Behavior of hafnium and neodymium isotopes in the crust: Constraints from Precambrian crustally derived granites. *Geochimica et Cosmochimica Acta*, 60(19): 3717-3733.
- Watson, E.B. and Harrison, T.M., 2005. Zircon Thermometer Reveals Minimum Melting Conditions on Earliest Earth. *Science*, 308(5723): 841-844.
- Wertz, K.L., 2003. From seafloor spreading to uplift; the structural and geochemical evolution of Macquarie Island on the Australian-Pacific Plate boundary. Doctoral Thesis, University of Texas, Austin, 169 pp.
- Wiedenbeck, M., Allé, P., Corfu, F., Griffin, W. L., Meier, M., Oberli, F., von Quadt, A., Roddick, J. C. and Spiegel, W., 1995. Three natural zircon standards for U-Th-Pb, Lu-Hf, trace element and REE analyses. *Geostandards and Geoanalytical Research*, 19(1): 1-23.
- Wiedenbeck, M., Hanchar, J. M., Peck, W. H., Sylvester, P., Valley, J., Whitehouse, M., Kronz, A., Morishita, Y., Nasdala, L., Fiebig, J., Franchi, I., Girard, J. P., Greenwood, R. C., Hinton, R., Kita, N., Mason, P. R. D., Norman, M., Ogasawara, M., Piccoli, P. M., Rhede, D., Satoh, H., Schulz-Dobrick, B., Skar, O., Spicuzza, M. J., Terada, K., Tindle, A., Togashi, S., Vennemann, T., Xie, Q. and Zheng, Y. F., 2004. Further characterisation of the 91500 zircon crystal. *Geostandards and Geoanalytical Research*, 28: 9-39.
- Workman, R.K. and Hart, S.R., 2005. Major and trace element composition of the depleted MORB mantle (DMM). *Earth and Planetary Science Letters*, 231(1-2): 53-72.
- Zindler, A. and Hart, S., 1986. Chemical geodynamics. *Annual Review of Earth and Planetary Sciences*, 14: 493-571.

Part 2:

Volcaniclastic rocks

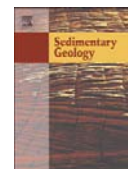
V:

**Glassy fragmental rocks of Macquarie Island
(Southern Ocean): Mechanism of formation and
deposition**

**DICKINSON, Julie A.¹, HARB, Nicole¹, PORTNER, Ryan A.¹, and
DACZKO, Nathan R.¹**

¹GEMOC ARC National Key Centre, Department of Earth and Planetary Sciences,
Macquarie University, NSW 2109, Australia

Published in Sedimentary Geology April 2009



Glassy fragmental rocks of Macquarie Island (Southern Ocean): Mechanism of formation and deposition

J.A. Dickinson, N. Harb, R.A. Portner*, N.R. Daczko

GEMOC ARC National Key Centre, Department of Earth and Planetary Sciences, Macquarie University, NSW 2109, Australia

ARTICLE INFO

Article history:

Received 24 June 2008

Received in revised form 30 January 2009

Accepted 12 February 2009

Keywords:

Australia–Pacific plate boundary

Hyaloclastite

Volcanogenic

Sedimentary

Breccia

ABSTRACT

Glassy fragmental rocks are interlayered with pillow basalt and tabular basalt on Macquarie Island (54°30' S, 158°54' E). These facies formed along the Proto-Macquarie Spreading Ridge between 6 and 12 Ma and have since been uplifted and exposed on the apex of the Macquarie Ridge Complex. Through a combination of field and microscopic analyses, we investigate the submarine production, transportation, deposition and lithification of basalt and sideromelane clasts within a spreading-ridge environment. The findings of this study indicate that these glassy grains form predominantly by cooling-contraction granulation of pillow lava rinds while crystalline basalt clasts are derived from the fragmentation of pillows along concentric and radial cooling joints. Hyaloclastite breccias consist of crystalline volcanic clasts in a matrix of glassy fragments, and are termed pillow-fragment breccias when clasts identifiable as pillows account for >25% of the cobble-sized fraction. This glassy fragmental sediment was transported predominantly by short-lived grain flows and deposited as a result of syn-eruptive talus accumulation. The above interpretations culminate in the production of a depositional model: these glassy fragmental rocks formed on the slopes of pillow cones following gravitational collapse of a destabilised cone flank along the Proto-Macquarie Spreading Ridge. Scanning electron microscopy reveals that palagonite alteration rims on glassy grains lithify the sediment. The findings may be used as an analogue for the formation of glassy fragmental rocks along past and present mid-oceanic ridges.

© 2009 Elsevier B.V. All rights reserved.

1. Introduction

Macquarie Island is the subaerial apex of an ~5 km high, ~50 km wide submarine ridge (Daczko et al., 2003) that constitutes part of what is known as the 'Macquarie Ridge Complex' (Fig. 1). The present-day ridge straddles the active boundary between the Australian Plate (on the west) and the Pacific Plate (on the east), and though presently a dextral transpressional-fault at this latitude, for much of the Tertiary (40 to ~6 Ma), this region of the plate boundary was an intra-oceanic axis of seafloor spreading (Wood et al., 1996; Daczko et al., 2005). These circumstances make Macquarie Island an ideal setting to study an in-situ exposure of oceanic crust that formed in a non-plume-related palaeo-intra-oceanic spreading-ridge setting. Though most aspects of the geology of Macquarie Island and its tectonic context and history have been studied (e.g. Griffin and Varne, 1980; Duncan and Varne, 1988; Kamenetsky et al., 2000; Varne et al., 2000; Goscombe and Everard, 2001; Daczko et al., 2003), there have been no detailed studies of its volcanogenic sedimentary rocks. Of these, glassy fragmental rocks predominate.

Glassy fragmental rocks have been described in some detail from intraplate, island arc, back arc and plume-related spreading-ridge settings (e.g. Jones, 1968; Lonsdale and Batiza, 1980; Batiza et al., 1984;

Yamagishi, 1991; Smellie and Hole, 1997; Tanner and Calvari, 1999; Templeton and Hanson, 2003). This investigation offers the first study of glassy fragmental rock associations within the plate tectonic setting preserved on Macquarie Island. We present the study of the submarine production, transportation, and deposition of basalt and sideromelane (basaltic glass) clasts within this palaeo-spreading-ridge environment, as well as their diagenesis.

2. Regional geology

Macquarie Island (54°30'S, 158°54'E) lies in the Southern Ocean 1500 km south-southeast of Tasmania, approximately midway between the southern tip of New Zealand and Antarctica (Fig. 1). The island is located 3–5 km east of the transpressional Australian–Pacific dextral-transform plate boundary. The oceanic crust that constitutes Macquarie Island formed 6–12 Ma (Duncan and Varne, 1988; Wertz, 2003; Armstrong et al., 2004; Quilty and Crundwell, 2004) at the slow-spreading Proto-Macquarie Spreading Ridge (Duncan and Varne, 1988; Varne et al., 2000; Goscombe and Everard, 2001; Davidson et al., 2004; Mosher and Massell-Symonds, 2008). The island's crust formed near a ridge-transform intersection (Wertz, 2003; Daczko et al., 2005). Though extension and volcanism at the spreading ridge continued up until 6 Ma, transpression along adjacent transforms initiated at the latitude of Macquarie Island by ~11 Ma (Massell et al., 2000; Goscombe and Everard, 2001; Meckel et al., 2005).

* Corresponding author. Tel.: +61 2 9850 4400.

E-mail address: rportner@els.mq.edu.au (R.A. Portner).

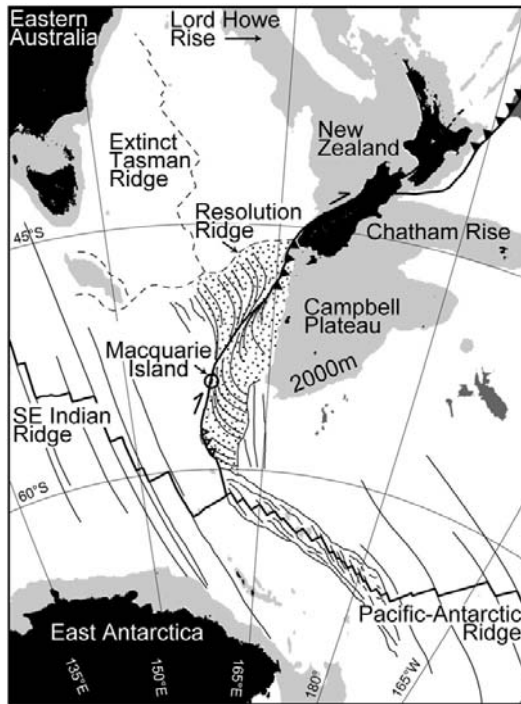


Fig. 1. Tectonic map of the South Pacific-Southern Ocean region showing Macquarie Island along the Macquarie Ridge Complex. Crust formed by Australian-Pacific spreading along the Proto-Macquarie Spreading Ridge between ca. 40 and ca. 10 Ma is stippled. Filled triangles indicate subduction zones; open triangle indicate recent incipient subduction. Light grey shows regions <2000 m below sea level. Dark grey shows regions >5500 m below sea level. Present plate boundaries are shown as bold black lines; fracture zones are shown as thin black lines; past plate boundaries are shown as dashed black lines (modified from Daczko et al., 2005).

The northernmost (ca. 15%) part of Macquarie Island consists mainly of sheeted dolerite dykes, gabbros and serpentinised peridotites together with minor volcanic and volcanoclastic rocks (Goscombe and Everard, 1998). The remainder of the island is composed mainly of pillow basalt and relatively minor tabular basalt. These rocks are associated with volcanoclastic breccias, glassy fragmental rocks and other sedimentary rocks that include mudstone, sandstone and minor chert and pelagic limestone (Daczko et al., 2005). Faulting is widespread and the island constitutes a complex of fault-bounded blocks (Goscombe and Everard, 2001). Volcanoclastic sedimentary rocks are spatially and temporally related to faults across the island, with volcanoclastic sediments formed by the breakdown of oceanic crust in fault zones (Daczko et al., 2005).

3. Methodology

Stratigraphic sections were measured at three locations on Macquarie Island: Bauer Bay, Green Gorge and Pyramid Peak (Fig. 2). These locations contain extensive exposure of glassy fragmental rocks and were selected based on previous mapping by Goscombe and Everard (1998). Petrographic features were analysed using transmitted-light microscopy on thin sections. Further investigation of morphologic and mineralogic variations was conducted using a Phillips XL30 CP scanning electron microscope (SEM) coupled with an EDAX energy-dispersive X-ray spectrometer (EDS) detector at The University of Sydney Electron Microscope Unit (EMU), Australian Key Centre for Microscopy and Microanalysis. Samples were analysed at a working distance of 11 mm with a 20.0 kV beam.

4. Stratigraphy

The stratigraphy of three sections at Bauer Bay, Green Gorge and Pyramid Peak (Fig. 3) are described (summarized in Table 1), where glassy fragmental rocks are exposed in association with pillow basalt. This presents the first detailed study of the outcrop characteristics of glassy fragmental rocks on Macquarie Island. Hyaloclastite breccias are defined as dominantly non-explosively derived glassy fragmental rocks with a dominant grain size greater than 4 mm (McPhie et al., 1993; Batiza and White, 2000). The hyaloclastite breccias found in this study are composed of crystalline volcanic clasts (commonly pillow basalt fragments with or without glassy rinds) in a matrix of glassy fragments (typically less than 16 mm), and compare with the 'angular

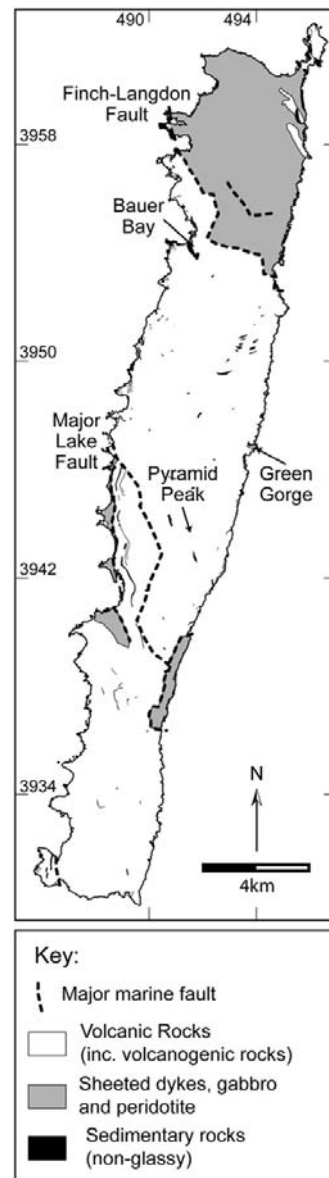


Fig. 2. Simplified geology map of Macquarie Island, showing major lithologic divisions, relict seafloor spreading faults and the location of field sections.

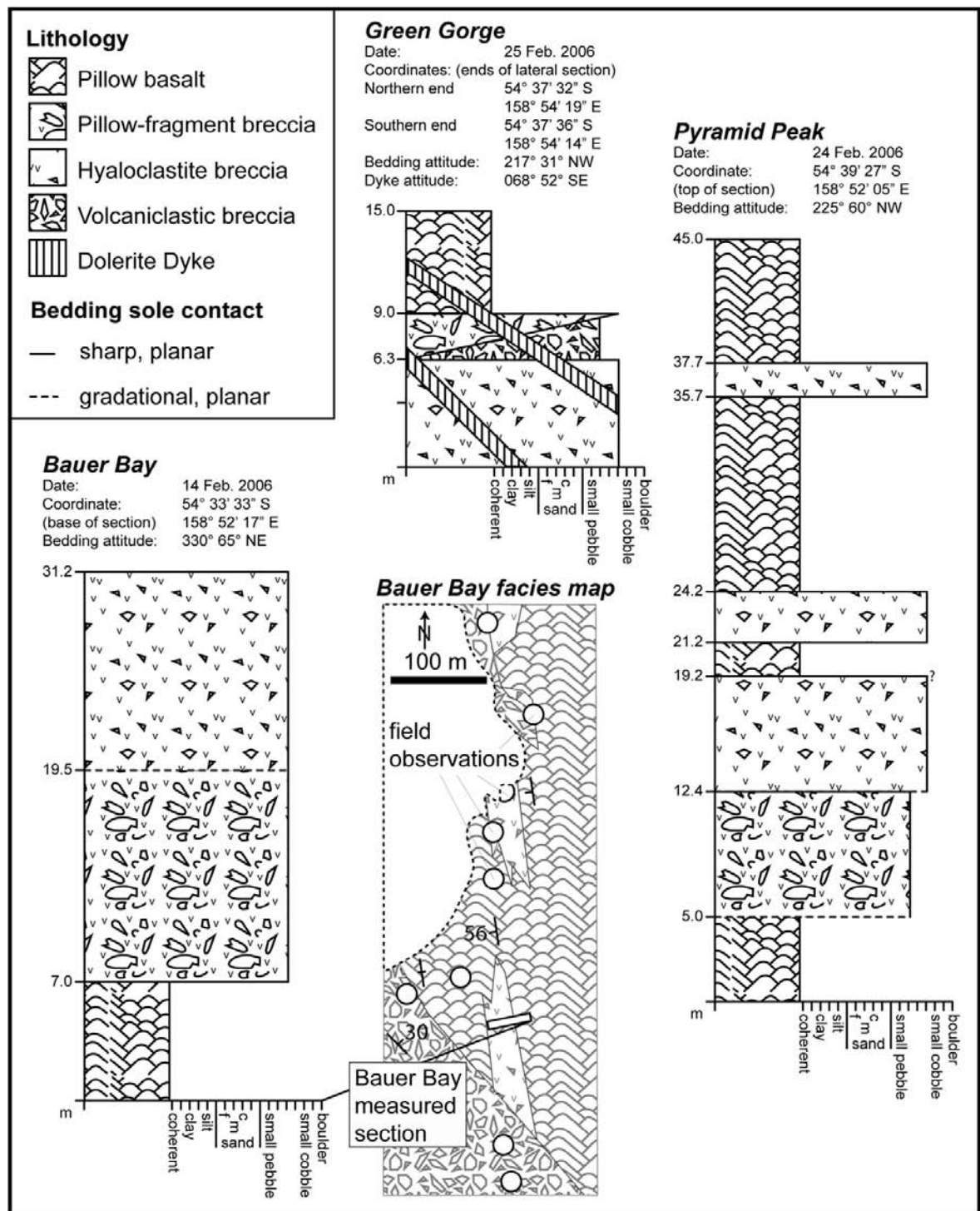


Fig. 3. Representative stratigraphic sections rich in glassy fragmental rocks from Bauer Bay, Green Gorge and Pyramid Peak. Each section begins and ends at an arbitrary position in the stratigraphy. A schematic representation of the lateral distribution of facies (all glassy fragmental rocks have hyaloclastite breccia map pattern) at Bauer Bay is shown in small inset map with reference to the location of the section measured.

Table 1

Summary of breccia clasts, breccia matrix and adjacent pillow basalt characteristics at the field sites.

	Matrix	Crystalline breccia clasts		Pillow basalt	
		Characteristics	Phenocrysts	Mineralogy	Phenocrysts
Bauer Bay	Med. sand–pebble (<15 mm) sized glassy grains	Dark grey to black	<5% porphyritic	Dark grey	Sparsely porphyritic
Green Gorge	Angular to sub-angular, blocky to sub-spherical shapes with radial fractures	Aphanitic	<1 mm size	Aphanitic	<2 mm size
	Palagonite between grains is common	Sparsely vesicular (<5%)	Olivine + Plagioclase	Sparsely vesicular	Olivine
	Med. sand–pebble (<15 mm) sized glassy grains	Dark to medium grey	Moderately porphyritic	Medium grey	Sparsely porphyritic
	Angular with straight surfaces to sub-spherical forms	Aphanitic	<3 mm size	Aphanitic	Plagioclase
Pyramid Peak	Rare concentric fractures	Moderately vesicular (<15%; laterally variable)	Plagioclase + olivine	Moderately vesicular (<30%)	
	Crs. sand-sized plagioclase and basalt fragments				
	Glassy grains <30 mm	Medium grey	Variably porphyritic	Medium grey	Moderately to non-porphyritic
	Angular to sub-spherical	Aphanitic	<3 mm size	Aphanitic	<2 mm size
	Pebble-sized basalt fragments	Moderately (<15%) to sparsely vesicular	Olivine (+ plagioclase)	Moderately vesicular (<30%) in pillow margins to sparsely vesicular in pillow cores	Olivine + plagioclase
	Crs. sand-sized plagioclase				
	Palagonite between grains is common				

fragment breccias' of Yamagishi (1991) and the 'hyaloclastites' of Tanner and Calvari (1999). Pillow-fragment breccias, defined by Staudigel and Schminke (1984) with reference to the broken pillow breccias of Carlisle (1963) and later described by others (e.g. Yamagishi, 1991; McPhie, 1995; Tanner and Calvari, 1999), are composed of isolated pillows and broken pillow fragments set in a glassy matrix (Yamagishi, 1991). In this study they are distinguished from hyaloclastite breccias by a larger proportion (>25%) of grains coarser than 150 mm that are recognisable as pillows or pillow fragments. Clast morphology is an important qualifier in this study for differentiating between the two types of breccias. Consequently, the encompassing terminology of hyaloclastite tuff breccia based on the new classification scheme of White and Houghton (2006) has not been adopted here.

4.1. Bauer Bay

A 31.2 m section of hyaloclastite breccia, pillow-fragment breccia and pillow basalt was logged ~300 m inland of the southern coastline of Bauer Bay, close to the Finch Langdon Fault (Fig. 2). A pillow basalt unit of unknown thickness (mapped by Goscombe and Everard, 1998) marks the base of the section (Fig. 3). The pillow basalt consists of pillows 40–55 cm in diameter. They are aphanitic, feature radial fractures and have thin (<10 mm) chilled margins. Some are highly amygdaloidal. A matrix of granule-sized glassy grains and minor crystalline basalt fragments fills the spaces between these pillows at the top of the unit. These granules have the same lithological characteristics as the overlying pillow-fragment breccia matrix and appear to have filtered down from above. The undulating upper surface of the top pillows marks the base of the overlying 12.5 m thick unit of matrix-supported pillow-fragment breccia, which grades upwards into a 11.7 m section of predominantly matrix-supported hyaloclastite breccia interspersed with two ~1 m thick intervals of clast-supported hyaloclastite breccia. These breccias are laterally continuous for up to ~200 m and pinch out into pillow basalt (Fig. 3).

The pillow-fragment breccia and hyaloclastite breccias are very poorly sorted and massive (Fig. 4A). Elongate clasts in the matrix-supported hyaloclastite breccias show a preferential orientation to the horizontal. All breccia units are characterised by monomict clast types composed of aphanitic and sparsely porphyritic (olivine phenocrysts up to 2 mm diameter) basalt. The clasts are sparsely vesicular and amygdaloidal, similar to underlying pillow basalt.

The basal pillow-fragment breccia contains isolated, intact sausage-shaped pillows. These pillows have long dimensions of 19–

59 cm, radial fracture patterns, and 10–20 mm thick chilled margins with glassy rinds. Pebble-sized pillow fragments also occur and are more common here than within the hyaloclastite breccias. The pillows and pillow fragments are aphanitic and exhibit low vesicularity.

Clasts in the hyaloclastite breccia units are predominantly angular to sub-rounded and pebble-sized. Some exhibit glassy rims. The clasts possess predominantly blocky and wedge-like morphologies that commonly have curved surfaces. Rare crystalline basalt clasts are pyramidal (Fig. 4B), while others have highly irregular morphologies with arcuate surfaces (Fig. 4A). The largest clasts in the hyaloclastite breccias have maximum dimensions in the range 10–26 cm, and are elongate and/or ellipsoidal with tapering tails. These clasts are aphanitic, non-vesicular, and have prominent chilled margins and hollowed cores (Fig. 4C).

The matrix of the breccia units consists of medium sand to medium pebbles that comprise sideromelane fragments. Sand- and granule-sized glassy grains are angular whereas the larger glassy fragments are sub-angular and have blocky to sub-spherical shapes, and some exhibit radial fractures. Rarely, they are bowl-shaped (Fig. 4D). A yellowish clay-like material (palagonite) rims the glassy grains and is common between the sideromelane fragments (Fig. 4A).

4.2. Green Gorge

The section measured on the rock platform exposed along the northern Green Gorge embayment (Fig. 2) contains a 9 m thick succession of predominately hyaloclastite breccia that is laterally extensive for over 150 m. This facies is laterally interstratified with non-glass fragment bearing volcanoclastic breccia to the north and locally overlain by minor pillow-fragment breccia with sharp contact (Fig. 3). The section is cut by numerous dolerite dykes (~1 m thick) that have quenched margins and capped by pillow basalt.

The hyaloclastite breccia is generally structureless and very poorly sorted (Fig. 5A). Though the breccia appears as one 9 m thick uniform package, subtle lateral variations in clast-support versus matrix-support are also apparent. The clasts in the hyaloclastite breccias are generally very large pebble-sized aphanitic basalt that is moderately porphyritic and vesicular. Olivine and plagioclase phenocrysts are present in equal amounts and up to 2 mm diameter. The clasts are variably of low or high sphericity, commonly angular, bounded by primary curved surfaces, and have blocky or wedge-like forms (Fig. 5A). The larger clasts (maximum exposed long-dimension of 60 cm; e.g., Fig. 5B) are clearly recognisable as discrete wedge-like or arcuate-shaped pillow fragments with radial fractures and 10–40 mm

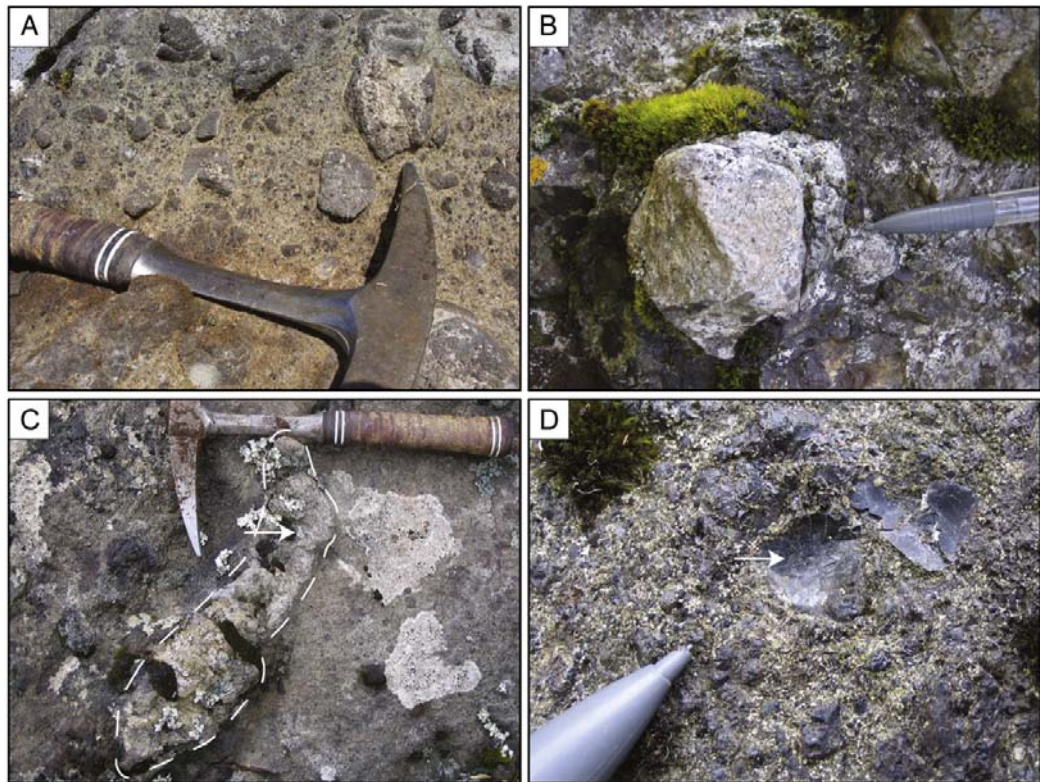


Fig. 4. Photographs illustrating typical field appearance of breccias at Bauer Bay. A. Hyaloclastite breccia at Bauer Bay. Crystalline basalt fragments are cemented by a mixture of glassy fragments and yellow palagonite. Note the irregular-shaped clasts with arcuate surfaces. Head of hammer is 17 cm long. B. Pyramidal-shaped clast with curved surfaces within the hyaloclastite breccia. Grey pencil tip is 4 cm long. C. Elongate clast within hyaloclastite breccia with tapered ends showing a prominent chilled margin and hollow core (arrow). Hammer is 31 cm long. D. Glassy grains within the hyaloclastite breccia. The larger grains can be seen to be bowl-shaped (arrow) and the creamy-yellow material surrounding glassy grains is palagonite. Pencil is 8 mm at its widest part.

thick chilled margins of an aphanitic inner and glassy exterior surface. Others are broken 'mini-pillows' (or buds) or large isolated pillows (Fig. 5C), which in rare instances exhibit zeolite-filled cores with diameters of 20–50 mm.

The breccia matrix predominantly consists of coarse sand- to medium pebble-sized glassy fragments. Coarse sand-sized fragments of basalt and plagioclase crystals also occur. The sand-sized glassy grains are typically angular with straight surfaces, whereas the larger fragments have curved outlines, sub-spherical (globule) forms (Fig. 5D), and rarely display concentric fractures. A greenish clay-like material occurs in outcrops within the present-day surf zone (Fig. 5A) and zeolite is common between the sideromelane fragments.

The pillow basalt unit at the top of the section consists of sausage-shaped pillows with normal (radial) joints and 10–30 mm thick chilled margins consisting of an aphanitic inner and glassy exterior surface. The 'sausages' have branches and buds but are tightly packed with typically less than 10 mm thickness of glassy matrix and zeolite present in the inter-pillow spaces. Pillow diameters range from 40 to 65 cm and are sparsely to moderately vesicular (and amygdaloidal). Some pillows contain sparse plagioclase phenocrysts.

4.3. Pyramid Peak

A 45 m thick section was measured on the northern face of the prominent near vertical bedding exposure west of Pyramid Peak (Fig. 2). The stratigraphy comprises a succession of pillow basalt intercalated with pillow-fragment and hyaloclastite breccia units

(Fig. 3). The basal pillow basalt (of undetermined thickness) is overlain by 7.4 m of pillow-fragment breccia, which grades upward into a 6.8 m thick bed of matrix-supported hyaloclastite breccia. Two thinner (2–3 m) matrix-supported hyaloclastite breccias occur within the overlying 18.5 m thick pillow basalt. The breccia units are very poorly sorted, internally structureless, and exhibit a lenticular geometry with a width of ~100 m.

The pillow-fragment breccia is clast-supported and consists of intact variably aphanitic and porphyritic (olivine and rarely plagioclase phenocrysts up to 3 mm across), 40–60 cm long, ovoid-shaped pillows and pillow fragments. The clasts are pebble-sized grains that have wedge-like or arcuate morphologies. The cross-sections of some pillows show fracture patterns indicative of pillow-rind and core-fragment morphologies (Fig. 6A). These morphologies are also evident in the crystalline basalt clasts surrounding them. The abundance of intact pillow-shaped clasts decreases up-section and the breccia grades into the overlying hyaloclastite breccia.

Clasts within the hyaloclastite breccias are predominantly fragments with arcuate, wedge, and blocky forms. Less common are spheroidal bodies with glassy rinds. Rare clasts exhibit cylindrical hollows, some filled with zeolite. The clasts commonly have at least one glassy surface and some exhibit grooves parallel to the clasts' long-axis (Fig. 6B). The clasts of all the hyaloclastite breccias in this measured section are monomict and consist of variably aphanitic and porphyritic basalt similar to the associated pillow basalt in the section.

The matrix of both the pillow-fragment breccia and the hyaloclastite breccias consists of coarse sand-sized fragments of plagioclase,

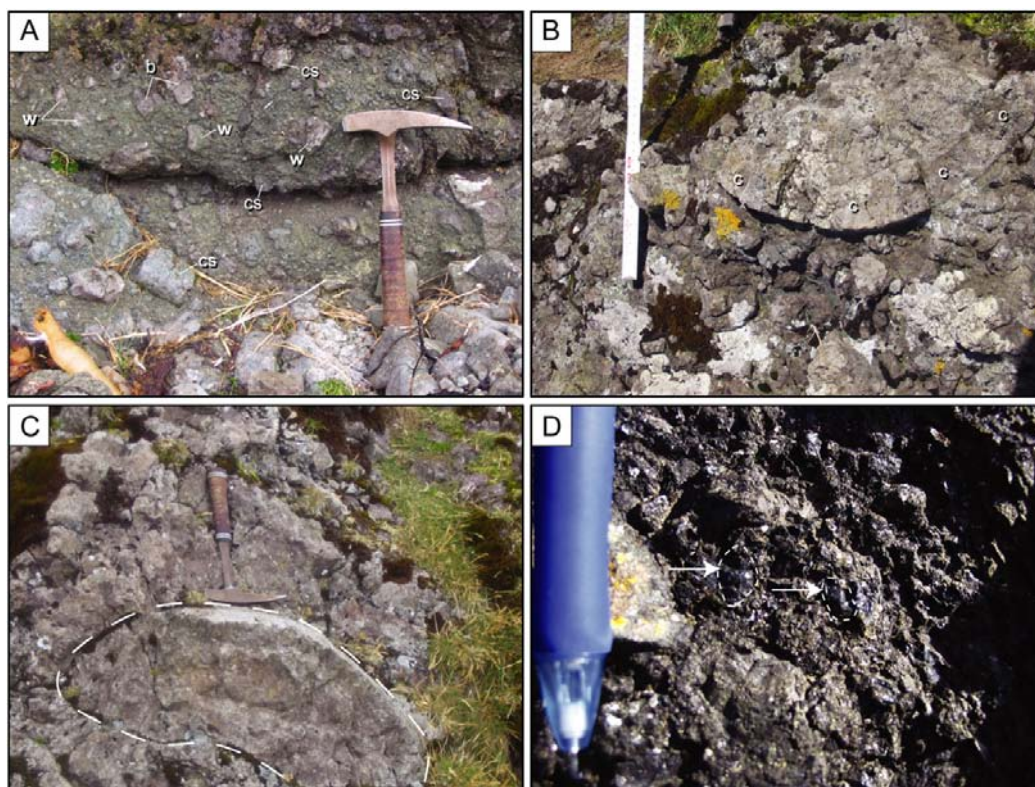


Fig. 5. Photographs illustrating typical field appearance of breccias at Green Gorge. A. Hyaloclastite breccia with blocky (b) and wedge-shaped (w) crystalline basalt clasts, some with curved surfaces (cs). Hammer is 31 cm long. B. Arcuate-shaped crystalline basalt clasts with chilled (c) margin on outer edge in hyaloclastite breccia. Folding ruler is 30 cm long. C. Intact flattened pillow (marked with a dashed line) in hyaloclastite breccia. Hammer is 31 cm long. D. Matrix of hyaloclastite breccia showing glassy pebbles with sub-spherical form. Pen is 8 mm wide.

pebble-sized basalt fragments, and glassy grains up to ~30 mm in size. The sand- and granule-sized glassy grains are angular, whereas those of pebble-size commonly have curved exteriors (Fig. 6C) and exhibit annular concentric fractures. One tear-drop-shaped glassy pebble observed has a ~3 mm rim that is roughened and pitted (Fig. 6D). A yellowish clay-like material (palagonite) (Fig. 6D) coats grains and along with zeolite is common between the sideromelane fragments.

The pillow basalt comprising the basal and topmost units of the measured section are very similar. Their component pillows are 30–55 cm in diameter, aphanitic and moderately porphyritic (with plagioclase and olivine phenocrysts), and they exhibit radial fractures. They contain a high percentage of zeolite-filled vesicles that are concentrated in 20 mm thick chilled margins. Many pillows have a 1–2 mm thick glassy rind. The matrix consists of coarse sand- to pebble-sized glassy grains.

5. Petrography of breccia matrix

The matrix of hyaloclastite and pillow-fragment breccias from Macquarie Island was examined using petrological and scanning electron microscopy (SEM).

Individual glassy grains (including their palagonitised rims) are 0.1 to 17 mm long, though most are 1–3 mm. The shape of the glassy material varies very little between samples and common morphologies observed are squarish, sub-rectangular, trapezoidal, triangular, elliptical and arcuate (Fig. 7A). Some also have irregular shapes and arcuate edges. Grains are typically sub-angular to angular, though the largest (>5 mm) have sub-oval forms.

The glassy grains are moderately to very closely packed and randomly oriented, except for elongate grains (particularly the <3 mm fraction) that are rarely aligned parallel to bedding. Many of the grain shapes are reflected in the fracture patterns of larger glassy grains. Squarish, sub-rectangular, trapezoidal and triangular fracture patterns are the most common, though parallel fractures are also present. Radial fractures are common around vesicles and many glassy grains have fractured along the boundary with phenocrysts. Large arcuate fractures separate granulated rinds from the cores of some large glassy grains. Sets of parallel fractures in separate glassy grains within any one sample are randomly oriented. Jigsaw-fit textures (McPhie et al., 1993) are observed between arcuate-shaped glassy fragments and adjacent olivine phenocrysts or the cores of glassy grains from Bauer Bay and Green Gorge samples (Fig. 7B). The glassy grains at Pyramid Peak have the least degree of internal fracturing. Those that are fractured do so in forms which resemble squares, rectangles and elongate triangles. Spalling rinds are also visible.

The samples consist of up to 60% fresh basaltic glass (sideromelane), which forms the core of the glassy grains. The glass is generally sparsely vesicular, the exception being samples from Green Gorge that are moderately vesicular. Vesicles are circular (rarely elongate) and filled with calcite and zeolite (Fig. 7C). Vesicles from Bauer Bay samples also have a thin rim of pyrite around the inner wall. Phenocrysts of euhedral to subhedral olivine (0.1–2 mm across) and rarely plagioclase are also a feature of the glass (Fig. 7D), more commonly so in Green Gorge breccia units.

1–5% of glassy grains in all samples contain scattered semi-opaque Fe-oxide spherulites. Initially star-shaped, they adopt a cross- and finally

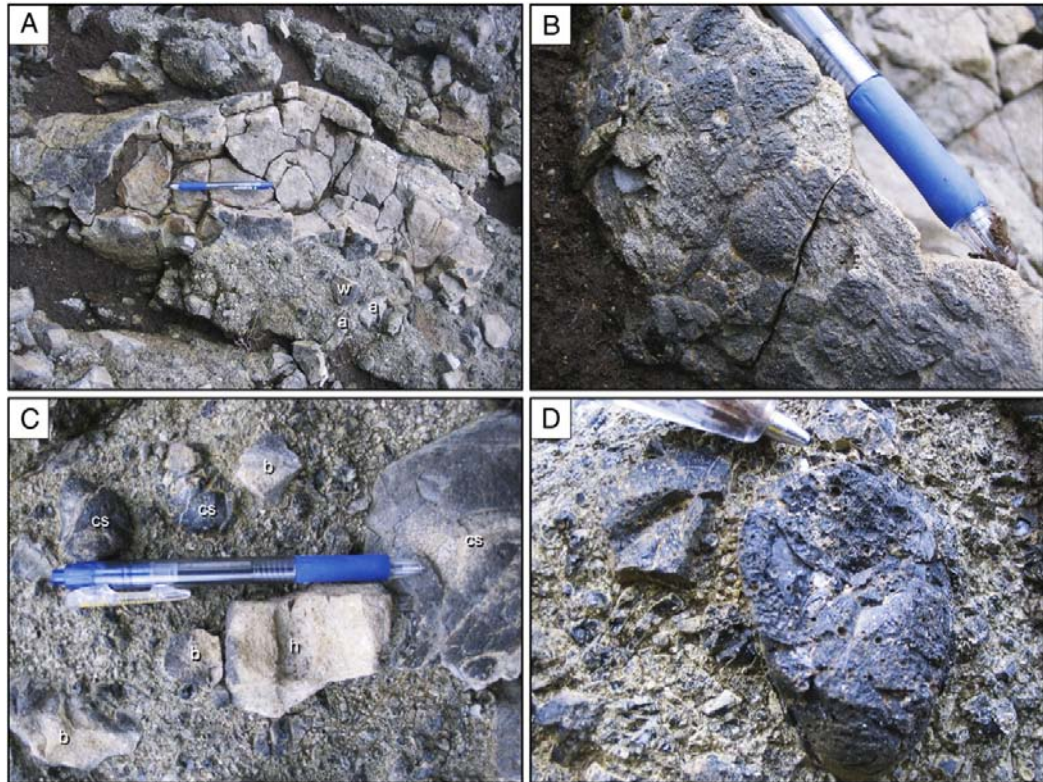


Fig. 6. Photographs illustrating typical field appearance of breccias at Pyramid Peak. A. Pillow-fragment breccia at Pyramid Peak with cross-section through a pillow tube. Note crystalline basalt clasts embedded in glassy matrix with wedge (w) and arcuate (a) shapes. Pillow tube shows fracturing patterns of chilled margin and core. Elongate amygdale-filled vesicles are observed in the chilled margin parallel to the pillow tube elongation. Pen is 15 cm long. B. Striations on glassy surface of hyaloclastite breccia clast. Pen is 8 mm wide. C. Clasts and glassy matrix of hyaloclastite breccia. One clast exhibits a cylindrical hollow (h) while others are blocky (b) or exhibit curved surfaces (cs). Pen is 15 cm long. D. Sub-spherical glassy globule with 3 mm pitted rind in hyaloclastite breccia. Pale green palagonite can be seen between glassy grains. Metallic pen tip is 2 mm wide.

square-shaped morphology as dendrites grow out perpendicular to the spherulite arms (Fig. 7D). Tachylite containing moderate concentrations of microlites of olivine and 'swallow tail' or 'belt buckle' plagioclase surrounded by Fe-oxide spherulites is also observed (Fig. 7E).

20–50% of each sample is palagonite (Drief and Schiffman, 2004), which makes up the altered rims of glassy grains, alteration haloes around vesicles and forms along fractures in glass. Palagonite completely replaces smaller (<1 mm) glassy grains (Fig. 7F) and sutures the rims of adjacent glassy grains (Fig. 7G). Replacement of the fresh basaltic glass by palagonite occurs from the outside inward as indicated by the diffuse inner boundary (Fig. 7F). Smectite makes up a further 5% of each sample and is limited to thin weakly birefringent bands around the rims of glassy grains, vesicles and along glass fractures. It is identified by its 2nd order brown interference colours in crossed polarized light (Fig. 7H) and typically does not occur in direct contact with fresh glass. The transition zone between smectite clay and fresh glass is commonly composed of palagonite with or without a minor component of weakly birefringent smectite-like material. This smectite-like material shares a diffuse inner boundary with either palagonite or fresh glass and has characteristics similar to reddened smectite grain replacement (RSGR, Drief and Schiffman, 2004). We use the term smectite for any birefringent clay-like material, including RSGR, and the term palagonite for any nearly isotropic alteration product that rims and locally completely replaces glassy grains.

Between 5 and 7% of each sample is void space or is filled with zeolite (including analcite), calcite, minor albite and smectite (Fig. 7H). These mineral precipitates are observed adjacent to glassy grains already sutured by palagonite alteration rims and are the same minerals that fill

vesicles at Bauer Bay. Smectite occurs between grains replacing the palagonite rims of adjacent grains. It is more abundant in samples from Pyramid Peak (40–50%). Minor (1–5%) fragments of fractured olivine and plagioclase phenocrysts occur between glassy grains.

6. Discussion

6.1. Fragmentation processes

The generation of glassy and associated crystalline (basalt) clasts to form hyaloclastites and hyaloclastite breccias, has been a topic of much debate (e.g. Lonsdale and Batiza, 1980; Batiza et al., 1984; Yamagishi, 1991; Maicher et al., 2000; Head and Wilson, 2003; Davis and Clague, 2006). Five modes of fragmentation have been identified in submarine settings: cooling-contraction granulation, joint fragmentation, contact-surface steam explosivity, bulk interaction steam explosivity, and magmatic explosivity (Kokelaar, 1986). The latter three processes are generally thought to be limited to shallower depths due to the increased hydrostatic pressures with depth. Cooling-contraction granulation and joint fragmentation are considered more likely at deep marine seafloor spreading centres.

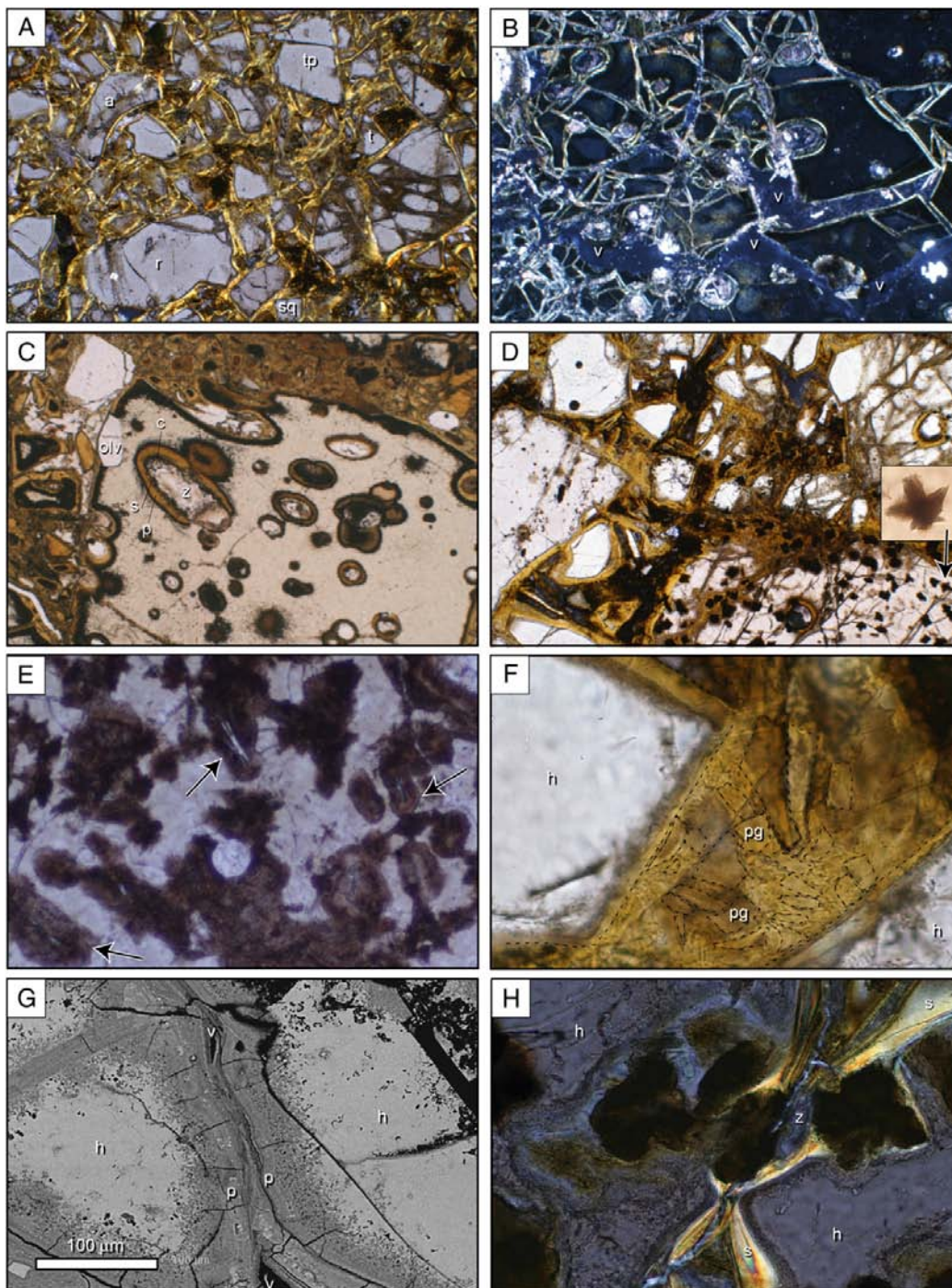
6.1.1. Fragmentation of glassy grains

The majority of glassy grains from all three field locations have a dominant grain size of 1 to 3 mm and grains in this size range typically have angular shapes and equant, rectangular, triangular or trapezoidal morphologies. They also exhibit sparse vesicularity. The production of

glassy sediment with these characteristics is generally attributed to cooling-contraction granulation of quenched pillow rinds (e.g. Clague et al., 2000; Maicher et al., 2000; Head and Wilson, 2003; Templeton and Hanson, 2003). If steam or magmatic explosivity were involved in their production, highly vesicular, elongate or limbo (thin flakes defined as glass bubble shards) fragments would be expected (Davis

and Clague, 2006). As this is not evident, cooling-contraction granulation is likely the dominant mechanism for the production of glassy grains in the breccias.

Rare sub-spherical (globule) glass pebbles, some of which exhibit radial fractures, are more consistent with fire-fountaining. Thin section analyses revealed common concentric fractures and less



commonly these grains are surrounded by spalled-off arcuate glassy fragments. SEM observations of these fragments (<1 mm) indicate very angular, triangular- to splinter-shaped morphologies, consistent with subsequent cooling-contraction granulation of magma droplets (Kokelaar, 1986; Maicher et al., 2000; Head and Wilson, 2003). The additional presence of sand-sized triangular-shaped glassy grains also supports this interpretation. Furthermore, the observation of bowl-shaped glassy grains (Bauer Bay), sub-spherical crystalline basalt clasts surrounded by concentric glassy shells (Pyramid Peak) and a sub-spherical (globule) glassy pebble with a 3 mm thick pitted rind (Pyramid Peak), suggest a fire-fountaining origin for these grains (lapilli). Though not expected along a spreading centre, experimental evidence for the occurrence of fire-fountaining at depths below 3000 m do support such an interpretation (Head and Wilson, 2003; Davis and Clague, 2006). Lapilli-sized glass droplets are also locally observed in high abundance west of the Pyramid Peak section shown here (unpublished data). However, the volume of lapilli produced along the Proto-Macquarie Spreading Ridge must have been minor (<2%), on the basis of the general rarity of these characteristic morphologies.

Microscopic jigsaw-fit texture, observed in glassy grains and phenocryst fragments, are consistent with in-situ fragmentation of these grains following deposition from a volcanic source. This texture in glass is traditionally interpreted as a product of the shattering of glassy grains deposited while hot (Carlisle, 1963; Batiza et al., 1984; Maicher et al., 2000). However, cooling rates, as slow as 0.15 °C/min (Maicher et al., 2000), enables cooling-contraction granulation to occur following deposition. So alternatively, fragmentation of cooled glassy grains or phenocryst fragments may have occurred along pre-existing partial fractures as they were deposited from mass flow, or while other sediment was deposited above them. Regardless of fragmentation process, this took place after deposition and the fragments remained adjacent to each other until diagenetic processes cemented them into place.

6.1.2. Fragmentation of crystalline basalt clasts

The crystalline basalt clasts that are volumetrically dominant in the breccias exhibit characteristics that are consistent with a pillow lava origin: (i) curved surfaces (e.g. Fig. 5A and B) similar to pillow surfaces, with rare glassy striated rinds (e.g. Fig. 6B); (ii) wedge-shaped and blocky morphologies (Fig. 4B) that resemble the shapes and sizes formed by fracturing of pillows along cooling joints (Fig. 6A); and (iii) hollow cores (Fig. 6C) as observed in rare pillow clasts at Green Gorge. Cooling-contraction fragmentation of pillows along joints is frequently cited as the mechanism from which basalt talus is derived in the marine environment (Jones, 1970; McPhie et al., 1993; Smellie et al., 1998; Tanner and Calvari, 1999; Lipman and Coombs, 2006). Where this occurs, the derived clasts are commonly pyramidal, wedge-shaped, blocky, or have glass encrusted on remnant pillow structures (McPhie, 1995; Sansone and Smith, 2006) as observed with the crystalline basalt clasts in this study. Consequently, a cooling-controlled joint-fragmentation mechanism is responsible for the production of the crystalline basalt clasts.

However, a different clast-forming mechanism is required to explain the rare fluidally-shaped clasts observed at Bauer Bay. These clasts are devoid of vesicles, have elongate morphologies and are

surrounded by chilled margins. Tearing apart of lava ejected during Hawaiian-style fire-fountaining has derived similar morphologies in submarine basaltic-andesite clasts (Simpson and McPhie, 2001). However, the clasts produced in that setting exhibit high vesicularity, which is common for volatile-rich magmas and magmatic explosivity. The nature of the fluidally-shaped clasts found at Bauer Bay, their lack of vesicles and the scarcity of quenched magma droplets suggest that these associations are not applicable here. Instead it is interpreted that their fluidal morphology is derived from lava being squeezed out of ruptures in flowing pillows or spilt out of fractures in the chilled margins of emptying pillows. These morphologies may also be explained as small pillow lava apophyses that have intruded into unconsolidated hyaloclastite breccia (Simpson and McPhie, 2001).

6.2. Sediment source

Examination of the breccia units indicates that the sideromelane glassy grains and crystalline basalt clasts are derived from the fragmentation of pillow lava, and that a small percentage of lapilli-sized droplets (either entirely glassy or with crystalline cores) originate from fire-fountaining. The rare tachylite grains are most likely derived from the tachylitic rim of pillows (positioned beneath the sideromelane outer rim; McPhie et al., 1993). As tachylite is partly crystalline, it is more likely to remain attached to the crystalline basalt core during cooling-contraction granulation, while the brittle non-crystalline sideromelane separates from the pillow rinds. Consequently, tachylite only rarely forms distinct grains.

A parallel study (Daczko et al., *in press*) of the major- and trace-element geochemistry of intra-sample glasses indicates that the glassy grains in any one stratigraphic section are supplied from a single geochemically distinct magma reservoir that may be feeding multiple local volcanic edifices (Fig. 8). This contrasts with polymict sedimentary rocks from Macquarie Island that have been interpreted as fault-scarp-derived (Daczko et al., 2005). A fault-scarp source for the glassy grains is ruled out by the geochemical results, as sediment wasted from an exposed cross-section of pillow basalt would likely contain material representing the products of several eruptions and Macquarie Island magmas have been shown to have significant compositional differences (Kamenetsky and Maas, 2002). Furthermore, though it is likely that the oceanic crust was highly faulted, observations of fault scarps along the mid-Atlantic ridge did not find significant volumes of talus at the base of these structures 'implying that uplift can take place without major dislocation and slumping' (Ballard and Moore, 1977, p. 87). A "cold" faulted source can also be negated by the in-situ fragmentation indicated by the jigsaw-fit texture and the glass globules, both a result of hot emplacement and active volcanism.

6.3. Transport mechanism

The pillow-fragment and hyaloclastite breccias are generally characterised by matrix-supported, massive and poorly sorted deposits that lack any primary mud-sized material. Processes

Fig. 7. Transmitted light microscope (TLM) photomicrographs and scanning electron microscope backscatter (BSE) images illustrating the texture of the glassy fragmental rocks. A. Typical morphologies of glassy grains include squarish (sq), sub-rectangular (r), trapezoidal (tp), triangular (t), and arcuate (a). Grains are surrounded by palagonite. Field of view is 3.5 mm, plain polarised light (PPL), Bauer Bay. B. Jigsaw-fit texture of glassy grains. Grains are rimmed by birefringent smectite. Void space (v) is labelled. Field of view is 1.75 mm, crossed polarised light (XPL), Green Gorge. C. Elongate vesicles within a glassy grain are filled with unidentified zeolite (z) and calcite (c). Smectite (s) lines the inner walls of vesicles and grades into brown palagonite (p) which is in contact with fresh glass. Small olivine (olv) phenocryst is not altered by palagonitisation. Field of view is 3.5 mm, PPL, Green Gorge. D. Typical glassy grains showing sub-angular morphology and extent of palagonite (straw-yellow to dark brown coloured material). Fe-oxide spherulites are evident in partly devitrified glassy grain in lower right. Inset shows highly magnified individual spherulite with cross-shaped morphology. Field of view is 3.5 mm wide in the large-scale image and 0.08 mm wide in the small scale inset, PPL, Bauer Bay. E. Tachylitic glassy grain with abundant plagioclase microlites (arrows) surrounded by dark brown Fe-oxide spherulites. Field of view is 1.17 mm, PPL, Green Gorge. F. The visible outlines of completely palagonitised grains (pg) between two larger fresh glassy grains (h) show that small palagonite grains fill much of the interstitial space. The fresh cores of the two larger grains share a diffuse boundary with their palagonite rims. The original edges of these grains are partially traced with a dashed line. Field of view is 0.5 mm, PPL, Bauer Bay. G. Two glassy grains (h) sutured by their respective palagonitised rims (p) with no interstitial material between them. The banded pattern is characteristic of amorphous palagonite. Dark areas in between them are void space (v). Scale shown is 100 µm, BSE image, Green Gorge. H. Authigenic smectite (s) with 2nd order brown birefringence fills glassy grain pore space, rims glassy grains and locally surrounds dark brown spherulites. Zeolite (z; locally analcite) fills some pore space. Field of view is 0.5 mm, XPL, Bauer Bay.

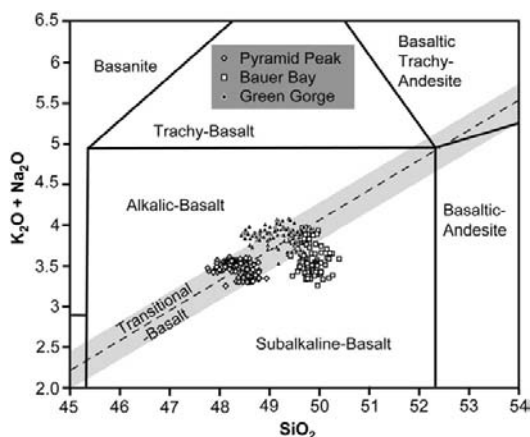


Fig. 8. Total alkali versus silica diagram (wt.%) for Macquarie Island glasses from the three sections studied. Data from Daczko et al. (in press).

synonymous with gravity-driven deposition in subaqueous settings (e.g. turbidity currents, fluidised flows, liquefied flows, mud flows, slides and slumps) have been evoked for glassy fragmental rocks. However, the textural characteristics of the breccia units in this study rule out these processes as plausible depositional mechanisms. For example, transport of the sediment by turbidity currents or traction carpets is discounted due to the absence of: (i) normal grading; (ii) good sorting; (iii) erosive basal contacts; and (iv) sedimentary structures such as laminations. Similarly, the lack of dewatering structures, good sorting and bedding rule out transportation by submarine liquefied flow or fluidised flow (Lowe, 1976; Leeder, 1999). These flows are also highly unlikely to occur in gravel-sized sediment, which is highly permeable allowing fluid to escape readily, and where the weight of clasts makes them resistant to lift (Reading, 1996). The limited primary mud-sized matrix of hyaloclastite breccia and pillow-fragment breccia in this study excludes mud flows, which require a matrix of mud-sized particles to provide the necessary buoyancy (Leeder, 1999). Submarine slumps or slides are also excluded as these mechanisms require evidence of a failure plane and sediments capable of maintaining a high degree of cohesion (e.g. mud; Leeder, 1999) not evident here.

The deposition of glassy fragmental rocks in a submarine setting is generally attributed to grain flows (cohesionless debris flows), talus accumulation by gravitational collapse and in-situ accumulation (e.g. Carlisle, 1963; Jones, 1966; Tasse et al., 1978; Wright, 1996; Yamagishi, 1991; Tanner and Calvari, 1999; Wright, 2001). Key evidence for transportation of volcanoclastic sediment by grain flow includes: (i) inverse grading; (ii) limited primary mud-sized fraction; (iii) non-erosive basal contacts (Fisher, 1984); (iv) a planar clast fabric indicative of laminar flow, and (v) the absence of tractional structures (Reading, 1996). All of these features were observed in hyaloclastite breccia in this study, with the exception of inverse grading. The glassy fragmental rocks in this study exhibited massive bedding. However, subaqueous grain flows are less effective at sorting than subaerial ones, as the interstitial water severely dampens the exchange of momentum experienced during grain-to-grain and grain-to-bed collisions (Leeder, 1999). The resultant short-lived flows may explain why inverse grading did not develop and massive bedding is observed. An interpretation of a grain flow mechanism is consistent with the angularity of clasts reflecting sediment immaturity and a proximal source.

Another possible transport mechanism is by a volcanic debris avalanche, which has been described in shallow and deep submarine settings (Trofimovs et al., 2004; Chiocci and de Alteriis, 2006). They result in deposits of volcanogenic sediment that consist of decimetre

to metre scale clasts with a sandy matrix and very little clay, and are associated with large-scale collapse of volcanic edifices (Schneider and Fisher, 1998; Trofimovs et al., 2004). Sector collapse of a volcanic vent and transportation by debris avalanche could provide an explanation for the mechanical breakage of pillows to create the large fragmented pillows (up to 90 cm) observed in the breccias of this study. However, submarine debris avalanche deposits are known to be mantled by normal-graded, stratified horizons indicative of hydraulic sorting (Trofimovs et al., 2004); a feature not identified in this study. Instead, there is an overall coarse-tail gradation as the largest clasts reduce in size up-section within structureless deposits.

Breccia units on Macquarie Island reach a maximum thickness of 12 m with no evidence for internal discordances to suggest the amalgamation of several depositional events. Consequently, it is unlikely that individual units of hyaloclastite breccia or pillow-fragment breccia were deposited in a series of single grain flow events. It is proposed that the entire package is the result of one eruptive event where new volcanoclastic material is constantly being produced and transported away from the vent. Destabilisation around the vent resulting in gravitational collapse would have produced and transported the coarsest fragments to form the base of the sequence. This appears to have coincided with an increase in eruption activity that provided a constant source of material for fragmentation, which is in part transported by grain flow mechanisms to form thick accumulations of hyaloclastite and pillow-fragment breccias. Ultimately, the system stabilises with a return to pillow extrusion. The overall waning of the eruption event explains the coarse-tail grading evident, while variations in breccia unit thickness are a function of eruption rate and duration. This interpretation is also consistent with all sediment at any one location being derived from a single magma chamber (as suggested by geochemical evidence; Daczko et al., in press). Contribution of sediment by in-situ accumulation cannot be ruled out and is likely to have occurred. The jigsaw-fit textures indicate transportation after fragmentation must have been minimal for some grains.

6.4. Lithification

The dominant phase between fresh glassy grains in Macquarie Island breccias is palagonite alteration rims, which have a very even thickness around the edges of glassy grains. The suturing of these rims on adjacent grains indicates that palagonitisation was the first phase of lithification. These findings are consistent with most studies of the production of basaltic glassy fragmental rocks (e.g. Lonsdale and Batiza, 1980; Wohletz and Sheridan, 1983; Maicher et al., 2000). Aggregates of small (<1.0 mm), sutured and totally palagonitised grains also contribute to lithification (Fig. 7F). The genesis for palagonite occurs during low-temperature hydrous alteration of volcanic glass (Thorseth et al., 1991), which suggests that the lithification process for Macquarie Island hyaloclastites began once the glass was exposed to sea-water following fragmentation. Continued circulation of pore waters and in-situ fragmentation in the unconsolidated breccia would have promoted palagonite alteration of the glass and further lithification.

Alteration rims around glassy grains and surrounding vesicle walls indicate that the primary formation of palagonite is followed by smectite clay precipitation, a common by-product of glass alteration with the formation of reddened smectite grain replacement (Drief and Schiffman, 2004). The progression from palagonite to smectite also indicates an increasing degree of low-grade metamorphism (McPhie et al., 1993; Giffkins et al., 2005), which is supported by the presence of zeolite (unidentified) + smectite + calcite + analcite and absence of chlorite in hyaloclastite pore fillings. This mineral array combined with local bedrock mapping of Griffin (1982) indicates diagenetic temperatures in the upper zeolite metamorphic grade between 100 and 200 °C (Giffkins et al., 2005).

Claystone, relatively impermeable to circulating pore fluids, in nearby sedimentary intervals at Bauer Bay contain corrensite (unpublished data) supporting low-grade metamorphic conditions (Neuhoff et al., 2006) for the mineralogy of breccia cements. These cements have a fresh appearance, authigenic habits and occupy the largest breccia pore spaces not filled with palagonite, indicating precipitation from a thermally-charged circulating pore fluid. This hydrothermal fluid was continually recharged by low-temperature sea-water alteration (halmyrolysis) of volcanic glass and lithified the breccia.

6.5. Depositional model

Possible depositional settings of glassy fragmental rocks in a mid-oceanic ridge environment include: (i) areas adjacent to seamounts (i.e. large-scale features here assumed to exceed >1000 m relief); (ii) pillow cones (i.e. smaller volcanic edifices comprised largely of pillows); and (iii) fissures (Batiza et al., 1984; Yamagishi, 1991). Volcaniclastic sediment can also be derived from fault scarps (Daczko et al., 2005), which are widespread in mid-ocean ridge settings (Ballard and Moore, 1977), but these are discounted because of the

monomict nature of the sediment, hot emplacement and homogenous geochemistry of the glassy grains as discussed above.

The occurrence of in-situ pillow cones exposed on Macquarie Island (called submarine volcanoes by Wertz, 2003) suggest a pillow cone setting is more likely than a seamount. Though numerous seamount-scale volcanoes have been identified in the Proto-Macquarie Spreading Ridge crust (Massell et al., 2000; Meckel et al., 2003) none are located near Macquarie Island. The close association between pillow basalt and pillow-fragment breccia (e.g. Pyramid Peak) also support a pillow cone setting. Furthermore, the hot emplacement of glassy grains and immaturity of the sediment are considered strong evidence for a proximal source.

The sequences examined were therefore deposited on the slopes of a growing pillow cone (Fig. 9). Destabilisation of the pillow cone resulted in a gravitational collapse and accumulation of fragmented material down slope (i.e. pillow-fragment breccias). This destabilisation was possibly triggered by seismic activity, the intrusions of dykes or over steepening of slopes from a voluminous eruption episode, but evidence to support one mechanism over the other is not sufficient. Prior to, concurrently or because of this destabilisation event, a voluminous eruption phase was initiated producing a large volume of

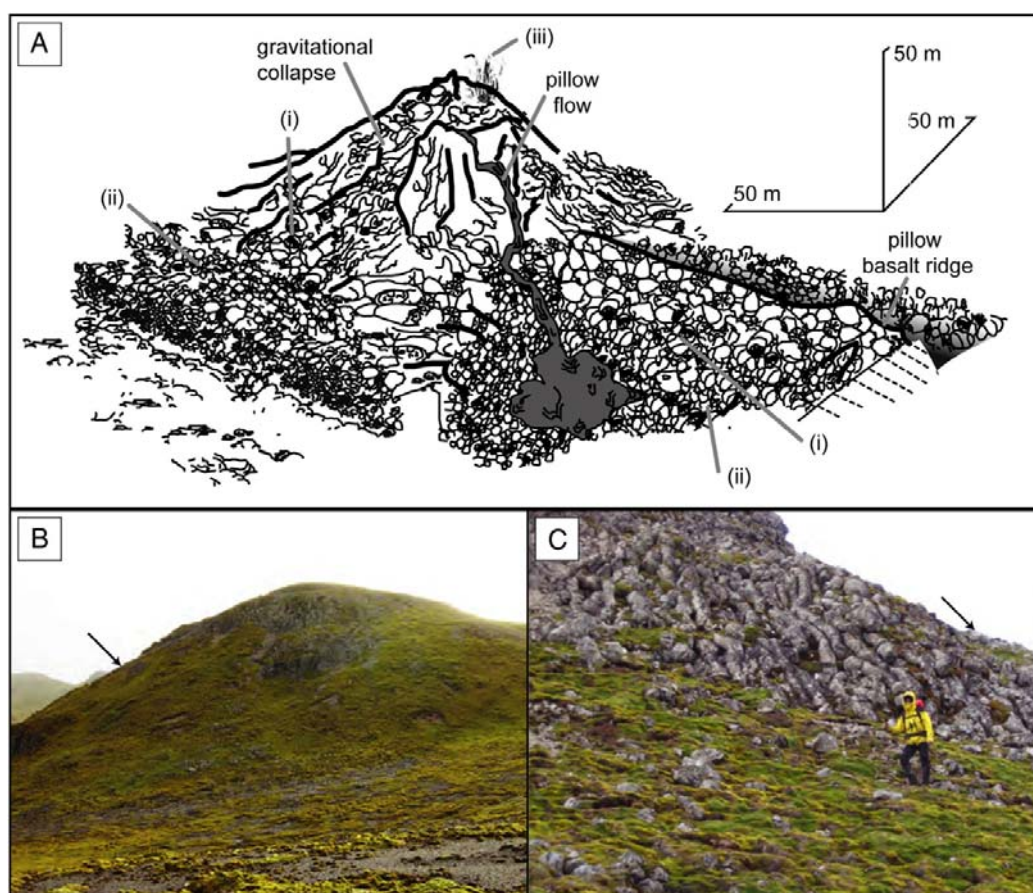


Fig. 9. A. Facies model for the production of glassy fragmental rocks in a mid-oceanic spreading-ridge environment. All glassy fragmental rocks examined in this study formed on the foot-slopes or in a basin proximal to a pillow cone. Processes include: (i) in-situ and/or talus accumulation of pillow-fragment breccia; (ii) grain flow deposits of hyaloclastite breccia derived from unconsolidated pillow-fragment breccia and pillow basalt above; and (iii) minor fire-fountaining. Gravity collapse from destabilisation of the erupting vent initiated the generation of thick hyaloclastite and pillow-fragment breccia aprons along pillow cone slopes. Flowing pillow lava tubes (labelled pillow flow) may push accumulated pillow-fragment breccia debris down slope. The scale of features is schematic. Thin black lines show cross-sectional relief. B. Field photograph looking west of a small pillow cone (approximately 50 m relief) exposed near Pyramid Peak. The arrow points to the pillow basalt ridge shown in C. C. Field photograph looking northeast of southerly plunging pillow basalt tubes. The arrow points to the pillow basalt ridge shown in B. Person is 1.75 m tall.

volcaniclastic sediment by a combination of cooling-contraction granulation, joint fragmentation and minor fire-fountaining (i.e. hyaloclastite breccias). Pillow basalt units cap the sequence marking a return to normal eruptive activity.

7. Conclusions

Two main types of glassy fragmental rocks formed along the Proto-Macquarie Spreading Ridge: (1) hyaloclastite breccia and (2) pillow-fragment breccia. These rocks form on the slopes or within the immediate vicinity of submarine pillow cones along the mid-oceanic ridge. Glassy grains in hyaloclastite breccia and pillow-fragment breccia form mainly by cooling-contraction granulation of pillow basalt rinds, but fire-fountaining eruptions and syn- or post-depositional compaction operate as minor fragmentation processes. Crystalline basalt clasts are derived from the fragmentation of pillows along concentric and radial cooling joints. The majority of basalt, sideromelane and tachylite fragments are therefore derived from proximally emplaced pillow lava while a small volume of clasts are derived from erupted magma droplets. Pillow-fragment breccias form as a result of destabilisation of the pillow cone causing a gravitational collapse and accumulation of talus down slope. A syn-depositional phase of intense volcanism produces an increase in eruptive material to be quenched. This is transported by short-lived grain flows driven by gravity and intergranular collisions to form the hyaloclastite breccias further down slope.

Acknowledgements

Australian Research Council funding to NRD and JAD (DP0663373) provided financial support to conduct this research. The Australian Antarctic Division (AAD) and Antarctic Research Assessment Committee (ARAC) funded the fieldwork and provided logistical support on Macquarie Island (Science Project 2515). We thank the Tasmanian Parks and Wildlife Service for the permission to visit and the sample localities on Macquarie Island. NH thanks the expeditioners of the 56th ANARE and especially Ryan Portner for their assistance in the field. Critical reviews by Kurt Panter and John Smellie, and careful editorial work improved an earlier version of this manuscript. This study used instrumentation [and/or geochemical laboratories] funded by ARC LIEF and DEST Systemic Infrastructure Grants, Macquarie University and industry. This is contribution no. 561 from the ARC GEMOC National Key Centre (www.es.mq.edu.au/GEMOC/).

References

- Armstrong, R.A., Kohn, B., Goscombe, B.D., Everard, J.L., 2004. U–Pb and fission track ages from oceanic crust at Macquarie Island. In: McPhie, J., McGoldrick, P. (Eds.), *Dynamic Earth: Past, Present and Future: 17th Australian Geological Convention: Program and Abstracts*. Geological Society of Australia, Sydney, p. 197.
- Ballard, R.D., Moore, J.G., 1977. *Photographic Atlas of the Mid-Atlantic Ridge Rift Valley*, vol. 114. Springer-Verlag, New York.
- Batiza, R., Fornari, D.J., Vanko, D.A., Lonsdale, P., 1984. Craters, calderas, and hyaloclastites on young Pacific seamounts. *Journal of Geophysical Research* 89 (B10), 8371–8390.
- Batiza, R., White, J.D.L., 2000. Submarine lavas and hyaloclastite. In: Sigurdsson, H. (Ed.), *Encyclopaedia of Volcanoes*. Academic Press, New York, pp. 361–381.
- Carlisle, D., 1963. Pillow breccias and their aquagene tuffs, Quadra Island, British Columbia. *The Journal of Geology* 71 (1), 48–71.
- Chiocci, F.L., de Alteris, G., 2006. The Ischia debris avalanche: first clear submarine evidence in the Mediterranean of a volcanic island prehistorical collapse. *Terra Nova* 18, 202–209.
- Clague, D.A., Davis, A.S., Bischoff, J.L., Dixon, J.E., Geyer, R., 2000. Lava bubble-wall fragments formed by submarine hydrovolcanic: explosions on L(o)over-bar'hi Seamount and Kilauea Volcano. *Bulletin of Volcanology* 61 (7), 437–449.
- Daczko, N.R., Wertz, K.L., Mosher, S., Coffin, M.F., Meckel, T.A., 2003. Extension along the Australian–Pacific transpressional transform plate boundary near Macquarie Island. *Geochemistry Geophysics Geosystems* (G³) 4 (9), 1080.
- Daczko, N.R., Mosher, S., Coffin, M.F., Meckel, T.A., 2005. Tectonic implications of fault-scarp-derived volcaniclastic deposits on Macquarie Island: sedimentation at a fossil ridge-transform intersection? *Geological Society of America Bulletin* 117 (1/2), 18–31.
- Daczko, N.R., Harb, N., Portner, R.A., Dickinson, J.A., in press (2009). Geochemical fingerprint of hyaloclasts in glassy fragmental rocks of Macquarie Island (Southern Ocean). *Australian Journal of Earth Sciences*.
- Davidson, G.J., Varne, R., Brown, A.V., Connell, R., 2004. Structural controls on sulphide deposition at the dyke-lava boundary, slow-spreading ocean crust, Macquarie Island. *Terra Nova* 16, 9–15.
- Davis, A.S., Clague, D.A., 2006. Volcaniclastic deposits from the North Arch volcanic field, Hawaii: explosive fragmentation of alkalic lava at abyssal depths. *Bulletin of Volcanology* 68 (3), 294–307.
- Drief, A., Schiffman, P., 2004. Very low-temperature alteration of sideromelane in hyaloclastites and hyalotuffs from Kilauea and Mauna Kea volcanoes: implications for the mechanism of palagonite formation. *Clays and Clay Minerals* 52 (5), 622–634.
- Duncan, R.A., Varne, R., 1988. The age and distribution of the igneous rocks of Macquarie Island. *Papers and Proceedings of the Royal Society of Tasmania* 122 (1), 45–50.
- Fisher, R.V., 1984. Submarine volcaniclastic rocks. In: Kokelaar, B.P., Howells, M.F. (Eds.), *Marginal Basin Geology: Volcanic and Associated Sedimentary and Tectonic Processes in Modern and Ancient Marginal Basins*. Blackwell scientific publications, Oxford, pp. 5–27.
- Gifkins, C., Herrmann, W., Large, R., 2005. *Altered Volcanic Rocks: A Guide to Description and Interpretation*. CODES Key Centre, Hobart, p. 275 pp.
- Goscombe, B.D., Everard, J.L., 1998. Macquarie Island. 1:25 000 Geological Map Series, Sheet 1 and 2. Mineral Resources Tasmania, Hobart, Australia.
- Goscombe, B.D., Everard, J.L., 2001. Tectonic evolution of Macquarie Island: extensional structures and block rotations in oceanic crust. *Journal of Structural Geology* 23, 639–673.
- Griffin, B.J., Varne, R., 1980. The Macquarie Island ophiolite complex: mid-Tertiary oceanic lithosphere from a major ocean basin. *Chemical Geology* 30, 285–308.
- Griffin, B.J. 1982. *Igneous and Metamorphic Petrology of Lavas and Dykes of the Macquarie Island Ophiolite Complex*. Ph.D. Thesis, University of Tasmania, Hobart, 220 pp.
- Head, J.W., Wilson, L., 2003. Deep submarine pyroclastic eruptions: theory and predicted landforms and deposits. *Journal of Volcanology and Geothermal Research* 121, 155–193.
- Jones, J.G., 1966. Intraglacial volcanoes of south-west Iceland and their significance in the interpretation of the form of the marine basaltic volcanoes. *Nature* 212, 586–588.
- Jones, J.G., 1968. Intraglacial volcanoes of the Laugarvatn region, south-west Iceland-I. *Quarterly Journal of the Geological Society of London* 124, 197–211.
- Jones, J.G., 1970. Intraglacial volcanoes of the Laugarvatn region, southwest Iceland, II. *The Journal of Geology* 78 (2), 127–140.
- Kamenetsky, V.S., Everard, J.L., Crawford, A.J., Varne, R., Eggins, S.M., Lanyon, R., 2000. Enriched end-member of primitive MORB melts: petrology and geochemistry of glasses from Macquarie Island (SW Pacific). *Journal of Petrology* 41 (3), 411–430.
- Kamenetsky, V.S., Maas, R., 2002. Mantle-melt evolution (dynamic source) in the origin of a single morb suite: a perspective from magnesian glasses of Macquarie Island. *Journal of Petrology* 43, 1909–1922.
- Kokelaar, B.P., 1986. Magma–water interactions in subaqueous and emergent basaltic volcanism. *Bulletin of Volcanology* 48, 275–289.
- Leeder, M., 1999. *Sedimentology and Sedimentary Basins: From Turbulence to Tectonics*. Blackwell Sciences Ltd, Oxford.
- Lipman, P.W., Coombs, M.L., 2006. North Kona slump: submarine flank failure during the early(?) tholeiitic shield stage of Hualalai Volcano. *Journal of Volcanology and Geothermal Research* 151 (1–3), 189–216.
- Lonsdale, P., Batiza, R., 1980. Hyaloclastite and lava flows on young seamounts examined with a submersible. *Geological Society of America Bulletin* 91 (1), 545–554.
- Lowe, D.R., 1976. Subaqueous liquefied and fluidized sediment flows and their deposits. *Sedimentology* 23 (3), 285–308.
- Maicher, D., White, J.D.L., Batiza, R., 2000. Sheet hyaloclastite: density–current deposits of quench and bubble-burst fragments from thin, glassy sheet lava flows, Seamount Six, Eastern Pacific Ocean. *Marine Geology* 171 (1–4), 75–94.
- Massell, C., Coffin, M.F., Mann, P., Mosher, S., Frohlich, C., Duncan, C.S., Karner, G., Ramsay, D., Lebrun, J.-F., 2000. Neotectonics of the Macquarie Ridge Complex, Australia–Pacific plate boundary. *Journal of Geophysical Research* 105, 13,457–13,480.
- McPhie, J., Doyle, M., Allen, R., 1993. *Volcanic Textures: A Guide to the Interpretation of Textures in Volcanic Rocks*. CODES Key Centre, Hobart, 198 pp.
- McPhie, J., 1995. A Pliocene shoaling basaltic seamount: Ba volcanic group at Rakiraki, Fiji. *Journal of Volcanology and Geothermal Research* 64, 193–210.
- Meckel, T.A., Coffin, M.F., Mosher, S., Symonds, P., Bernardel, G., Mann, P., 2003. Underthrusting at the Hjort Trench, Australian–Pacific plate boundary: incipient subduction? *Geochemistry Geophysics Geosystems* (G³) 4 (12), 1099.
- Meckel, T.A., Mann, P., Mosher, S., Coffin, M.F., 2005. Influence of cumulative convergence on lithospheric thrust fault development and topography along the Australian–Pacific plate boundary south of New Zealand. *Geochemistry Geophysics Geosystems* (G³) 6, Q09010.
- Mosher, S., Massell-Symonds, C., 2008. Ridge reorientation mechanisms: Macquarie Ridge Complex, Australia–Pacific plate boundary. *Geology* 36, 119–122.
- Neuhoff, P.S., Rogers, K.L., Stannius, L.S., Bird, D.K., Pedersen, A.K., 2006. Regional very low-grade metamorphism of basaltic lavas, Disko-Nuussuaq region, West Greenland. *Lithos* 92, 33–54.
- Quilty, P., Crundwell, M.P., 2004. The age of seafloor spreading that formed the foundation rocks of Macquarie Island. In: McPhie, J., McGoldrick, P. (Eds.), *Dynamic Earth: Past, Present and Future: 17th Australian Geological Convention: Program and Abstracts*. Geological Society of Australia, Sydney, p. 220.
- Reading, H.G., 1996. *Sedimentary Environments: Processes, Facies and Stratigraphy*, 3rd Ed. Blackwell Scientific Publications, Oxford, 687pp.
- Sansone, F.J., Smith, J.R., 2006. Rapid mass wasting following nearshore submarine volcanism on Kilauea volcano, Hawaii. *Journal of Volcanology and Geothermal Research* 151, 133–139.
- Schneider, J., Fisher, R.V., 1998. Transport and emplacement mechanisms of large volcanic debris avalanches: evidence from the northwest sector of Cantal Volcano, France. *Journal of Volcanology and Geothermal Research* 83, 141–165.

- Simpson, K., McPhie, J., 2001. Fluidal-clast breccia generated by submarine fire-fountaining, Trooper Creek Formation, Queensland, Australia. *Journal of Volcanology and Geothermal Research* 109 (4), 339–355.
- Smellie, J.L., Hole, M.J., 1997. Products and processes in Pliocene–Recent, subaqueous to emergent volcanism in the Antarctic Peninsula: examples of englacial Surtseyan volcano construction. *Bulletin of Volcanology* 58 (8), 628–646.
- Smellie, J.L., Millar, I.L., Rex, D.C., Butterworth, P.J., 1998. Subaqueous, basaltic lava dome and carapace breccia on King George Island, South Shetland Islands, Antarctica. *Bulletin of Volcanology* 59 (4), 245–261.
- Staudigel, H., Schmincke, H.-U., 1984. The Pliocene seamount series of La Palma/Canary Islands. *Journal of Geophysical Research* 89 (B13), 11,195–11,215.
- Tanner, L.H., Calvari, S., 1999. Facies analysis and depositional mechanisms of hydroclastite breccias, Acicastello, eastern Sicily. *Sedimentary Geology* 129 (1–2), 127–141.
- Tasse, N., Lajoie, J., Dimroth, E., 1978. The anatomy and interpretation of an Archean volcanoclastic sequence, Noranda region, Quebec. *Canadian Journal of Earth Sciences* 15, 874–888.
- Templeton, J.H., Hanson, R.E., 2003. Jurassic submarine arc–apron deposits and associated magma/wet–sediment interaction, northern Sierra Nevada, California. *Journal of Volcanology and Geothermal Research* 128 (4), 299–326.
- Thorseth, I.H., Furnes, H., Tumyr, O., 1991. A textural and chemical study of Icelandic palagonite of varied composition and its bearing on the mechanism of the glass–palagonite transformation. *Geochimica et Cosmochimica Acta* 55, 731–749.
- Trofimovs, J., Cas, R.A.F., Davis, B.K., 2004. An Archean submarine volcanic debris avalanche deposit, Yilgarn Craton, western Australia, with komatiite, basalt and dacite megablocks: the product of dome collapse. *Journal of Volcanology and Geothermal Research* 138 (1–2), 111–126.
- Varne, R., Brown, A.V., Falloon, T., 2000. Macquarie Island: its geology, structural history, and the timing and tectonic setting of its N-MORB to E-MORB magmatism. In: Dilek, Y., Moores, E.M., Elthon, D., Nicolas, A. (Eds.), *Ophiolites and Oceanic Crust: New Insights from Field Studies and the Ocean Drilling Program*. Geological Society of America, Boulder, Colorado, pp. 301–320.
- Wertz, K.L., 2003. From Seafloor Spreading to Uplift: The Structural and Geochemical Evolution of Macquarie Island on the Australian–Pacific Plate Boundary. Ph.D. Thesis, The University of Texas at Austin, Austin, 169 pp.
- White, J.D.L., Houghton, B.F., 2006. Primary volcanoclastic rocks. *Geology* 34 (8), 677–680.
- Wohletz, K.H., Sheridan, M.F., 1983. Hydrovolcanism: basic considerations and review. *Journal of Volcanology and Geothermal Research* 17, 1–29.
- Wood, R., Lamarche, G., Herzer, R., Delteil, J., Davy, B., 1996. Paleogene seafloor spreading in the southeast Tasman Sea. *Tectonics* 15, 966–975.
- Wright, I.C., 1996. Volcanoclastic processes on modern submarine arc stratovolcanoes: sidescan and photographic evidence from the Rumble IV and V volcanoes, southern Kermadec Arc (SW Pacific). *Marine Geology* 136, 21–39.
- Wright, I.C., 2001. In situ modification of modern submarine hyaloclastic/pyroclastic deposits by oceanic currents: an example from the Southern Kermadec arc (SW Pacific). *Marine Geology* 172, 287–307.
- Yamagishi, H., 1991. Morphological and sedimentological characteristics of the Neogene submarine coherent lavas and hyaloclastites in Southwest Hokkaido, Japan. *Sedimentary Geology* 74, 5–23.

VI:

Geochemical fingerprint of hyaloclasts in glassy fragmental rocks of Macquarie Island (Southern Ocean): implications for volcanogenic sedimentary processes at a waning mid-ocean ridge

DACZKO, Nathan R.¹, HARB, Nicole¹, PORTNER, Ryan A.¹, and DICKINSON, Julie A.¹

¹GEMOC ARC National Key Centre, Department of Earth and Planetary Sciences, Macquarie University, NSW 2109, Australia

Published in Australian Journal of Earth Sciences August 2009



Geochemical fingerprint of hyaloclasts in glassy fragmental rocks of Macquarie Island (Southern Ocean): implications for volcanogenic sedimentary processes at a waning mid-ocean ridge

N. R. DACZKO*, N. HARB, R. A. PORTNER AND J. A. DICKINSON

GEMOC ARC National Key Centre, Department of Earth and Planetary Sciences, Macquarie University, NSW 2109, Australia.

Two main types of glassy fragmental rocks formed along the Proto-Macquarie Spreading Ridge: (i) hyaloclastite breccia; and (ii) pillow-fragment breccia. Examples now exposed on Macquarie Island, Southern Ocean, were largely sourced from proximal pillow lavas. In each of seven samples examined, hyaloclasts (basaltic glass grains) have a narrow major- and trace-element geochemical range, consistent with derivation of each sample from a single volcanic eruption event. Moreover, every sample analysed within the one stratigraphic section (at three sites) displays distinctive major- and trace-element geochemistry compared with the other two sections. This suggests that hyaloclasts at each site represent discrete magma batches. A single source for these glassy fragmental rocks contrasts with the dominant fault-scarp-derived polymict sedimentary rocks on Macquarie Island. We suggest that the hyaloclasts analysed in this study were deposited in small basins between the slopes of growing pillow cones along the mid-ocean ridge. The geochemical analyses presented here encompass (weakly) fractionated (e.g. Bauer Bay) to near-primitive (e.g. Pyramid Peak) compositions. All samples presented here lie within the range of the enriched- to normal-MORB suites previously reported for the island that include the least fractionated MORB melts known globally. The interpretation of geochemically distinct magma batches over the small area of the island suggests very limited magma mixing consistent with an immature or waning magmatic system. We relate these geochemical characteristics to: (i) volcanism near a very long offset transform; and (ii) genesis of magmas during the waning stages of slow seafloor spreading within a very narrow (<50 km-wide) spreading corridor.

KEY WORDS: Australia–Pacific plate boundary, geochemistry, glass, Macquarie Island, MORB, provenance.

INTRODUCTION

Mid-ocean ridge environments produce a remarkable range of volcanogenic units and underwater landforms. Deep-sea submersible diving has provided rare access to the relatively inaccessible mid-ocean ridge environment (Heirtzler & Grassle 1976; Fryer 1990) and many studies have examined, for example, the broad geological products including ridge and seamount geology (Ballard & Van Andel 1977; Lonsdale & Batiza 1980; Lonsdale & Fornari 1980; Karson *et al.* 1987; Ondreas *et al.* 1997; Fornari *et al.* 1998; Mitchell 2001), hydrothermal activity (Ballard *et al.* 1984; Hekinian *et al.* 1985), ridge-transform intersections (Mamaloukas-Frangoulis *et al.* 1991; Tivey *et al.* 1998), backarc basin spreading (Lagabrielle *et al.* 1994), spreading discontinuities (Ruellan *et al.* 1994), explosivity or rapidity of eruptions (Gregg *et al.* 1996; Fouquet *et al.* 1998), scarp topography (Mitchell *et al.* 2000) and oceanic core complexes (Blackman *et al.*

2002). Observations made during these studies show that most eruptions at mid-ocean ridges produce flows of pillow basalt and sheet lava. Quenching of basaltic lava by seawater interaction produces glassy crusts that spall off and contribute to glassy fragmental sedimentary deposits (Batiza & White 2000). These hyaloclastic deposits are the most abundant type of volcanoclastic sediment in the modern oceans.

Glassy fragmental rocks have been described in detail from intraplate, island arc, backarc and plume-related spreading ridge settings (Jones 1968; Lonsdale & Batiza 1980; Batiza *et al.* 1984; Yamagishi 1991; Tanner & Calvari 1999; Templeton & Hanson 2003). Despite the extensive nature of the global mid-ocean ridge system, studies of glassy fragmental rocks produced at non-plume-related spreading centres are limited to dredged samples, submersible observations and cores. One key limitation is that these samples and observations lack stratigraphic context for the sedimentary rocks

examined. An understanding of the production of glassy fragmental rocks in modern and ancient intra-oceanic spreading ridge environments is restricted by: (i) the practical difficulty of *in situ* study of deep ocean-floor crust and its processes of formation; and (ii) the limitations (such as glass alteration) of studies on typically highly deformed and attenuated ophiolites where exposed on land.

The Macquarie Island ophiolite is the world's only subaerially exposed remnant of a non-plume-related, relatively little-deformed paleosspreading ridge that still lies within the ocean basin in which it formed. This extraordinary exposure of oceanic crust permits a detailed characterisation of stratigraphic relationships and sampling of glassy fragmental rocks. Though many aspects of Macquarie Island geology, tectonic context and history have been studied (Griffin & Varne 1980; Duncan & Varne 1988; Varne 1989; Fröhlich *et al.* 1997; Kamenetsky *et al.* 2000; Varne *et al.* 2000; Goscombe & Everard 2001; Daczko *et al.* 2003; Wertz *et al.* 2003; Davidson *et al.* 2004; Rivizzigno & Karson 2004), there have been no detailed sedimentological studies of its glassy fragmental rocks. However, detailed geochemical studies of pillow-rim and hyaloclastite glasses by Kamenetsky *et al.* (2000) and Wertz (2003) indicated a remarkable range of primitive and fractionated MORB that ranges from normal- to highly enriched-MORB (N-MORB to E-MORB).

In this contribution, we summarise field and petrological observations and present stratigraphically controlled geochemical data from glassy fragmental rocks on Macquarie Island. We place these data into the context of more detailed geochemical studies that have examined mid-ocean ridge basalt (MORB) genesis on the island (Kamenetsky *et al.* 2000; Kamenetsky & Maas 2002). We then focus on how the geochemical fingerprinting informs on: (i) volcanogenic sedimentary processes at mid-ocean ridges; and (ii) the tectonic setting and evolution of this paleosspreading ridge.

The key aims of this contribution include: (i) to document the geochemical variation of individual hyaloclasts within stratigraphic sections rich in glassy fragmental rocks; (ii) to explore the relative contribution of fault-scarp *vs* pillow cone sources for the glassy fragments; and (iii) to explore the implications this study has for volcanogenic sedimentary processes within the tectonic context of Macquarie Island.

REGIONAL GEOLOGY

Macquarie Island (54°30'S, 158°54'E) lies in the Southern Ocean 1500 km south-southeast of Tasmania, approximately midway between the southern tip of New Zealand and Antarctica (Figure 1a). The island is located 3–5 km east of the transpressional Australian-Pacific dextral transform plate boundary. Macquarie Island forms the subaerial apex of a 5 km-high, 50 km-wide submarine ridge, a segment of the Macquarie Ridge Complex. The complex is defined by a series of ridges and troughs that delineate the active Australian-Pacific plate boundary in the Southern Ocean (Figure 1a). The plate boundary at this latitude was an intra-oceanic axis of seafloor spreading for much of the Tertiary (40 to ~6

Ma; Wood *et al.* 1996; Daczko *et al.* 2005) and the crust of Macquarie Island formed at the end of the spreading history (<12 Ma).

The oceanic crust that constitutes Macquarie Island formed at 12–6 Ma (Duncan & Varne 1988; Wertz 2003; Armstrong *et al.* 2004; Quilty & Crundwell 2004) within a narrow (<50 km wide) spreading corridor of the slow-spreading Proto-Macquarie Spreading Ridge (Duncan & Varne 1988; Varne *et al.* 2000; Goscombe & Everard 2001; Davidson *et al.* 2004; Mosher & Massell-Symons 2008). The island's crust formed near a ridge–transform intersection (Wertz *et al.* 2003; Daczko *et al.* 2005) adjacent to a very long offset transform that linked the Proto-Macquarie Spreading Ridge to the Australian–Pacific–Antarctic triple junction (Figure 1b) (Mosher & Massell-Symons 2008). Though extension and volcanism at the spreading ridge continued up until 6 Ma, transpression along adjacent transforms had initiated near the latitude of Macquarie Island by ~27 Ma (Massell *et al.* 2000; Goscombe & Everard 2001; Meckel *et al.* 2005; Mosher & Massell-Symons 2008).

Macquarie Island comprises fault-bounded blocks made up of all levels of oceanic crust and upper mantle from pillow and tabular basalt and minor sedimentary rocks to sheeted dolerite dykes, gabbros and serpentinised peridotites (Figure 2) (Varne *et al.* 1969, 2000; Varne & Rubenach 1972; Griffin 1982; Christodoulou *et al.* 1984; Goscombe & Everard 1998). The volcanic rocks are associated with volcanoclastic breccias, glassy fragmental rocks and minor sedimentary rocks that include mudstone, sandstone, chert and limestone (Daczko *et al.* 2005). Volcanoclastic sedimentary rocks on Macquarie Island are largely fault-scarp-derived (Daczko *et al.* 2005).

METHODS

Field methods

Three well-exposed stratigraphic sections were measured at Bauer Bay, Green Gorge and Pyramid Peak (Figure 2). The sections are laterally extensive (200–150 m) and rich in fresh glassy fragmental rocks (units >5 m thick). Two sections were measured perpendicular to strike (Bauer Bay and Pyramid Peak) and a representative section was produced from several observations along strike at Green Gorge to reveal any lateral changes in facies or geochemistry. We use 'hyaloclastite breccia' to include dominantly non-explosively-derived glassy fragmental rocks composed of grains finer or coarser than 4 mm respectively (McPhie *et al.* 1993 p. 11). Hyaloclastite breccias that contain a larger proportion (>25%) of grains coarser than 150 mm that are recognisable as whole pillows and broken pillow fragments within their glassy matrix are termed 'pillow-fragment breccia' (Yamagishi 1991).

Geochemical methods and analytical techniques

The geochemical analyses outlined below were conducted at the Geochemical Analysis Unit housed in the

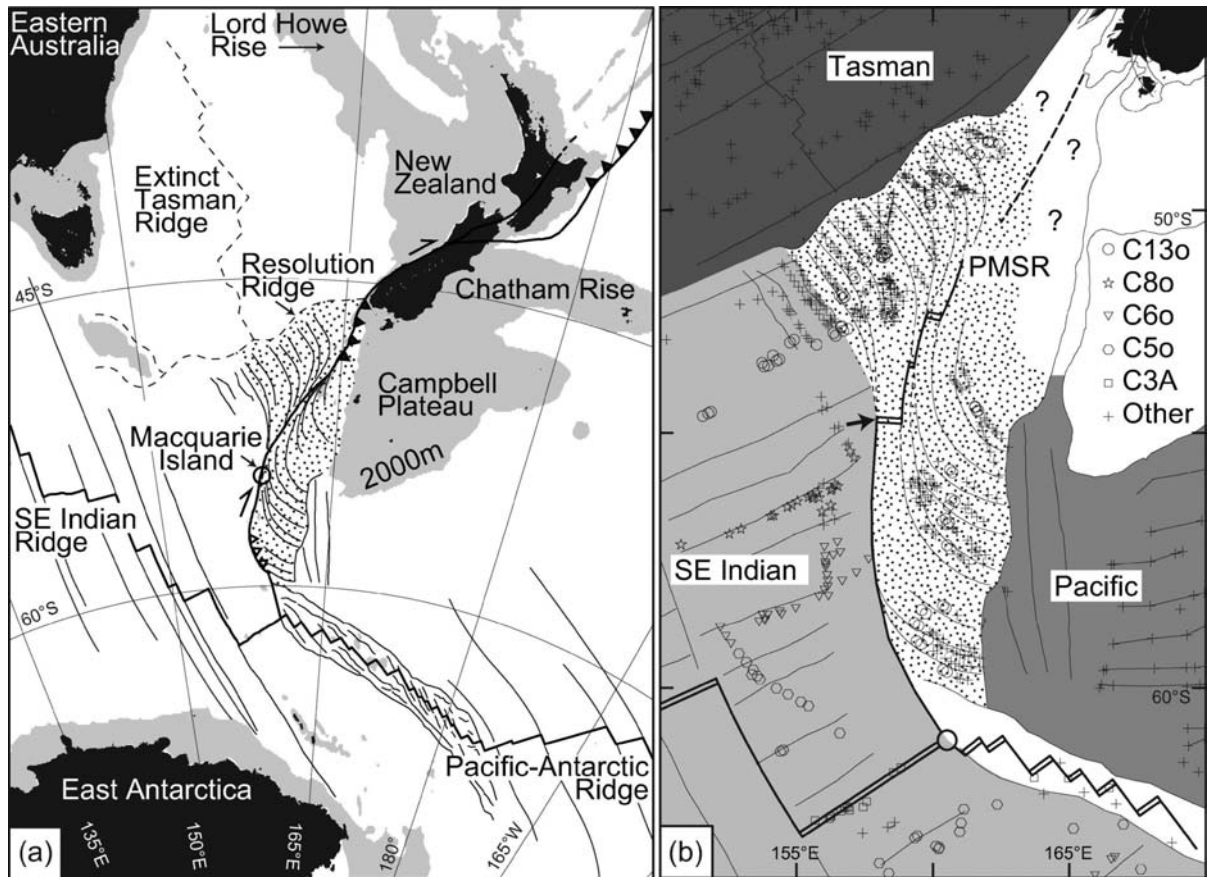


Figure 1 (a) Location map of Macquarie Island and the Australian-Pacific transform plate boundary south of New Zealand (Macquarie Ridge Complex). Crust formed by Australian-Pacific spreading along the (now extinct) Proto-Macquarie Spreading Ridge (PMSR) between ~40 and ~6 Ma is stippled. Filled triangles along the plate boundary are subduction zones; open triangles (in the Hjort region) represent incipient subduction (Meckel *et al.* 2003). Light-grey illustrates regions ≤ 2000 m below sea level. Present plate boundaries are shown as thick black lines. Past plate boundaries are shown as dashed black lines. Fracture zones are shown as thin black lines. Azimuthal equidistant projection centred at 60°S, 180°E (after Daczko *et al.* 2003). (b) Plate-tectonic reconstruction for Chron 3A (5.9 Ma). Stippled crust formed at the PMSR (now inactive), light-grey crust formed at the Southeast Indian spreading ridge (still active), medium-grey crust formed at the Pacific-Antarctic spreading ridge (still active), and dark-grey crust formed at the Tasman spreading ridge (extinct) (after Daczko *et al.* 2005; Mosher & Massell-Symons 2008). Macquarie Island formed at the westernmost mid-ocean ridge spreading corridor of the PMSR (arrow).

Australian Research Council National Key Centre for Geochemical Evolution and Metallogeny of Continents (GEMOC) based in the Department of Earth and Planetary Sciences at Macquarie University, Sydney. Samples were selected for geochemical analyses on the basis of their preservation of fresh glass.

Electron microprobe (EMP) analyses were employed to quantify the major element geochemistry of sideromelane (fresh basaltic glass) in seven hyaloclastite breccia and pillow-fragment breccia samples from Macquarie Island. Samples selected for analysis exhibited the least degree of glass alteration based on petrographic analysis and are from Bauer Bay (BB1-1B, BB1-1C2 and BB1-3A), Green Gorge (GG1-14A and GG1-22) and Pyramid Peak (PP4-2 and PP4-3B). The stratigraphic location of each sample is shown in Figure 2.

The analysed samples represent the matrix of pillow-fragment and hyaloclastite breccias, as these parts of the

rocks allow better geochemical characterisation of the hyaloclasts. In addition, the finer fraction is likely to record the most diverse provenance on the thin-section scale as it contains more grains. The vast majority of analyses are of different grains within a given sample, but duplicate analyses were made of ~10% of the grains analysed. Analyses were made using a Cameca SX100 electron microprobe equipped with five wavelength dispersive spectrometers. The operating conditions were: accelerating voltage, 15 kV; beam current, 20 nA; beam size, 10 μm ; and counting time total 20 s (10 s peak, 10 s background). The PAP matrix correction procedure (Pouchou & Pichoir 1984) was applied to the raw data.

Major element oxides (SiO_2 , TiO_2 , Al_2O_3 , FeO , MnO , MgO , CaO , Na_2O and K_2O) and minors (Cr_2O_3 , NiO , P_2O_5 , F , Cl and SO_2) were measured. Special care was taken to avoid the vicinity of microphenocrysts and altered areas (see below) within hyaloclasts, where compositional

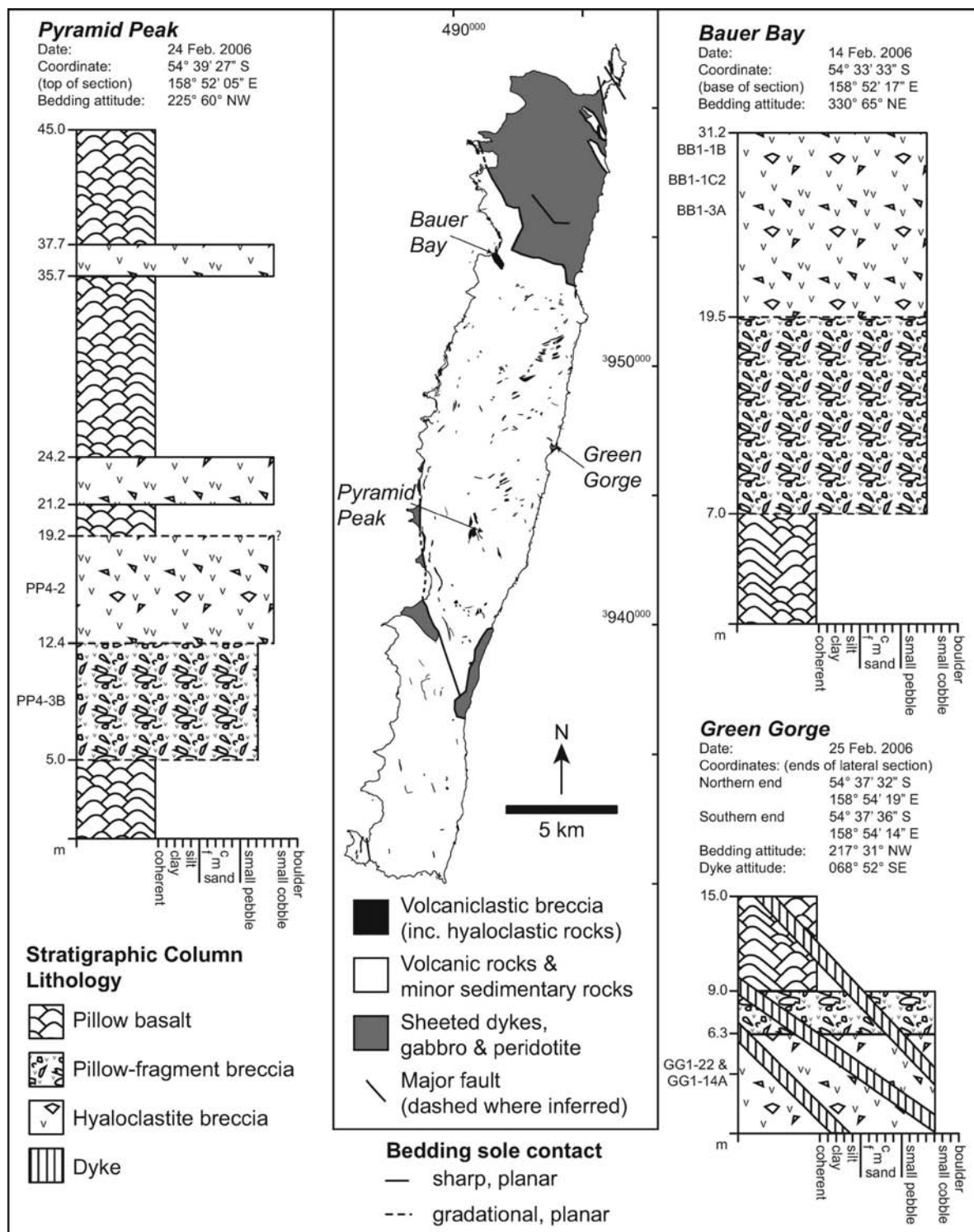


Figure 2 Simplified geological map (UTM 57S) of Macquarie Island showing the location of stratigraphic sections (tip of arrows). Each section begins or ends at an arbitrary position in bounding pillow basalt units or in unexposed portions. The locations of samples discussed in the text are noted at their stratigraphic position. The Green Gorge section represents 100 m of lateral (parallel to strike) exposure and the two samples were taken 75 m apart.

heterogeneities are more likely to occur (Kamenetsky *et al.* 2000). Analyses of glass with totals of $100 \pm 2\%$ and $\text{Na}_2\text{O} > 2.5 \text{ wt}\%$ are defined as 'pristine' for the purposes

of this study, as low Na_2O contents ($< 2.5 \text{ wt}\%$) are consistent with the petrographically identified palagonised grains. In support of these criteria for 'pristine'

glass, the analyses excluded also show high MgO and TiO₂ consistent with alteration.

Thick sections (200 µm) of four samples (BB1-1C2, BB1-1B, GG1-14A and PP4-2) were analysed by laser ablation inductively coupled plasma mass spectrometry (LA-ICP-MS) to determine the trace-element geochemistry of constituent sideromelane hyaloclasts. A 7500cs Agilent ICP-MS Octopole Reaction System was operated in standard mode with no reaction cell gas. A platinum (Pt) shield plate was used on the torch. The plasma conditions were: reflective power, 1200 W; sample depth, 5.0 mm; makeup gas (Ar), 0.86 L/min (high purity, liquid argon); and optional gas (He), 75.5% (high purity). The laser used was a Merchantek 266 nm Nd: YAG laser (New Wave) and the conditions were: frequency, 5 Hz; spot size, 60 µm; laser output, 45–50%; energy output, 0.1 mJ; and gases, ablation with He gas then mixing with Ar gas.

CaO wt% data from the EMP analyses were used as internal standards for all analyses of sideromelane included in this study. The calibrating standard used was a multi-element NIST 610 glass standard. The data reduction software used was GLITTER (GEMOC Laser ICP-MS Total Trace Element Reduction), version 4.4 (van Achterbergh *et al.* 1999). Trace-element concentrations were normalised to the primitive mantle compositions recommended by Sun & McDonough (1989) for the construction of normalised multi-element diagrams (spider diagrams).

CIPW norms were calculated for the average glass compositions of each sample. As is commonly done for glassy rocks, norms were calculated to estimate the modal proportions of the mineralogy of hyaloclasts, had they been crystalline. Furthermore, as there was minimal variation in the geochemistry of hyaloclasts within locations, CIPW norms were calculated to help enable comparison between hypersthene-normative N-MORB and nepheline-normative E-MORB (Varne *et al.* 2000). Since data for Fe₂O₃ concentrations were not available, a value of Fe²⁺ = 0.9Fe^{total} (following Kamenetsky *et al.* 2000) was used in the norm calculations. The Mg# reported in this study were calculated using the formula: $100 \times \text{Mg}/(\text{Mg} + \text{Fe}^{2+})$, again where Fe²⁺ = 0.9Fe^{total}.

OBSERVATIONS AND RESULTS

Field relationships

The field relationships are briefly summarised here (see Dickinson *et al.* 2009 for details). Hyaloclastite is rare on Macquarie Island, and our three stratigraphic sections contain only hyaloclastite breccia (Figure 3a) and pillow-fragment breccia (Figure 3b) in variable stratigraphic relationship to pillow basalt. The breccias analysed are well indurated, massively bedded and primarily matrix-supported. Units rich in glassy fragmental facies are laterally continuous from >150 m wide at Bauer Bay and Green Gorge to 20–50 m wide at Pyramid Peak. A lateral and vertical transition from pillow lava to pillow-fragment breccia to hyaloclastite breccia is observed at both Pyramid Peak and Bauer Bay (Figure 2). All breccia units are very poorly sorted (Figure 3a) and are characterised by unimodal basalt clast types.

The clasts are angular to subrounded (with blocky and wedge-like forms) and predominantly very large pebble size (Figure 3a). Intact sausage-shaped pillows, pillow tubes (190–600 mm long) with radial fracture patterns and pillow fragments are common in the pillow-fragment breccia units (Figure 3b). These components have 10–40 mm-thick chilled margins with glassy rinds. The grainsize of the matrix in both types of glassy fragmental rocks ranges from medium sand to medium pebbles. However, most hyaloclasts are granule-sized (Figure 3c). Sand- and granule-sized fragments of glass are very angular and rimmed by palagonite (Figure 3c).

Petrography

The preservation of fresh basaltic glass (sideromelane) in the matrix of glassy fragmental rocks ranges from 0 to 60%, predominantly controlled by the proximity of samples to minor faults. Fresh sideromelane is restricted to the cores of hyaloclasts (Figure 3d). Hyaloclasts from Bauer Bay (Figure 3d) and Pyramid Peak are sparsely vesicular (<5%). Hyaloclasts from Green Gorge vary from sparsely vesicular (sample GG1-14A) to moderately vesicular (<15%, sample GG1-22). Hyaloclasts are sparsely to moderately olivine-plagioclase porphyritic (Figure 3d). Phenocryst fragments of mainly plagioclase and olivine make up to 10% of matrix at Green Gorge. Hyaloclasts (including their palagonised rims) are commonly 1–3 mm across (Figure 3d). Grains are typically subangular to very angular, though the largest hyaloclasts rarely have suboval forms. Blocky, triangular- and splinter-shaped fragments predominate.

Major-element geochemistry of glasses

Figure 4 shows six of the major-element-oxide compositions of the Macquarie Island glasses against increasing Mg# and shows that glass grains within individual samples have remarkable similarity in major element compositions and Mg#. Analyses from different stratigraphic units at a given location show the next highest degree of similarity to each other. Data from each sample have therefore been averaged (Table 1).

Averaged Macquarie Island glasses analysed in this study have Mg# ranging from 65.70 to 67.75 and 48.27 to 50.04 wt% SiO₂. The plots of SiO₂, Al₂O₃, CaO and TiO₂ vs Mg# show a trend for the group of seven samples (Figure 4). The greatest difference between locations can be observed in CaO concentrations: samples from each location have distinct CaO concentrations with 10.93 ± 0.09 wt%, 12.21 ± 0.10 wt% and 12.62 ± 0.07 wt% for Bauer Bay, Green Gorge and Pyramid Peak, respectively (Figure 4). CaO concentrations at Green Gorge show a weak difference with Mg# between samples, whereas there is no difference in CaO concentrations between samples at the other two sites. Samples from Green Gorge generally have <7.6 wt% FeO, whereas samples from Bauer Bay and Pyramid Peak generally have >7.6 wt% FeO (Figure 4). Samples from Pyramid Peak generally have <0.64 wt% K₂O, whereas samples from Bauer Bay and Green Gorge generally have >0.64 wt% K₂O (Figure 4).

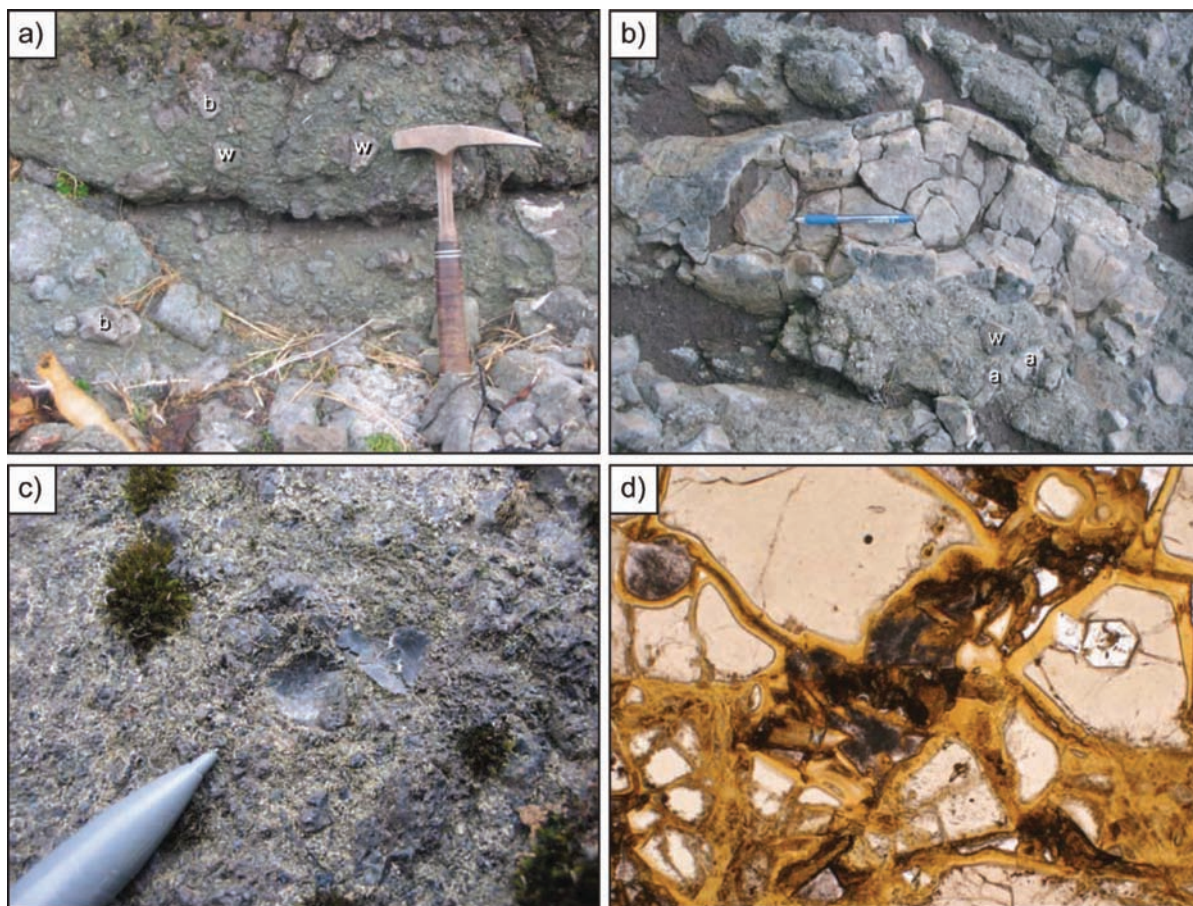


Figure 3 (a) Hyaloclastite breccia with blocky (b)- and wedge (w)-shaped basalt clasts, Green Gorge; head of hammer is 170 mm long. (b) Pillow tube cross-section in pillow-fragment breccia, Pyramid Peak. Wedge (w)- and arcuate (a)-shaped basalt clasts are embedded in a glassy matrix surrounding the pillow tube. Pen is 160 mm long. (c) Fresh arcuate-shaped basaltic glass hyaloclasts (black). Note the thin rims of palagonite (creamy-yellow) on the finer-grained matrix, Bauer Bay; visible tip of pencil is 15 mm long. (d) Plane-polarised-light photomicrograph of sample BB1-3A showing angular fresh sideromelane cores with palagonised rims. Note an olivine microphenocryst at the middle right; field of view is ~ 3 mm. Sample reposited in the Department of Earth and Planetary Sciences, Macquarie University. See Figure 2 for coordinates of localities.

After removal of rare analyses with Na_2O concentrations < 2.5 wt%, all hyaloclasts have similar Na_2O concentrations with Green Gorge slightly higher ($\text{Na}_2\text{O} = 3.17 \pm 0.10$ wt%), Pyramid Peak slightly lower ($\text{Na}_2\text{O} = 2.87 \pm 0.08$ wt%), and Bauer Bay intermediate with a broader range in data ($\text{Na}_2\text{O} = 2.94 \pm 0.19$ wt%). Concentrations of P_2O_5 follow a similar trend to that displayed by TiO_2 with the lower P_2O_5 concentrations at higher Mg#. P_2O_5 concentrations range from 0.22 ± 0.03 wt% at Pyramid Peak to 0.25 ± 0.03 wt% at Green Gorge to 0.30 ± 0.03 wt% at Bauer Bay. There are no systematic trends in the concentrations of MnO (0.14–0.16 wt%), F (0.01–0.03 wt%), Cl (0.04–0.05 wt%) and SO_2 (0.13–0.17 wt%) between the seven samples. The concentrations of Cr_2O_3 and NiO are below the lower limit of detection for this technique.

The three samples from Bauer Bay were collected within less than 5 m of each other (true stratigraphic thickness) from a laterally extensive and > 10 m-thick hyaloclastite breccia unit (Figure 2). The three samples

show overlapping compositions of major elements (within 1σ of the average; Figure 4). The two samples from Green Gorge were collected ~ 75 m apart (along strike) and within 5 m stratigraphically of each other in a laterally extensive and > 10 m-thick hyaloclastite breccia unit. The northernmost sparsely vesicular sample (GG1-14A) has a higher Mg# compared with the southernmost moderately vesicular sample (GG1-22). Sub-trends between the two Green Gorge samples in SiO_2 , TiO_2 and FeO, and to a lesser extent CaO and K_2O , follow the broad trend observed across the group of seven samples (Figure 4); the minor geochemical differences between the two laterally equivalent samples from Green Gorge are discussed below. Though from different unit types, the two samples from the laterally discontinuous Pyramid Peak section [PP4-2 (hyaloclastite breccia) and PP4-3B (pillow-fragment breccia) (Figure 2)] show a very similar Mg# and virtually identical ranges in major-element-oxide concentrations (Figure 4).

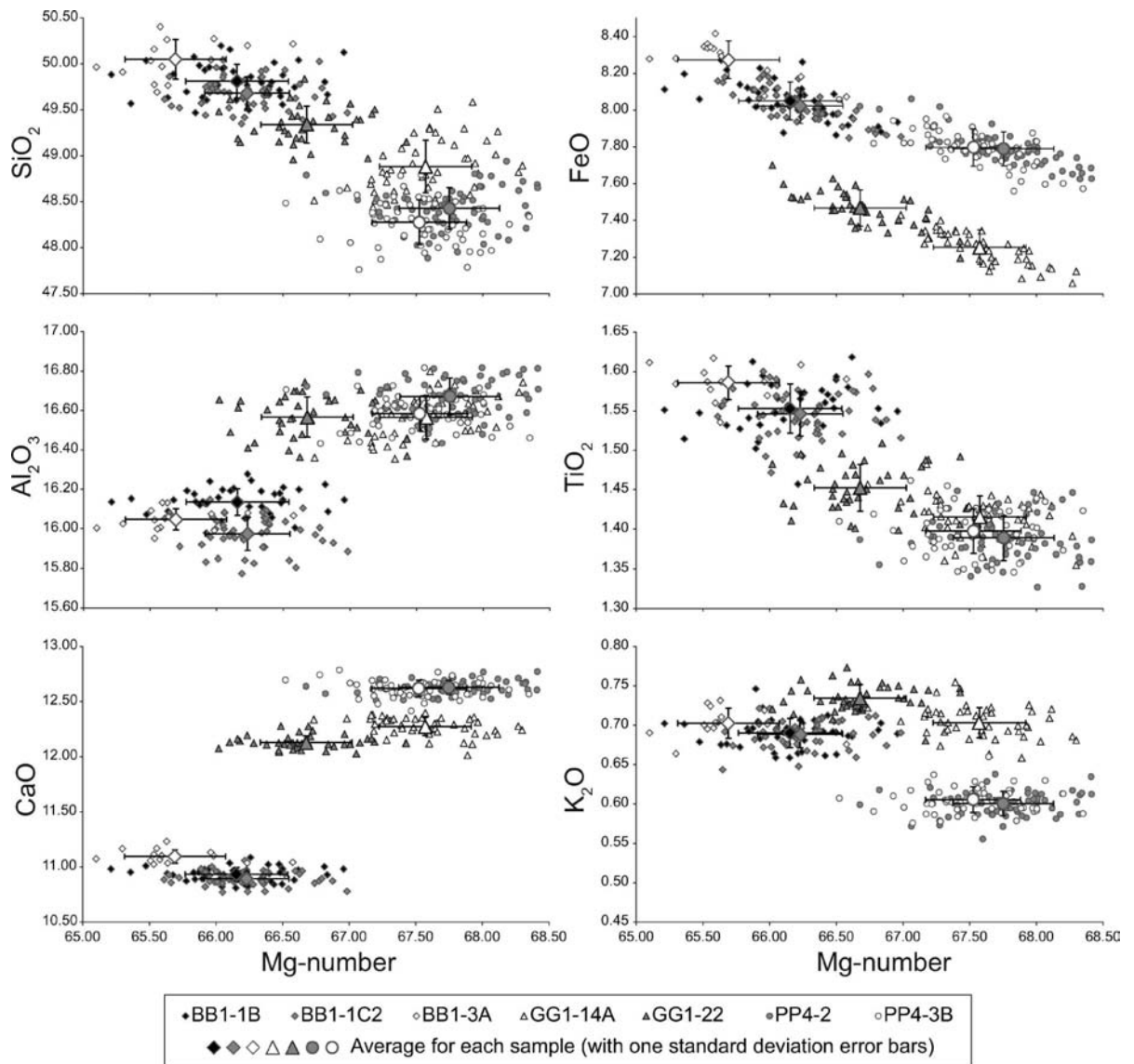


Figure 4 Macquarie Island glass major-element composition (wt% oxide) *vs* Mg-number [$Mg\# = 100 \times Mg/(Mg + Fe)$]. Data points with 1σ error bars are the average for each sample.

Glass classification and CIPW normative mineralogy

The analysed sideromelane grains are each basaltic in composition and classify as medium-K series subalkaline to transitional basalts (Le Maitre 1989). Table 1 shows CIPW norms for the average glass composition in each sample. The basaltic glass varies from hypersthene-normative (saturated) at Bauer Bay to weakly nepheline-normative (undersaturated) at Green Gorge and Pyramid Peak (Table 1). The average glasses from all three localities contain between 51–53 wt% normative plagioclase and ~4 wt% orthoclase. Bauer Bay samples contain ~8 wt% normative olivine, approximately two-thirds of that in the Green Gorge and Pyramid Peak samples (~12–14 wt%).

Trace-element geochemistry of glasses

Figure 5 shows remarkably similar primitive mantle-normalised trace-element concentrations for grains in samples from Bauer Bay, Green Gorge and Pyramid Peak along with published results from Kamenetsky *et al.* (2000: discussed below). On the basis of the data obtained here, the hyaloclasts in individual samples of hyaloclastite breccia and pillow-fragment breccia matrix at all three locations show very limited compositional variation. The compositions are characteristic of E-MORB. All trace-element patterns exhibit positive Nb and Ta anomalies and negative K and Pb anomalies. The Green Gorge samples are slightly more large-ion lithophile-element-enriched, whereas the Bauer Bay samples are slightly more heavy rare-earth-element-enriched, compared with the other samples (Figure 5).

Table 1 Average sideromelane geochemical analyses.

Section	BB1						GG1				PP4			
Sample No. (major, trace) ^a	1B 41, 1	1 σ	1C2 49, 3	1 σ	3A 14, –	1 σ	14A 46, 6	1 σ	22 39, –	1 σ	2 62, 7	1 σ	3B 55, –	1 σ
EMP (wt%)														
SiO ₂	49.81	0.18	49.68	0.17	50.04	0.22	48.88	0.29	49.33	0.20	48.42	0.23	48.27	0.24
TiO ₂	1.55	0.03	1.55	0.03	1.59	0.02	1.42	0.03	1.45	0.03	1.39	0.03	1.40	0.03
Al ₂ O ₃	16.13	0.07	15.97	0.08	16.04	0.05	16.56	0.11	16.56	0.10	16.67	0.09	16.58	0.09
Cr ₂ O ₃	<0.05	–	<0.05	–	0.05	0.01	<0.05	–	<0.05	–	<0.05	–	<0.05	–
FeO	8.05	0.10	8.02	0.09	8.27	0.10	7.25	0.09	7.47	0.10	7.79	0.09	7.80	0.10
MnO	0.15	0.02	0.15	0.02	0.16	0.02	0.14	0.02	0.15	0.02	0.15	0.02	0.15	0.02
MgO	7.95	0.10	7.95	0.07	8.00	0.09	7.63	0.07	7.55	0.08	8.27	0.08	8.19	0.09
CaO	10.93	0.06	10.89	0.06	11.09	0.06	12.27	0.08	12.13	0.06	12.63	0.06	12.62	0.07
Na ₂ O	2.94	0.20	2.98	0.17	2.81	0.13	3.17	0.06	3.16	0.13	2.87	0.10	2.87	0.07
K ₂ O	0.69	0.02	0.69	0.02	0.70	0.02	0.70	0.02	0.73	0.02	0.60	0.02	0.61	0.02
NiO	<0.04	–	<0.04	–	<0.04	–	<0.04	–	<0.04	–	<0.04	–	<0.04	–
P ₂ O ₅	0.29	0.03	0.30	0.03	0.29	0.03	0.26	0.03	0.25	0.03	0.22	0.03	0.23	0.03
F	0.02	0.02	0.02	0.02	0.01	0.01	0.02	0.02	0.03	0.02	0.02	0.01	0.02	0.02
Cl	0.05	0.01	0.05	0.01	0.05	0.01	0.05	0.01	0.05	0.01	0.04	0.01	0.04	0.01
SO ₂	0.17	0.02	0.17	0.02	–	–	0.14	0.02	0.13	0.02	0.16	0.02	0.17	0.02
Total	98.73	–	98.42	–	99.10	–	98.49	–	98.99	–	99.23	–	98.95	–
Mg #	66.16	0.39	66.23	0.32	65.70	0.38	67.58	0.35	66.68	0.34	67.75	0.38	67.53	0.36
LA-ICP-MS (ppm)														
Li	5.45	–	4.42	1.12	–	–	4.83	0.28	–	–	4.58	0.19	–	–
Be	0.91	–	0.92	0.19	–	–	0.78	0.19	–	–	0.69	0.21	–	–
B	2.90	–	3.60	0.58	–	–	2.66	0.36	–	–	4.59	0.50	–	–
Sc	32.68	–	35.30	0.50	–	–	35.08	0.31	–	–	39.34	1.09	–	–
V	227.73	–	218.01	12.50	–	–	209.44	1.66	–	–	225.08	2.00	–	–
Cr	258.12	–	249.17	14.84	–	–	247.55	1.75	–	–	262.85	3.13	–	–
Co	36.93	–	35.98	1.72	–	–	34.03	0.50	–	–	37.90	0.37	–	–
Ni	120.04	–	115.23	5.95	–	–	98.29	2.53	–	–	113.64	3.91	–	–
Cu	64.83	–	62.43	2.42	–	–	77.49	2.48	–	–	82.30	1.52	–	–
Zn	63.95	–	57.64	9.95	–	–	53.52	1.15	–	–	57.69	2.38	–	–
Ga	17.96	–	17.27	1.31	–	–	17.01	0.47	–	–	17.62	0.23	–	–
Ge	1.70	–	1.64	0.13	–	–	1.50	0.28	–	–	1.62	0.16	–	–
As	0.54	–	0.39	0.04	–	–	0.69	0.22	–	–	0.42	0.09	–	–
Rb	19.83	–	18.54	1.14	–	–	22.00	0.55	–	–	18.01	0.28	–	–
Sr	297.61	–	299.61	0.52	–	–	317.67	1.60	–	–	297.05	0.97	–	–
Y	26.94	–	28.71	1.64	–	–	24.35	0.24	–	–	24.21	0.35	–	–
Zr	128.13	–	133.89	4.85	–	–	108.37	1.05	–	–	99.12	0.44	–	–
Nb	34.16	–	35.10	0.20	–	–	42.50	0.38	–	–	34.69	0.24	–	–
Cs	0.23	–	0.21	0.01	–	–	0.23	0.02	–	–	0.18	0.01	–	–
Ba	193.39	–	193.34	1.94	–	–	227.15	3.02	–	–	192.90	1.21	–	–
La	18.48	–	19.43	0.63	–	–	21.01	0.15	–	–	17.82	0.09	–	–
Ce	35.38	–	35.30	0.58	–	–	38.63	0.26	–	–	33.08	0.30	–	–
Pr	4.42	–	4.64	0.10	–	–	4.68	0.04	–	–	4.14	0.06	–	–
Nd	18.46	–	19.52	0.55	–	–	18.88	0.21	–	–	17.10	0.23	–	–
Sm	4.35	–	4.52	0.06	–	–	4.15	0.06	–	–	3.88	0.08	–	–
Eu	1.44	–	1.51	0.05	–	–	1.40	0.02	–	–	1.36	0.01	–	–
Gd	4.89	–	4.88	0.25	–	–	4.35	0.10	–	–	4.25	0.13	–	–
Tb	0.76	–	0.79	0.04	–	–	0.67	0.01	–	–	0.66	0.02	–	–
Dy	5.12	–	5.21	0.22	–	–	4.52	0.13	–	–	4.43	0.14	–	–
Ho	1.03	–	1.10	0.05	–	–	0.94	0.02	–	–	0.95	0.02	–	–
Er	2.91	–	3.02	0.15	–	–	2.58	0.11	–	–	2.60	0.06	–	–
Tm	0.41	–	0.44	0.02	–	–	0.38	0.02	–	–	0.37	0.02	–	–
Yb	2.87	–	2.89	0.10	–	–	2.54	0.09	–	–	2.57	0.09	–	–
Lu	0.41	–	0.42	0.02	–	–	0.38	0.01	–	–	0.38	0.01	–	–
Hf	3.03	–	3.30	0.14	–	–	2.73	0.06	–	–	2.51	0.07	–	–
Ta	1.93	–	2.01	0.02	–	–	2.42	0.04	–	–	2.02	0.03	–	–
Pb	1.16	–	1.05	0.14	–	–	1.12	0.07	–	–	0.95	0.03	–	–
Th	2.62	–	2.79	0.10	–	–	3.29	0.09	–	–	2.65	0.05	–	–
U	0.69	–	0.67	0.03	–	–	0.79	0.03	–	–	0.68	0.02	–	–

Table 1 (Continued).

Section	BB1						GG1				PP4			
Sample	1B	1 σ	1C2	1 σ	3A	1 σ	14A	1 σ	22	1 σ	2	1 σ	3B	1 σ
No. (major, trace) ^a	41, 1		49, 3		14, –		46, 6		39, –		62, 7		55, –	
CIPW norms (wt%)														
Quartz	0.00	–	0.00	–	0.00	–	0.00	–	0.00	–	0.00	–	0.00	–
Plagioclase	52.71	–	52.43	–	52.52	–	51.68	–	53.30	–	51.44	–	51.44	–
Orthoclase	4.22	–	4.22	–	4.14	–	4.35	–	4.31	–	3.69	–	3.60	–
Nepheline	0.00	–	0.00	–	0.00	–	1.71	–	0.83	–	1.53	–	1.41	–
Diopside	18.44	–	18.72	–	19.18	–	23.96	–	23.33	–	24.03	–	24.00	–
Hypersthene	10.08	–	9.35	–	10.05	–	0.00	–	0.00	–	0.00	–	0.00	–
Olivine	8.02	–	8.41	–	8.10	–	12.04	–	12.35	–	13.82	–	13.71	–
Ilmenite	2.94	–	2.94	–	3.02	–	2.70	–	2.75	–	2.64	–	2.66	–
Magnetite	1.29	–	1.29	–	1.33	–	1.17	–	1.20	–	1.26	–	1.26	–
Apatite	0.70	–	0.72	–	0.70	–	0.63	–	0.60	–	0.53	–	0.55	–

^aNumber of analyses averaged to produce the values presented: e.g. 41, 1 indicates 41 EMP analyses were averaged to obtain the major element oxide wt% data, and 1 LA_ICPMS analysis was averaged to obtain the trace ppm data; 1 σ is given on these averages.

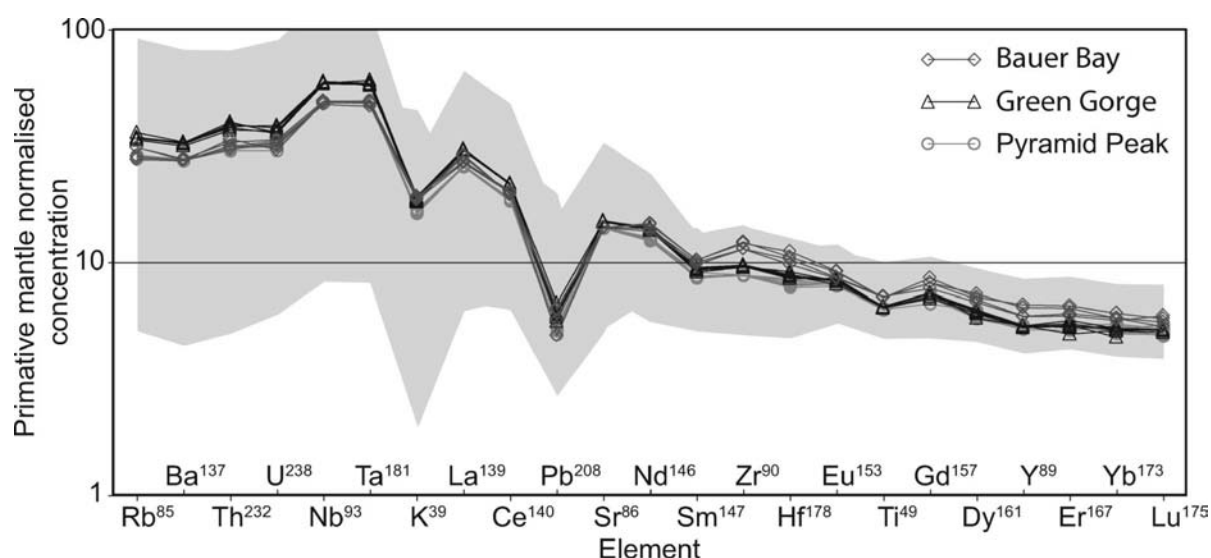


Figure 5 Primitive mantle-normalised (Sun & McDonough 1989) trace-element patterns for hyaloclasts in samples BB1-1B ($n=3$) and BB1-1C2 ($n=1$; Bauer Bay), GG1-14 ($n=6$; Green Gorge) and PP4-2 ($n=7$; Pyramid Peak). Grey-shaded region is the range of data presented in Kamenetsky *et al.* (2000).

DISCUSSION

Comparison of geochemical results with previous work

Varne *et al.* (2000) summarised the petrogenesis of the compositions observed in Macquarie Island basalts, dolerites and gabbros. Basaltic and doleritic rocks range from tholeiitic to alkalic, where tholeiitic compositions are more common in the northern third (excluding North Head) of the island and the southernmost part of Macquarie Island (Griffin 1982). Alkalic compositions are more common in the central part of the island. The basalts and sheeted dykes have normative compositions ranging from olivine- and hypersthene-normative tholeiites, similar to N-MORB, to nepheline-normative compositions similar to E-MORB (Varne *et al.* 2000). However, the volcanic rocks on Macquarie Island

include rare compositions more alkalic than E-MORB and this is reflected in high Nb concentrations as well as their nepheline-normative compositions.

Kamenetsky *et al.* (2000) found that Macquarie Island basaltic glasses exhibit a broad range of K_2O (0.1–1.8 wt%) and a strong positive covariation of K_2O with other incompatible major, minor and trace elements (e.g. TiO_2 , Na_2O , P_2O_5 and La). Kamenetsky *et al.* (2000) divided their samples into two compositional groups according to their $Mg\#$ – K_2O , $-TiO_2$, $-La$ and $-Sm$ relationships. Group I glasses are near-primitive and have the highest $Mg\#$ (63–69) along with high Al_2O_3 and CaO contents at a given K_2O content. They also carry microphenocrysts of Mg-rich olivine ($Fo_{86-89.5}$). Group II are fractionated glasses saturated with olivine + plagioclase \pm clinopyroxene and have a slightly lower $Mg\#$ (57–67) and relatively low Al_2O_3 and CaO contents

(Kamenetsky *et al.* 2000). The two groups are genetically related via the magmatic process of olivine±plagioclase±clinopyroxene crystallisation (Kamenetsky *et al.* 2000).

Wertz (2003) did not sample glasses with Mg# as low as Kamenetsky *et al.*'s (2000) basaltic glasses, and her lowest Mg# was 62. Like Kamenetsky *et al.* (2000), Wertz (2003) found that Macquarie Island glasses are characterised by a broad range of incompatible-element enrichment but discovered that there are basaltic glasses with higher K_2O/TiO_2 at a given MgO than previously recognised.

Kamenetsky *et al.*'s (2000) analyses show a greater range in all major and minor-element-oxides than the samples from the present study. Figure 6 shows the average glass compositions presented here compared with those of both groups defined by Kamenetsky *et al.* (2000). The samples of this study form a very small subset of the compositional range of Macquarie Island glasses. Using K_2O/TiO_2 or La/Sm as an index of the degree of enrichment, all the samples of this study sit toward the middle of the compositional range of Macquarie Island glasses (Figure 6). Samples from

Pyramid Peak are the most primitive and align with Group I of Kamenetsky *et al.* (2000), whereas samples from Bauer Bay are the most fractionated of the present study and align with their Group II. At Green Gorge, sample GG1-14A is primitive whereas sample GG1-22 is weakly fractionated (Figure 6). We therefore interpret the trends in Figure 4 to represent fractionation trends rather than different degrees of enrichment, where Bauer Bay samples are the most fractionated and Pyramid Peak samples are the least.

Though a thorough geochemical analysis in terms of MORB genesis is not a focus of this study, our results support the key interpretations of the detailed studies of Kamenetsky *et al.* (2000) and Kamenetsky & Maas (2002). Below we focus on the implications this study has for volcanogenic sedimentary processes within the tectonic context of Macquarie Island.

Implications for provenance

Examination of hyaloclastite breccia and pillow-fragment breccia units at Bauer Bay, Green Gorge and Pyramid Peak indicates that quench fragmentation of pillow lavas is the dominant source of sideromelane hyaloclasts and crystalline basalt clasts (Dickinson *et al.* 2009). Every hyaloclast analysed from a given sample displays virtually identical major- and trace-element geochemistry. This observation is consistent with a single volcanic eruption acting as provenance for each sample. Moreover, every sample analysed at a given site displays distinctive major- and trace-element geochemistry compared with other sites, consistent with discrete magma batches controlling the geochemistry of hyaloclasts at each site.

The slight difference in geochemistry between the two laterally equivalent samples at Green Gorge warrants some discussion. On the one hand, it is remarkable that the two samples are so similar given they were sampled 75 m apart. However, these two samples show the greatest intra-site difference in geochemistry in this study. If the difference in geochemistry is real then it is consistent with eruption and deposition from a single evolving magma chamber. This would require that the more primitive sample (GG1-14A) be deposited before the apparently coeval weakly fractionated sample (GG1-22). This may imply lateral filling of a small sedimentary basin, but no break in section was observed. An alternate interpretation is that each sample was deposited at the same time but sourced from different components of a poorly mixed magma chamber that involved near-primitive and weakly fractionated parts. The latter is consistent with the large volume of material erupted and deposited at Green Gorge. Additional geochemical studies in this section may resolve this further.

We note that the similar intra-site data at Bauer Bay and Pyramid Peak suggests that the glassy fragmental rocks are chemically homogeneous at vertical scales of at least 5 m. Furthermore, we note that the similar geochemistry of sideromelane in hyaloclastite breccia and pillow-fragment breccia at Pyramid Peak suggests that facies type is not a function of geochemistry, but more likely a function of proximity to source.

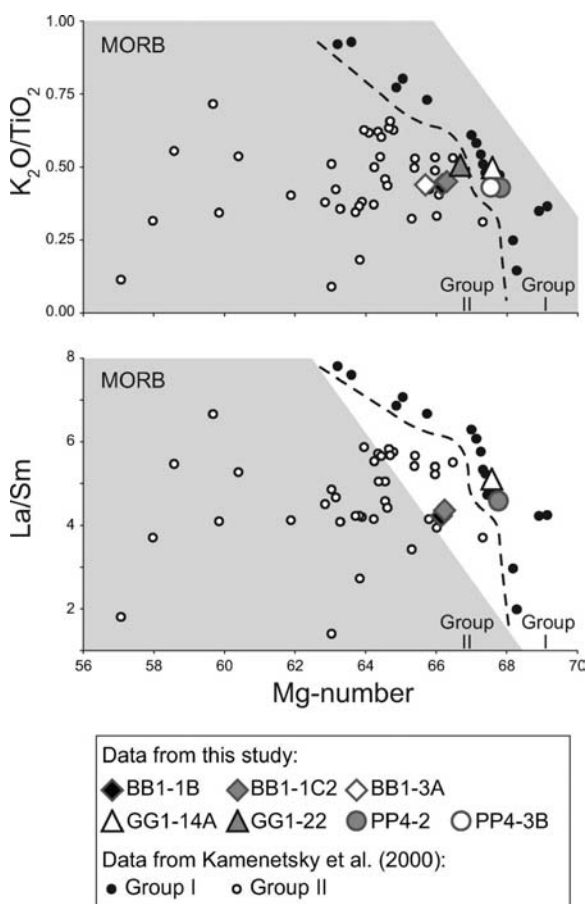


Figure 6 Incompatible major-element oxide and trace-element ratios (K_2O/TiO_2 and La/Sm) vs Mg-number for Macquarie Island glasses. The field of MORB (grey-shaded region) and Group I and II analyses are from Kamenetsky *et al.* (2000).

Therefore, three key interpretations are made: (i) hyaloclasts within a single sample are sourced from a single proximal eruption event; (ii) hyaloclasts within any given stratigraphic section are sourced from a single evolving magma reservoir that may be feeding multiple local seamounts, pillow cones or fissures; and (iii) distinct magma reservoirs feed the local eruptive events at each site. These findings are consistent with previous studies that found products of cooling-contraction granulation are derived from a single eruption (Batiza *et al.* 1984; Clague *et al.* 2000; Templeton & Hanson 2003). In addition, the immature fabric/texture (Dickinson *et al.* 2009), preservation of fresh sideromelane, and grain size are consistent with proximity of the glassy fragmental rocks to their source.

A single source for these glassy fragmental rocks contrasts with polymict sedimentary rocks on Macquarie Island that generally lack 'fresh' hyaloclasts and have been interpreted as fault-scarp-derived (Daczko *et al.* 2005). It is suggested here that the extensive hydrothermal alteration of sediment '... produced by the physical disintegration and tectonic abrasion of oceanic crust in fault zones and mass wasting of these tectonic features' (Daczko *et al.* 2005 p. 18) limits the preservation of 'fresh' hyaloclastic sediment in fault-derived sedimentary rocks. As a corollary, it is very difficult to produce abundant monomict 'fresh' hyaloclastic sediment with homogeneous geochemistry from a fault-scarp source. In addition, it is noteworthy that in spite of the close proximity of the three sites to each other and their geochemically distinct nature, there is no evidence of hyaloclasts being derived from more than one source. This implies that the glassy sediment travelled only a very short distance prior to being deposited, as discussed below.

Depositional settings

Possible depositional settings of glassy fragmental rocks in a mid-ocean ridge environment include areas adjacent to: (i) seamounts (elevations >1000 m); (ii) pillow cones (smaller than seamounts and comprised largely of pillows); (iii) fault scarps; and (iv) fissures (Batiza *et al.* 1984; Yamagishi 1991; Daczko *et al.* 2005). Fault scarps are widespread in mid-ocean ridge settings. However, a fault-scarp setting is excluded in this study on the basis of the homogeneous geochemistry of hyaloclasts. As discussed above, the facies must be proximal to source. Pillow-fragment breccia invariably forms adjacent to pillow lava, whereas hyaloclastite breccia is sourced from both pillow-fragment breccia and pillow lava and is deposited more distally. We suggest that the sections measured in this study all formed on the flanks of elongate fissures or the slopes of growing pillow cones in small sedimentary basins. We cannot exclude the possibility that sediments are derived from multiple adjacent cones that tap a common magma reservoir as opposed to a single pillow cone. A better understanding of the paleobathymetry at the time of deposition or paleocurrent data is needed to resolve this. Though our model for the production of glassy fragmental rocks may be broadly applicable to seafloor-spreading centres in general, the unusual geochemical diversity of these

rocks on Macquarie Island reflects the unique tectonic setting at which these rocks were produced.

Implications for the cessation of seafloor spreading at the Proto-Macquarie Spreading Ridge

Mosher & Massell-Symons (2008) showed that the young crust of Macquarie Island formed in a narrow (48 km wide) corridor of seafloor spreading at ~6 Ma. They also demonstrated that this corridor was one of three remaining active along the Proto-Macquarie Spreading Ridge at this time and that the other two corridors were only 21 and 5 km wide (Figure 1b). The corridors were separated by long offset transforms (160 and 117 km long). The dramatic 60–90° change in spreading direction and 47–88% shortening of these spreading corridors accompanied the transition of the Proto-Macquarie Spreading Ridge into a transform plate boundary (Mosher & Massell-Symons 2008). Having formed at the waning stages of seafloor spreading, Macquarie Island provides exceptional insight into volcano-sedimentary processes in analogous low-magmatic settings that include slow to ultra-slow spreading ridges and ridge-transform intersections.

The very unusual and diverse geochemical characteristics of Macquarie Island volcanism reflect this unique tectonic setting. The existence of compositions, ranging from N-MORB to E-MORB through a highly enriched end member of MORB, is indicative of a very limited degree of magma mixing in the asthenosphere (Kamenetsky *et al.* 2000; Varne *et al.* 2000). The slow spreading rates coupled with ridge segmentation by long transform faults (thus also segmenting magma reservoirs) is believed to have inhibited mixing that would have otherwise resulted in a typical N- to E-MORB suite for Macquarie Island crust (Varne *et al.* 1969; Batiza 1996). For example, Kamenetsky *et al.* (2000) reported their Group I glasses as being among the least-fractionated MORB melts known and argued that their enriched Group I glasses define a new primitive end-member within the known compositional spectrum of MORB. Our data are within the broad range of geochemically distinct compositions presented by Kamenetsky *et al.* (2000). The preservation of many geochemically distinct magma batches over the small area of the island and between the closely spaced three sites of this study suggests very limited magma mixing consistent with an immature or waning magmatic system. We suggest that the unique tectonic setting most likely permitted very small volume percentage melts to segregate from their mantle source regions and to rapidly migrate toward the point of eruption, at which stage they contribute to building a patchwork of geochemically distinct eruptive products that include the glassy fragmental rocks of this study.

Though the textural and geochemical features of glassy fragmental rocks on Macquarie Island may fit a seamount setting, the lack of pelagic sediment between the basalt and hyaloclastite layers suggests eruption very close to a spreading ridge. We suggest that these features reflect an unusual tectonic setting that involved seafloor spreading that was: (i) slow; (ii) at a very

narrow ridge segment (and therefore likely near to a ridge-transform intersection); and (iii) where spreading continued for at least a few million years after the adjacent long offset transforms were experiencing transpression (Meckel *et al.* 2005). All these factors probably resulted in very low degrees of partial melting that produced low rates of magma production and patchy volcanism with unusual and diverse geochemistry.

CONCLUSIONS

Two main types of glassy fragmental rocks formed along the Proto-Macquarie Spreading Ridge: (i) hyaloclastite breccia; and (ii) pillow-fragment breccia. Each sample contains a single geochemical population of hyaloclasts that are distinctive to a given site. These rocks form on the slopes or immediate vicinity of submarine pillow cones, seamounts or fissures along the mid-ocean ridge. Geochemical analyses confirm that the volcanic section on Macquarie Island includes enriched basalts that formed by low degrees of melting and that the glassy fragmental rocks of this study formed very close to source. An outstanding feature of the Macquarie Island volcanic section is the diversity of geochemistry preserved and we relate this to the unique tectonic setting that involved limited magma production at a waning seafloor-spreading system.

ACKNOWLEDGEMENTS

Australian Research Council funding to NRD and JAD (DP0663373) provided financial support to conduct this research. The Australian Antarctic Division (AAD) and Antarctic Research Assessment Committee (ARAC) funded the fieldwork and provided logistical support on Macquarie Island (Science Project 2515). We thank the Tasmanian Parks and Wildlife Service for permission to visit and sample localities on Macquarie Island. NH and RAP thank the expeditioners of the 56th ANARE for their assistance in the field and Norman Pearson and Suzy Elhlou for their assistance with the geochemical analyses. Critical reviews by John Everard and an anonymous reviewer improved an earlier version of this manuscript. This study used instrumentation (and/or geochemical laboratories) funded by ARC LIEF and DEST Systemic Infrastructure Grants, Macquarie University and industry. This is contribution no. 550 from the ARC GEMOC National Key Centre (URL: <<http://www.es.mq.edu.au/GEMOC/>>).

REFERENCES

- ARMSTRONG R. A., KOHN B., GOSCOMBE B. D. & EVERARD J. L. 2004. U-Pb and fission track ages from oceanic crust at Macquarie Island. *Geological Society of Australia Abstracts* **73**, 197.
- BALLARD R. D., HEKINIAN R. & FRANCHETEAU J. 1984. Geological setting of hydrothermal activity at 12°50'N on the East Pacific Rise: a submersible study. *Earth and Planetary Science Letters* **69**, 176–186.
- BALLARD R. D. & VAN ANDEL T. H. 1977. Morphology and tectonics of the inner rift valley at lat 36°50'N on the Mid-Atlantic Ridge. *Geological Society of America Bulletin* **88**, 507–530.
- BATIZA R. 1996. Magmatic segregation in mid-oceanic ridges: a review. In: MacLeod C. J. & Walker C. L. eds. *Tectonic, magmatic, hydrothermal, and biological segmentation of mid-ocean ridges*, pp. 103–130. Geological Society of London Special Publication **118**.
- BATIZA R., FORNARI D. J., VANKO D. A. & LONSDALE P. 1984. Craters, calderas, and hyaloclastites on young Pacific seamounts. *Journal of Geophysical Research* **89**, 8371–8390.
- BATIZA R. & WHITE J. D. L. 2000. Submarine lavas and hyaloclastite. In: Sigurdsson H., Houghton B. F., McNutt S. R., Rymer H. & Stix J. eds. *Encyclopedia of volcanoes*, pp. 361–381. Academic Press, San Diego.
- BLACKMAN D. K., KARSON J. A., KELLEY D. S., CANN J. R., FRUEH-GREEN G. L., GEE J. S., HURST S. D., JOHN B. E., MORGAN J., NOONER S. L., ROSS D. K., SCHROEDER T. J. & WILLIAMS E. A. 2002. Geology of the Atlantis Massif (Mid-Atlantic Ridge, 30°N): implications for the evolution of an ultramafic oceanic core complex. *Marine Geophysical Researches* **23**, 443–469.
- CHRISTODOULOU C., GRIFFIN B. J. & FODEN J. 1984. The geology of Macquarie Island. *Australian National Antarctic Research Expeditions Research Notes* **21**, 1–15.
- CLAGUE D. A., DAVIS A. S., BISCHOFF J. L., DIXON J. E. & GEYER R. 2000. Lava bubble-wall fragments formed by submarine hydro-volcanic explosions on Lo'ihi Seamount and Kilauea Volcano. *Bulletin of Volcanology* **61**, 437–449.
- DACZKO N. R., MOSHER S., COFFIN M. F. & MECKEL T. A. 2005. Tectonic implications of fault-scarp-derived volcanoclastic deposits on Macquarie Island: sedimentation at a fossil ridge-transform intersection? *Geological Society of America Bulletin* **117**, 18–31.
- DACZKO N. R., WERTZ K. L., MOSHER S., COFFIN M. F. & MECKEL T. A. 2003. Extension along the Australian-Pacific transpressional transform plate boundary near Macquarie Island. *Geochemistry Geophysics Geosystems* **4**, 1080, doi:10.1029/2003GC000523.
- DAVIDSON G. J., VARNE R., BROWN A. V. & CONNELL R. 2004. Structural controls on sulphide deposition at the dyke-lava boundary, slow-spreading ocean crust, Macquarie Island. *Terra Nova* **16**, 9–15.
- DICKINSON J. A., HARB N., PORTNER R. A. & DACZKO N. R. 2009. Glassy fragmental rocks of Macquarie Island (Southern Ocean): mechanism of formation and deposition. *Sedimentary Geology* **216**, 91–103.
- DUNCAN R. A. & VARNE R. 1988. The age and distribution of the igneous rocks of Macquarie Island. *Papers and Proceedings of the Royal Society of Tasmania* **114**, 45–50.
- FORNARI D. J., HAYMON R. M., PERFIT M. R., GREGG T. K. P. & EDWARDS M. H. 1998. Axial summit trough of the East Pacific Rise 9°–10°N: geological characteristics and evolution of the axial zone on fast spreading mid-ocean ridges. *Journal of Geophysical Research* **103**, 9827–9855.
- FOUQUET Y., ELISSEN J., ONDREAS H., BARRIGA F., BATIZA R. & DANYUSHEVSKY L. V. 1998. Extensive volcanoclastic deposits at the Mid-Atlantic Ridge axis: results of deep-water basaltic explosive volcanic activity? *Terra Nova* **10**, 280–286.
- FROHLICH C., COFFIN M. F., MASSELL C., MANN P., SCHUUR C. L., DAVIS S. D., JONES T. & KARNER G. 1997. Constraints on Macquarie Ridge tectonics provided by Harvard focal mechanisms and teleseismic earthquake locations. *Journal of Geophysical Research* **102**, 5029–5041.
- FRYER P. 1990. Deep submersibles and potential marine geological research. *Marine Technical Society Journal* **24**, 22–31.
- GOSCOMBE B. D. & EVERARD J. L. 1998. *Geology of Macquarie Island, geological atlas 1:10,000 series*. Mineral Resources of Tasmania, Hobart.
- GOSCOMBE B. D. & EVERARD J. L. 2001. Tectonic evolution of Macquarie Island: extensional structures and block rotations in oceanic crust. *Journal of Structural Geology* **23**, 639–673.
- GREGG T. K. P., FORNARI D. J., PERFIT M. R., HAYMON R. M. & FINK J. H. 1996. Rapid emplacement of a mid-ocean ridge lava flow on the East Pacific Rise at 9°46'–51°N. *Earth and Planetary Science Letters* **144**, E1–E7.
- GRIFFIN B. J. 1982. Igneous and metamorphic petrology of lavas and dykes of the Macquarie Island ophiolite complex. PhD thesis, University of Tasmania, Hobart (unpubl.).

- GRIFFIN B. J. & VARNE R. 1980. The Macquarie Island ophiolite complex: mid-Tertiary oceanic lithosphere from a major ocean basin. *Chemical Geology* **30**, 285–308.
- HEIRTZLER J. R. & GRASSLE J. F. 1976. Deep sea research by manned submersibles. *Science* **194**, 294–299.
- HEKINIAN R., FRANCHETEAU J. & BALLARD R. D. 1985. Morphology and evolution of hydrothermal deposits at the axis of the East Pacific Rise. *Oceanologica Acta* **8**, 147–155.
- JONES J. G. 1968. Intraglacial volcanoes of the Laugarvatn region, south-west Iceland-I. *Quarterly Journal of the Geological Society* **124**, 197–211.
- KAMENETSKY V. S., EVERARD J. L., CRAWFORD A. J., VARNE R., EGGINS S. M. & LANYON R. 2000. Enriched end-member of primitive MORB melts: petrology and geochemistry of glasses from Macquarie Island (SW Pacific). *Journal of Petrology* **41**, 411–430.
- KAMENETSKY V. S. & MAAS R. 2002. Mantle-melt evolution (dynamic source) in the origin of a single MORB suite: a perspective from magnesium glasses of Macquarie Island. *Journal of Petrology* **43**, 1909–1922.
- KARSON J. A., THOMPSON G., HUMPHRIS S. E., EDMOND J. M., BRYAN W. B., BROWN J. R., WINTERS A. T., POCKALNY R. A. & CASEY A. J. F. 1987. Along-axis variations in seafloor spreading in the MARK area. *Nature* **328**, 681–685.
- LAGABRIELLE Y., AUZENDE J., EISSEN J., JANIN M. & COTTEN J. 1994. Geology and geochemistry of a 800 m section through young upper oceanic crust in the North Fiji Basin (Southwest Pacific). *Marine Geology* **116**, 113–132.
- LE MAITRE R. W. (Editor) 1989. *A classification of igneous rocks and glossary of terms*. Blackwell, Oxford.
- LONSDALE P. & BATIZA R. 1980. Hyaloclastite and lava flows on young seamounts examined with a submersible. *Geological Society of America Bulletin* **91**, 545–554.
- LONSDALE P. & FORNARI D. 1980. Submarine geology of Malpelo Ridge, Panama Basin. *Marine Geology* **36**, 65–83.
- MAMALOUKAS-FRANGOULIS V., AUZENDE J., BIDEAU D., BONATTI E., CANNAT M., HONNOREZ J., LAGABRIELLE Y., MALAVIEILLE J., MEVEL C. & NEEDHAM H. D. 1991. In-situ study of the eastern ridge-transform intersection of the Vema Fracture Zone. *Tectonophysics* **190**, 55–71.
- MASSELL C., COFFIN M. F., MANN P., MOSHER S., FROHLICH C., DUNCAN C. S., KARNER G., RAMSAY D. & LEBRUN J.-F. 2000. Neotectonics of the Macquarie Ridge Complex, Australia–Pacific plate boundary. *Journal of Geophysical Research* **105**, 13457–13480.
- MCPHIE J., DOYLE M. & ALLEN R. 1993. *Volcanic textures: a guide to the interpretation of textures in volcanic rocks*. CODES, University of Tasmania, Hobart.
- MECKEL T. A., COFFIN M. F., MOSHER S., SYMONDS P., BERNARDEL G. & MANN P. 2003. Geophysical characterization of incipient subduction at the Hjort Trench, Australian–Pacific plate boundary. *Geochemistry Geophysics Geosystems* **4**, 1099, doi:10.1029/2002GC000498.
- MECKEL T. A., MANN P., MOSHER S. & COFFIN M. 2005. Influence of cumulative convergence on lithospheric thrust fault development and topography along the Australian–Pacific plate boundary south of New Zealand. *Geochemistry Geophysics Geosystems* **6**, Q09010, doi:10.1029/2005GC000914.
- MITCHELL N. C. 2001. Random sequences of lithologies exposed on the Mid-Atlantic Ridge. *Journal of Geophysical Research* **106**, 26365–26378.
- MITCHELL N. C., TIVEY M. A. & GENTE P. 2000. Seafloor slopes at mid-ocean ridges from submersible observations and implications for interpreting geology from seafloor topography. *Earth and Planetary Science Letters* **183**, 543–555.
- MOSHER S. & MASSELL-SYMONS C. 2008. Ridge reorientation mechanisms: Macquarie Ridge Complex, Australia–Pacific plate boundary. *Geology* **36**, 119–132.
- ONDREAS H., FOUQUET Y., VOISSET M. & RADFORD-KNOERY J. 1997. Detailed study of three contiguous segments of the Mid-Atlantic Ridge, South of the Azores (37°N to 38°30'N), using acoustic imaging coupled with submersible observations. *Marine Geophysical Researches* **19**, 231–255.
- POUCHOU J. L. & PICOIR F. 1984. A new model for quantitative X-ray microanalysis of homogenous samples. *Recherche Aerospatiale* **5**, 13–38.
- QUILTY P. & CRUNDWELL M. P. 2004. The age of seafloor spreading that formed the foundation rocks of Macquarie Island. *Geological Society of Australia Abstracts* **73**, 220.
- RIVIZZIGNO P. A. & KARSON J. A. 2004. Structural expression of oblique seafloor spreading in the Macquarie Island ophiolite, Southern Ocean. *Geology* **32**, 125–128.
- RUELLAN E., HUCHON P., AUZENDE J. & GRACIA E. 1994. Propagating rift and overlapping spreading center in the North Fiji Basin: the STARMER French–Japanese joint project, 1987–1992. *Marine Geology* **116**, 37–56.
- SUN S.-S. & McDONOUGH W. F. 1989. Chemical and isotopic systematics of oceanic basalts: implications for mantle composition and processes. In: Saunders A. D. & Norry M. J. eds. *Magmaism in the ocean basins*, pp. 313–345. Geological Society of London Special Publication **42**.
- TANNER L. H. & CALVARI S. 1999. Facies analysis and depositional mechanisms of hydroclastite breccias, Acicastello, eastern Sicily. *Sedimentary Geology* **129**, 127–141.
- TEMPLETON J. H. & HANSON R. E. 2003. Jurassic submarine arc-apron deposits and associated magma/wet-sediment interaction, northern Sierra Nevada, California. *Journal of Volcanology and Geothermal Research* **128**, 299–326.
- TIVEY M., TAKEUCHI A. & SCIENTIFIC PARTY 1998. A submersible study of the western intersection of the Mid-Atlantic Ridge and Kane Fracture Zone (WMARK). *Marine Geophysical Researches* **20**, 195–218.
- VAN ACHTERBERGH E., RYAN C. G. & GRIFFIN W. L. 1999. GLITTER: on-line interactive data reduction for the laser ablation ICPMS microprobe. In: *Proceedings of the 9th V. M. Goldschmidt Conference*, pp. 305–306. Lunar and Planetary Institute, Houston.
- VARNE R. 1989. Macquarie Island. In: Burrett C. F. & Martin E. L. eds. *Geology and mineral resources of Tasmania*, pp. 398–402. Geological Society of Australia Special Publication **15**.
- VARNE R., BROWN A. V. & FALLOON T. 2000. Macquarie Island: its geology, structural history, and the timing and tectonic setting of its N-MORB to E-MORB magmatism. In: Dilek Y., Moores E. M., Elthon D. & Nicolas A. eds. *Ophiolites and oceanic crust: new insights from field studies and the Ocean Drilling Program*, pp. 301–320. Geological Society of America Special Paper **349**.
- VARNE R., GEE R. D. & QUILTY P. G. 1969. Macquarie Island and the cause of oceanic linear magnetic anomalies. *Science* **166**, 230–232.
- VARNE R. & RUBENACH M. J. 1972. Geology of Macquarie Island and its relationship to oceanic crust. In: Hayes D. E. ed. *Antarctic oceanology II: The Australian–New Zealand sector*, pp. 251–266. American Geophysical Union Antarctic Research Series **19**.
- WERTZ K. L. & 2003. From seafloor spreading to uplift: the structural and geochemical evolution of Macquarie Island on the Australian–Pacific plate boundary. PhD thesis, University of Texas at Austin, Austin (unpubl.).
- WERTZ K. L., MOSHER S., DACZKO N. R. & COFFIN M. F. 2003. Macquarie Island's Finch–Langdon fault: a ridge-transform inside-corner structure. *Geology* **31**, 661–664.
- WOOD R., LAMARCHE G., HERZER R., DELTEIL J. & DAVY B. 1996. Paleogene seafloor spreading in the southeast Tasman Sea. *Tectonics* **15**, 966–975.
- YAMAGISHI H. 1991. Morphological and sedimentological characteristics of the Neogene submarine coherent lavas and hyaloclastites in Southwest Hokkaido, Japan. *Sedimentary Geology* **74**, 5–23.

Received 4 August 2008; accepted 17 April 2009

VII:

Vitriclastic lithofacies from Macquarie Island (Southern Ocean): compositional influence on abyssal eruption explosivity in a dying spreading ridge

PORTNER, Ryan A.¹, DACZKO, Nathan R.¹, and HARB, Nicole¹

¹GEMOC ARC National Key Centre, Department of Earth and Planetary Sciences,
Macquarie University, NSW 2109, Australia

Published in Bulletin of Volcanology August 2009

Vitriclastic lithofacies from Macquarie Island (Southern Ocean): compositional influence on abyssal eruption explosivity in a dying Miocene spreading ridge

Ryan A. Portner · Nathan R. Daczko ·
Julie A. Dickinson

Received: 29 October 2008 / Accepted: 20 July 2009
© Springer-Verlag 2009

Abstract Macquarie Island is composed of a complete section of oceanic crust that formed in a slow-spreading mid-ocean ridge 2.0 to 3.5 km below sea level. Vitriclastic facies preserved on the island have both pyroclastic and hyaloclastic characteristics. Monomict hyaloclastic breccia facies are widespread across the island and are predominantly composed of near-primitive (~7.9 wt% MgO) subalkaline/transitional (~0.7 wt% K₂O) sideromelane shards and crystalline basalt clasts with low vesicularity (LV, < 15% vesicles). Breccias are thick bedded and structureless with matrix-supported angular pillow fragments, bomb-sized fluidal mini-pillows, and globular glass lapilli. Clasts are lithologically similar to interbedded pillow basalts and laterally grade into fine-grained sandstone facies. These sandstones are normal-graded, well-laminated, thin bedded, and interstratified with red pelagic mudstone. Lithofacies associations indicate that the hyaloclastic breccias were formed proximal to a source vent via quench-fragmentation, and subsequently reworked by ocean-bottom currents into distal epiclastic sandstone facies. During eruption, co-genetic pillow lava and hypabyssal intrusions mingled with the breccia, forming fluidal peperite. Rare polymict pyroclastic facies only occur in the highest stratigraphic levels and are mostly composed of highly vesicular (HV, 15–50% vesicles) sideromelane shards and

crystalline basalt clasts with alkaline (~1.0 wt% K₂O) fractionated (~6.8% MgO) compositions. Minor lithic grains are composed of subalkaline (~0.7 wt% K₂O) to very highly alkaline (~1.7 wt% K₂O) LV sideromelane shards, and amphibole-bearing diabase. The pyroclastic facies contains medium to thick beds of lapilli-tuff that exhibit both reverse and normal grading, diffuse lamination, and planar-grain fabric. These beds are locally overlain by thin fine-grained tuff beds entirely composed of cusped to very thin elongate bubble-wall shards. These characteristics indicate that explosive deep-marine eruptions produced high-density coarse-grained gravity flows that were covered by slower suspension settle-out of delicate bubble-wall shards. Stratigraphic relationships suggest that explosive eruptions started during the waning stages of more alkaline volcanism along the proto-Macquarie spreading center.

Keywords Mid-ocean ridge · Deep-marine · Volcaniclastic · Hyaloclastite · Pyroclastic · Macquarie Island · Explosive

Introduction

Oceanic crust formed in mid-ocean ridges typically forms above the carbonate compensation depth between 2–3 km below sea level (b.s.l.; Orton 1996). At these water depths explosive volcanic activity is greatly suppressed due to the hydrostatic pressure created by the overlying water column (Fouquet et al. 1998; Clague et al. 2003). The maximum depth for significant submarine explosivity and generation of pyroclastic debris is commonly believed to be between 0.5 and 1.8 km b.s.l. (McBirney 1963; Staudigel and Schmincke 1984; Kokelaar 1986; Gill et al. 1990; Fouquet et al. 1998), although explosive hydrovolcanism can theoretically occur at depths of ~ 4 km b.s.l. (Wohletz

Editorial responsibility: J. White

Electronic supplementary material The online version of this article (doi:10.1007/s00445-009-0312-8) contains supplementary material, which is available to authorized users.

R. A. Portner (✉) · N. R. Daczko · J. A. Dickinson
GEMOC ARC National Key Centre,
Department of Earth and Planetary Sciences, Macquarie University,
Sydney, NSW 2109, Australia
e-mail: rportner@els.mq.edu.au

Published online: 18 August 2009

 Springer

2003). In addition, Head and Wilson (2003) postulated that foam buildup by upward migrating bubble accumulation in the tops of confined submarine conduits, may induce magmatic fragmentation and explosive eruptions at these depths. Recent work using submersibles has documented highly vesicular alkalic basalt pyroclasts along the Hawaiian North Arch volcanic field (Davis and Clague 2006) and variably volatile-rich poorly vesicular MORB Limu o Pele along the global mid-ocean ridge system (Sohn et al. 2008; Clague et al. 2009), providing rare insight into explosive volcanism in deep-marine settings >4 km b.s.l..

Subaqueous eruption explosivity is controlled by depth of eruption (hydrostatic pressure), discharge rate and volume, magmatic properties (i.e. temperature, volatile content, viscosity and crystallinity), magma/water interaction characteristics (including particulate-contaminated water), conduit properties, and vent geometry (Kokelaar 1986; White 1996; White et al. 2000). The fragmentation mechanism is reflected in the resulting volcanoclast particle morphology, and includes vesicularity, grain size, texture and shape (Wohletz 1983; Fisher and Schmincke 1994). It has been well-documented that vesicle-poor detritus is replaced by vesicle-rich detritus with an overall increase in clastic production and eruption explosivity relative to effusive volcanism, as depth below sea level decreases (Staudigel and Schmincke 1984; Lackschewitz et al. 1994; Eissen et al. 2003). This change is gradual and partly dependent upon magma composition. A correspondence between volcanoclast morphology and geochemical composition has also been documented from modern deep-sea volcanoclastic sediments (Hekinian et al. 2000; Clague et al. 2003), where poorly vesicular basalts are typically tholeiitic (subalkaline) to transitional and highly vesicular basalts have more alkalic compositions. Although analysis of modern day deep-marine pyroclastic deposits provides good constraint on the eruptive environment (i.e. eruption depth), the deposits rarely allow observation of detailed vertical and lateral sedimentary characteristics. This lack of outcrop inhibits evaluation of depositional processes and the stratigraphic significance of explosively formed deposits along mid-ocean spreading ridges. Few works document present day exposures of explosively derived volcanoclastics formed in abyssal (~2 km b.s.l.) deep-sea environments (e.g. Simpson and McPhie 2001) and preserve fresh volcanic glass shards for geochemical analysis.

In this study, we present evidence for explosively formed alkaline sideromelane and non-explosively formed subalkaline to transitional sideromelane from a Miocene mid-ocean spreading ridge. By comparing grain morphology, sedimentologic characteristics and stratigraphic architecture of Macquarie Island's vitriclastic lithofacies, we are able to document modes of eruption, fragmentation mechanisms, transport dynamics and depositional processes. Major

element geochemistry trends within the different lithofacies described reveal magma compositional controls on the resulting eruption process.

Geologic background and previous research

Located in the Southern Ocean halfway between New Zealand and Antarctica, Macquarie Island exposes a nearly complete section of oceanic crust (Fig. 1a). Extrusive rocks of the island formed along the Proto-Macquarie Spreading Ridge (PMSR) between 8 and 12 Ma (Duncan and Varne 1988; Quilty et al. 2008). This slow spreading ridge separated the Indo-Australian and Pacific plates during Middle Eocene through Late Miocene time, with spreading

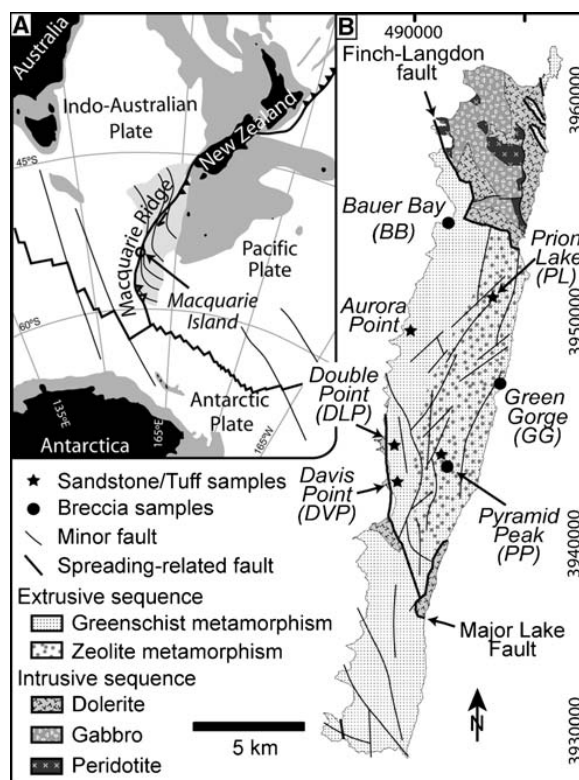


Fig. 1 Location maps. **a** Present day position of Macquarie Island in the Southern Ocean at 54.65°S, 158.83°E. Light grey represents oceanic crust formed at the Proto-Macquarie Spreading Ridge (PMSR). Dark grey represents bathymetric depths shallower than 2 km b.s.l.. Heavy black lines represent active plate boundaries, solid teeth on hanging walls of active subduction zones (hollow teeth on incipient subduction zones). Thin black lines represent spreading-related fracture zones. **b** Simplified geologic map after Goscombe and Everard (1998) showing sample locations. Extrusive sequence consists of pillow basalt, tabular basalt, volcanoclastic breccias, and minor sedimentary rocks. Some minor faults and modern alluvium omitted for clarity. Metamorphic grade is from Griffin (1982). Map projection is UTM 57 S and grid is in meters

rates between 28 and 4.4 mm/yr (half rates) during its evolution (Mosher and Massell-Symons 2008). The plate boundary evolved from a divergent setting (~47–15 Ma) through a transtensional episode (~15–10 Ma) to the currently active dextral-transpressional phase (Goscombe and Everard 2001). Therefore, rocks of the island most likely formed during the waning stages of volcanism in a transtensional to transpressional regime.

A paleo-ridge depth >1 km b.s.l. is constrained by dissolution-resistant benthic foraminifera (e.g. *Pullenia*, *Globocassidulina*, *Melonis*) from inter- and intra-pillow calcareous oozes that do not show evidence of being transported down-slope from shallow water (Quilty et al. 2008). These taxa compare with southern Pacific fauna associations (Hayward et al. 2004) that indicate upper abyssal depths between 2.0–3.5 km b.s.l., above the Late Miocene carbonate compensation depth of ~4 km b.s.l. (Quilty et al. 2008). This is supported by *Zoophycos* and *Nereites* ichnofacies in mudstone interbeds (unpublished data 2007).

Seventy five percent of the rocks exposed on Macquarie Island consist predominantly of enriched mid-ocean ridge basalt (E-MORB) and minor amounts of normal mid-ocean ridge basalt (N-MORB; Goscombe and Everard 1998; Kamenetsky and Mass 2002). Based on zeolite metamorphic grade and basalt geochemistry, Griffin (1982) concluded that alkalic compositions are more common in upper stratigraphic levels (Fig. 1b). Vitriclastic breccias represent only 1% of the mapped extrusive sequence (Goscombe and Everard 1998), but occur at all stratigraphic levels. Harb (2006) described these breccias from three separate stratigraphic sections and concluded that they were primarily derived through quench-granulation processes (hyaloclastites). The major and trace element geochemistry of sideromelane shards, from these three field sites (Daczko et al. 2009) along with petrography and measured stratigraphic sections (Dickinson et al. 2009), suggest that they were primarily formed by discrete volcanic eruptions and subsequent mass flows down pillow cone slopes. Vitriclastic rocks with <2 mm average grain size have previously not been documented on Macquarie Island, but do occur in very minor amounts and are described in this study.

Lithofacies

Results from previous studies and new field data presented here are combined into a lithofacies scheme that highlights key associations. Vitriclastic rocks are divided into five lithofacies based on vesicularity, grain size, particle morphology, bedforms, and bedding characteristics. Measured stratigraphic sections, field mapping, and petrography

using transmitting light and stereo microscopes are used to define the lithofacies. Results are presented in Table 1 and diagnostic characteristics and associations are described below. Lithofacies that are intercalated within pillow basalt are classified according to the volcanoclastic scheme of White and Houghton (2006) along with a diagnostic characteristic as a prefix (e.g. pillow-fragment breccia). Where lithofacies are interbedded within thicker sedimentary sequences we use sedimentary terms (e.g. sandstone). We restrict the term shard to <4 mm sized particles of volcanic glass.

For the purpose of this study we distinguish between low vesicularity (LV; 0–15% vesicles) and high vesicularity (HV; 15–50% vesicles). We estimated the maximum degrees of vesicularity by tracing photomicrographs of volcanoclastic particles and then calculating the total area of the images occupied by vesicles. Vesicles in all lithofacies are on average 0.13 mm in diameter with a maximum of 0.33 mm, highly spherical, and are filled with zeolites or clay. Pyrite commonly occurs along inner vesicle walls.

Low vesicularity (LV) lithofacies characteristics

Pillow-Fragment Breccia (PFB)

Low vesicularity pillow-fragment breccia (LV-PFB) is distinguished by a high proportion of well-preserved pillow fragments (Table 1) that have polyhedral shapes and discontinuous/partial chilled-margins (Fig. 2a). Coarser grained mini-pillows are 20 to 60 cm in diameter, have round exteriors, contain columnar joints that radiate outward from the core to the rim, and have continuous/complete glassy chilled-margins (Fig. 2b). Mini-pillows exhibit fluidal, amoeboid, irregular and ragged morphologies. Vitriclastic matrix is mostly composed of 1–4 mm LV shards that exhibit jigsaw-fit texture (Table 1).

Globule Tuff-Breccia (GTB)

The relatively low proportion of pillow fragments compared to LV-PFB facies (Table 1) and the abundance of very round glassy coarse lapilli, referred to here as glass globules, characterizes low vesicularity globule tuff-breccia (LV-GTB). The globules are spherical to elongate, very round, droplet-like (Fig. 2c), and locally have grooved surfaces. Glass globules >30 mm have crystalline cores with <5 mm thick glassy exteriors that exhibit concentric fractures. Rare 10–26 cm size clasts are bulbous, elliptical and tapered-cylindrical in shape and share a morphological affinity with mini-pillows described above (Fig. 2d). These mini-pillows commonly have surface corrugations that run parallel to elongate clast dimension (inset in Fig. 2d). Matrix is identical to LV-PFB facies (Table 1).

Table 1 Lithofacies descriptions for vitriclastic rocks on Macquarie Island. LV-PFB/GTB grain/clast and matrix compositions compiled from Dickinson et al. (2009)

Facies; cement; clast/grain diversity	<ul style="list-style-type: none"> Grain/clast composition Breccia matrix description 	Grain/clast texture: average size, texture and shape	Bedding: fabric; structures; breccia matrix %	Bedding: geometry; extent; thickness; nature of basal contacts
LV-PFB (low vesicularity pillow-fragment breccia); palagonite, zeolite and calcite cement	Monomict: <ul style="list-style-type: none"> >50% coarse lapilli, angular, blocky 	<ul style="list-style-type: none"> >25% pillow fragments >15 cm, angular, polyhedral >25% mini-pillows, 20–60 cm, well-rounded, fluidal 	Very poorly sorted, matrix- to locally framework-supported; structureless; <20% matrix	Lenticular-shaped; <100 m laterally continuous; <13 m thick; gradational basal contact with pillow basalt
LV-GTB (low vesicularity globule tuff-breccia); palagonite, zeolite and calcite cement	- Matrix: 0.25–30 mm, very angular, very poorly sorted; >90% low vesicularity sideromelane/ palagonite, planar to curvilinear fracture surfaces, squarish, subrectangular, trapezoidal, triangular and arcuate shapes, jigsaw-fit texture, quench microclites common; <10% basalt, tachylite and monocrySTALLINE fragments Polymict: <ul style="list-style-type: none"> >50% relict-shards altered to clay, calcite, zeolite 30% monocrySTALLINE fragments (plag, cpx), 10% chloritic basalt and <5% amphibolite/ diabase lithics, minor epidote and zeolite <5% calcareous microfossils (e.g. foraminifera) 	<ul style="list-style-type: none"> <25% pillow fragments >15 cm 40–50% glass lapilli 2–10 cm, very round, spherical-elongate ~10% mini-pillows, 10–26 cm, tapered-cylindrical >20% coarse lapilli, angular, blocky 	Poorly sorted, open matrix-supported; structureless; planar-clast fabric; surface corrugations parallel to elongate dimension of mini-pillows; 20–40% matrix Moderately to well- sorted; normal grading; well-defined laminations are parallel, planar and continuous; diffuse ripple cross-laminae; grain-imbriication; mudstone rip-up clasts; load casts	Lenticular- to wedge-shaped with abrupt pinching; <700 m laterally extensive; <30 m thick; basal contact gradational with LVG-PFB or sharp with pillow basalt
LV-VS* (low vesicularity vitric sandstone); smectitic clay and fossiliferous micrite (carbonate ooze) cement	Polymict: <ul style="list-style-type: none"> >50% relict-shards altered to clay, calcite, zeolite 30% monocrySTALLINE fragments (plag, cpx), 10% chloritic basalt and <5% amphibolite/ diabase lithics, minor epidote and zeolite <5% calcareous microfossils (e.g. foraminifera) 	<ul style="list-style-type: none"> Relict-shards: coarse- to fine-grained sand; angular, wedge- and blocky-shaped; planar fracture surfaces Lithics: coarse- to medium-grained sand; angular Microfossils: unfragmented 	Moderately to well- sorted; normal grading; well-defined laminations are parallel, planar and continuous; diffuse ripple cross-laminae; grain-imbriication; mudstone rip-up clasts; load casts	Planar- to lenticular-shaped, <150 m laterally extensive; 1–12 cm thick; basal contact: sharp with mudstone/carbonate, draping with pillow basalt, laterally correlate with LV-PFB/GTB
HV-LLT (highly vesicular laminated lapilli-tuff); palagonite, zeolite and minor calcite cement	Polymict: <ul style="list-style-type: none"> 60–80% HV, yellowish gray, highly porphyritic (>20% plag, ol, cpx) sideromelane shards 40–15% LV, yellowish gray, poorly porphyritic (<10% plag, ol, cpx) sideromelane shards <5% LV brownish orange aphyric sideromelane shards <5% basalt (HV and LV), diabase (plag, amph, cpx) <10% monocrySTALLINE fragments (plag, cpx, ol) very rare microfossils (e.g. radiolarian) 	<ul style="list-style-type: none"> Shards: very fine- to very coarse-grained ash; angular to subround; platy, cusped, blocky and irregular shapes; irregular to curved fracture surfaces Shard phenocrysts: <1.5 mm euhedral/ subhedral to fragmented PolyCRYSTALLINE clasts: medium lapilli (<13 cm); angular; blocky MonocrySTALLINE: 0.25 mm; angular 	Moderately to well-sorted very fine tuff and poorly sorted lapilli-tuff; reverse and normal grading; diffuse laminations with parallel wavy/planar discontinuous geometries; rare low-angle cross-laminae; planar-grain/clast fabric	Planar and interbedded, <30 m laterally extensive (poorly exposed), 3–30 cm thick well-defined beds, sharp to draping basal contact with pillow basalt
HV-BST* (highly vesicular bubble-wall shard tuff); zeolite cement	Monomict: <ul style="list-style-type: none"> Bubble-wall shards completely altered to palagonite 	<ul style="list-style-type: none"> Very fine to fine ash (range 0.5 mm to 0.05 mm); >80% cusped, <20% wispy (<0.75 mm long and <0.05 mm thick) 	Well- to very well- sorted, structureless, crude grain alignment, high porosity	Planar, <15 m (very poorly exposed), 10–30 cm thick, basalt contact not exposed

* Average grain size is less than average vesicle size (<0.5 mm). Primary vesicularity estimated from grain shapes and rare coarse grains.

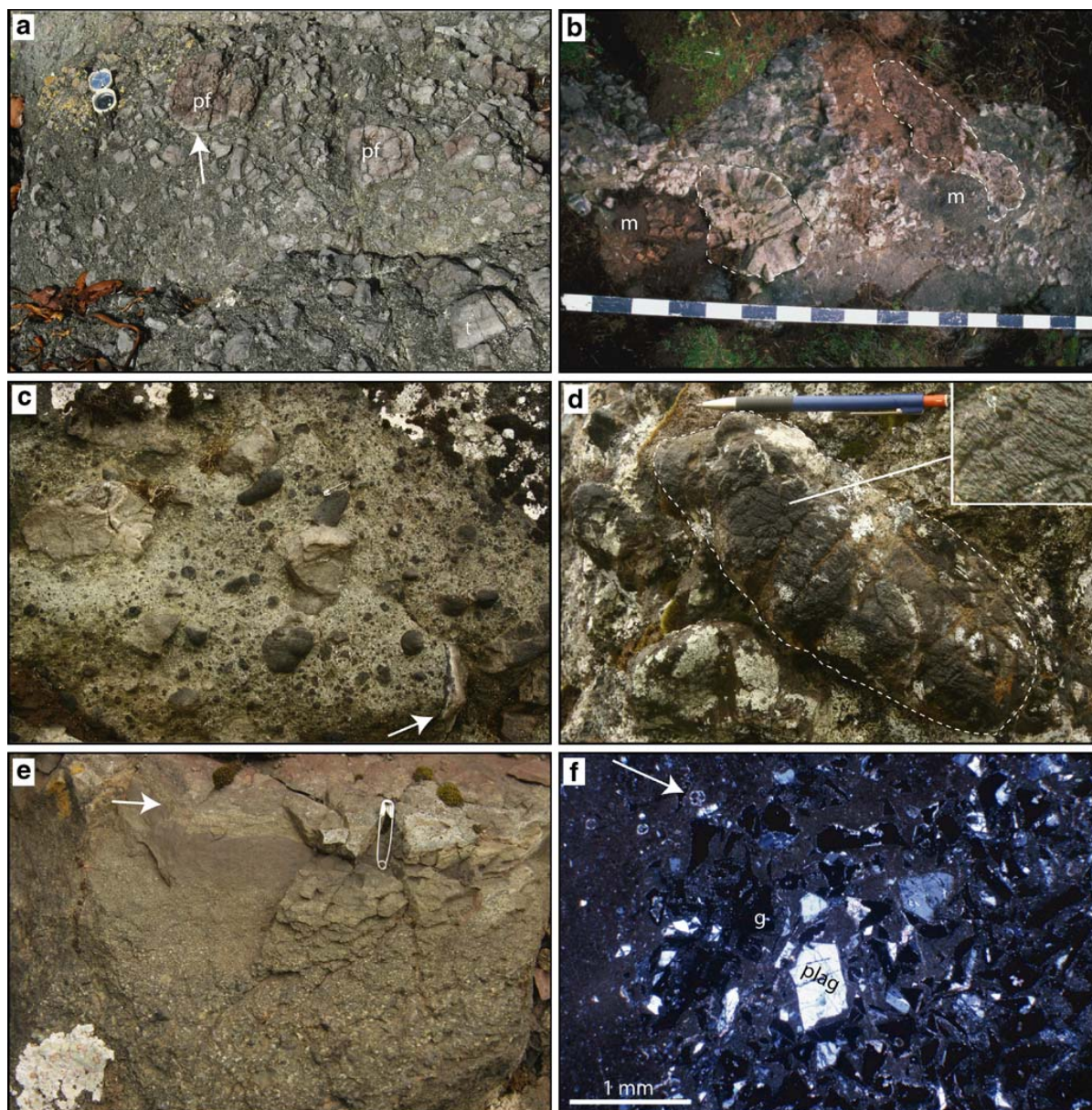
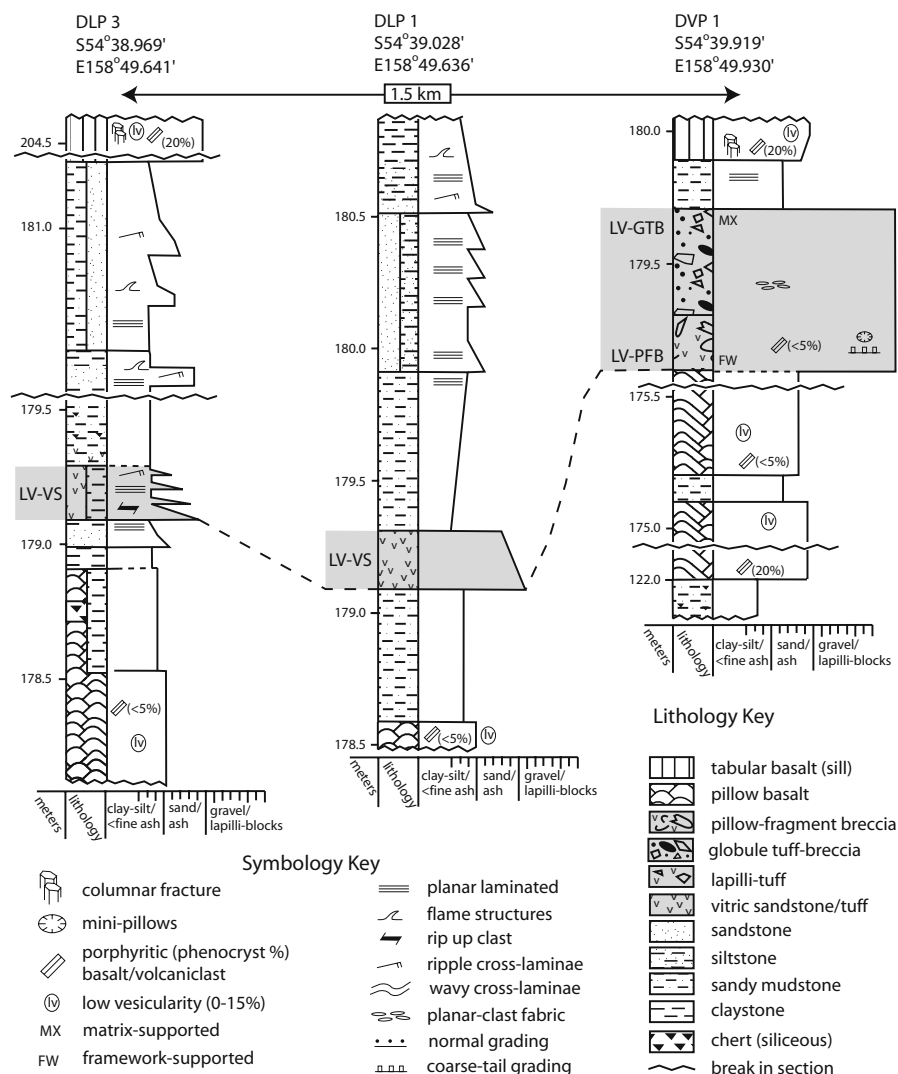


Fig. 2 LV lithofacies characteristics. **a** Pillow fragments (pf) with discontinuous chilled-margins (arrow) and trapezoidal (t) clasts from LV-PFB facies at Green Gorge. Brunton compass is 20 cm long. **b** Isolated fluidal-shaped mini-pillows set in a lapilli-sized LV vitriclastic matrix (m) from LV-PFB facies at Bauer Bay. Mini-pillow in lower left exhibits radial cooling fractures and a complete chilled-margin. Scale is in 10 cm intervals. **c** Spherical and drop-like lapilli-sized glass globules intermixed with angular basalt clasts from LV-GTB facies near Pyramid Peak. Note discontinuous chilled-margin on pillow fragment in lower right (arrow). Safety pin in center of photo is 3 cm. **d** Large tapered

cylindrical-shaped mini-pillow with corrugated outer glassy surface (inset) from LV-GTB facies near Pyramid Peak. Pencil is 15 cm. **e** Normal grading from granules through fine-grained sand in LV-VS facies at Davis Point. Unit is capped by red sandy mudstone with very thin vitriclastic laminae (arrow). Safety pin is 3 cm. **f** Petrographic photomicrograph (crossed polarized light) of LV-VS facies within foraminifera-bearing (arrow) carbonate ooze from Aurora Point. Relict-glass (g) shards are blocky to wedge shaped and are interspersed with plagioclase (plag) crystals

Fig. 3 Representative stratigraphic sections that contain LV facies. LV lithofacies bearing units are indicated in gray. See Fig. 1b for location of sections



Vitric Sandstone (VS)

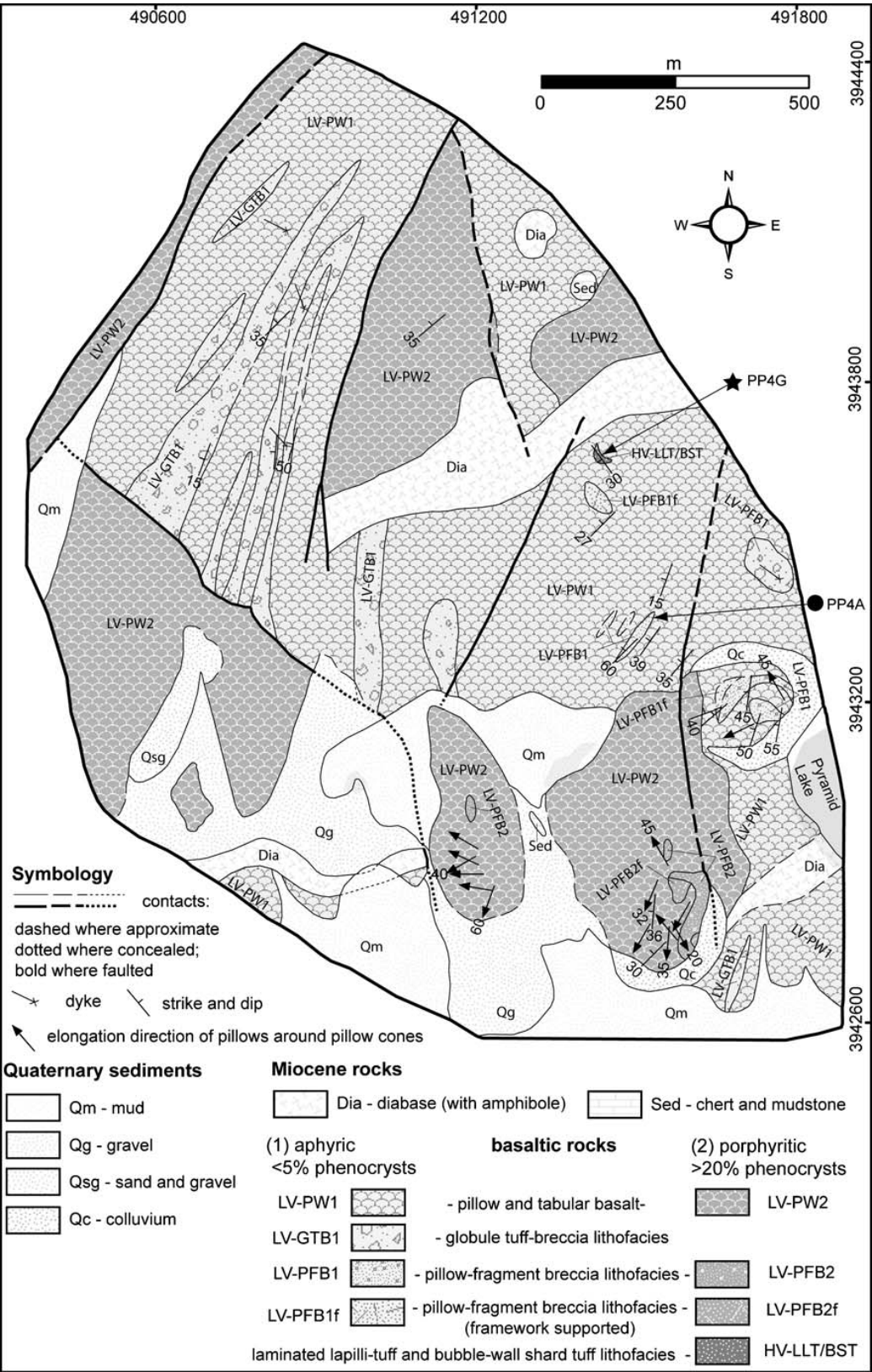
Low vesicularity vitric sandstone (LV-VS) facies consist of well-stratified sandstone beds that exhibit normal grading and well-developed horizontal lamination (Fig. 2e). This facies is commonly interbedded within thicker sedimentary sections (Fig. 3) that locally consist of foraminifera-bearing carbonate ooze (Fig. 2f). Relict-glass shards are entirely altered to clay and/or zeolite. Greenschist facies lithics typically occur (Table 1) and are very common within interbedded sedimentary rocks.

LV facies associations

LV-VS facies commonly occur directly above pillow basalt and laterally correlate with LV-PFB/GTB facies up to

1.5 km away (Fig. 3). LV-PFB facies have gradational basal contacts with pillow basalt and typically grade upward into LV-GTB facies with coarse-tail grading of mini-pillows. LV-GTB facies have sharp basal contacts with pillow basalt and are commonly penetrated by numerous subvertical dykes with quenched margins. Both facies have sharp upper and lateral contacts with pillow basalt. Breccia clast lithologies (i.e. mineralogy and phenocryst content) ubiquitously resemble adjacent basalt lithologies (Fig. 4) and breccias locally mantle small hills of pillow basalt near Pyramid Peak interpreted to be pillow cones (Goscombe and Everard 1998).

Fig. 4 Geologic map of Pyramid Peak area showing lithofacies | distributions. Lithofacies descriptions in text and in Table 1



High vesicularity (HV) lithofacies characteristics

Laminated Lapilli-Tuff (LLT)

Laminated lapilli-tuff with high vesicular grains comprises HV-LLT facies, which is composed of well stratified polymict lapilli-tuff to very fine tuff (Table 1). Diffuse planar to wavy lamination (Fig. 5a), planar-grain fabric (Fig. 5b), and basal reverse grading (Fig. 6) is characteristic of this facies. Basalt clast and shard vesicularity is bimodal in lapilli-tuff beds (Fig. 5c), but highly vesicular grains predominate (Table 1). Some highly vesicular shards have coalesced and stretched vesicles (Fig. 5d) with feldspar microphenocrysts aligned parallel to vesicle elongation.

Bubble-wall Shard Tuff (BST)

Diagnostic features of the bubble-wall shard tuff facies HV-BST include the ubiquitous presence of cusped bubble-wall shards (Fig. 5e) and a fine-grained well-sorted nature (Table 1). Very thin wispy-shaped shards resembling fragmented glass-partitions between stretched vesicles also occur and are typically parallel to each other (Fig. 5f). This facies is nearly devoid of crystal fragments and has a very open porosity now filled with zeolites.

HV facies associations

Where HV-BST facies is exposed at Pyramid Peak, it forms a very thin cap above underlying coarser grained HV-LLT facies (Fig. 6). The Pyramid Peak section is primarily composed of porphyritic HV vitriclastic facies, yet it is intercalated within a thick sequence of aphyric LV pillow basalt and associated LV-PFB/GTB facies that strike at nearly 90 degrees (Fig. 4). Amphibole-bearing diabase sills that intrude this pillow basalt sequence have mineralogical similarities to some polycrystalline lithic grains in HV-LLT facies (Table 1).

Major element geochemistry

Methodology

Representative samples containing fresh unaltered volcanic glass shards were taken from both HV-LLT and LV-PFB/GTB facies exposed at Pyramid Peak (PP), Prion Lake (PL), Green Gorge (GG), and Bauer Bay (BB; see Fig. 1b for location). Unaltered shards and olivine phenocrysts were analyzed for major element geochemistry using a Cameca SX100 electron microprobe

maintained by the Macquarie University Geochemical Analysis Unit in Sydney, Australia. The complete dataset is available online (vclastic_geochem.xls). The instrument was operated with a 15 kV accelerating voltage, 20 nA beam current, 10 μ m beam size and 20 s counting time. Only glass data with total compositions >98 wt % and Na₂O compositions >2.5 wt % were deemed “fresh”, as alteration is concomitant with liberation of Na and low totals. These data were reduced following procedures outlined in Deer et al. (1992) and Mg number was calculated by $100 \cdot \text{Mg} / (\text{Mg} + \text{Fe}^{2+})$ where $\text{Fe}^{2+} = 0.9 \text{Fe}^{\text{total}}$. Olivine forsterite (Fo) number is equal to $\text{Mg} / (\text{Fe}^{\text{total}} + \text{Mg} + \text{Mn})$.

Glass shard geochemistry

We recognize three different geochemical groups (A, B, and C) based on Mg# contents and incompatible elements K and Ti (Fig. 7). Average compositions of geochemical groups within selected samples are presented in Table 2. Groups were delineated by data points that fall within a 95% confidence limit of a weighted mean. Subclustering of data within lithofacies/groups is based on different Mg values (Fig. 8) and primarily reflects different degrees of crystal fractionation between sample locations (Daczko et al. 2009). Subalkaline to transitional basalt compositions of group A primarily consist of LV shards from LV-PFB/GTB facies (crosses). A minor amount of LV shards from group A make up of 7–38% of the total shards analyzed in HV-LLT samples (boxes). The majority of shards in HV-LLT samples comprise the more alkaline group B (triangles), which is entirely composed of HV shards. Very rare pale brownish orange LV shards from HV-LLT facies (sample PL1-b1) fall into group C. Group C compositions make up the most alkaline end of negative variation trends between incompatible elements and MgO (Fig. 8). These trends are weakly corroborated by relatively low magnesium olivine phenocryst forsterite numbers ($\text{Fo}_{83.5-87.9}$, $n=15$) in more alkaline group B and group C host shards compared to generally higher Mg olivine crystals ($\text{Fo}_{85.7-88.6}$, $n=25$) in group A host shards.

All samples analyzed here fall within the wide N-MORB to E-MORB compositional range of near-primitive and fractionated Macquarie Island glasses of Kamenetsky et al. (2000). Group B shards typically have fractionated compositions whereas group A shards yield near-primitive compositions (Fig. 7). Group C shards have hawaiite compositions following the classification scheme outlined in Le Maitre (2002) and plot with Kamenetsky et al.’s (2000) uppermost highly enriched near-primitive compositions (Fig. 7). The volatile component measured by Cl shows a positive covariation with K₂O across the spectrum of Macquarie

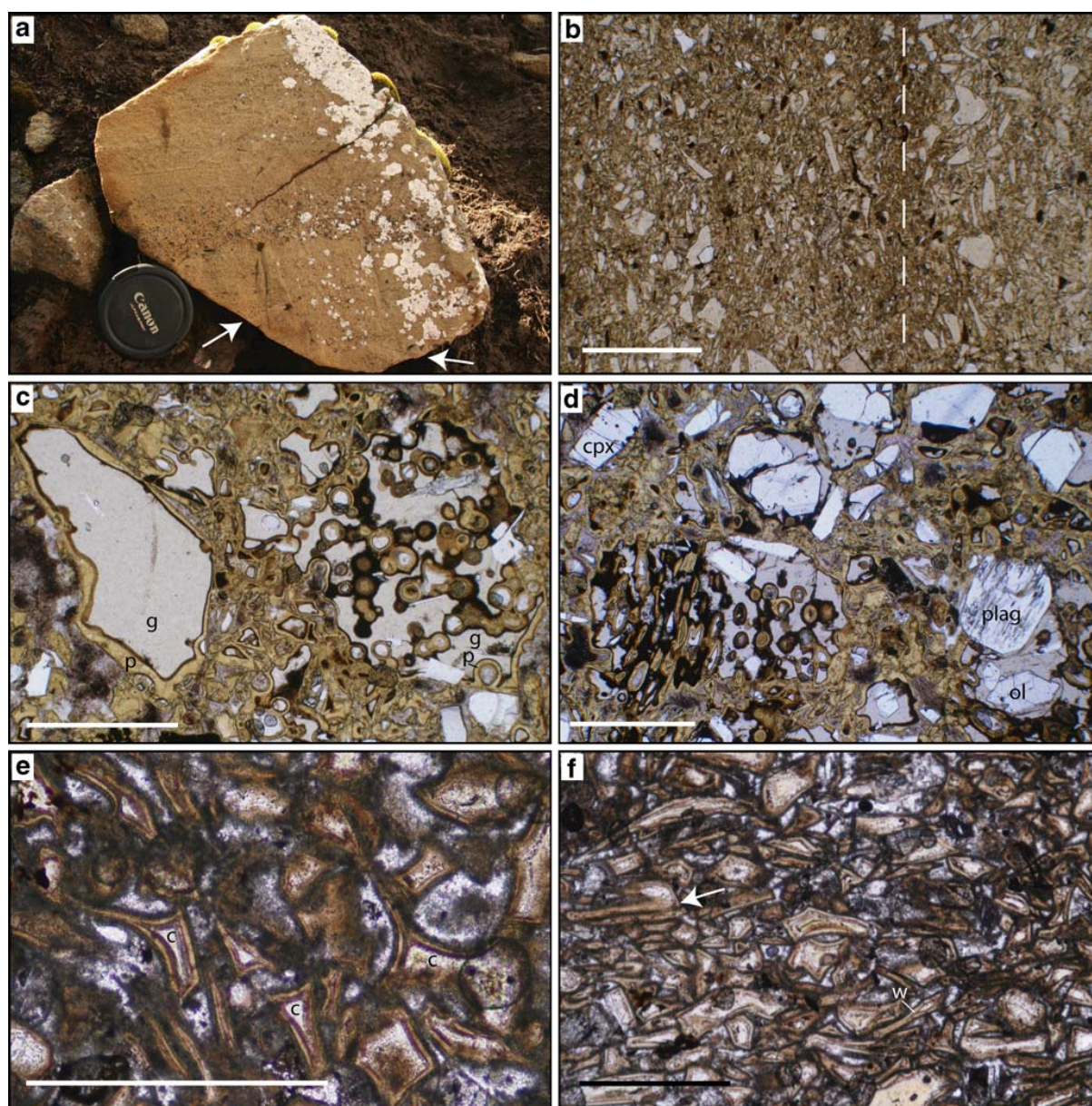
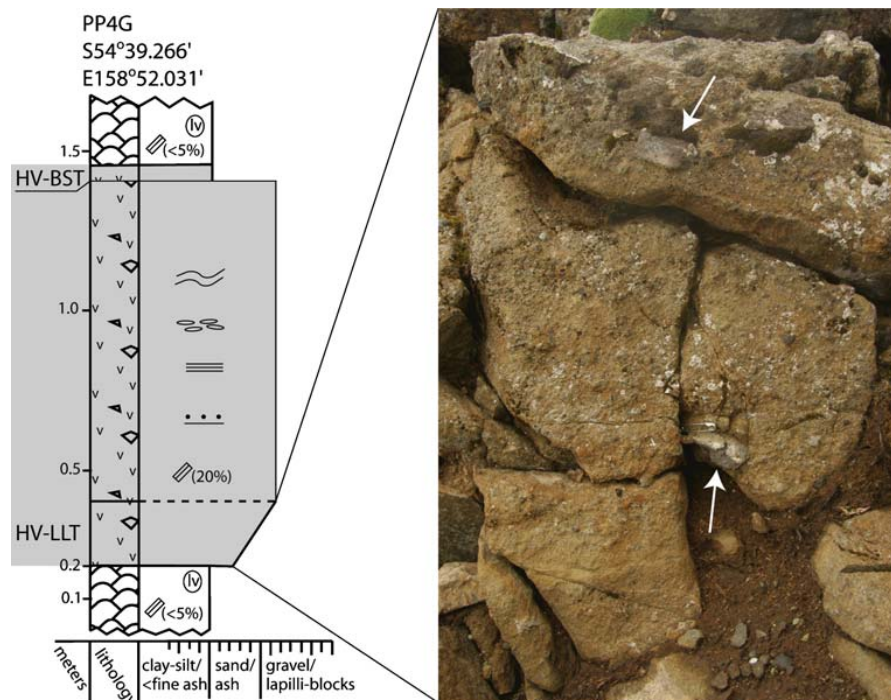


Fig. 5 HV lithofacies characteristics. All photomicrographs taken with uncrossed-polars and scales shown are 1 mm (Fig. 5b-f). **a** Planar laminated fine- to very coarse-grained tuff from HV-LLT facies at Prion Lake. Sample exhibits low angle inclined laminations (arrows) and thin normal-graded intervals (above lens cap [60 mm across]). **b** Blocky and platy shards in very fine- to medium-grained tuff from HV-LLT facies. Lamination shown by dashed line is parallel to planar-grain fabric. **c** Shards with low vesicularity (*LV*) and high vesicularity (*HV*) from HV-LLT facies at Pyramid Peak. Light yellowish gray fresh

glass (*g*) is devitrified to dark grayish yellow palagonite (*p*) and semi-opaque Fe-Ti oxides along shard and vesicle margins. **d** Stretched vesicles in a highly vesicular shard from HV-LLT facies at Prion Lake. Phenocrysts include plagioclase (*plag*), clinopyroxene (*cpx*), and olivine (*olv*). **e** Cusate (*c*) bubble-wall shards from HV-BST facies at Pyramid Peak. **f** Parallel alignment of wispy (*w*) and cusate bubble-wall shards from HV-BST facies at Pyramid Peak. Note remnant stretched vesicle morphology in larger shard (*arrow*)

Island glass data indicating higher volatile components with more alkali-enriched group B and C compositions (Fig. 9). Kamenetsky et al. (2000) also found that H₂O contents increased with Cl and K₂O. By projecting the

line of best fit through H₂O vs. Cl contents from Kamenetsky et al. (2000), approximately 1.5 wt % H₂O would be expected in the most alkalic compositions of this study (group C).



LV facies

LV-PFB/GTB facies fragmentation mechanisms

Dickinson et al. (2009) concluded that the matrix of LV-PFB/GTB facies was primarily formed by quench-granulation of pillow basalt chilled-margins and that the angular basalt clasts making up part of the LV-PTB/GTB framework were produced by cooling-contraction fragmentation along cooling joints in pillow interiors. A proximal origin for these hyaloclastite breccia lithofacies (Daczko et al. 2009) minimized any modification by mechanical fragmentation during transport. Fragmentation of quenched pillow basalt rims is reflected by the high abundance of quench microlites and tachylite in the breccia's vitriclastic matrix.

Mini-pillows and globular lapilli do not have angular broken morphologies akin to cooling- and transport-related fragmentation. Dickinson et al. (2009) suggested that these clasts may have been derived by effusive pillow basalt budding and fire fountaining (respectively). However, the upward gradational reduction in size and abundance (coarse-tail grading) of these rounded clasts from underlying pillow basalt contacts suggests that they were likely produced by an effusion-related process. The thermohydrodynamic morphologies of these clasts resemble

volcanic bombs and fluidal lapilli that form subaerially in fire fountains (Vergnolle and Mangan 2000) and have previously been suggested to indicate explosive submarine eruptions elsewhere (Staudigel and Schmincke 1984; ‘fluidal clasts’ of Simpson and McPhie 2001; ‘spheroidal clasts’ of Cas et al. 2003). However, the clasts of inferred

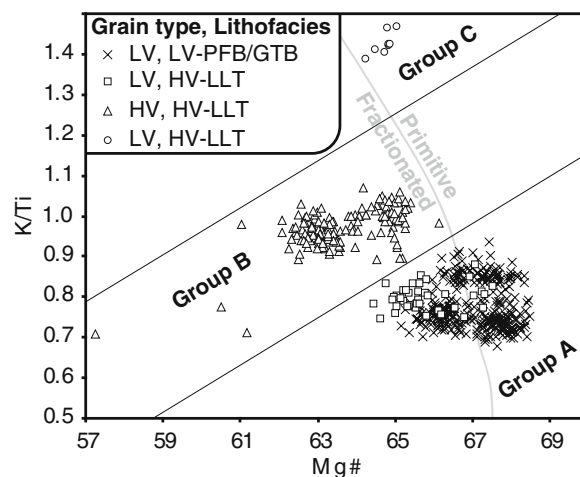


Fig. 7 K/Ti vs. Mg# discrimination plot subdividing volcanic glass compositions into three groups. Group A (*crosses and squares*) is near primitive and subalkaline to transitional. Group B (*triangles*) is fractionated and moderately alkaline. Group C (*circles*) is primitive and strongly alkaline. Primitive/fractionated boundary inferred from Kamenetsky et al. (2000)

Table 2 Average microprobe analyses of volcanic glasses from different vitriclastic facies expressed in wt%. Group symbols refer to legend used in Fig. 7.

Sample Group-symbol	PL1-b1 A - □	PL1-b1 B - Δ	PL1-b1 C - O	PP4G-4 A - □	PP4G-4 B - Δ	PP4G-5 A - □	PP4G-5 B - Δ	BB1 A - □	GG1 A - □	PP4A A - □
Shard type, % within lithofacies	LV, <40% of HV-LLT	HV, >60% of HV-LLT	LV, <5% of HV-LLT	LV, <15% of HV-LLT	HV, >80% of HV-LLT	LV, <15% of HV-LLT	HV, >80% of HV-LLT	LV, 100% of LV-PFB/ GTB	LV, 100% of LV-PFB/ GTB	LV, 100% of LV-PFB/ GTB
SiO ₂	49.62	49.14	47.63	48.32	49.25	48.77	49.32	49.84	49.11	48.35
TiO ₂	1.38	1.71	1.99	1.53	1.76	1.53	1.76	1.56	1.43	1.39
Al ₂ O ₃	16.03	16.53	17.80	17.38	16.50	16.63	16.48	16.05	16.56	16.63
Cr ₂ O ₃	0.04	0.03	0.04	0.04	0.03	0.03	0.03	0.04	0.04	0.04
FeO ^{total}	7.85	7.46	6.77	7.62	7.76	7.88	7.82	8.11	7.36	7.79
MnO	0.15	0.14	0.14	0.15	0.15	0.14	0.15	0.15	0.14	0.15
MgO	7.50	6.88	6.30	7.96	6.71	7.51	6.71	7.97	7.59	8.23
CaO	12.54	11.99	10.89	11.79	11.73	12.03	11.85	10.97	12.20	12.62
Na ₂ O	2.73	3.39	4.37	3.36	3.48	3.14	3.46	2.91	3.17	2.87
K ₂ O	0.65	1.00	1.67	0.73	0.99	0.72	0.98	0.69	0.72	0.60
NiO	0.01	0.02	0.01	0.02	0.01	0.01	0.02	0.02	0.02	0.02
P ₂ O ₅	0.24	0.36	0.61	0.26	0.41	0.29	0.40	0.30	0.25	0.22
F	0.03	0.04	0.06	0.02	0.03	0.02	0.02	0.02	0.02	0.02
Cl ^a	548	606	1145	435	665	543	677	471	496	374
S ^a	612	555	671	844	661	-	669	845	680	834
Total	98.74	98.56	98.21	99.25	98.75	98.75	98.87	98.79	98.80	99.14
N ^b	33	52	17	11	49	2	49	104	85	117
Mg#	65.43	64.59	64.83	67.43	63.14	65.35	62.92	66.03	67.13	67.64
Na ₂ O + K ₂ O	3.38	4.39	6.04	4.10	4.47	3.86	4.44	3.60	3.89	3.47
K/Ti	0.79	0.99	1.43	0.81	0.96	0.8	0.95	0.75	0.85	0.73

^a Expressed in parts per million (ppm)^b Number (n) of analyses for P₂O₅, F, Cl, and S are not equal to “n” value. See [volcanic_geochem.xls](#) online

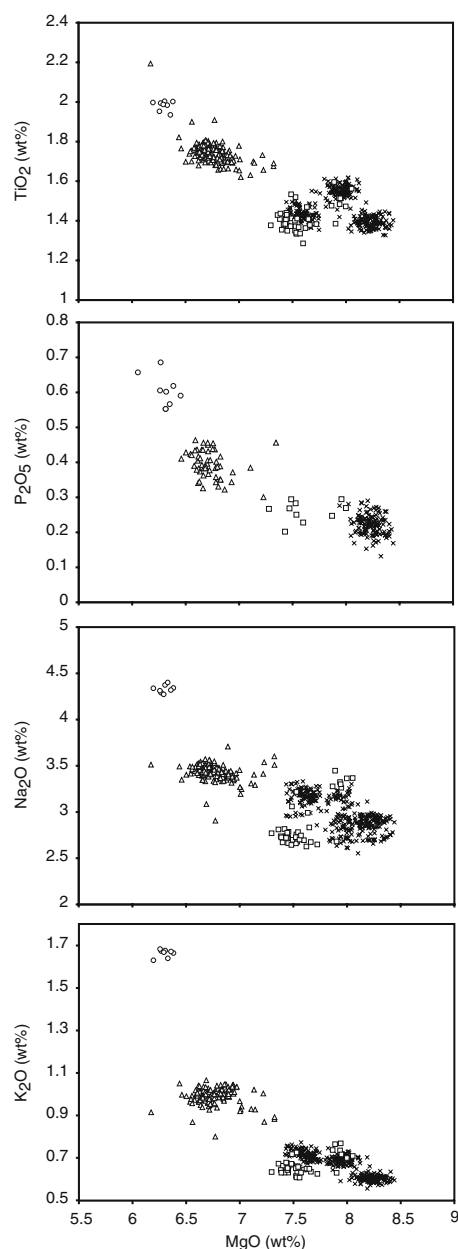


Fig. 8 Harker diagrams showing a negative covariation between incompatible elements (expressed as wt% oxides) TiO_2 , P_2O_5 , Na_2O and K_2O with MgO . Symbol legend is shown in Fig. 7

explosive origin in the cited studies are typically highly vesicular, a texture not observed in the fluidal and globular clasts of Macquarie Island hyaloclastite breccias. Corrugations on the surfaces of clasts described here are similar to the scratching scars found on pillow basalt exteriors that form during pillow growth (Yamagishi 1991).

Another plausible mechanism for the formation of these poorly vesicular fluidal and globular clasts is through

magma-hyaloclastite mingling, i.e. peperite generation. Carlisle (1963) described matrix-supported fluidal form mini-pillows up to several 10's of centimeters in diameter that are isolated in a matrix of smaller spherical, ovoid, teardrop- and spindle-shaped basalt droplets (globules). Carlisle's mini-pillows typically have a gradational lower contact with pillow basalt and diminish in abundance upward into globule-rich facies, similar to Macquarie Island facies associations. In comparison, it has been shown that dismemberment of dyke tops or intrusive tongues into wet unconsolidated breccia during late eruption episodes produces isolated mini-pillows set in a finer grained vitriclastic matrix (Simpson and McPhie 2001; Cas et al. 2003). We envision similar processes where the encounter of flowing pillow lava or hypabyssal dykes with adjacent or overlying unconsolidated hyaloclastite breccia, causes the pillow lobes to intrude and detach into isolated fluidal and globular forms (Fig. 10a). The coarse-tail grading of block-sized mini-pillows to lapilli-sized glass globules is an artifact of the host's proximity to intrusive contacts. A fluidal peperite origin for these hydrodynamic clasts is supported by the gradational facies association away from pillow basalt contacts, complete quenched margins, structureless nature, and fluidal/globular clast morphologies (Squire and McPhie 2002).

Fluidal peperite is formed by ductile fragmentation of low-viscosity magma that intrudes into unconsolidated host sediment (Skilling et al. 2002). This magma must have sufficient heat for ductile deformation and also be insulated from the surrounding fluid-saturated pore space by a steam envelope that would prohibit brittle fragmentation. The

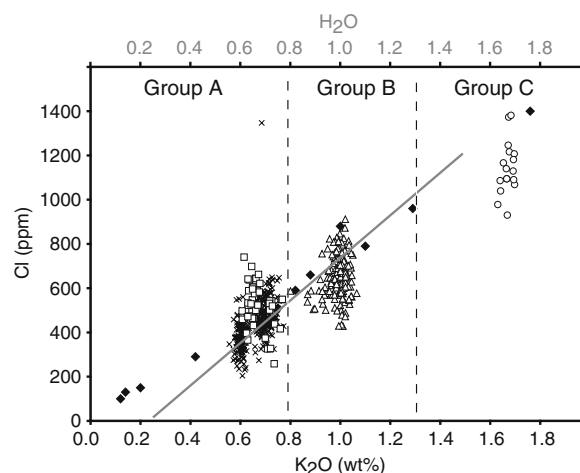


Fig. 9 Cl vs. K_2O plot of Macquarie Island volcanic glass groups. Symbol legend is shown in Fig. 7 with data from Kamenetsky et al. (2000; black diamonds) shown for comparison. Grey line is a best fit of Cl vs. H_2O data from Kamenetsky et al. (2000) and shows that both Cl and H_2O increase with increasing K_2O



VS lithofacies. **b** Rare explosive volcanism generates pyroclastic flows down vent flanks that transport material via density-stratified gravity currents. This material is ponded in distal basins between pillow cones

The upward morphological change from angular pillow fragments to hydrodynamic glass globules is similar to the shift from blocky to fluidal peperite observed by Busby-Spera and White (1987). This change from blocky to fluidal peperite has been attributed to host characteristics (i.e. permeability; Busby-Spera and White 1987) and intruding magma properties (i.e. viscosity; Squire and McPhie 2002). Significant changes in these properties would not be expected within the uniform composition and lithology of Macquarie Island host breccias at single stratigraphic sections (Daczko et al. 2009). The absence of: 1) mineral filled cavities, 2) complete chilled-margins around angular clasts, and 3) entrapment of host matrix within polyhedral-shaped pillow fragments; indicates that these polyhedral pillow fragments are not of a blocky peperite origin (Squire and McPhie 2002). This supports the cooling-contraction/transport-related origin for angular pillow fragments in Macquarie Island hyaloclastite breccias (Dickinson et al. 2009).

LV facies transport mechanisms

The structureless nature, very poor sorting, coarse grain-size and planar-clast fabric typical of LV-PFB/GB facies is suggestive of grain-flow or cohesionless debris flow processes (Dickinson et al. 2009). This type of mass flow lacks the turbulence necessary for suspension settle-out and hydraulic sorting that would otherwise produce the coarse-tail grading observed between the two breccia facies. Dickinson et al. (2009) attributes this coarse tail grading to waning eruptive periods, but results from lithofacies associations outlined above show that it can be produced during the generation of peperite subsequent to transport.

Normal grading, sandy grain size, and rip-up clasts, indicate that LV-VS facies were deposited in part by turbidity currents (Sanders 1965; Shanmugam 1997). Exotic lithic grains, such as amphibolite, are common in overlying sandstones that were derived from hydrothermally altered fault scarps (Daczko et al. 2005), indicating that this facies incorporated lithic material during transport. Its common occurrence directly above pillow basalt may indicate that relict-glass shards and unaltered monocrystalline lithics were derived in part through reworking of the fragmented chilled exteriors of underlying porphyritic pillow basalts. Stratigraphic correlation of LV-VS facies with LV-PFB/GB facies suggests that LV-VS facies are also derived from reworking of hyaloclastite breccia facies (Fig. 10a). Resedimentation of deep-marine hyaloclastite detritus has been documented in modern ocean basins where currents rework unconsolidated deposits by in-situ winnowing and down-slope entrainment (Wright 2001). This process likely produced the ripple bedded, well-sorted, and graded LV-VS facies. Epiclastic debris entrained by ocean-bottom contour currents would have locally evolved into turbidity currents where sufficient slope existed.

LV facies depositional environment

Dickinson et al. (2009) suggested that the LV hyaloclastite breccias of Macquarie Island were deposited by mass flow along the basal slopes of pillow cones that underwent gravitational flank collapse during voluminous eruption episodes. This interpretation is based upon maximum lateral extents of 0.7 km and thicknesses of 30 m for LV breccia units produced by a single eruption episode and the expected low volume ratio of quenched pillow rinds to crystalline pillow basalt. Rapid emplacement shortly following eruption is supported by hot in-situ fragmentation inferred for the breccia matrix.

The lithological similarity of monomict breccia framework clasts to interbedded pillow basalt at specific field sites (Fig. 4) indicates that hyaloclastites were proximally derived from similar source vents to interbedded lavas

(Fig. 10a). This is supported by the low geochemical variability of breccia matrix at individual field sites, which is attributed to single eruption events of spatially isolated magma batches (Daczko et al. 2009). Hyaloclastites produced by this eruptive activity were subsequently and/or contemporaneously intruded by hypabyssal dikes and co-genetic pillow basalt. This formed an unstable peperitic-hyaloclastite apron that surrounded pillow cones. The surface of the apron was reworked down slope where it was entrained by ocean-bottom currents into distal basin floor settings. The overall abundance of LV vitriclastic lithofacies on Macquarie Island suggests that effusive volcanism was the dominant eruption style along the PMSR.

HV facies

HV-LLT juvenile vs. non-juvenile shards

The variable compositions of sideromelane shards that occur in HV-LLT facies suggest a polymodal source. The volumetric abundance of group B shards, compared to other geochemical groups, combined with the sedimentary and eruptive characteristics outlined below suggests a juvenile origin for group B shards. In comparison, less voluminous compositional groups A and C in HV-LLT facies were likely incorporated into the sample through transport processes (accidental lithics) or by incorporation of wall-rock in the volcanic conduit during eruption (accessory lithics). This is supported by: 1) the presence of group A shards in adjacent LV hyaloclastite breccias, 2) the disparate lithology and geochemistry for group C, and 3) the presence of coarse-grained diabase and basalt lithics.

HV facies fragmentation mechanisms

The fine-grained size (<0.25 mm), ubiquitous presence of bubble-wall shards and general lack of straight/planar shard surfaces in HV-BST facies are typical characteristics of explosively derived pyroclastic deposits (Honnorez and Kirst 1975; Wohletz 1983; Büttner et al. 1999; Zimanowski et al. 2003). Quench granulation products are commonly coarser, between 0.25–4.0 mm (Maicher et al. 2000). The close association between HV-BST and HV-LLT facies at Pyramid Peak suggests that they were likely derived by the same eruption. Fragmented stretched vesicle walls from these facies indicate deformation and rapid quenching (Clague et al. 2009) of a vesiculating magma with subsequent and/or contemporaneous fragmentation. These shard characteristics are comparable to those of Wohletz (1983) and have been found along the Mid-Atlantic Ridge where they imply high submarine effusion rates and/or explosive activity (Fouquet et al. 1998; Hekinian et al. 2000).

A magmatically explosive origin for HV facies is supported by the general lack of extremely fine ash ($<64\ \mu\text{m}$; Zimanowski et al. 2003) and relatively high clast vesicularity. However, maximum vesicularities in HV facies are generally lower than the minimum suggested threshold of 50–70% for explosive subaerial basaltic eruptions (Houghton and Wilson 1989). Such high vesicularities would not be expected in the deep-marine environment due to the great hydrostatic pressure (Kokelaar 1986), but ranges of 30–80% vesicularity have been documented from pyroclasts erupted at depths $>1.5\ \text{km b.s.l.}$ (Gill et al. 1990; Fouquet et al. 1998; Hekinian et al. 2000; Davis and Clague 2006). Higher density basaltic pyroclasts, like that described in this study, are more commonly associated with bubble accumulation and strombolian-style eruptions (Vergnolle and Mangan 2000). Work on basaltic magmatic foams by Mangan and Cashman (1996) has shown that disequilibria vesiculation increases the rates of magma expansion and acceleration, which causes explosive magmatic fragmentation. They also suggest that the final pyroclast vesicularity is dependent upon the timing of quenching and that clast formation is not directly controlled by magma vesicularity. This is supported by textures, such as vesicle gradients, that indicate post-eruptive degassing. In the submarine environment post-eruptive vesiculation would be minimal due to quenching effects upon eruption into the water column and hence lower vesicularities might be expected in explosive eruptions. Dense pyroclasts with $<60\%$ vesicularity can also form by rapid decompression induced fragmentation in a confined conduit (Cashman et al. 2000), which would produce a mixture of country rock fragments and juvenile material (Head and Wilson 2003) similar to what is observed in some Macquarie Island HV facies.

In contrast to a magmatic fragmentation mechanism, the high percentage of lithic clasts in HV facies is more typical of a phreatomagmatic origin (Morrisey et al. 2000). Such lithics include amphibole-bearing diabase that would have come from subsurface sills. The wide range in Macquarie Island HV facies pyroclast vesicularities from $\sim 15\%$ to 50% is more typical of a phreatomagmatic eruption (Houghton and Wilson 1989), but can be due to eruptions of a heterogeneously degassed magma (Noguchi et al. 2006). Although this range in vesicularity is in part due to the presence of non-juvenile lithics (discussed above), variably vesiculated domains within single lapilli have been observed elsewhere in deep-water tholeiitic pyroclasts (Gill et al. 1990). MFCI drives phreatomagmatic eruptions and can theoretically occur in the deep-marine environment by repeated expansion and collapse of supercritical vapor films along magma/water contact surfaces (Wohletz 2003). For this to occur, a high fuel:coolant ratio is needed (Zimanowski et al. 1997a) and could conceivably exist in

a submarine confined conduit where hydrothermal circulation is restricted (Davis and Clague 2006). Dissolved compounds would likely increase the density and viscosity of the hydrothermal coolant and potentially improve the initial coarse mixing stage of the MFCI process (White 1996). The presence or absence of MFCI can be resolved by identification of μm -scale surface features (Büttner et al. 2002), but were not observed in this study due to the physical difficulty of grain separation and surface modification by palagonite alteration. However, mm-scale wispy pyroclast morphologies in HV-BST facies are comparable to some experimentally produced elongate basaltic pyroclasts of MFCI origin (c.f. Zimanowski et al. 1997b).

These observations lead us to conclude that the HV particles in Macquarie Island pyroclastic lithofacies were fragmented by magmatic and possibly MFCI mechanisms. The high phenocryst content of this facies suggests that there was sufficient crystal fractionation to have caused volatile enrichment in the parent magma and bubble nucleation (Vergnolle and Mangan 2000). Magma degassing and expansion caused the rapid acceleration of a magmatic foam through a confined conduit where it was injected into a shallow hydrothermal coolant. The vesicular nature of the magma would promote bulk mixing of the magma and coolant (Heiken and Wohletz 1991) and initiate MFCI fine fragmentation processes. However, explosive expansion due to steam generation, i.e. stage 3 of MFCI (White 1996), would be suppressed at the high hydrostatic pressure. Decompression of the finely fragmented magmatic foam would disrupt the conduit seal and cause an explosive burst of variably degassed pyroclasts and lithic fragments. Upon eruption into the water column secondary quench granulation would likely occur around the vent.

HV facies transport mechanisms

Planar lamination and planar-grain fabric in HV-LLT facies indicate deposition by rapidly depositing upper plane bed conditions (Hiscott and Middleton 1980; Lowe 1988; Cheel 1990). This laminar flow rheology is supported by the presence of reverse grading and large outsized clasts (Fisher 1971), and typifies high-density sandy gravity current deposits (Lowe 1982; Arnott and Hand 1989). Intergranular friction produced by dispersive pressures would have destroyed the delicate bubble-wall shapes that are preserved in the HV-BST facies. The preservation of these delicate primary shard morphologies suggests that HV-BST facies formed from suspended load fall-out without significant reworking. This is supported by the absence of both traction current structures and mineral fragments. The density contrast between mineral fragments and buoyant bubble-wall shards would have concentrated the former into underlying HV-LLT facies.

HV facies depositional environment

The HV lithofacies association observed at Pyramid Peak indicates that a high-density gravity flow deposit was overlain by less dense suspension settle-out (Fig. 10b). This stratigraphy is comparable to the idealized depositional sequence from a submarine pyroclastic eruption visualized by Schneider (2000), which includes a lithic-rich vesicular lapilli base and a fine-grained ash top. The separation of these two facies at Pyramid Peak is characteristic of internal decoupling in a density stratified turbidity current (Kneller and McCaffery 1999).

High-density gravity currents would have been initiated by lateral movement of pyroclastic debris from a collapsing eruption column (Fig. 10b). Head and Wilson (2003) calculated eruption column heights to be <240 m at depths greater than 1.0 km b.s.l. in volatile-rich magmas (1.9 wt% H₂O) and negligible below 0.5 km b.s.l. in moderately volatile magmas (0.54 wt% H₂O). Due to the great eruption depth (>2 km b.s.l.) and moderate volatile contents (~1 wt% H₂O) for Macquarie Island HV pyroclastic rocks, eruption column heights would have been minimal and akin to a “boil-over” eruption style. Nevertheless, the eruption would generate rising plumes of heated seawater and expelled hydrothermal fluids that could promote wide pyroclast dispersal (Clague et al. 2009). The discrepancy between porphyritic HV facies clasts and interbedded LV aphyric pillow basalts on Macquarie Island indicates that pyroclastic material was transported to distal basins as envisioned by previous workers (e.g. Smith and Batiza 1989; Lackschewitz et al. 1994). The high angle between bedding attitudes of HV facies and the encompassing extrusive sequence of Pyramid Peak is the result of pyroclastic flows ponding in bathymetric lows between pillow cones (Fig. 10b).

Eruptive explosivity and geochemistry

Magmatic eruptive explosivity is generated in part by exsolving volatiles that expand and fragment the magma (Houghton and Wilson 1989). A magmatic origin for volatile gasses in HV lithofacies described in this study is implied by the positive co-variation between H₂O and Cl with incompatible elements (Hekinian et al. 2000). Furthermore, the presence of pyrite on the interior vesicle walls indicates that S was exsolving out of the magma and reacting with Fe during vesicle formation (Davis and Clague 2006). This is supported by generally lower S contents in HV facies compared to LV facies (Table 2). Degassing of the relatively highly volatile HV facies compared to LV breccia facies suggests that magmatic

volatile exsolution may have contributed to the production of ubiquitous bubble-wall shards in HV facies.

Kokelaar (1986) showed that the volatile fragmentation depth is greater with more alkalic magmas (2 wt% H₂O) at about 1 km, than tholeiitic magmas (<0.5 wt% H₂O) at about 200 m. Chemical trends documented by Hekinian et al. (2000) along the Mid-Atlantic Ridge, indicate that eruption of N- and T-MORB basalts will generate effusive non-explosive processes that produce poorly vesicular (<15% vesicles) hyaloclasts; and E-MORB and alkalic magmas will generate explosive magmatic processes that produce more highly vesicular (>15% vesicles) pyroclasts. This relationship between magma geochemistry, vesicularity and eruption explosivity is also observed between LV hyaloclastites and HV pyroclastites in this study. In general, juvenile shards from LV facies (group A) have less alkaline magma compositions than juvenile shards from HV facies (group B), specifically in incompatible elements Na, K, P and Ti. This is complimented by lower Mg#’s and higher volatile contents in HV facies. These trends broadly compare to findings by Kokelaar (1986) and Hekinian et al. (2000), and suggest that more alkaline basalts can produce explosive submarine eruptions. However, the most alkaline and volatile-rich shards of this study (group C) are poorly vesicular and would imply non-magmatic explosivity. Speculation about the significance of group C is moot at this point considering that they are non-juvenile and their primary eruptive origin is uncertain. Nevertheless, poorly vesicular groups A and C outlined here are comparable to the normal and highly enriched (respectively) near-primitive glasses of Kamenetsky et al. (2000), whereas group B fits within their fractionated glass compositions (Fig. 7). Crystal fractionation for group B indicates sufficient crustal residence time to have caused magmatic degassing (discussed above). Therefore, we suggest that both high volatile content/alkalinity and crystal fractionation time were required to produce deep-marine explosive eruptions along the PMSR.

The stratigraphically restricted position of pyroclastic facies in the uppermost alkaline interval of Macquarie Island’s extrusive sequence indicates the late development of explosive volcanism during crustal construction (Fig. 1b; Griffin 1982). Several factors may account for this and include off-axis volcanism, seamount shoaling, tectonic uplift, low magma-rate supply, short spreading-segments along the PMSR, and proximity to an amagmatic inside corner structure (Staudigel and Schmincke 1984; Batiza 1996; Naumann and Geist 1999; Goscombe and Everard 2001; Georgen and Lin 2003; Wertz et al. 2003; Mosher and Massell-Symons 2008). These factors are partly dependent upon one another and reflect the eruption of the Macquarie Island extrusive sequence during the demise of the slow-spreading PMSR.

Conclusions

Vitriclastic rocks from Macquarie Island formed through both non-explosive and explosive processes at water depths exceeding 2 km b.s.l.. Thick structureless beds of monomict hyaloclastite breccias primarily consist of blocky pillow fragments, mini-pillows, and spherical glass globules supported by a co-genetic poorly vesicular very coarse ash matrix with near-primitive subalkaline to transitional basalt compositions. This facies was formed by quench-fragmentation and subsequent short lived grain-flows proximal to a source vent. In this vicinity intrusion of pillow basalt tongues produced coarse-grained fluidal peperite. These breccias were reworked and transported to distal locations to form very thin fine-grained sandstone beds.

In contrast, polymict pyroclastic facies consist of planar laminated lapilli-tuffs that are primarily composed of highly vesicular basalt clasts and sideromelane shards with fractionated alkaline compositions. This coarser unit is locally overlain by a very thin non-laminated bed of fine-grained bubble-wall shards that were formed by volatile gas buildup, magma expansion, and MFCI induced fragmentation in a confined conduit. This material was transported by density-stratified gravity currents. Juvenile highly vesicular pyroclasts were mixed with subalkaline poorly vesicular basalt, highly alkaline poorly vesicular hawaiite, and amphibole-bearing diabase lithics during eruption and transport.

A connection between vesicularity, magma composition, volatile content and magmatic explosivity is not necessarily corroborated by highly volatile poorly vesicular lithic shards. We suggest that both high volatile enrichment and fractionation time were required to produce deep-marine explosive eruptions along the PMSR. The abyssal eruption explosivity evident on Macquarie Island likely reflects the evolution of the PMSR into the present day transform boundary.

Acknowledgements The authors would like to acknowledge I. Skilling, D. Maicher, and JDL White for providing comments that greatly improved this manuscript. We thank the Australian Antarctic Division (AAD project number 2515) and the Tasmanian Parks and Wildlife Service for providing support and access to our remote field locations on Macquarie Island during summer field seasons of 2006 and 2007. We thank the crews of the *Marina Svateava* (summer 2006) and the *Spirit of Enderby* (summer 2007) along with Aurora and Heritage expeditions for providing transport to Macquarie Island. N. Pearson provided numerous insights and instrumentation support for the geochemical aspect of the study. This project was supported by an ARC discovery grant to NRD and JAD (DP0663373). This is contribution number 581 from the ARC GEMOC National Key Centre (www.es.mq.edu.au/GEMOC/).

References

- Arnott RWC, Hand BM (1989) Bedforms, primary structures and grain fabric in the presence of suspended sediment rain. *J Sed Petrol* 59:1062–1069
- Batiza R (1996) Magmatic segregation in mid-ocean ridges: A review. In: MacLeod CJ, Walker CL (eds) Tectonic, magmatic, hydrothermal, and biological segmentation of mid-ocean ridges. *Geol Soc London Spec Pub* 118:103–130
- Busby-Spera CJ, White JDL (1987) Variation in peperite textures associated with differing host-sediment properties. *Bull Volcanol* 49:765–776
- Büttner R, Dellino P, Zimanowski B (1999) Identifying magma-water interaction from the surface features of ash aarticles. *Nature* 401:688–690
- Büttner R, Dellino P, La Volpe L, Lorenz V, Zimanowski B (2002) Thermohydraulic explosions in phreatomagmatic eruptions as evidenced by the comparison between pyroclasts and products from molten fuel coolant interaction experiments. *J Geophys Res* 107:2277. doi:10.1029/2001JB000511
- Carlisle D (1963) Pillow breccias and their aquagene tuffs, Quadra Island, British Columbia. *J Geol* 71:48–71
- Cas RAF, Yamagishi H, Moore L, Scutler C (2003) Miocene submarine fire fountain deposits, Ryugasaki Headland, Oshoro Peninsula, Hokkaido, Japan: implications for submarine fountain dynamics and fragmentation processes. In: White JDL, Smellie JL, Clague DA (eds) Explosive subaqueous volcanism. *Am Geophys Union Mon* 140:299–316
- Cashman KV, Sturtevant B, Papale P, Navon O (2000) Magmatic fragmentation. In: Sigurdsson H, Houghton BF, McNutt SR, Rymer H, Stix J (eds) *Encyclopedia of volcanoes*. Academic, San Diego, pp 421–430
- Cheel RJ (1990) Horizontal lamination and the sequence of bed phases and stratification under upper-flow-regime conditions. *Sedimentology* 37:517–529
- Clague DA, Batiza R, Head JW, Davis AS (2003) Pyroclastic and hydroclastic deposits on Loihi Seamount, Hawaii. In: White JDL, Smellie JL, Clague DA (eds) Explosive subaqueous volcanism. *Am Geophys Union Mon* 140:73–95
- Clague DA, Paduan JB, Davis AS (2009) Widespread strombolian eruptions of mid-ocean ridge basalt. *J Volcanol Geotherm Res* 180:171–188
- Daczko NR, Mosher S, Coffin MF, Meckel TA (2005) Tectonic implications of fault-scarp-derived volcanoclastic deposits on Macquarie Island; sedimentation at a fossil ridge-transform intersection? *Geol Soc Am Bull* 117:18–31
- Daczko NR, Harb N, Portner RA, Dickinson JA (2009) Geochemical fingerprint of hyaloclasts in glassy fragmental rocks of Macquarie Island (Southern Ocean): implications for volcanogenic sedimentary processes at a waning mid-ocean ridge. *Aus J Earth Sci* 56:951–963
- Davis A, Clague D (2006) Volcanoclastic deposits from the North Arch volcanic field, Hawaii: explosive fragmentation of alkalic lava at abyssal depths. *Bull Volcanol* 68:294–307
- Deer WA, Howie RA, Zussman J (1992) An introduction to the rock-forming minerals. Longman Scientific Technical, Harlow Cambridge
- Dickinson JA, Harb N, Portner RA, Daczko NR (2009) Glassy fragmental rocks of Macquarie Island (Southern Ocean): Mechanism of formation and deposition. *Sed Geol* 216:91–103
- Duncan RA, Varne R (1988) The age and distribution of the igneous rocks of Macquarie Island. *Pap Proc Roy Soc Tas* 122:45–50
- Eissen JP, Fouquet Y, Hardy D, Ondreas H (2003) Recent MORB volcanoclastic explosive deposits formed between 500 and 1750 m.b.s.l. on the axis of the Mid-Atlantic Ridge, south of the

- Azores. In: White JDL, Smellie JL, Clague DA (eds) Explosive subaqueous volcanism. *Am Geophys Union Mon* 140:143–166
- Fisher RV (1971) Features of coarse-grained, high-concentration fluids and their deposits. *J Sed Petrol* 41:916–927
- Fisher RV, Schmincke H-U (1994) Volcaniclastic sediment transport and deposition. In: Pye K (ed) *Sediment transport and depositional processes*. Blackwell Scientific, Edinburgh, pp 351–388
- Fouquet Y, Eissen JP, Ondreas H, Barriga F, Batiza R, Danyushevsky L (1998) Extensive volcaniclastic deposits at the Mid-Atlantic Ridge axis; results of deep-water basaltic explosive volcanic activity? *Terra Nova* 10:280–286
- Georgen JE, Lin J (2003) Plume-transform interactions at ultra-slow spreading ridges; implications for the Southwest Indian Ridge. *Geochim Geophys Geosyst* 4:9106. doi:10.1029/2003GC000542
- Gill J, Torssander P, Lapierre H, Taylor R, Kaiho K, Koyama M, Kusakabe M, Aitchison J, Cisowski S, Dadey K, Fujioka K, Klaus A, Lovell M, Marsaglia K, Pezard P, Taylor B, Tazaki K (1990) Explosive deep water basalt in the Sumisu backarc rift. *Science* 248:1214–1217
- Goscombe BD, Everard JL (1998) Geology of Macquarie Island. Geological Atlas 1:10,000 Series, Mineral Resources Tasmania, Hobart:7 sheets
- Goscombe BD, Everard JL (2001) Tectonic evolution of Macquarie Island; extensional structures and block rotations in oceanic crust. *J Struct Geol* 23:639–673
- Griffin BJ (1982) Igneous and metamorphic petrology of lavas and dikes of the Macquarie Island ophiolite complex. PhD thesis, University of Tasmania, Hobart
- Harb N (2006) Fragmentation processes, depositional mechanisms and lithification of glassy fragmental rocks, Macquarie Island. BSc (hons) thesis, Macquarie University, Sydney
- Hayward BW, Grenfell HR, Carter R, Hayward JJ (2004) Benthic foraminiferal proxy evidence for the Neogene palaeoceanographic history of the Southwest Pacific, east of New Zealand. *Mar Geol* 205:147–184
- Head JW, Wilson L (2003) Deep submarine pyroclastic eruptions; theory and predicted landforms and deposits. *J Volcanol Geotherm Res* 121:155–193
- Heiken G, Wohletz K (1991) Fragmentation processes in explosive volcanic eruptions. *Soc Econ Paleontol Mineral Spec Publ* 45:19–26
- Hekinian R, Pineau F, Shilobreeva S, Bideau D, Gracia E, Javoy M (2000) Deep sea explosive activity on the Mid-Atlantic Ridge near 34 degrees 50'N; magma composition, vesicularity and volatile content. *J Volcanol Geotherm Res* 98:49–77
- Hiscott RN, Middleton GV (1980) Fabric of coarse deep-water sandstones, Tourelle Formation, Quebec, Canada. *J Sed Petrol* 50:703–721
- Honnorez J, Kirst P (1975) Submarine basaltic volcanism: morphometric parameters for discriminating hyaloclastites from hyalotuffs. *Bull Volcanol* 39:441–465
- Houghton BF, Wilson CJN (1989) A vesicularity index for pyroclastic deposits. *Bull Volcanol* 51:451–462
- Kamenetsky VS, Everard JL, Crawford AJ, Varne R, Eggins SM, Lanyon R (2000) Enriched end-member of primitive MORB melts; petrology and geochemistry of glasses from Macquarie Island (SW Pacific). *J Petrol* 41:411–430
- Kamenetsky VS, Maas R (2002) Mantle-melt evolution (dynamic source) in the origin of a single MORB suite: a perspective from magnesian glasses of Macquarie Island. *J Petrol* 43:1909–1922
- Kneller B, McCaffrey W (1999) Depositional effects of flow nonuniformity and stratification within turbidity currents approaching a bounding slope; deflection, reflection, and facies variation. *J Sed Res* 69:980–991
- Kokelaar P (1986) Magma-water interactions in subaqueous and emergent basaltic volcanism. *Bull Volcanol* 48:275–289
- Lackschewitz KS, Dehn J, Wallrabe-Adams H-J (1994) Volcaniclastic sediments from mid-oceanic Kolbeinsey Ridge, north of Iceland; evidence for submarine volcanic fragmentation processes. *Geology* 22:975–978
- Le Maitre RW (2002) *Igneous rocks a classification and glossary of terms*. Cambridge University, Cambridge
- Lowe DR (1982) Sediment gravity flows; II, depositional models with special reference to the deposits of high-density turbidity currents. *J Sed Petrol* 52:279–297
- Lowe DR (1988) Suspended-load fallout rate as an independent variable in the analysis of current structures. *Sedimentology* 35:765
- Maicher D, White JDL, Batiza R (2000) Sheet hyaloclastite; density-current deposits of quench and bubble-burst fragments from thin, glassy sheet lava flows, Seamount Six, eastern Pacific Ocean. *Mar Geol* 171:75–94
- Mangan MT, Cashman KV (1996) The structure of basaltic scoria and reticulite and inferences for vesiculation, foam formation, and fragmentation in lava fountains. *J Volcanol Geotherm Res* 73:1–18
- McBirney AR (1963) Factors governing the nature of submarine volcanism. *Bull Volcanol* 26:455–469
- Morrissey MM, Zimanowski B, Wohletz K, Büttner R, Ballard RD (2000) Phreatomagmatic fragmentation. In: Sigurdsson H, Houghton BF, McNutt SR, Rymer H, Stix J (eds) *Encyclopedia of volcanoes*. Academic, San Diego, pp 431–445
- Mosher S, Massell-Symons CM (2008) Ridge reorientation mechanisms: Macquarie Ridge Complex, Australia-Pacific plate boundary. *Geology* 36:119–122
- Naumann TR, Geist DJ (1999) Generation of alkalic basalt by crystal fractionation of tholeiitic magma. *Geology* 27:423–426
- Noguchi S, Toramaru A, Shimano T (2006) Crystallization of microlites and degassing during magma ascent: Constraints on the fluid mechanical behavior of magma during the Tenjo eruption on Koze Island, Japan. *Bull Volcanol* 68:432–449
- Orton GJ (1996) Volcanic environments. In: Reading HG (ed) *Sedimentary environments: Processes, facies and stratigraphy*. Blackwell Science, Oxford, pp 485–567
- Quilty PG, Crundwell M, Wise SW Jr (2008) Microplankton provide 9 Ma age for sediment in the Macquarie Island ophiolite complex. *Aus J Earth Sci* 55:1119–1125
- Sanders JE (1965) Primary sedimentary structures formed by turbidity currents and related resedimentation mechanisms. In: Middleton GV (ed) *Primary sedimentary structures and their hydrodynamic interpretation*. Soc Econ Paleontol Mineral Spec Publ, pp 192–219
- Schneider J-L (2000) Volcaniclastic sedimentation in submarine settings; products and processes. In: Leyrit H, Montenat C (eds) *Volcaniclastic rocks from magmas to sediments*. Gordon and Breach Science Publishers, Amsterdam, pp 175–191
- Shanmugam G (1997) The Bouma sequence and the turbidite mind set. *Earth-Sci Rev* 42:201–229
- Simpson K, McPhie J (2001) Fluidal-clast breccia generated by submarine fire fountaining, Trooper Creek Formation, Queensland, Australia. *J Volcanol Geotherm Res* 109:339–355
- Skilling IP, White JDL, McPhie J (2002) Peperite: a review of magma sediment mingling. *J Volcanol Geotherm Res* 114:1–17
- Smith TL, Batiza R (1989) New field and laboratory evidence for the origin of hyaloclastite flows on seamount summits. *Bull Volcanol* 51:96–114
- Sohn RA, Willis C, Humphris S, Shank TM, Singh H, Edmonds HN, Kunz C, Hedman U, Helmke E, Jakuba M, Liljebladh B, Linder J, Murphy C, K-i N, Sato T, Schlindwein V, Stranne C, Tausenfreund M, Upchurch L, Winsor P, Jakobsson M, Soule A (2008) Explosive volcanism on the ultraslow-spreading Gakkel Ridge, Arctic Ocean. *Nature* 453:1236–1238
- Squire RJ, McPhie J (2002) Characteristics and origin of peperite involving coarse-grained host sediment. *J Volcanol Geotherm Res* 114:45–61

- Staudigel H, Schmincke H-U (1984) The Pliocene seamount series of La Palma/Canary Islands. *J Geophys Res* 89:11,195–11,215
- Vergnolle S, Mangan M (2000) Hawaiian and strombolian eruptions. In: Sigurdsson H, Houghton BF, McNutt SR, Rymer H, Stix J (eds) *Encyclopedia of volcanoes*. Academic, San Diego, pp 447–461
- Wertz KL, Mosher S, Daczko NR, Coffin MF (2003) Macquarie Island's Finch-Langdon Fault; a ridge-transform inside-corner structure. *Geology* 31:661–664
- White JDL (1996) Impure coolants and interaction dynamics of phreatomagmatic eruptions. *J Volcanol Geotherm Res* 74:155–170
- White JDL, Houghton BF, Ballard RD (2000) Surtseyan and related phreatomagmatic eruptions. In: Sigurdsson H, Houghton BF, McNutt SR, Rymer H, Stix J (eds) *Encyclopedia of volcanoes*. Academic, San Diego, pp 495–512
- White JDL, Houghton BF (2006) Primary volcaniclastic rocks. *Geology* 34:677–680
- Wohletz KH (1983) Mechanisms of hydrovolcanic pyroclast formation: grain-size, scanning electron microscopy, and experimental studies. *J Volcanol Geotherm Res* 17:31–63
- Wohletz KH (2003) Water/magma interaction: physical considerations for the deep submarine environment. In: White JDL, Smellie JL, Clague DA (eds) *Explosive subaqueous volcanism*. *Am Geophys Union Mon* 140:25–49
- Wright IC (2001) In situ modification of modern submarine hyaloclastic/pyroclastic deposits by oceanic currents; an example from the southern Kermadec Arc (SW Pacific). *Mar Geol* 172:287–307
- Yamagishi H (1991) Morphological and sedimentological characteristics of the Neogene submarine coherent lavas and hyaloclastites in Southwest Hokkaido, Japan. *Sed Geol* 74:5–23
- Zimanowski B, Büttner R, Lorenz V (1997a) Premixing of magma and water in MFCI experiments. *Bull Volcanol* 58:491–495
- Zimanowski B, Büttner R, Lorenz V, Haefele H-G (1997b) Fragmentation of basaltic melt in the course of explosive volcanism. *J Geophys Res* 102:803–814
- Zimanowski B, Wohletz K, Dellino P, Büttner R (2003) The volcanic ash problem. *J Volcanol Geotherm Res* 122:1–5

VIII:

**Discussion about a fault-scarp source for
hyaloclastite breccias**

The problem:

A key conclusion from Chapter V and the work of Harb (2006) indicates that hyaloclastite breccias from Macquarie Island were not produced by movement along fault-scarps as is interpreted for gabbroic and basaltic lithofacies presented in Chapters I and II. This conclusion is based upon the low geochemical diversity of vitric grains within individual stratigraphic sections around the island and the assumption that a fault-derived source would consist of polymodal compositions from several different eruption episodes. Furthermore, Chapters V and VI also conclude that the fresh nature of vitric grains in the sampled sections would not be possible in hydrothermally altered fault zones interpreted as the source for the gabbroic sedimentary rocks described in Chapter II. Therefore, based on these premises the chosen hyaloclastic sections in Chapter V and VI were interpreted to be the result of pillow cone flank collapse during voluminous eruption episodes. Therefore, lava extrusion onto the steep slopes surrounding pillow cones is considered the primary caveat in causing gravity flows of the syneruptive quench-fragmented hyaloclastic debris. This interpretation is supported by the presence of jig-saw fit texture and spherical glassy globules, which indicate fragmentation while hot. Hence, refuting a “cold” faulted source.

Chapters V and VI do not mention hyaloclastic breccias observed at Aurora Point, Davis Bay, northern Bauer Bay, and Davis Point, which occur adjacent to fault scarps and are interstratified with fault scarp-derived polymodal basaltic breccia (Fig. 8.1). The fault-scarp associated hyaloclastic breccias are lithologically similar to those described in chapters V and VI, being comprised of monomict basalt clasts and a vitric granule matrix. The spatial association between fault-derived basaltic breccias and hyaloclastites may be explained by several interpretations: 1) eruption along the

edge or above active fault scarps; 2) active eruptive vents (i.e. pillow cones, fissures) located along the base of fault scarps; or 3) fault scarps along the edges of active calderas. In all these cases, the erupting vent would have to have produced hyaloclastic debris in close proximity to steep slopes associated with a fault. Evidence for and against a fault-scarp influenced source for hyaloclastite breccias are presented below from two specific field locations.

The Davis Point example:

Description

A relationship between fault-scarps and hyaloclastite is best demonstrated in the uppermost units of the Davis Point stratigraphic section where an extrusive section including key hyaloclastite breccia and thin sedimentary marker units are offset 13-25 m by a 58° east dipping 330° oriented fault scarp (Figure 8.2A). Well-exposed slicken lines that plunge 65° toward 227° indicate normal/dextral offset. Across ~50 m of exposure, a wedge shaped hyaloclastite unit thickens from 0.8 to 2.0 m in the hangingwall and thins from 0.7 to 0.0 m in the footwall, going from east to west (Figure 8.2B-D). Locally, pillow basalt associated with the co-genetic overlying hyaloclastite rapidly thins to 0 m in the immediate footwall (Figure 8.2D). The hyaloclastite breccia is coarse-tail graded and laterally correlates with very thin epiclastic sandstone lithofacies (LV-VS) 1.5 km to the north (see Figure 7.3). Vitriclastic material is replaced by basalt clasts in more fault-proximal locations, thereby producing interstratified hyaloclastic and basaltic breccia. Together, hyaloclastic debris and basalt clasts from over- and underlying faulted basalt units fill a 4 m wide gouge zone adjacent to the fault. This gouge zone locally contains a

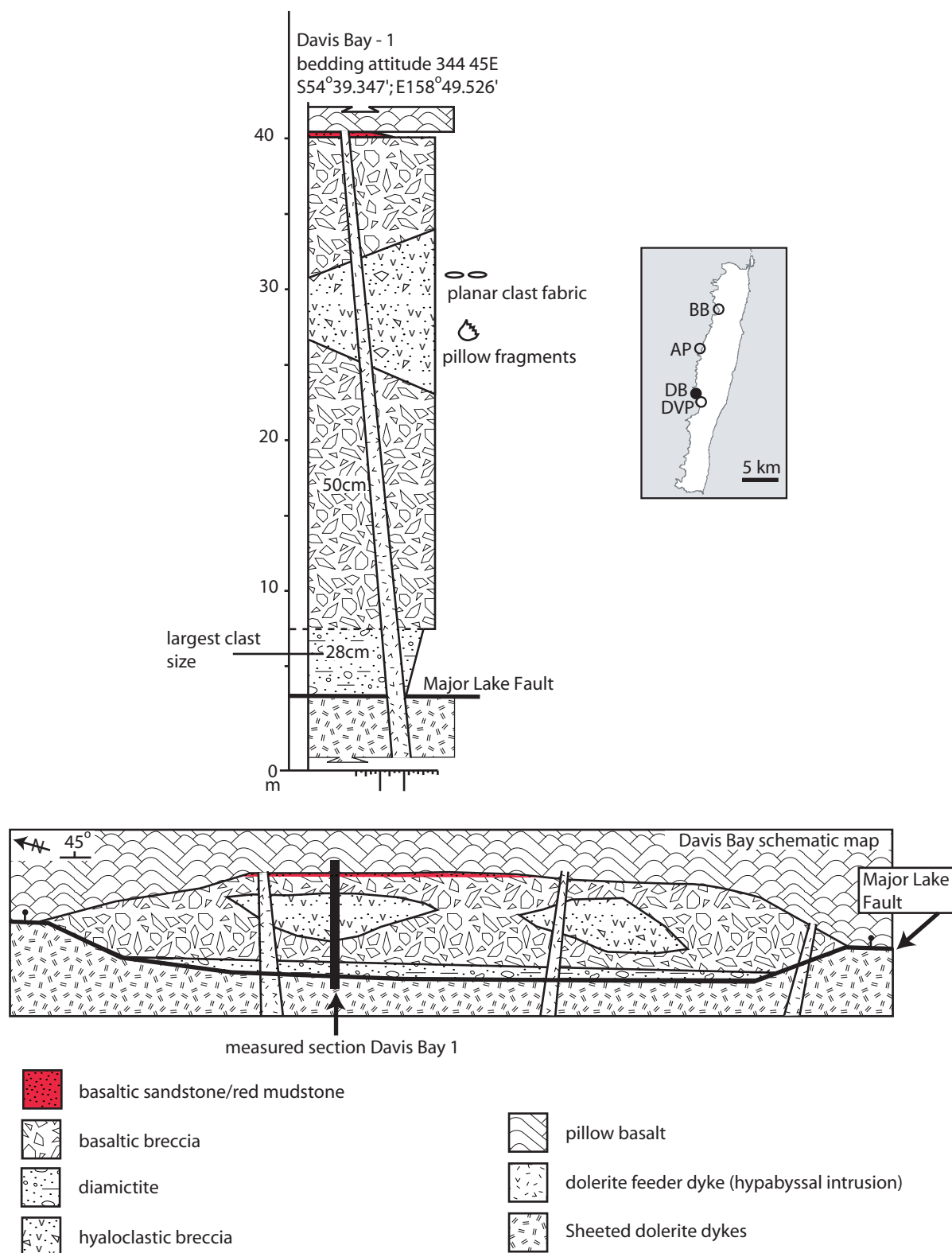


Figure 8.1:
Representative measured section and schematic map from Davis Bay illustrating the spatial relationship between monomict hyaloclastic breccia and oligomict basaltic breccia lithofacies. Lensoid shaped hyaloclastic breccias units occur within thick basaltic breccia, which mantles the Major Lake Fault along strike. Section corresponds to base of Davis Point (DVP) composite section shown in Figure 3.1. Basaltic breccia and sandstone lithofacies described on page 32 in Chapter I. Hyaloclastic breccias described in Chapter V. Inset shows other locations on Macquarie Island containing similar relationships to that observed at Davis Bay (DB; closed circle) and include Davis Point (DVP), northern Bauer Bay (BB), and Aurora Point (AP; open circles).

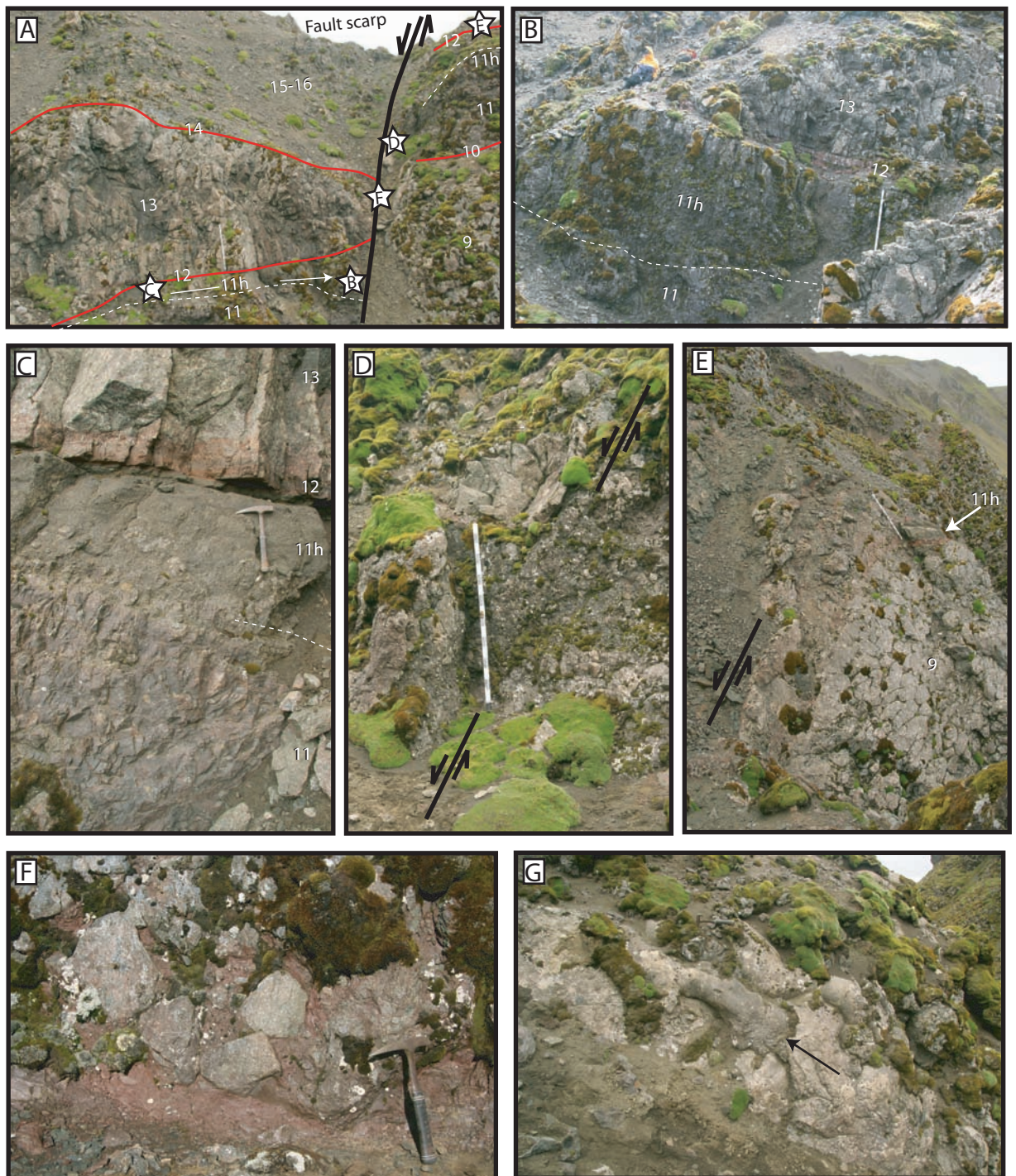


Figure 8.2:

Photographic montage from upper Davis Point stratigraphic section (DVP). Numbers on each photo represent unit number in stratigraphic column DVP1 in Figure 2.2B. Unit 11h refers to hyaloclastic breccia top to unit 11 pillow basalt. Measuring staff in A, B, C, and D is 1.8 meters. Hammer in B and E is 30 cm. A) Davis Point fault looking south showing offset in very thin sedimentary interbeds (units 10, 12 and 14; red lines) and hyaloclastite breccia (base marked by dashed line). Lettered stars refer to other photographs. Arrow between C and B represents decreasing vitric grain component. B) Hyaloclastite breccia in proximal hangingwall location. Basalt breccia in base of unit 11h. C) Hyaloclastite breccia in distal hangingwall location. D) Steeply dipping (black lines) basaltic breccia from unit 13 and hyaloclastite breccia from unit 11h. E) Fault gouge (black line) and footwall south of photo shown in A. Pillow basalt unit 11 is absent with thin hyaloclastite breccia 11h. F) Fault gouge composed of unit 13 basalt clasts within red mudstone matrix. G) Elongate pillows from units 9 extending down fault scarp face. Note brecciation of pillow tubes (arrow). Fault dips to lower right of photo.

red mudstone matrix and is bound in the footwall by elongate pillow tubes that are oriented vertically down the face of the fault scarp (Figure 8.2F-G). Hyaloclastite breccia and overlying pelagic red mudstone beds dip steeply into the fault zone, but interbedded basalt units primarily show brittle deformation or strung-out extrusive (i.e. elongate pillows) characteristics.

Interpretation

Observations outlined above indicate that a fault scarp influenced the thickness of an actively forming hyaloclastite breccia unit. Furthermore, the presence of red pelagic mudstone within fault gouge and elongate pillow tubes down the face of the scarp indicate that faulting occurred during pelagic sedimentation and volcanism. Deformation of the hyaloclastite unit and bounding pillow basalt units suggests that the fault was also active after volcanism ceased. These features are analogous to volcanic growth faults that form along abyssal hills within modern day mid-ocean ridges (Macdonald et al. 1996). Considering the 3 possible fault-scarp influenced hyaloclastite interpretations listed above, field relationships observed at Davis Point suggest that a relatively shallow fault-tip propagated into an actively forming vent field and continued activity throughout the duration of volcanism in the area and long after.

A general lack of hydrothermal fault minerals in the breccias and fault gouge is most likely due to the minor nature and relatively shallow-crustal position of the upper crustal Davis Point fault-tip when compared to much larger faults that expose deeper plutonic rocks (i.e. Finch-Langdon fault). Hence, small shallow-crustal fault-tips would not tap the hot hydrothermal fluids that produced the relatively high-grade hydrothermal detrital minerals (e.g. laumontite, epidote, and prehnite) in

gabbroic sandstone and breccias. This is also supported by the general absence of “high” grade hydrothermal minerals in basaltic and hyaloclastic breccia clasts, which contain the “lower” grade alteration minerals analcime, corrensite, red hematitic oxides, calcite, thomsonite, and natrolite? (see Chapter I and III). These low grade hydrothermal minerals are prevalent as pore-space fillings and clay-altered rims of fresh vitric grains in vitriclastic rocks of Macquarie Island (see Chapter V and VII).

The Green Gorge example:

Description

Hyaloclastite breccias from the Green Gorge measured section of Chapters V and VI were examined in more detail during the 2007 field season. Several low angle reverse faults that strike $\sim 75^\circ$ and verge to the northwest cut the massive hyaloclastite breccia units. A sequence of dolerite units with thin tabular geometries occur within the hyaloclastite breccia and are oriented nearly parallel to the reverse faults. These dolerite units are mapped as tabular basalt flows on the geologic map of Goscombe and Everard (1996) and were used by Harb (2006) as bedding surfaces to measure the Green Gorge hyaloclastite stratigraphic section. The method employed by Harb (2006) was used due to the lack of bedding in hyaloclastite breccias. However, measurement of the flattened top and bottoms of pillow surfaces and “Y-form” selvage geometries between pillows that overlie and are laterally equivalent to the hyaloclastite breccias show that regional bedding is nearly perpendicular to the orientations of the dolerite units (Fig. 8.3 A-B). In addition, the dolerite units have fine grained chilled margins on both surfaces, lack surficial flow corrugations/striations, exhibit a very thin extensive nature, and have very well

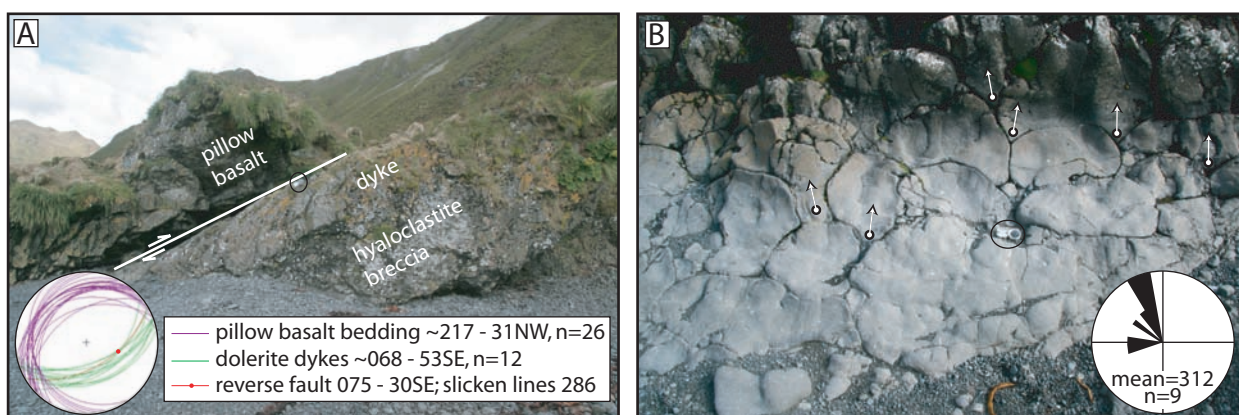


Figure 8.3:
Structural data and photographs from Green Gorge hyaloclastite breccia locality described in Chapters IV and V. A) Folded columnar fractures in dolerite dyke from footwall below a west-northwest verging reverse fault. Dyke cross cuts pillow basalt and hyaloclastite breccia at a high angle (stereonet). Ba) Stratigraphic up-indication from "Y"-from in pillow basalt selvages (arrows) have a northwesterly younging orientation (rose diagram). Brunton compass for scale (circled).

preserved contact-orthogonal cooling fractures. Locally, fault planes occur along the competence discontinuity between the dolerite units and the host hyaloclastite breccia. Along this discontinuity the upper surface of columnar fractures bounded by the fault's hangingwall, are folded into the direction of fault vergence (Fig. 8.3A).

Interpretations

Field relationships mentioned above suggest that the "thin basalt flows" immediately north of Green Gorge on the Goscombe and Everard (1996) geologic map are dolerite dykes. This interpretation is also supported by a lack of depositional breaks within the bounding hyaloclastite breccia. A stereonet plot shows that dyke attitudes are nearly perpendicular to pillow basalt bedding (Fig. 8.3A). An intrusive, rather than extrusive, origin for the Green Gorge dolerite swarm is implemented into both chapters V and VI of this dissertation. Furthermore, the Green Gorge field relationships suggest that hyaloclastite breccias were deposited and lithified long before dyke intrusion and subsequent faulting occurred. This is indicated by the deflection of cooling fractures in some dykes, which is the likely result of movement along overriding reverse faults shortly after dyke intrusion (Fig. 8.3A). Therefore, observations from Green Gorge suggest that the formation of hyaloclastite did not have any relationship with localized faults and would have been derived from purely volcanic processes as described in Chapter V.

Conclusion:

Examples illustrated above indicate that hyaloclastites on Macquarie Island were derived from volcanic eruptions that occurred in close proximity to steep slopes associated with active fault scarps and volcanic constructional features (i.e. pillow

cones). The relationship of hyaloclastite units within encompassing polymict basaltic breccia without depositional breaks between them suggests that both formed simultaneously. Chapter I showed that polymict basaltic breccia on Macquarie Island is derived by the abrasion and disintegration of oceanic crust within spreading-related fault zones. They are comparable to basaltic breccias along the global mid-ocean ridge system, which mantle uplifted fault blocks of basalt with typical slopes of $\sim 43^\circ$ (Mitchell, et al., 2000). Chapter 4 showed that hyaloclastite breccias formed from gravitational collapse of steep slopes along pillow cone flanks during voluminous eruption episodes. Therefore, the presence of a steep slope, whether it be from a pillow cone or fault scarp etc., close to active volcanic vents is the important variable when considering the origin of thick hyaloclastite breccias. Such steep slopes in the mid-ocean ridge environment would exist adjacent to pillow cones, fissures, seamounts and faults. It therefore seems reasonable that seismic activity in the presence of steep slopes, as would be expected along a faulted mid-ocean spreading ridge, would produce gravitational instability along eruption vent flanks and influence hyaloclastic generation as described in Chapter V. This conclusion extends the proposed mode of formation for hyaloclastic rocks within mid-ocean spreading ridges to fault scarp influenced.

References Cited:

- Harb, N., 2006. Fragmentation processes, depositional mechanisms and lithification of glassy fragmental rocks, Macquarie Island. BSc (hons) Thesis, Macquarie University, Sydney, 86 pp.
- Macdonald, K.C., Fox, P.J., Alexander, R.T., Pockalny, R. and Gente, P., 1996. Volcanic growth faults and the origin of Pacific abyssal hills. *Nature*, 380(6570): 125-129.
- Goscombe, B.D. and Everard, J.L., 1998. 1:10,000 Geological Map of Macquarie Island, series of 7 maps, Mineral Resources Tasmania.

Mitchell, N.C., Tivey, M.A. and Gente, P., 2000. Seafloor slopes at mid-ocean ridges from submersible observations and implications for interpreting geology from seafloor topography. *Earth and Planetary Science Letters*, 183(3-4): 543-555.

Synthesis:

Sedimentary and volcanoclastic record of a mid-ocean spreading ridge: Macquarie Island, Southern Ocean

Together, debrites, densites, turbidites, contourites, hemipelagites, pyroclastites, and hyaloclastites formed within mid-ocean ridge systems, comprise a unique lithofacies assemblage that has received relatively little documentation compared to the vast database of continental- and volcanic arc-derived deep-marine sedimentary rocks. Results presented here would suggest that the so-called pelagic “sediment” that occurs close to transform intersections on young spreading ridge seafloors, namely in nodal basins and transform valley floors, likely overlies a plethora of gravity flow and bottom current deposits. This is supported by modern observations of pelagic “sediment” that drape talus accumulations along the base of spreading-ridge fault-scarps (e.g. Tivey et al. 1998).

Apart from coarse-grained breccias/landslide deposits, most submersible dive studies and geophysical surveys tend to passively assume a pelagic origin for “sediment” observed along active-mid ocean ridges without any detailed documentation of specific lithologies other than chalk (Karson and Dick 1983; Goud and Karson 1985; Auzende et al. 1994; Juteau et al. 1995; Blackman et al. 1998). This is puzzling considering geophysical observations of 100 to 700 m of sedimentary fill within transform valleys and nodal basins that are flanked by fault-scarp derived talus piles (Karson et al., 1984; Dick et al. 1991). Such a thick basin fill solely from pelagic suspension fall-out seems unlikely on such young oceanic crust. For example, Mitchell et al. (1998) suggest that an anomalously thick pelagic cover within bathymetric lows along active mid-ocean ridges is due to variable particle load in the bottom nepheloid layer and that turbidite deposition becomes more dominant 30 km away from the ridge axis. This interpretation goes against the long-held idea that pelagic sediments increase in thickness going away from young to old oceanic crust

and therefore should not be very thick along the active spreading ridges (Tucholke et al. 1982). Alternatively, this dissertation would suggest that bathymetric lows along active mid-ocean ridges are likely filled with the sandy portions of gravity flow deposits and later draped by the dilute fine-grained tails of turbidity currents and/or pelagic settle-out. This is supported by, aside from a supra-subduction zone affinity (Robinson et al. 2003), 150 m thick sedimentary sequences intercalated within very thick pillow basalt sections of the Troodos ophiolite (Simonian and Gass, 1978). Hence, submersible and shallow dredge or coring operations may only provide a surficial glimpse of the complete sedimentary lithofacies preserved in active mid-ocean rift basins.

Interbedded talus breccias and lava flows exposed in modern ocean ridge fault-scarps clearly indicates the occurrence of mass wasting that is associated with active tectonism and volcanism (Karson and Dick 1983; Tucholke et al., 1997; Mitchell et al. 2000; Gao 2006). In addition, observation of finer-grained sandy deposits with mineralogies akin to a spreading-ridge source provide the essential link between very coarse-grained talus breccias and the commonly observed fine-grained “pelagic” sediment (Fox and Heezen 1965; Siever and Kastner 1967; Bonatti et al. 1973; Andel and Bowin 1968; Flier-Keller 1991; Swift 1991; Karson et al. 2002). Results from this dissertation have explored this link by describing a plethora of very coarse- to fine-grained sedimentary and volcanoclastic lithofacies from the Macquarie Island ophiolite.

Sedimentary and volcanoclastic lithofacies on Macquarie Island provide convincing evidence for syntectonic mass wasting and volcanism along the proto-Macquarie Spreading ridge (PMSR). Chapters I-IV of this thesis showed that lateral

gravity flow variations preserved by sedimentary rock sequences and their spatial association with fault scarps record the magmatic and unroofing history of upper to lower oceanic crust along the PMSR. This lateral variation in gravity flow lithofacies is also preserved by primary volcanoclastic rocks, which preserve syneruptive features characteristic of volcanic growth faults and explosive to effusive seamount volcanism (Chapter V-VIII). A rugged seafloor bathymetry associated with the fault scarps and volcanic constructional features, as preserved by the primary volcanoclastic rocks, in turn influenced the stratigraphic architecture of sedimentary lithofacies (Chapter II). Together these clastic lithofacies record the tectonic, hydrothermal, magmatic, and volcanic evolution of the PMSR system.

Unusual degrees of enrichment preserved in the late stage pyroclastic rocks are also preserved by “E-zircon” collected from gabbroic colluvium in the island’s north (Chapter IV). The enriched character of magmatism within the last stages of PMSR volcanism is drastically different to the more depleted nature of magmatism recorded by sediment derived from older crust exposed within bounding transforms (Chapters I, II, IV). This evolution from a depleted source to an enriched source was explored in discussions of Chapter IV and predicts a generally effusive style of volcanism within the Oligocene SEIR-PMSR system, considering conclusions made in Chapter VII. Furthermore, shortening of spreading segments and complimentary lengthening of transforms during changing plate motion directions between 30-6 Ma (Chapter I), likely influenced more enriched magmatism by segregating magma chambers and suppressing large-scale partial melting (Chapter VI). This is supported by geochemical provenance studies in Chapters III, IV, VI, and VII, which demonstrated the value of sedimentary and volcanoclastic detrital grains as registrars

for the mid-oceanic rift engine. Therefore, future research in light of igneous, tectonic, and metamorphic processes along mid-ocean ridges and within ophiolites should take a closer look at the so-called “sediment” that fills in the gaps.

References Cited:

- Auzende, J.-M., Cannat, M., Gente, P., Henriët, J.-P., Juteau, T., Karson, J., Lagabriele, Y., Mevel, C. and Tivey, M., 1994. Observation of sections of oceanic crust and mantle cropping out on the southern wall of Kane FZ (N. Atlantic). *Terra Nova*, 6(2): 143-148.
- Blackman, D.K., Cann, J.R., Janssen, B. and Smith, D.K., 1998. Origin of extensional core complexes; evidence from the Mid-Atlantic Ridge at Atlantis fracture zone. *Journal of Geophysical Research*, 103(B9): 21,315-21,333.
- Bonatti, E., Honnorez, J. and Gartner, S., Jr., 1973. Sedimentary serpentinites from the Mid-Atlantic Ridge. *Journal of Sedimentary Petrology*, 43(3): 728-735.
- Flier-Keller, E.V.d., 1991. Geochemistry and mineralogy of sediments, Atlantis II fracture zone, Southwest Indian Ocean. In: R.P. Von Herzen and P.T. Robinson (Editors), *Proceedings of the Ocean Drilling Program, Scientific Results*. Ocean Drilling Program, College Station, TX, pp. 145-151.
- Fox, P.J. and Heezen, B.C., 1965. Sands of the Mid-Atlantic Ridge. *Science*, 149(3690): 1367-1370.
- Gao, D., 2006. Gravitational sliding on the Mid-Atlantic Ridge at the Kane Transform; implications for submarine basin-slope degradation and deformation. *AAPG Bulletin*, 90(2): 159-176.
- Goud, M.R. and Karson, J.A., 1985. Tectonics of short-offset, slow-slipping transform zones in the FAMOUS area, Mid-Atlantic Ridge. *Marine Geophysical Researches*, 7(4): 489-514.
- Juteau, T., Cannat, M., Gente, P., Henriët, J.-P., Juteau, T., Karson, J., Lagabriele, Y., Mevel, C. and Tivey, M., 1995. A submersible study of the western Blanco fracture zone, N.E. Pacific; structure and evolution during the last 1.6 Ma. *Marine Geophysical Researches*, 17(5): 399-430.
- Karson, J.A. and Dick, H.J.B., 1983. Tectonics of ridge-transform intersections at the Kane fracture zone. *Marine Geophysical Researches*, 6(1): 51-98.
- Karson, J.A., Fox, P. J., Sloan, H., Crane, K. T., Kidd, W. S. F., Bonatti, E., Stroup, J. B., Fornari, D. J., Elthon, D., Hamlyn, P., Casey, J. F., Gallo, D. G., Needham, D. and Sartori, R., 1984. The geology of the Oceanographer Transform: The ridge-transform intersection. *Marine Geophysical Researches*, 6(2): 109-141.
- Karson, J.A., Tivey, M.A. and Delaney, J.R., 2002. Internal structure of uppermost oceanic crust along the western Blanco transform scarp; implications for subaxial accretion and deformation at the Juan de Fuca Ridge. *Journal of Geophysical Research*, 107: no.B9, 24.
- Mitchell, N.C., Allerton, S. and Escartin, J., 1998. Sedimentation on young ocean floor at the Mid-Atlantic Ridge, 29 degrees N. *Marine Geology*, 148(1-2): 1-8.

- Mitchell, N.C., Tivey, M.A. and Gente, P., 2000. Seafloor slopes at mid-ocean ridges from submersible observations and implications for interpreting geology from seafloor topography. *Earth and Planetary Science Letters*, 183(3-4): 543-555.
- Robinson, P.T., Malpas, J. and Xenophontos, C., 2003. The Troodos Massif of Cyprus; its role in the evolution of the ophiolite concept. *Special Paper - Geological Society of America*, 373: 295-308.
- Siever, R. and Kastner, M., 1967. Mineralogy and petrology of some Mid-Atlantic Ridge sediments. *Journal of Marine Research*, 25(3): 263-278.
- Simonian, K.O. and Gass, I.G., 1978. Arakapas fault belt, Cyprus: A fossil transform fault. *Geological Society of America Bulletin*, 89(8): 1220-1230.
- Swift, S.A., 1991. Gravels in the Atlantis II fracture zone. In: R.P. Von Herzen and P.T. Robinson (Editors), *Proceedings of the Ocean Drilling Program, Scientific Results*. Ocean Drilling Program, College Station, TX, pp. 431-438.
- Tivey, M., Takeuchi, A. and Scientific Party, W., 1998. A submersible study of the western intersection of the Mid-Atlantic ridge and Kane fracture zone (WMARK). *Marine Geophysical Researches*, 20(3): 195-218.
- Tucholke, B.E., Houtz, R.E. and Ludwig, W.J., 1982. Sediment thickness and depth to basement in western North Atlantic Ocean basin. *AAPG Bulletin*, 66(9): 1384-1395.
- Tucholke, B.E., Kenneth Stewart, W. and Kleinrock, M.C., 1997. Long-term denudation of ocean crust in the central North Atlantic Ocean. *Geology*, 25(2): 171-174.
- van Andel, T.H. and Bowin, C.O., 1968. Mid-Atlantic ridge between 22 degrees and 23 degrees north latitude and the tectonics of mid-ocean rises. *Journal of Geophysical Research*, 73(4): 1279-1298.